Ministry of
Northern Development
and Mines
Ontario

Geoscience Research Grant Program
Summary of Research 1990–1991

Ontario Geological Survey
Miscellaneous Paper 156

1991

92-03609/

© Queens' Printer for Ontario, 1991
Printed in Ontario, Canada

ISSN 0704-2752 (Series)
ISSN 0225-5316 (Sub-series)

Publications of the Ontario Geological Survey and the Ministry of Northern Development and Mines are available from the following sources. Orders for publications should be accompanied by cheque or money order payable to the *Treasurer of Ontario*.

Reports, maps and price lists (personal shopping or mail order):

Public Information Centre, Ministry of Natural Resources
Room 1640, Whitney Block, Queen's Park
Toronto, Ontario M7A 1W3

Reports and accompanying maps only (personal shopping):

Publications Ontario
Main Floor, 880 Bay Street
Toronto, Ontario M7A 1N8

Reports and accompanying maps (mail order or telephone orders):

Publications, Ontario, Ministry of Government Services
5th Floor, 880 Bay Street
Toronto, Ontario M7A 1N8
Telephone (local calls), 965-5300
Toll-free long distance, 1-800-668-9938

Every possible effort is made to ensure the accuracy of the information contained in this report, but the Ministry of Northern Development and Mines does not assume any liability for errors that may occur. Source references are included in the report, and users may wish to verify critical information.

If you wish to reproduce any of the text, tables or illustrations in this report, please write for permission to the Director, Ontario Geological Survey, Ministry of Northern Development and Mines, 11th Floor, 77 Grenville Street, Toronto, Ontario M7A 1W4.

Parts of this publication may be quoted if credit is given. It is recommended that reference be made in the following form:

Macfie, R.I. and Dixon, J.M. 1991. New information on tectonic relations among the Parry Sound, Sequin and Rosseau domains; *in* Geoscience Research Grant Program, Summary of Research 1990-1991, Ontario Geological Survey, Miscellaneous Paper 156, p.65-73.

Scientific Editing: SOTA Production

Deyell-1000-91

Contents

Introductory Remarks, *V.G. Milne* vi

Grant 351 Stratigraphy and Sedimentology of the Upper Ordovician Georgian Bay Formation, Manitoulin Island and Bruce Peninsula—Evaluation of Hardgrounds, Biostromes and Storm Beds for Regional Correlation
M. Byerley and M. Coniglio 3

Grant 357 Mineralogy and Geochemistry of Diagenetic Carbonates in Cambro—Ordovician Sedimentary Rocks, Southwestern Ontario
M.A. Wadleigh, F.J. Longstaffe, R.H. McNutt and S.K. Frape 17

Grant 359 Structural Geology and Stratigraphic Correlations in the Midlothian Lake—Peterlong Lake Area, Abitibi Subprovince
R.B. Hrabi and H. Helmstaedt 31

Grant 363 Seismotectonic Framework and Microearthquake Monitoring Program in the Western Lake Ontario Region: a Progress Report
A.A. Mohajer, H.C. Halls and R. McGrory 41

Grant 364 Multiple Fluid-Inclusion Generations in Variably Deformed Quartz: Hollinger—McIntyre and Kerr Addison—Chesterville Archean Gold-Bearing Quartz Vein Systems, Northern Ontario
D.M. DeR. Channer and E.T.C. Spooner 47

Grant 370 New Information on Tectonic Relations among the Parry Sound, Seguin and Rosseau Domains
R.J. Macfie and J.M. Dixon 65

Grant 375 Sedimentary Evolution in the Michipicoten Greenstone Belt, Wawa Subprovince, Superior Province
R.J. Rice and J.A. Donaldson 75

Grant 382 The Role of the Crust as a Source of PGE in the Sudbury Nickel Deposit: Re/Os Isotope Evidence
A.P. Dicken 99

Grant 384 Geochronology of Hydrothermal Alteration around Volcanic-Hosted Massive Sulphide Deposits in the Superior Province
E.S. Schandl, D.W. Davis, M.P. Gorton and H.A. Wasteneys 105

Grant 386 Modification of the Shallow Reflection Seismic Method for Urban Geophysical Studies in Southern Ontario
J.P. Greenhouse, D.C. Nobes, G.W. Schneider and M.A. Lockhard 121

Grant 389 Hydrogeological Implications of Buried Eskers in Essex County, Ontario: Results from Year 1
M.G. Sklash and O.A. Ibrahim 131

Grant 393 Metamorphic Petrology and Alteration Assemblages of the Hemlo Gold District
Yuanming Pan and Michael E. Fleet 147

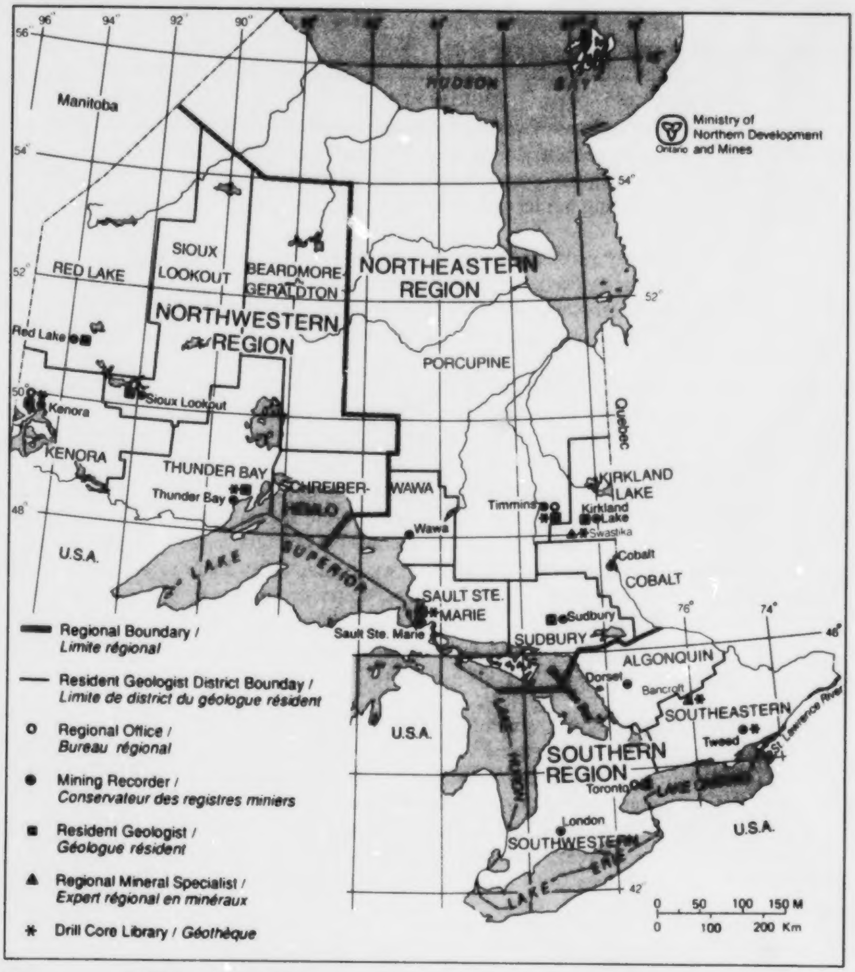
Manitoba
RED LAKE
SIOUX LOOKOUT
BEARDMORE-GERALDTON
NORTHWESTERN REGION
NORTHEASTERN REGION
PORCUPINE
Red Lake
Sioux Lookout
Kenora
KENORA
THUNDER BAY
Thunder Bay
SCHREIBER-HEMLO
WAWA
Wawa
Timmins
KIRKLAND LAKE
Kirkland Lake
Swastika
Cobalt
COBALT
SAULT STE. MARIE
Sault Ste. Marie
Sudbury
SUDBURY
ALGONQUIN
Dorset
Bancroft
SOUTHEASTERN
Tweed
SOUTHERN REGION
Toronto
London
SOUTHWESTERN
U.S.A.
Quebec
HUDSON BAY
LAKE SUPERIOR
LAKE HURON
LAKE ONTARIO
LAKE ERIE
St. Lawrence River
Ontario
Ministry of Northern Development and Mines
Regional Boundary / Limite régional
Resident Geologist District Bounday / Limite de district du géologue résident
○ Regional Office / Bureau régional
● Mining Recorder / Conservateur des registres miniers
■ Resident Geologist / Géologue résident
▲ Regional Mineral Specialist / Expert régional en minéraux
✱ Drill Core Library / Géothèque
0 50 100 150 M
0 100 200 Km
56°
54°
52°
50°
48°
46°
42°
96°
94°
92°
90°
76°
74°

CITY *VILLE*	OFFICE(S) *BUREAU(X)*	ADDRESS *ADRESSE*	TELEPHONE *TÉLÉPHONE*	FAX *TÉLÉCOPIEUR*
Kenora	○	Box 5050, 12 Main St. S. P9N 3X9	(807) 468-3135	(807) 468-6298
	●	Box 5200, 808 Robertson St. P9N 3X9	(807) 468-3658	(807) 468-9451
	■	Box 5200, 808 Robertson St. P9N 3X9	(807) 468-8492	(807) 468-9451
	✱	860 Fourth Ave. S. P9N 2A1	(807) 468-3658	--
Red Lake	●	Box 324, Ont. Govt. Bldg. P0V 2M0	(807) 727-3272	(807) 727-3553
	■	Box 324, Ont. Govt. Bldg. P0V 2M0	(807) 727-3284	(870) 727-3553
Sioux Lookout	●	Box 3000, OPP Bldg. P0V 2T0	(807) 737-2039	(807) 737-1727
	■	Box 3000, OPP Bldg. P0V 2T0	(807) 737-2034	(807) 737-1727
Thunder Bay	● (3)	435 James St. S. P7E 6E3	(807) 475-1331	(807) 475-5312
	■	435 James St. S. P7E 6E3	(807) 475-1311	(807) 475-5312
	✱	335 Euclid Ave. P7E 6G6	(807) 475-1331	--
Wawa	●	Box 530, Mine Rd. P0S 1K0	(705) 856-4883	(705) 856-4282
Sault Ste. Marie	● ■	875 Queen St. E. P6A 2B3	(705) 949-1231	(705) 949-0014
	✱	64 Church St. P6A 5L5	(705) 949-1231	--
Timmins	○ ● ■	60 Wilson Ave. P4N 2S7	(705) 267-1401	(705) 264-8723
	✱	896 Riverside Dr. P4N 3W2	(705) 267-1401	--
Kirkland Lake	●	4 Government Rd. E. P2N 1A2	(705) 567-5242	(705) 567-5621
	■	4 Government Rd. E. P2N 1A2	(705) 567-9242	(705) 567-5621
Swastika	▲ ✱	Box 129 P0K 1T0	(705) 642-3222	(705) 642-3323
Cobalt	●	Box 230, Presley St. P0J 1C0	(705) 679-8558	(705) 679-5584
Sudbury	●	2nd floor, 159 Cedar St. P3E 6A5	(705) 670-7325	(705) 670-7223
	■	2nd floor, 159 Cedar St. P3E 6A5	(705) 670-7321	(705) 670-7223
Dorset	●	Box 190 P0A 1E0	(705) 766-2494	(705) 766-9976
Tweed	● ✱	B.S. 43, Old Troy Rd. K0K 3J0	(613) 478-2330	(613) 478-6247
Bancroft	▲ ✱	Box 3000, Highway 28 K0L 1C0	(613) 332-4875	(613) 332-1800
Toronto	■	1st floor, 10 Wellesley St. E. M4Y 1G2	(416) 965-1322	(416) 963-0257
	○	1st floor, 10 Wellesley St. E. M4Y 1G2	(416) 965-3611	(416) 963-0257
London	●	Box 5463, 659 Exeter Rd. N6A 4L6	(519) 661-2773	(519) 661-2819

Introductory Remarks

The Ontario Geoscience Research Grants Program was initiated by the Ontario Geological Survey (OGS) in 1978 to support geoscience research at Ontario universities. By encouraging mission-oriented research, the program complements the work of the Geoscience Branch, Ontario Geological Survey in carrying out its mandate:

> *to gather geoscience information on provincial geology and mineral resources, to stimulate and guide mineral exploration and development and in the planning and development of provincial land and water resources*

The program supports applied geoscience research, for up to three years, in the following areas: identifying the characteristics of mineral deposits by studying specific occurrences, or a group of occurrences, selected by common mineral content or geological characteristics; petrologic, rock geochemistry, structural geology, stratigraphic and geochronologic studies leading to an improved understanding of the factors influencing the origin and localization of mineral deposits, and better definition of the characteristics of their environments; field and laboratory studies, leading to the development of new geophysical or geochemical concepts and techniques to assist the exploration for ore bodies concealed beneath the bedrock surface, a cover of younger rocks of glacial overburden; identifying, through engineering and environmental geology, the terrain suitable for urban and industrial development, transportation routes, subsurface storage and waste disposal, or identifying geological characteristics of potentially hazardous terrain in Ontario; and developing methods of interpreting and improving the automated or manual processing of geoscience data.

To be eligible to receive funding, researchers must forward applications to the Geoscience Branch, Ontario Geological Survey by November 15. Project proposals are subject to review by a committee reporting to the Director of the Geoscience Branch. This committee advises the Minister of Northern Development and Mines concerning geoscience research priorities at Ontario universities and of the scientific merit and relevance of the proposals submitted. The committee consists of 3 representatives from the private sector geological community, 3 representatives from Ontario universities, 4 representatives from the OGS and a chairperson from industry. Members of the 1990-1991 committee were:

Dr. I.G.L. Sinclair, Chairperson; Minscan Consulting Ltd.
Dr. J.M. Morganti; Placer Dome Inc.
Mr. B.R. Krause; Inco Exploration and Technical Services
Dr. H. Helmstaedt; Queen's University
Dr. R.S. James; Laurentian University
Mr. C.L. Baker; Ontario Geological Survey
Dr. R.H. Sutcliffe; Ontario Geological Survey
Dr. J.A. Fyon; Ontario Geological Survey
Mr. R.B. Barlow; Ontario Geological Survey

Successful grant recipients are required to submit progress reports for publication in the annual Summary of Research and to participate in the Ontario Mines and Minerals Symposium held each December. Publication in other scientific journals is encouraged, and a final report summarizing the research results will be released as an OGS open file report. These reports are published periodically and are available at the Mines Library, 77 Grenville Street, Toronto, or at Ministry of Northern Development and Mines regional offices. During 1990–1991, 22 projects were funded under this program; of these, 12 were renewal projects.

University	Value of Grants	No. of Grants
Brock	$18,650.00	1
Carleton	$50,380,00	1
Guelph	$35,050.00	1
Laurentian	$39,500.00	2
McMaster	$30,981.00	1
Ottawa	$14,500.00	1
Queen's	$74,510.00	1
Toronto	$119,486.00	5
Waterloo	$14,000.00	1
Western	$99,427.50	4
Windsor	$11,000.00	1
Total	$507,484.50	22

I would like to thank Dr. I.G.L. Sinclair, Committee Chairperson, and the review committee members, all of whom gave freely of their time. The efforts of the researchers are of course fundamental and are acknowledged. The following are also acknowledged for their participation in producing this volume; T.C. Chin, Grants Administrator and Secretary to the Committee; staff geologists who reviewed the papers; and SOTA Production, who edited and co-ordinated the production of this publication.

V.G. Milne
Director, Geoscience Branch
Ontario Geological Survey

Geoscience Research Grant Program
Summary of Research 1990-1991

---

edited by V.G. Milne
Director, Ontario Geological Survey

Grant 351 Stratigraphy and Sedimentology of the Upper Ordovician Georgian Bay Formation, Manitoulin Island and Bruce Peninsula—Evaluation of Hardgrounds, Biostromes and Storm Beds for Regional Correlation

M. Byerley[1] and M. Coniglio[2]

[1]Phillips Petroleum Resources Ltd., 2800-144 Fourth Ave. SE, Calgary, Alberta.
[2]Department of Earth Sciences, University of Waterloo, Waterloo, Ontario.

The Georgian Bay Formation of Manitoulin Island and the Bruce Peninsula contains hardgrounds, biostromes and storm beds. Although widespread geographically, their utility as regional correlation tools is minimal, a reflection of the local complexity of the depositional facies mosaic. The storm-controlled distribution of potential "marker beds" precludes lithostratigraphic "bed-to-bed" correlation of the Georgian Bay Formation between Manitoulin Island, the Bruce Peninsula and the rest of southern Ontario. Presently, traditional lithostratigraphy, based on the upward increase in carbonate relative to siliciclastic sediment, offers the best approach to correlation within the Georgian Bay Formation.

INTRODUCTION

The Georgian Bay Formation is a mixed carbonate-siliciclastic, shallowing-upward shelf succession; it outcrops in the study area in a broad belt that extends from the western end of Manitoulin Island to the southern limit of the Bruce Peninsula (Figure 351.1). The distribution of the Georgian Bay Formation in outcrop and subsurface has been clearly delineated through mapping and drilling carried out on Manitoulin Island and the Bruce Peninsula by the Ontario Geological Survey (OGS) (Johnson and Telford 1981a, b, 1985; Armstrong 1987, 1988, 1989) and the Geological Survey of Canada (GSC) (Liberty and Bolton 1971). Previous studies, however, have not attempted lithostratigraphic correlation of Georgian Bay Formation outcrops between Manitoulin Island and the Bruce Peninsula.

Strata of the Georgian Bay Formation are of interest because of their importance in understanding the role of storm events in shelf sedimentation. By integrating outcrop, core and petrographic data, this report examines regional and local facies relationships and correlation. In order to further refine lithostratigraphic correlation below the member and submember level, storm beds, biostromes and hardgrounds were evaluated as possible marker horizons. Further information concerning the sedimentology and stratigraphy of the Georgian Bay Formation is provided in Byerley and Coniglio (1989).

Field work was carried out in the summer of 1988 with other short visits made in 1987 and 1989. Attempts at refining correlation have been largely based upon outcrop data. Five cores, stored at the Sudbury Regional Geologist's office, were also logged in detail in an attempt to correlate individual beds or bedding sequences. Bedding thickness and composition of all the cores were plotted and compared using a spreadsheet program. Comparison between measured sections and core was made based on facies (outcrop, slab) and microfacies (stained peel and thin section) analysis.

STRATIGRAPHIC UNITS

The Georgian Bay Formation is the youngest Ordovician formation in areas where it is not overlain by shales of the Queenston Formation (*see* Figure 351.2). It conformably overlies organic-rich shales of the Blue Mountain Formation. The base of the Georgian Bay Formation is defined at the first 10 cm or more thick calcisiltite limestone (hardband, *sensu* Liberty 1969) interbedded with shale. On Manitoulin Island dolostones of the Lower Silurian Manitoulin Formation rest unconformably on the Georgian Bay Formation. On the Bruce Peninsula the Upper Ordovician Queenston Formation lies between the Manitoulin and Georgian Bay formations.

The Georgian Bay Formation is divided into Upper and Lower members (*see* Figure 351.2). The Upper Member is further subdivided into Upper and Lower submembers (Liberty and Bolton 1971), informally referred to as the Lookout and Sextant Falls submembers, respectively, by Byerley and Coniglio (1989). The bottom of the Sextant Falls submember occurs at the base of the first 20 cm or thicker argillaceous limestone or dolostone bed (Photo 351.1a, 1b). The base of the first 1 m thick, pervasively dolomitized interval defines the contact between the Lookout Submember and the underlying Sextant Falls Submember.

Stratigraphic data gathered from approximately 50 outcrop sections measured for this study is not of sufficient

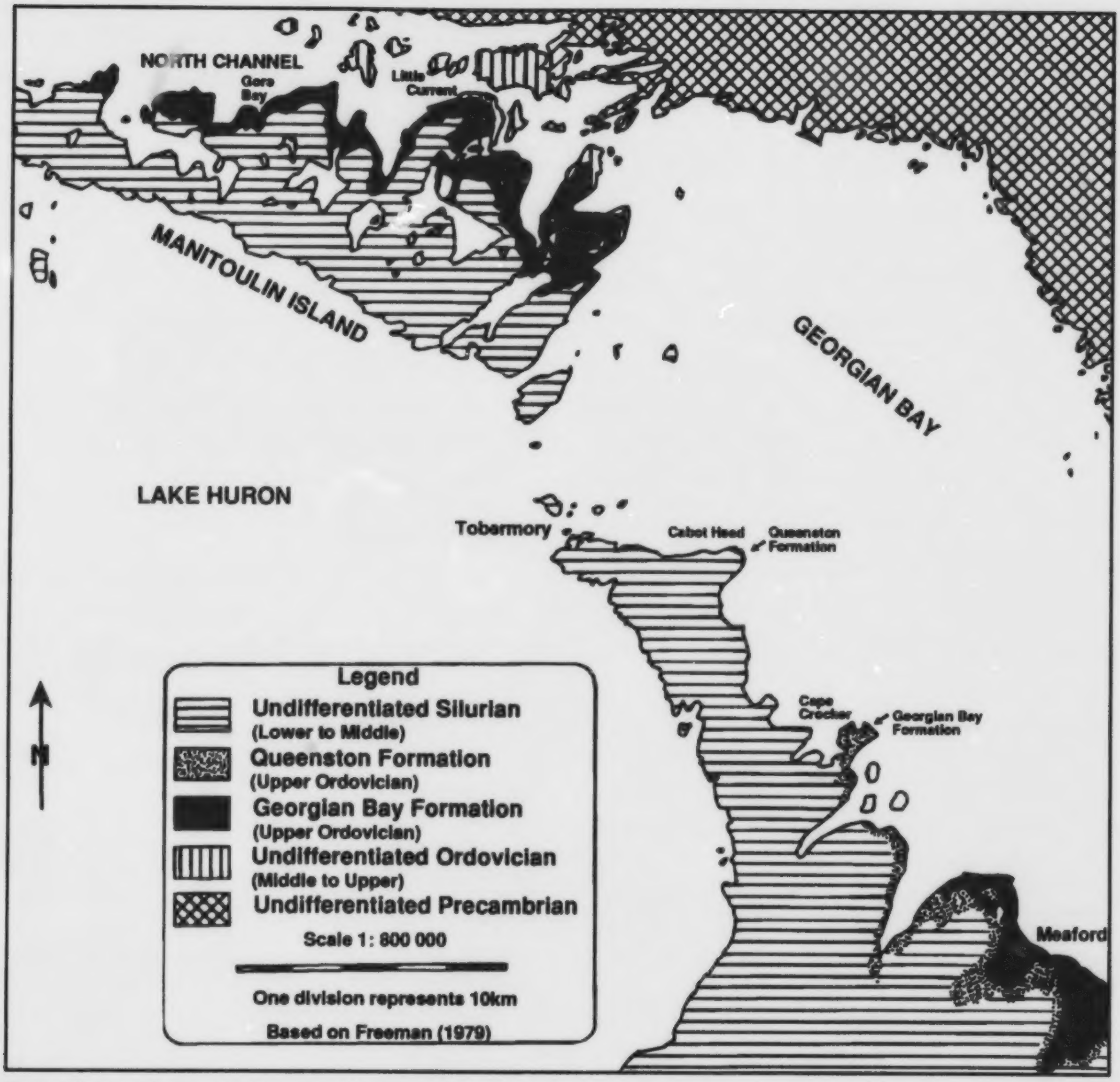
NORTH CHANNEL
Gore Bay
Little Current
MANITOULIN ISLAND
GEORGIAN BAY
LAKE HURON
Tobermory
Cabot Head
Queenston Formation
Cape Crocker
Georgian Bay Formation
Meaford
N
Legend
Undifferentiated Silurian (Lower to Middle)
Queenston Formation (Upper Ordovician)
Georgian Bay Formation (Upper Ordovician)
Undifferentiated Ordovician (Middle to Upper)
Undifferentiated Precambrian
Scale 1: 800 000
One division represents 10km
Based on Freeman (1979)

Figure 351.1. Location map showing geographic extent of the Georgian Bay Formation.

resolution to enable correlation beyond the submember level. Due to the weathered nature of the outcrop, the contacts between members and individual facies are commonly obscured, especially in argillaceous intervals. Cores provide the only continuous section through the entire formation. Existing lithologic logs (Johnson and Telford 1981a, 1981b, 1985) were not recorded at a scale suitable for detailed stratigraphic study. However, detailed logging of 5 cores (this study) also did not allow for correlation to be made below the submember level. Drill core does provide, however, the only means to accurately study many of the sedimentological features (such as biostromes, hardgrounds and storm beds) in these strata .

SEDIMENTS AND STRUCTURES

Five principal lithologic assemblages comprise the Georgian Bay Formation (Figure 351.3). Shales and small amounts of interbedded siltstones and calcisiltite limestones comprise the majority of the Lower Member. The Upper Member consists predominantly of interbedded limestones, argillaceous limestones and dolostones. These carbonates are thin- to medium- bedded and include bioclastic grainstones, packstones and wackestones. Brachiopods and ramose bryozoans with lesser amounts of bivalves and trilobites, are dominant allochems. Due to the influence of the Appalachian Basin-derived Queenston clastic wedge, the Upper Member is more poorly developed on the Bruce Peninsula than on Manitoulin Island (Figure 351.2). The effects of bioturbation are pervasive throughout the formation.

Sedimentary structures in the fine-grained Lower Member include well-developed scour features (gutter and flute casts), tool marks and various cross-lamination types, encompassing the spectrum from oscillation ripples to hummocky cross-stratification (*see* Figure 351.3). Coarser-grained, carbonate-rich sediments of the Upper Member characteristically contain more high energy sedimentary structures, such as scoured and sharp-based beds, normally-graded (or inversely-graded) beds, ripples, megaripples, hummocky cross-stratification, and amalgamated beds (*see* Photo 351.2). All of these features and their associated biogenic structures are interpreted to be the result of storm deposition (Byerley and Coniglio 1989).

Parautochthonous and *in situ* accumulations of bryozoans, large corals and stromatoporoids occur as biostromal floatstones predominantly in the Sextant and Lookout submembers of the Upper Member (*see* Photos 351.3, 351.4). Within the Lower Member biostromes represent reworked or transported deposits. Trace fossils of the Skolithos and Cruziana Ichno facies (Byerley and Coniglio 1989) are commonly well developed in associated sediments. Within the Sextant Submember,

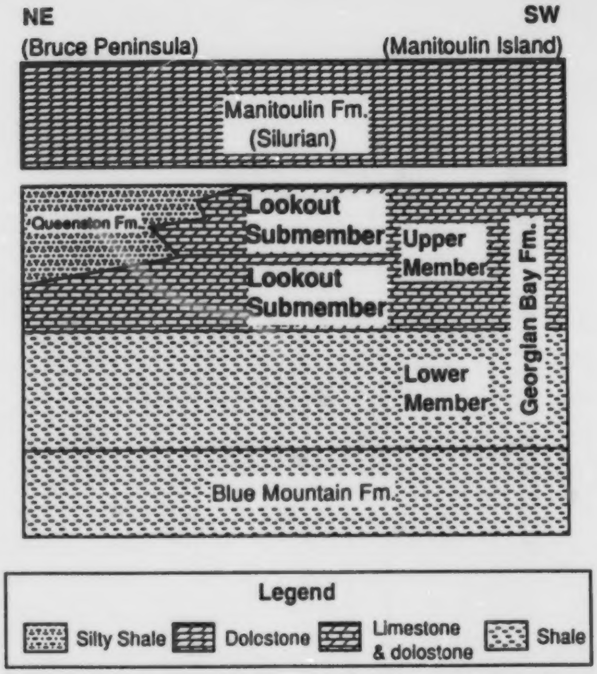
NE
(Bruce Peninsula)
SW
(Manitoulin Island)
Manitoulin Fm.
(Silurian)
Queenston Fm.
Lookout
Submember
Lookout
Submember
Upper
Member
Lower
Member
Georgian Bay Fm.
Blue Mountain Fm.
Legend
Silty Shale
Dolostone
Limestone
& dolostone
Shale

Figure 351.2. Regional stratigraphic setting of the Georgian Bay Formation.

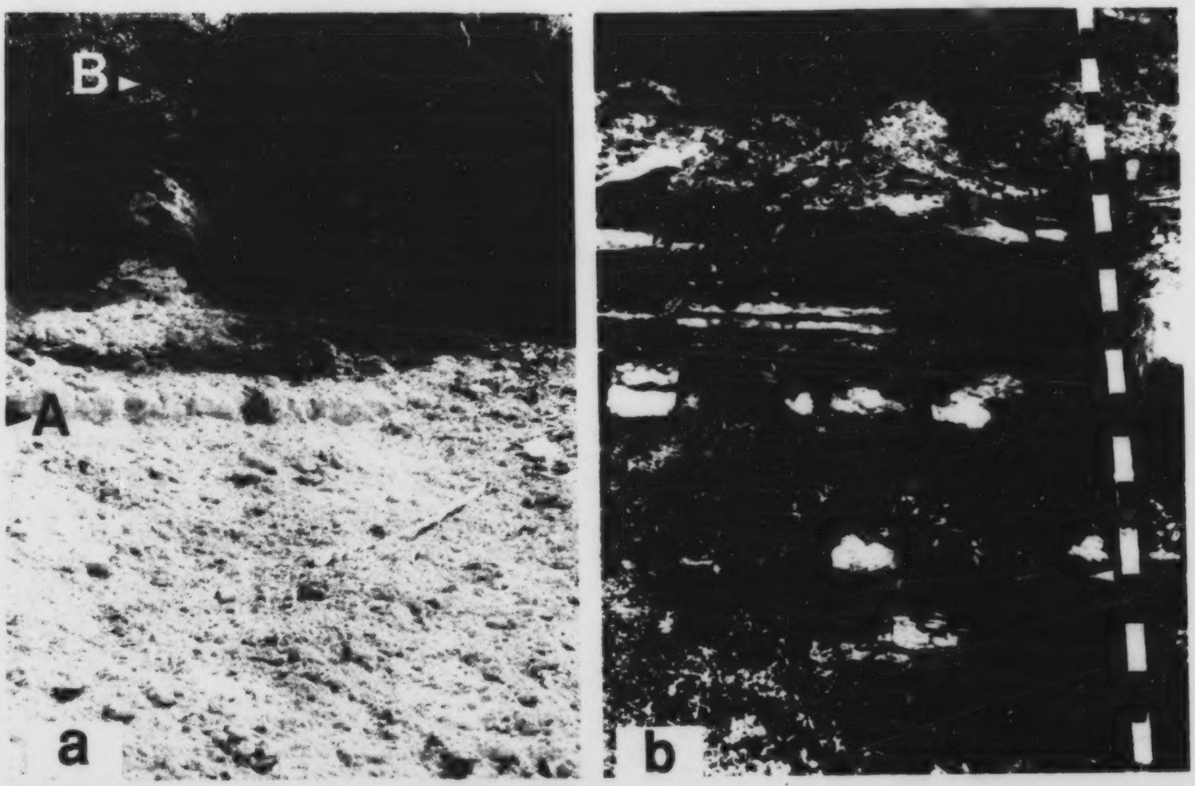

Photos 351.1a and 351.1b Outcrop photographs of the Georgian Bay Formation.
a) View showing Lower Member/Sextant Falls Submember (of the Upper Member) contact (A) and Sextant Falls Submember/Lookout Submember contact (B).
b) Silty shale of the Lower Member overlain by interbedded argillaceous limestones and shales of the Upper Member's Sextant Falls Submember. Contact at arrow. Scale divisions area 10 cm.

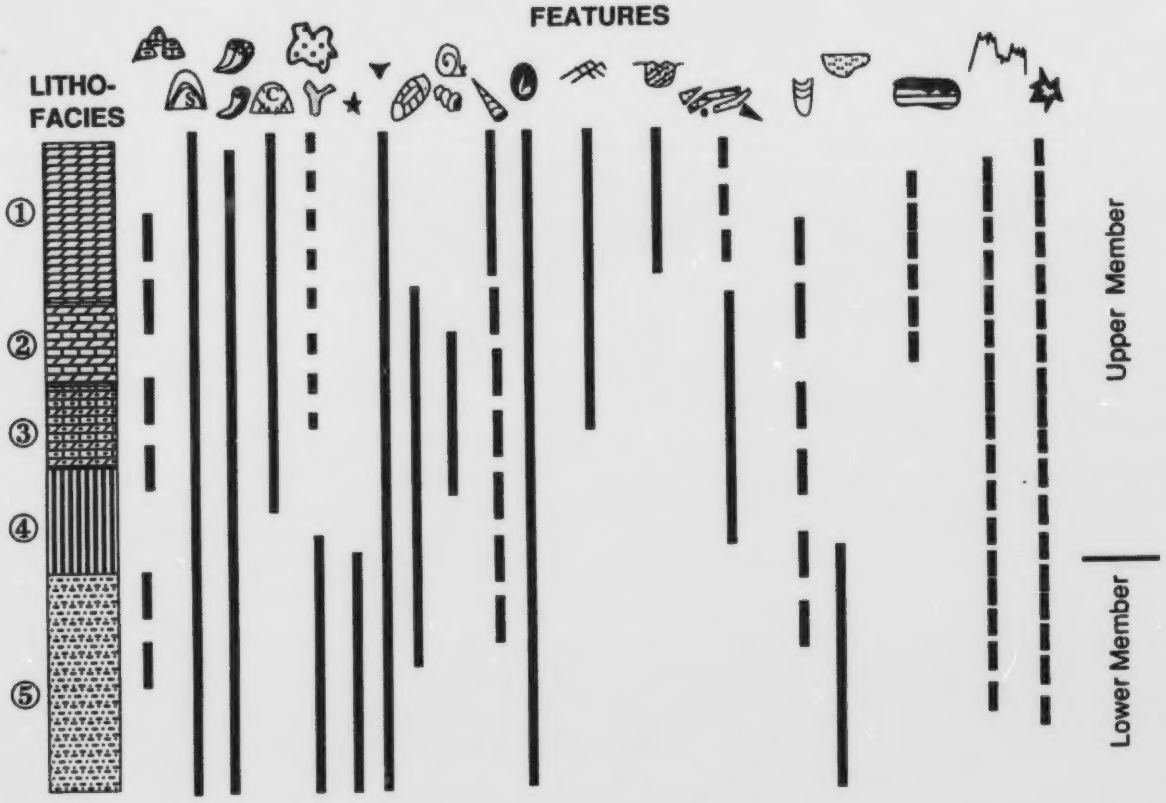

Lithofacies Notes

① **Dolostone**: pervasively dolomitized; silicified brachiopods, bryozoa, corals; thinly bedded (10-20 cm); stylolitized and/or parted bedding planes.

② **Interbedded limestone (dolostone) with shale partings**: very low siliciclastic content ≤1%; allochems are well preserved.

③ **Interbedded shale and limestone (dolostone)**: matrix has a siliciclastic/carbonate mixture similar to that given for calcisiltite (lithofacies 5); limestone/dolostone rarely argillaceous; allochem preservation is variable.

④ **Interbedded shale, argillaceous limestone (dolostone) and calcisiltite (litholfacies 5)**: shale seams/partings 0.1-50 cm thick.

⑤ **Interbedded shale and limestone/dolostone (calcisiltite)**: silt-sized carbonate particles; minor 10-15% siliciclastic silt content, finely laminated or rippled; storm layers common, trace fossils well preserved in core. Shale: 20-30% terrigenous silts; grey, black, olive brown.

Figure 351.3. Lithofacies descriptions and presence of fossils, sedimentary structures and diagenetic features in the Georgian Bay Formation. Symbol legend is provided in Figure 351.4.

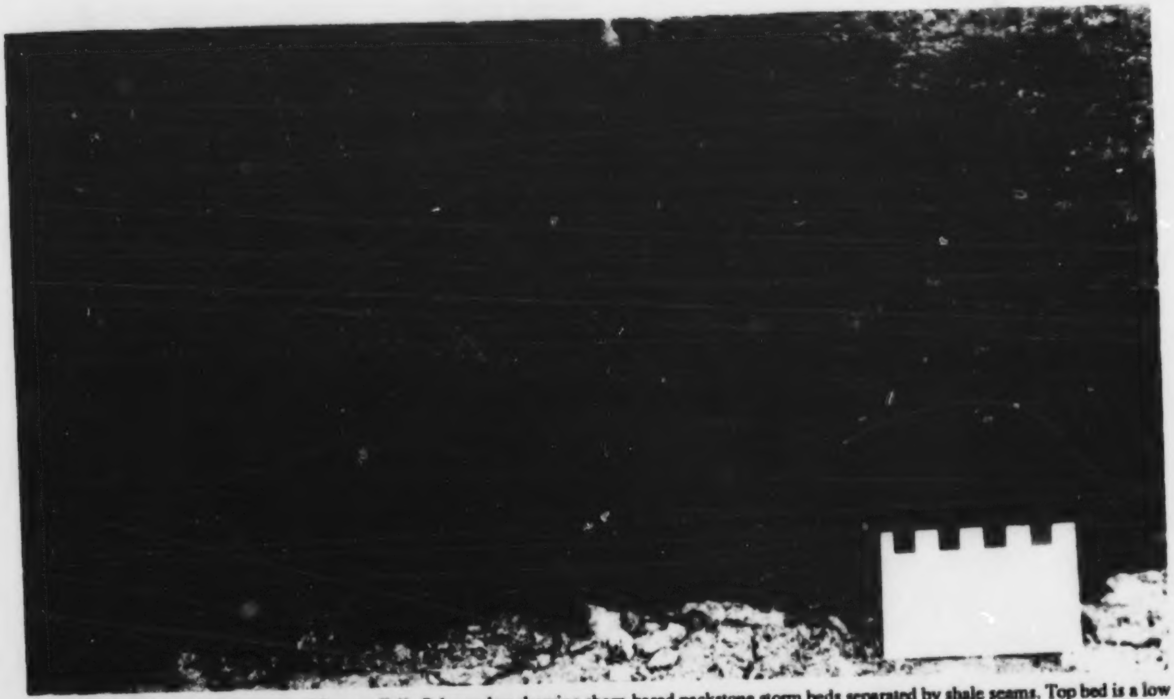

Photo 351.2. Outcrop photograph of Sextant Falls Submember showing sharp-based packstone storm beds separated by shale seams. Top bed is a low angle cross-stratified limestone, containing scattered shale intraclasts. Bed immediately above scale card has erosionally truncated upper surface crosscut by light grey vertical escape burrows. Divisions on scale card are 1 cm.

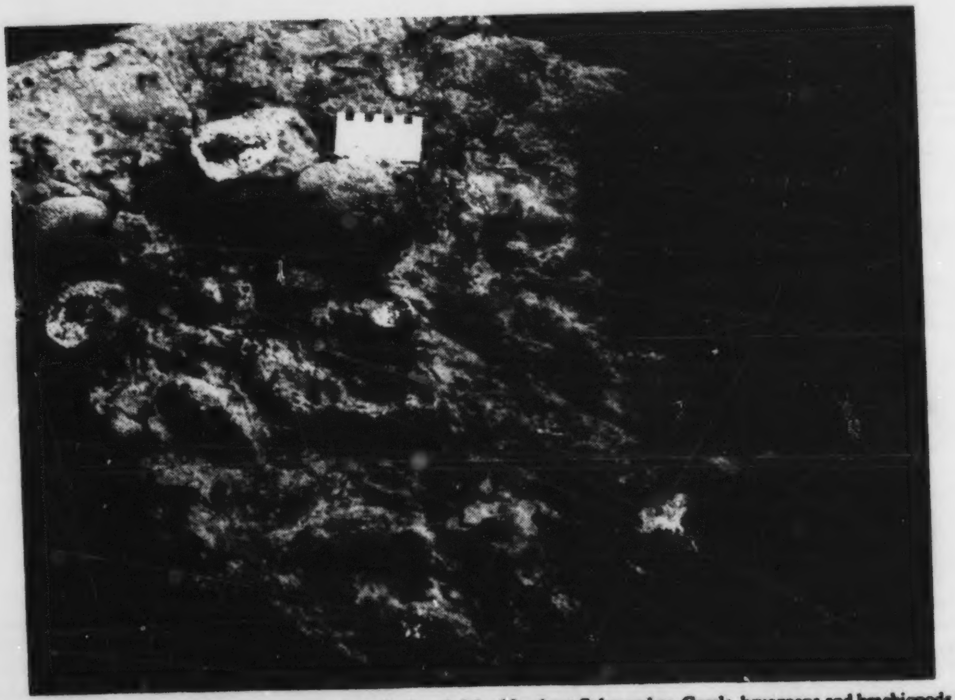

Photo 351.3. Outcrop photograph of biostrome preserved on displaced slab of Lookout Submember. Corals, bryozoans and brachiopods form a parautochthonous assemblage. The floatstone rests over a thinly bedded (10 to 15 cm) bioclastic packstone. Trace fossils (*Chondrites*, *Rusophycus*, *Planolites* and *Palaeophycus*) are well developed within the floatstone matrix. Divisions on scale card are 1 cm.

hardgrounds commonly occur in close stratigraphic proximity to storm layers (*see* Photo 351.5 and Figures 351.4 and 351.5)

HARDGROUNDS

The distribution of hardgrounds allows for local correlation of "packages" of hardgrounds over distances of approximately 30 km along the eastern side of Manitoulin Island. These individual hardgrounds do not have enough spatial distribution to extend detailed bed-by-bed correlations beyond this local scale.

Hardgrounds occur within grainstones and wackestones to packstones. Two styles of hardground development are recognized: 1) digitate high-relief surfaces, commonly contained within composite beds and 2) planar corrasion surfaces (*sensu* Wilson 1975). In most cases allochems and sedimentary fabrics are clearly preserved. In hardgrounds with truncated corrasion surfaces, however, later dolomitization has typically obliterated much of the original fabric.

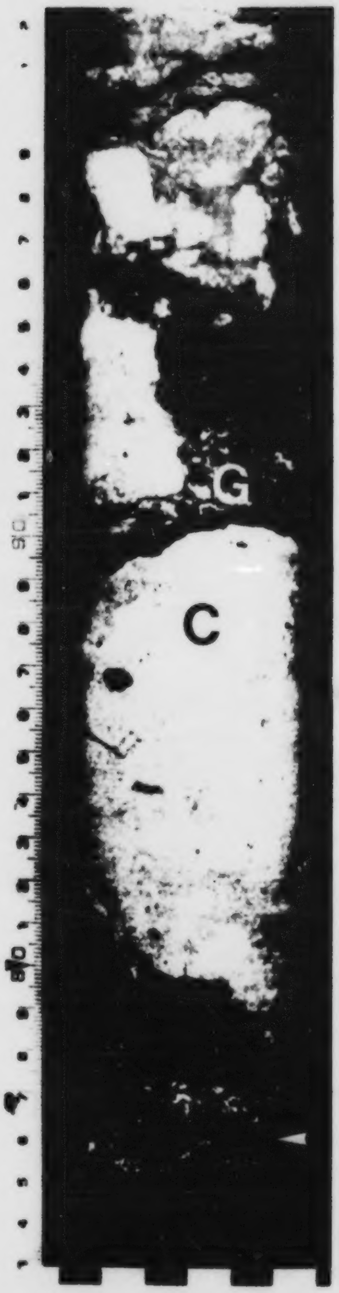

Photo 351.4. Core photograph of stromatoporoid-tabulate coral biostrome from Lookout Submember. Base of biostrome is in shale (at 79 cm on scale), overlying a coarse bioclastic packstone bed. Biostrome top (96 cm) has approximately 10 cm relief, filled by bioclastic packstone grading up to silty shale. A graded storm layer with a sharp and scoured base extends from 96 cm to top of photo. C-coral head; G-normal grading. OGS core M80-10: 101 feet 6 inches (at white arrow). Divisions on tape measure are 1 cm.

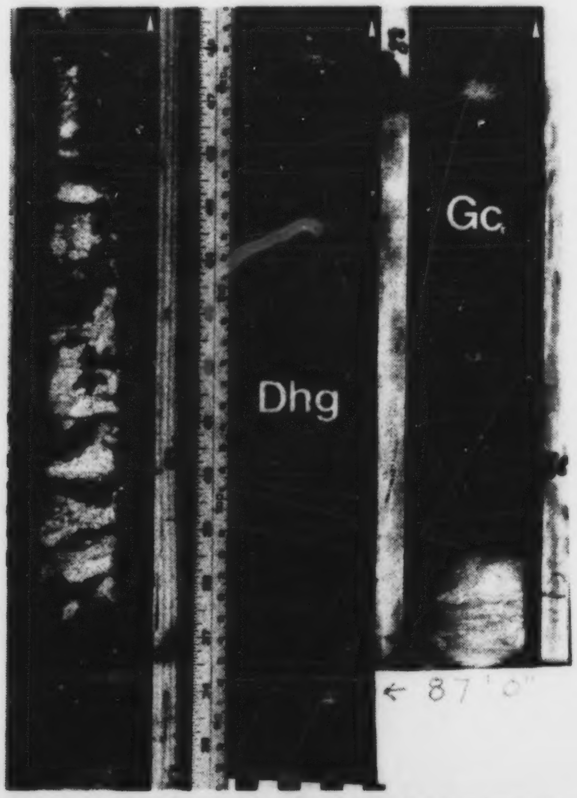

Photo 351.5. Core photograph of Lookout Submember displaying storm layers and hardgrounds. Graded siltstone to calcisiltstone storm beds (Gc) show weakly developed bioturbation. Digitate hardgrounds (Dhg) are developed on moderately bioturbated grainstone beds. Divisions on tape measure are 1 cm and 1 inch. White arrows show up orientation. OGS core M79-14.

Digitate surfaces show up to 5 cm relief, steep sides and overhangs that created numerous shelter cavities (*see* Photo 351.6). These cavities were subsequently filled with post-omission sediment, recording multiple cementation/sedimentation episodes that generated composite beds. The cause of the digitate surface is uncertain. The crest of each digit is commonly covered by a dark rind of pyrite mineralization (*see* Photo 351.7). The rind typically occurs only along the top of hardground "pinnacles". Its origin is unknown, but it may represent bacterial sulphate reduction near the sediment surface during a period of stagnant bottom water. Regardless of origin it appears that the rind was a thin surficial crust that was subsequently penetrated by burrowing organisms in order to reach softer sediment below

Corrasion surfaces have not been widely mapped. They are recognized by truncated allochems, borings (*Trypanites*), striations (tool marks?) and a suite of pre-lithification firmground traces. Planar corrasion surfaces, which are easily recognized only on bedding surfaces, probably resulted from either the erosional truncation of digitate hardground surfaces or exhumation of semi-consolidated concretionary layers, probably lithified a few to tens of centimetres below the sediment-water interface.

Most beds with hardgrounds contain evidence of multiple sedimentation/bioturbation events. Omission and post-omission trace fossils indicate that corrasion hardgrounds passed through 3 stages: 1) normal burrowing in a shifting substrate (*Skolithos* and other vertical to inclined traces); 2) "plastic" firmground marked by striations, tool marks and the trapping of some omission sediments in open burrows and 3) borings (*Trypanites*) which crosscut traces and structures formed at earlier stages (*see* Figure 351.6).

Digitate hardgrounds have a more complex history (Photo 351.8 and Figure 351.7). The elaborate pinnacled topography, undercuttings and overhangs of the digitate surface indicate early lithification. The overlying sediments consist of multiple generations of wackestone or packstone, suggesting repeated episodes of sedimentation and burrowing occurred within troughs between lithified pinnacles.

The digitate surface appears to be the result of modification by fauna. No clasts of broken hardground surface are encountered nor is there any evidence that erosion by currents produced the complex relief of the digitate hardground. Rather, the intense bioturbation seen in composite beds suggests that the digitate topography resulted from bioturbation between storm events. Borings have not been observed on the digitate surface, although microbored shells and bored corals are commonly encountered lying along the hardground surface. This suggests that the sediment surface was not attractive to boring organisms.

The composite nature of beds in which digitate hardground commonly occur can be explained as the result of storms. During low intensity sedimentation (from distant

Photo 351.6. Core photograph showing digitate high-relief hardground developed in limestone in Sextant Falls Submember. OGS core M83-5. Divisions on scale card are 1 cm.

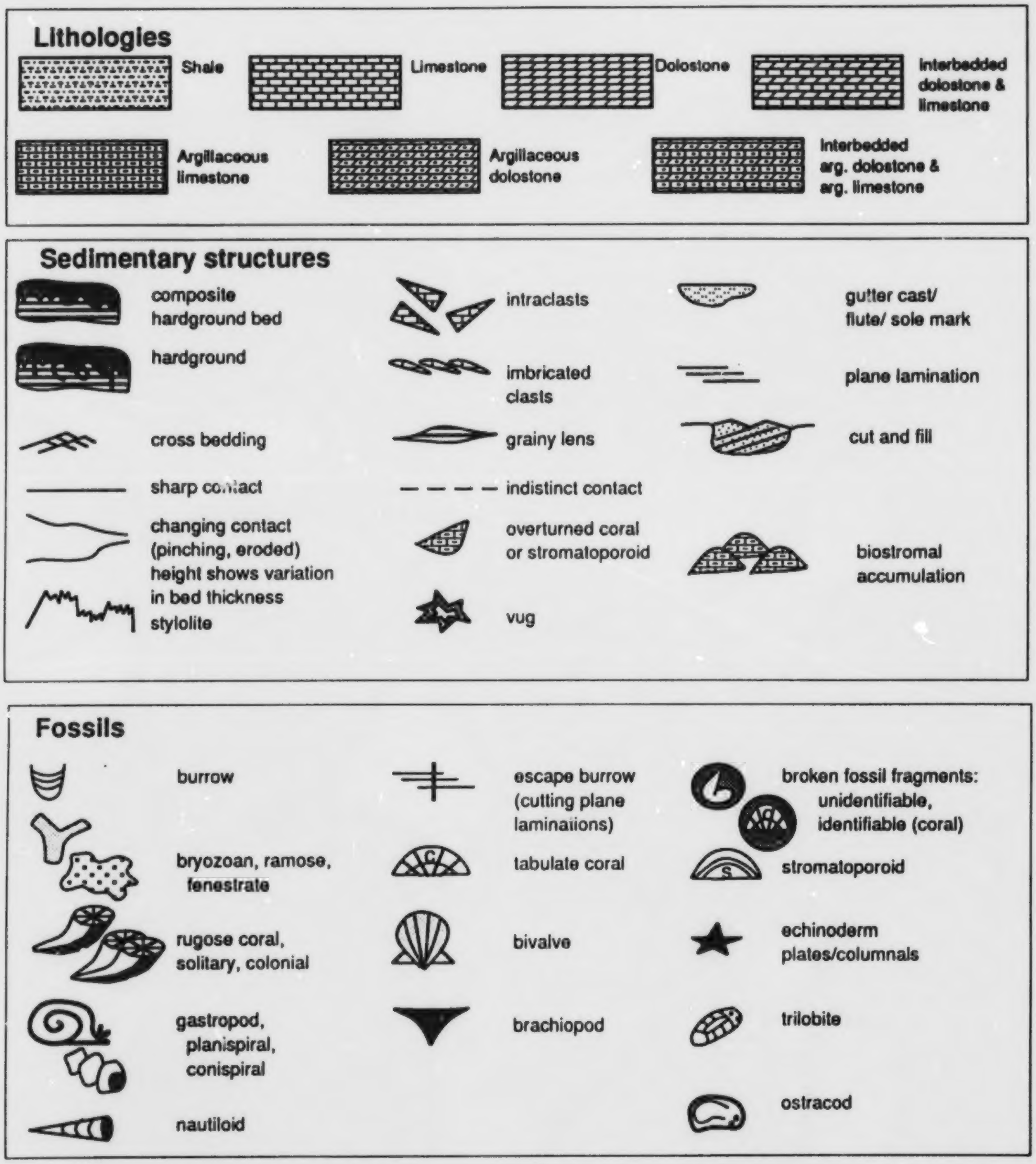
Lithologies
Shale
Limestone
Dolostone
Interbedded dolostone & limestone
Argillaceous limestone
Argillaceous dolostone
Interbedded arg. dolostone & arg. limestone
Sedimentary structures
composite hardground bed
hardground
cross bedding
sharp contact
changing contact (pinching, eroded) height shows variation in bed thickness
stylolite
intraclasts
imbricated clasts
grainy lens
indistinct contact
overturned coral or stromatoporoid
vug
gutter cast/ flute/ sole mark
plane lamination
cut and fill
biostromal accumulation
Fossils
burrow
bryozoan, ramose, fenestrate
rugose coral, solitary, colonial
gastropod, planispiral, conispiral
nautiloid
escape burrow (cutting plane laminations)
tabulate coral
C
bivalve
brachiopod
broken fossil fragments: unidentifiable, identifiable (coral)
stromatoporoid
S
echinoderm plates/columnals
trilobite
ostracod

Pk packstone
Fs floatstone
Wk wackestone
Sh shale
Gs grainstone

→ An arrow beside a symbol indicates that this feature occurs only at this specific point in the unit. Unmarked symbols indicate that a feature occurs throughout the unit.

Figure 351.4. Symbol legend for lithologies, sedimentary structures and fossils of the Georgian Bay Formation.

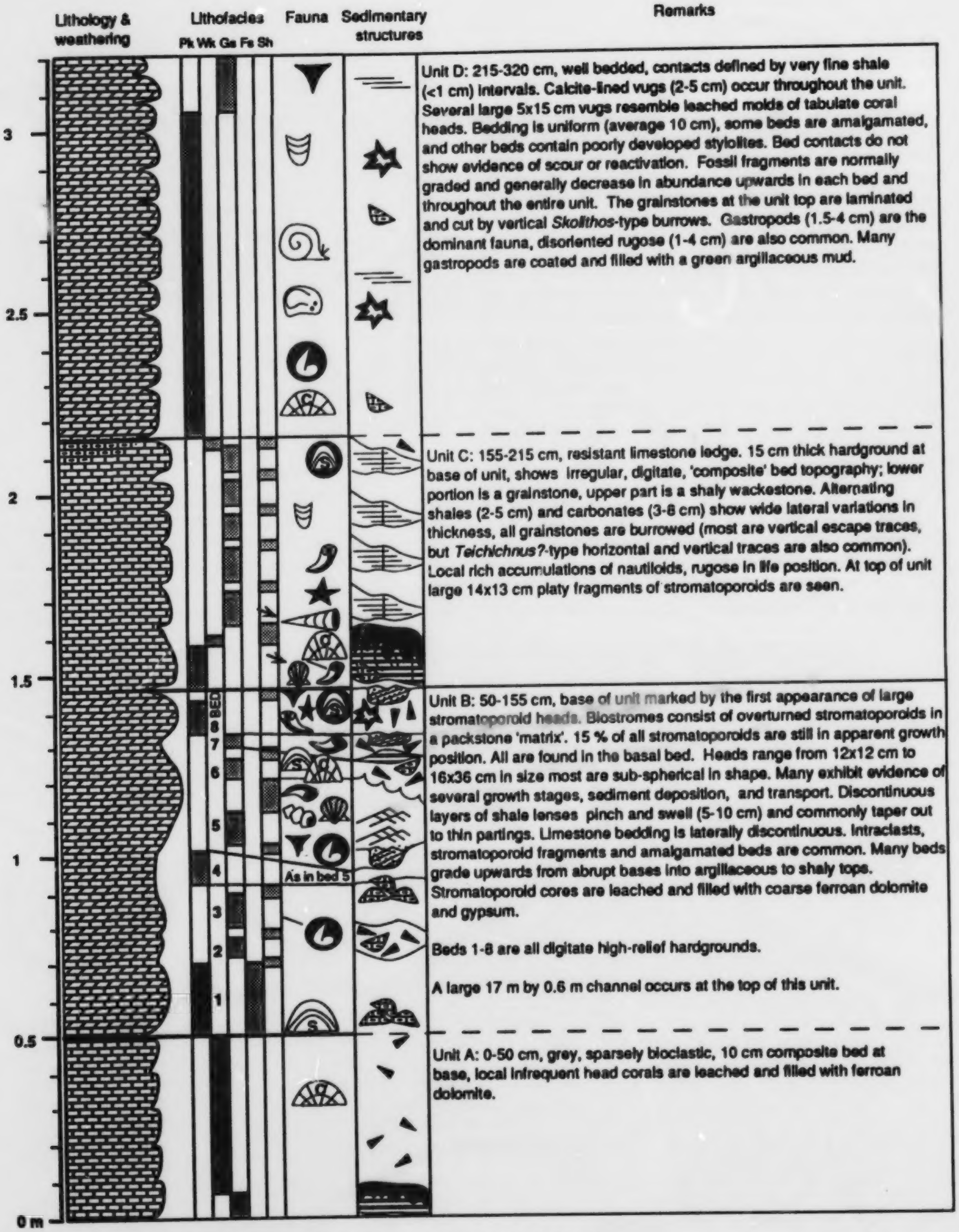

Unit D: 215-320 cm, well bedded, contacts defined by very fine shale (<1 cm) intervals. Calcite-lined vugs (2-5 cm) occur throughout the unit. Several large 5x15 cm vugs resemble leached molds of tabulate coral heads. Bedding is uniform (average 10 cm), some beds are amalgamated, and other beds contain poorly developed stylolites. Bed contacts do not show evidence of scour or reactivation. Fossil fragments are normally graded and generally decrease in abundance upwards in each bed and throughout the entire unit. The grainstones at the unit top are laminated and cut by vertical *Skolithos*-type burrows. Gastropods (1.5-4 cm) are the dominant fauna, disoriented rugose (1-4 cm) are also common. Many gastropods are coated and filled with a green argillaceous mud.

Unit C: 155-215 cm, resistant limestone ledge. 15 cm thick hardground at base of unit, shows irregular, digitate, 'composite' bed topography; lower portion is a grainstone, upper part is a shaly wackestone. Alternating shales (2-5 cm) and carbonates (3-8 cm) show wide lateral variations in thickness, all grainstones are burrowed (most are vertical escape traces, but *Teichichnus?*-type horizontal and vertical traces are also common). Local rich accumulations of nautiloids, rugose in life position. At top of unit large 14x13 cm platy fragments of stromatoporoids are seen.

Unit B: 50-155 cm, base of unit marked by the first appearance of large stromatoporoid heads. Biostromes consist of overturned stromatoporoids in a packstone 'matrix'. 15 % of all stromatoporoids are still in apparent growth position. All are found in the basal bed. Heads range from 12x12 cm to 16x36 cm in size most are sub-spherical in shape. Many exhibit evidence of several growth stages, sediment deposition, and transport. Discontinuous layers of shale lenses pinch and swell (5-10 cm) and commonly taper out to thin partings. Limestone bedding is laterally discontinuous. Intraclasts, stromatoporoid fragments and amalgamated beds are common. Many beds grade upwards from abrupt bases into argillaceous to shaly tops. Stromatoporoid cores are leached and filled with coarse ferroan dolomite and gypsum.

Beds 1-8 are all digitate high-relief hardgrounds.

A large 17 m by 0.6 m channel occurs at the top of this unit.

Unit A: 0-50 cm, grey, sparsely bioclastic, 10 cm composite bed at base, local infrequent head corals are leached and filled with ferroan dolomite.

Figure 351.5. Graphic log of High Falls section (Sextant Falls Submember), Manitoulin Island.

storms, weak storms and "normal" background sedimentation) interpinnacle sediments were deposited, bioturbated and eventually lithified. Further hardground modification was arrested by blankets of storm-deposited, fine-grained siliciclastic sediment, now preserved as 2 to 5 cm shale seams or interbeds, which killed or displaced most of the bioturbating fauna and cut off water circulation to the areas of cementation.

STRATIGRAPHIC IMPLICATIONS OF STORM SEDIMENTATION

The primary stratigraphic subdivision of the Georgian Bay Formation is based upon the progressive shift from terrigenous clastic to carbonate-dominated sedimentation thus defining the Upper and Lower members. Mixing of terrigenous and carbonate sediments occurred through short-lived episodes of storm-induced erosion and sedimentation. The time interval between storm events determined: 1) the proportions of siliciclastic and fine-grained carbonate sediment introduced to any single area; 2) the intensity of bioturbation and 3) the degree of primary sedimentary structure preservation.

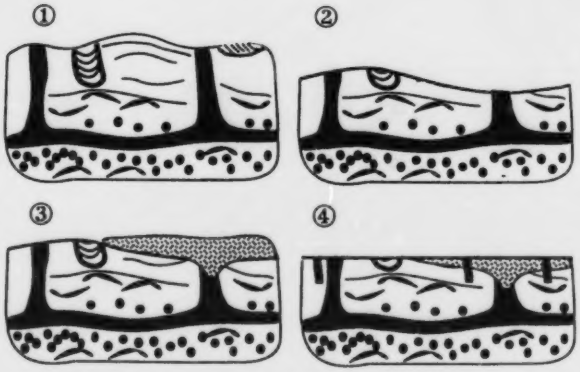

Figure 351.6. Trace fossil tiering and development of planar corrasion hardgrounds in Georgian Bay Formation: 1) unconsolidated sediment: burrowing by fauna; 2) unconsolidated to plastic sediment: erosional truncation of top portion of bed, formation of striae and tool marks; 3) plastic to hard: second sediment is loose and fills in surface depressions and open traces; 4) cementation of all sediments: borings cross-cut second and initial sediments and trace fossils. Variations on this model are possible and there may be multiple episodes of burrowing, erosion and boring.

Based upon core and outcrop evidence a depositional model for the Upper Member of the Georgian Bay Formation is proposed (Figure 351.8). Deposition occurred over a low sloping inner shelf dotted with shoals. Overall shallowing in the succession (eventually reaching subaerial exposure in the area of the Bruce Peninsula) resulted in the generation of a large expanse of very shallow water formed along the shoreward margin. The combination of low shelf gradient and shallow water depth dampened the effects of storm processes farther offshore. Reduced wave action in the nearshore prevented wide-scale mixing of nearshore carbonate and ter-

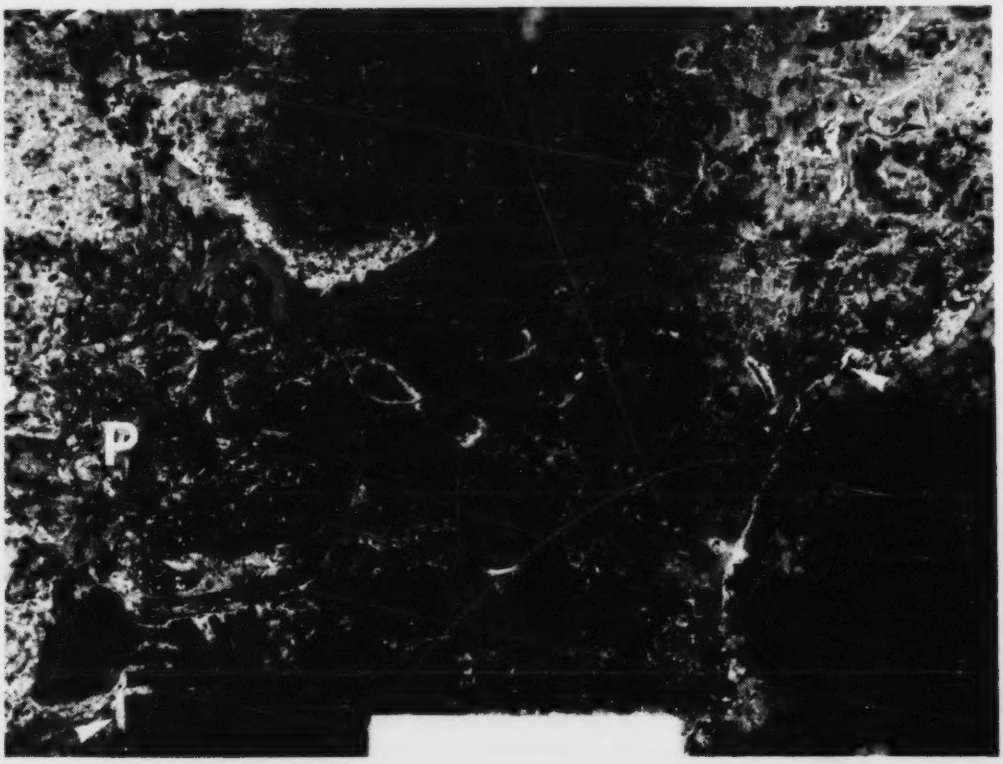

Photo 351.7 Negative thin section print showing pyrite rind (arrow) developed on tabulate and rugose corals. Coarse packstone (P) is post-omission sediment. Scale bar is 1 cm.

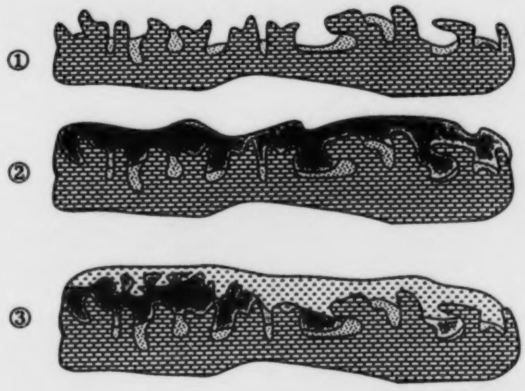

Figure 351.7. Development of composite high-relief digitate hardgrounds in Georgian Bay Formation: 1) creation of original pinnacled surface: lithification proceeded from base towards top, omission sediments trapped in cavities; 2) storm deposited layer blankets entire hardground, followed by development of new pinnacled surface; 3) storm deposited layer blankets entire hardground and erodes part of earlier storm layer.

restrial clastic sediments on the shallow shelf. When strong storms swept the entire shelf, returning flows containing abundant fine siliciclastic sediments and associated continental runoff, bypassed the inner shelf via a cross-shelf network of "storm-surge-maintained" channels, analogous to that of tidal flat channels, where they mixed with more offshore sediments. As a consequence, siliciclastic sedimentation in the nearshore region of the shelf was low. Sedimentation in the Upper Member was dominantly the product of *in situ* carbonate generation.

Relict, storm-generated bathymetric highs became preferred areas for hardground development possibly due to better water circulation and opportunity for winnowing and storm scour. Furthermore, the highs could stand above thin, storm-generated blankets of siliciclastic fines and thus were more favoured sites for subsequent colonization. Normal bioturbation would incorporate the siliciclastics with the "normal" shelf carbonate sediments, removing most of the siliciclastic sedimentary record of the storm. Thicker storm beds or frequent storms would limit bioturbation and bury developing hardgrounds. Once carbonate sedimentation was re-established, carbonate lithification over areas of the seafloor exhibiting local relief would continue. A modern example of topographically-influenced hardground formation can be found in the Arabian Gulf (Shinn 1969).

CONCLUSIONS

Storms assisted seafloor cementation by generating erosional and depositional relief on the sea bottom. Higher areas were periodically swept clean and kept in contact with circulating sea water. Other high areas generated by storms were sites of

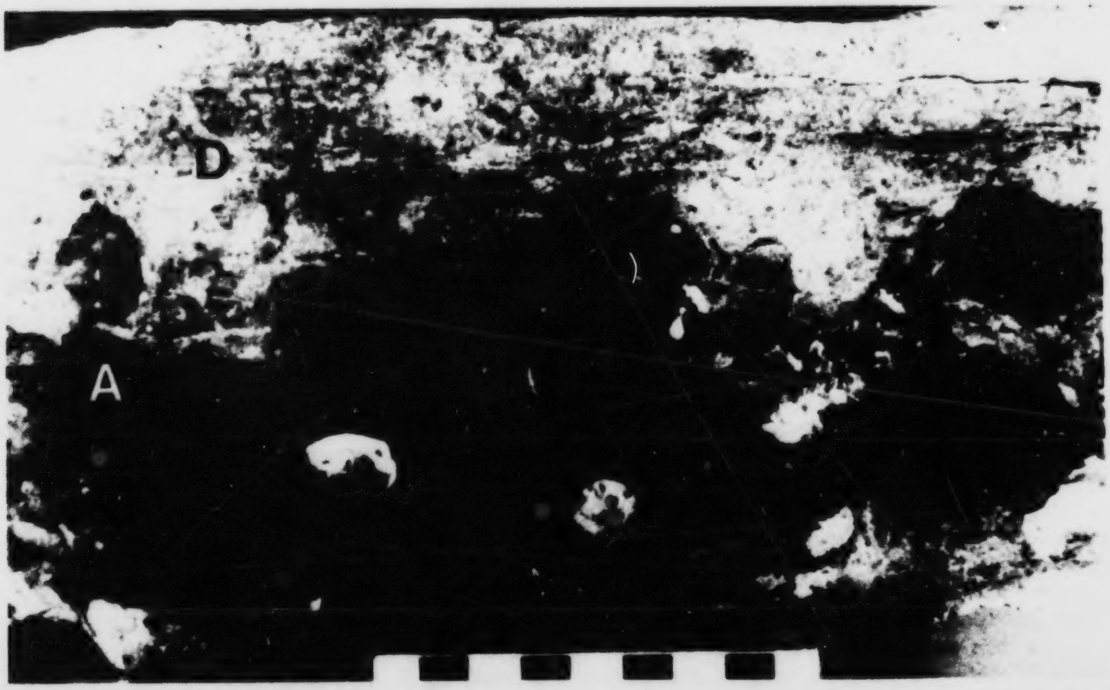

Photo 351.8. Slab photograph of composite high-relief digitate hardground (A) developed in Sextant Falls Submember at High Falls (bed 4 in Figure 351.5). B, C and D are post-omission deposits. Divisions on scale card are 1 cm.

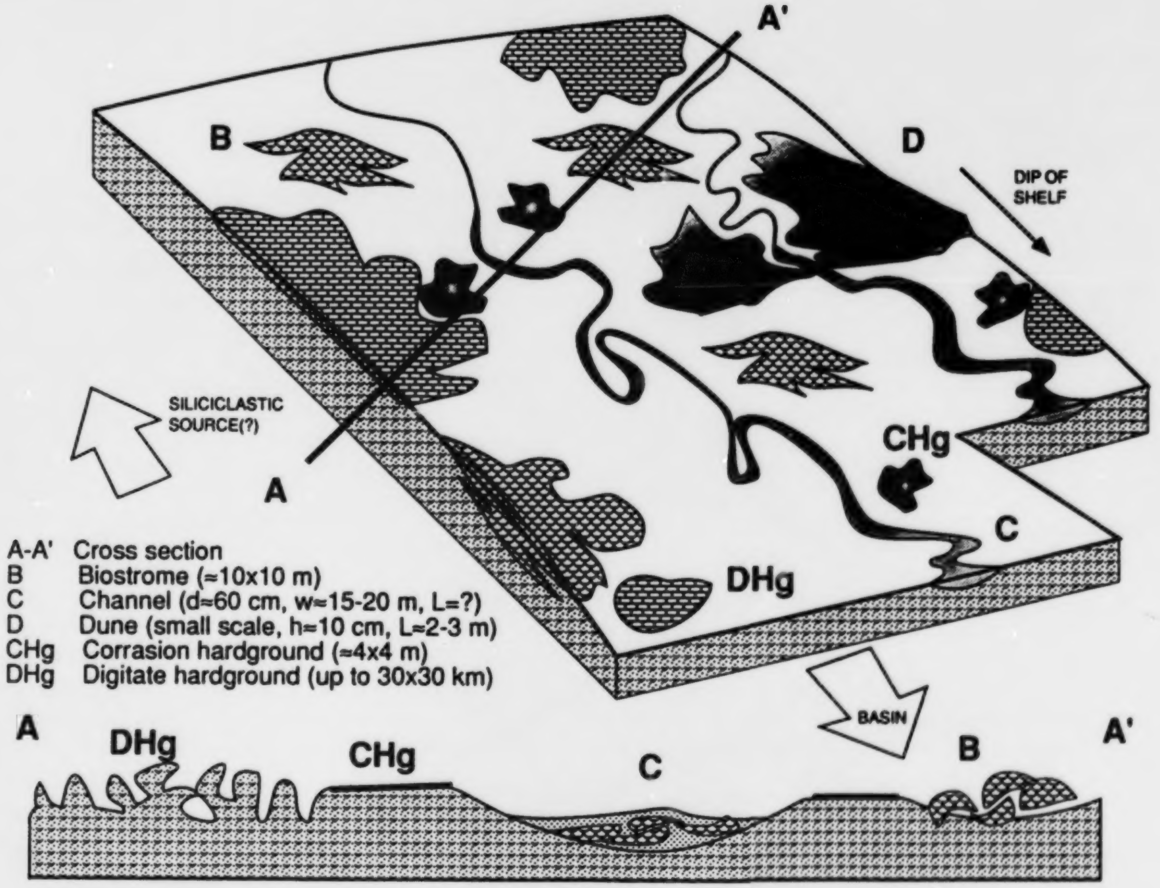
A'
B
D
DIP OF SHELF
SILICICLASTIC SOURCE(?)
A
CHg
C
DHg
A-A' Cross section
B Biostrome (≈10x10 m)
C Channel (d≈60 cm, w≈15-20 m, L=?)
D Dune (small scale, h≈10 cm, L≈2-3 m)
CHg Corrasion hardground (≈4x4 m)
DHg Digitate hardground (up to 30x30 km)
BASIN
A
DHg
CHg
C
B
A'

Figure 351.8. Depositional model for the Upper Georgian Bay Formation (not to any scale, *see* text for discussion).

in situ biostrome development with coarse bioclastic debris accumulating in the lows. The recurrence interval between storm events was the controlling factor on the development of submarine-cemented layers, intensity of bioturbation and the generation of biostromes.

The presence of numerous biostromes in the Georgian Bay Formation clearly indicate that hardground and firmground colonizing organisms were abundant. Hardground surfaces, however, contain little evidence of colonization but otherwise resemble hardgrounds known from the Trenton Group of Ontario (Brett and Brookfield 1984). This lack of colonization is attributed to be, in part, the result of intense storm influence. Sedimentation from frequent storms did not leave lithified surfaces exposed long enough for colonization by boring organisms to occur.

The complex mosaic of high and low relief areas on the seafloor and their distinct sediments precludes the use of hardgrounds, coarse-grained storm beds, or biostromes as marker beds over any large distance. The storm-controlled distribution of potential marker beds makes previous biostratigraphic bed-to-bed correlations (Horst 1978) within the Georgian Bay Formation between Manitoulin Island and areas including Toronto and the Bruce Peninsula questionable. Presently, traditional lithostratigraphy offers the best approach to correlation within the Georgian Bay Formation.

Research carried out thus far has focused upon outcrop data. In the future emphasis should be placed upon improving outcrop-based correlations through systematic usage of all available core. Most core is in outdoor storage at Sudbury and its quality is deteriorating rapidly. It is urgent that this material be examined in the near future if this information is to be retained.

ACKNOWLEDGMENTS

The authors thank D. Long (Laurentian University), W. Meyer and R. Henry (Sudbury District Office, MNR), M. Johnson and D. Armstrong (OGS) for their assistance with the core study portion of this project. P. Fisher (University of Waterloo) provided photographic support. Research was supported through Ontario Geoscience Research (OGR) Grant 351 and Natural Sciences and Engineering Council Operating Grant 1889 to M. Coniglio.

REFERENCES

Armstrong, D. K. 1987. Paleozoic geology of the Northern Bruce Peninsula; *in* Summary of Field Work and Other Activities 1987, Ontario Geological Survey, Miscellaneous Paper 137, p.392-395.

——1988. Paleozoic geology of the central Bruce Peninsula; *in* Summary of Field Work and Other Activities 1988, Ontario Geological Survey, Miscellaneous Paper 141, p.446-453.

——1989. Project unit 88-2. Paleozoic geology of the southern Bruce Peninsula; *in* Summary of Field Work and Other Activities 1989, Ontario Geological Survey, Miscellaneous Paper 146, p.222-227.

Brett , C.E. and Brookfield, M.E. 1984. Morphology, faunas and genesis of Ordovician hardgrounds from southern Ontario, Canada; Paleogeography, Paleoclimatology and Paleoecology, v.46, p.233-290.

Byerley, M.C. and Coniglio, M. 1989. Stratigraphy and sedimentology of the Upper Ordovician Georgian Bay Formation, Manitoulin Island and Bruce Peninsula; *in* Geoscience Research Grant Program Summary of Research 1988-1989, Ontario Geological Survey, Miscellaneous Paper 143, p.227-237.

Freeman, E. B. ed. 1979. Geological Highway Map, Southern Ontario; Ontario Geological Survey, Map 2441.

Horst, R. 1978. Paleoecology and stratigraphy of Late Ordovician (Ashgillian) Biostromes of Manitoulin Island, Ontario; unpublished MSc thesis, Laurentian University, Sudbury, Ontario, 184p.

Johnson, M. D. and Telford, P. G. 1981a. Preliminary Results of 1980 Drilling Programme, Manitoulin Island Limestone-Dolostone Assessment Project; Ontario Geological Survey, Open File Report 5364, 44p.

——1981b. Preliminary Results of the Northern Ontario Geological Survey programme, Manitoulin Island Limestone-Dolostone Assessment Project; Ontario Geological Survey, Open File Report 5360, 81p.

——1985. Paleozoic geology of the Little Current Area, District of Manitoulin; Ontario Geological Survey, Geological Series Preliminary Map P.2670, Geology 1979-1981.

Liberty, B.A. 1969. Paleozoic geology of the Lake Simcoe area, Ontario; Geological Survey of Canada, Memoir 355, 173p.

Liberty, B. A. and Bolton, T. E. 1971. Paleozoic geology of the Bruce Peninsula area, Ontario; Geological Survey of Canada, Memoir 360, 163p.

Shinn, E. A. 1969. Submarine lithification of Holocene carbonate sediments in the Persian Gulf; Sedimentology, v.12, p.109-144.

Wilson, J. L. 1975. Carbonate facies in geologic history; Springer–Verlag, New York, 471p.

Grant 357 Mineralogy and Geochemistry of Diagenetic Carbonates in Cambro–Ordovician Sedimentary Rocks, Southwestern Ontario

---

M.A. Wadleigh[1]*, F.J. Longstaffe[1], R.H. McNutt[2] and S.K. Frape[3]

[1]Department of Geology, University of Western Ontario, London, Ontario.
[2]Department of Geology, McMaster University, Hamilton, Ontario.
[3]Department of Earth Sciences, University of Waterloo, Waterloo, Ontario.

Mineralogical and geochemical analyses are being used to deduce the diagenetic history of Cambro–Ordovician mixed carbonate and clastic sedimentary rocks in southwestern Ontario. These rocks are stratigraphically located at the interface between the Michigan and Appalachian basins making them ideally situated for examination of water-rock interaction involving multiple-fluid sources. The section contains mostly quartz arenites, dolomitic quartz sandstones, dolomitic arkoses and sandy dolostones. Feldspar in these rocks is almost exclusively potassic (Or_{96-100}). It occurs as framework (detrital) grains, overgrowths and euhedral, authigenic crystals. Detrital potassium feldspar is varying shades of bright blue and purple when viewed under cathodoluminescence, while all authigenic varieties are non-luminescent. Clay minerals are also present dominated by illite, ferric illite and glauconite. Ferroan dolomite, present in several different textural varieties, is the major cement. It is most common as zoned rhombs containing alternating Fe-rich and Fe-poor bands. Diagenetic calcite is less abundant than dolomite but in shallower parts of the section can be the only carbonate phase present. Formation of these carbonates postdates diagenetic feldspar crystallization. Stable O-, C- and $^{87}Sr/^{86}Sr$-isotope results for the carbonates suggest that both seawater (or possibly brines) and meteoric water have influenced this diagenetic system. The most ^{18}O-enriched calcites and dolomites are in apparent isotope equilibrium with present formation waters. Most Cambrian dolomites have $\delta^{18}O$ and $^{87}Sr/^{86}Sr$ values compatible with derivation from Cambrian seawater at low temperatures.

INTRODUCTION

Chemical and isotopic compositions of formation waters reflect a variety of physical and chemical processes that occur during deposition and diagenesis (Clayton et al. 1966; Hitchon and Friedman 1969). McNutt et al. (1987) and Dollar et al. (1988) have examined formation waters for units within the Appalachian and Michigan basins. The data indicate that present pore waters are the end product of multiple-fluid mixing and water-rock interactions which may have involved components of deep fluids and downward-migrating freshwaters (during Pleistocene and more recent time?).

Cambrian and Ordovician mixed carbonate and clastic units in southwestern Ontario should have been strongly influenced by such waters. Diagenetic minerals formed in equilibrium with pore waters obtain chemical and isotopic signatures characteristic of that pore water. These compositions can be used to reconstruct pore-water evolution throughout diagenesis, provided the prerequisite information on mineralogy, mineral chemistry and paragenesis of the units has been obtained (Longstaffe 1987, 1988, 1989). However, except for a few isotopic analyses of carbonates and sulphate minerals (McNutt et al. 1987; Fritz et al. 1988; O'Shea et al. 1988), no isotopic data for diagenetic minerals from southwestern Ontario, and in particular Cambrian sandstones, have been reported in the literature.

OBJECTIVES

The general objectives of the project are 1) to deduce the diagenetic history of Cambro–Ordovician clastic sedimentary rocks and intercalated dolostones using mineralogy, isotope geochemistry and fluid chemistry and 2) to relate variations in the diagenetic minerals to basin-wide phenomena such as fluid fluxes, mass transport, burial history, thermal gradients, detrital mineralogy and sedimentary facies.

There are several specific objectives, but to date research has focussed on: 1) regional sampling and lithological, mineralogical and geochemical characterization of the basal Cambrian sandstones of the Mt. Simon (Potsdam) Formation, the dolostones of the Eau Claire (Theresa) and Trempealeau (Little Falls) formations and the mixed shales, siltstones and dolostones of the Ordovician Shadow Lake Formation and 2) O-, C- and Sr-isotope studies of diagenetic carbonate minerals contained within these units. Lithologic and petrographic examination of altered Precambrian basement overlain by Cambrian sandstones was also initiated to determine its genetic relationship to diagenesis in the sandstones.

---

* Present Address: Department of Earth Sciences, Memorial University of Newfoundland, St. John's, Newfoundland, A1B 3X5.

SAMPLING AND ANALYTICAL METHODS

The Cambro–Ordovician section in 76 cores was logged for lithological variability. From 35 of these cores, 271 samples of sandstone and dolostone have been selected. Most cores are located on the Appalachian Basin side of the Algonquin Arch, but 4 cores are from the Michigan Basin side (cores 21, 38, 39 and 44) and 10 are located east of the Frontenac Axis in the Ottawa lowlands (cores 22, 23, 43, 65 to 69, 75 and 76) (Figure 357.1). Many of the cores cluster about the locations of established oil fields. However, a limited number of cores are also located away from areas of known hydrocarbon accumulation and should contribute significantly to the regional aspect of this study. A few samples of the Cambrian–Precambrian contact have also been collected and detailed sampling of altered portions of the Precambrian basement has been initiated; 12 cores have been described and petrographic and X-ray-diffraction (XRD) examination is in progress.

More than 250 new chemical analyses of detrital and diagenetic minerals, including matrix clays, have been obtained using a JEOL 8600 electron microprobe and appropriate standards. Analyses were performed at an accelerating voltage of 15 kV, a sample current of 10 nA, a beam diameter of 1 to 5 mm and counting times of 20 s. Results are summarized in Table 357.1 which also includes approximately 230 analyses that were obtained during the first year of this project (Longstaffe et al. 1990). Textural relationships among the minerals were determined using transmitted light microscopy, backscattered electron imaging (BEI), scanning electron microscope (SEM) and cathodoluminescence microscopy.

Calcite and dolomite were chemically separated from all carbonate-bearing samples and measured for their stable O- and C- isotope compositions. Whole-rock samples were treated with HCl and the resulting leachate, comprised of dolomite ± calcite, was analyzed for $^{87}Sr/^{86}Sr$ isotope.

RESULTS

Whole-rock XRD patterns obtained for all 271 samples are consistent with the earlier classification of these rocks (*after* Folk 1968) into 4 major categories: quartz arenites, dolomitic

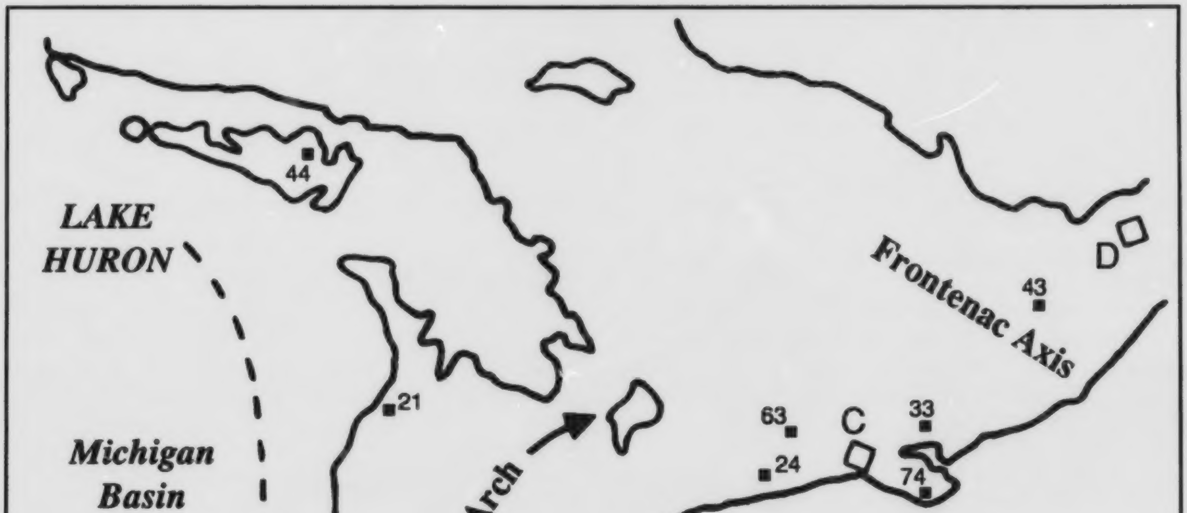

Figure 357.1. Map of southwestern Ontario study area showing numbers and locations of described core relative to structural features. A=cores 1 to 3, 19, 23, 26 to 29, 31, 34 to 36; B=cores 5, 10 to 18, 51 to 61, 72, 73; C=cores 45 to 50; D=cores 22, 23, 65 to 69, 75, 76.

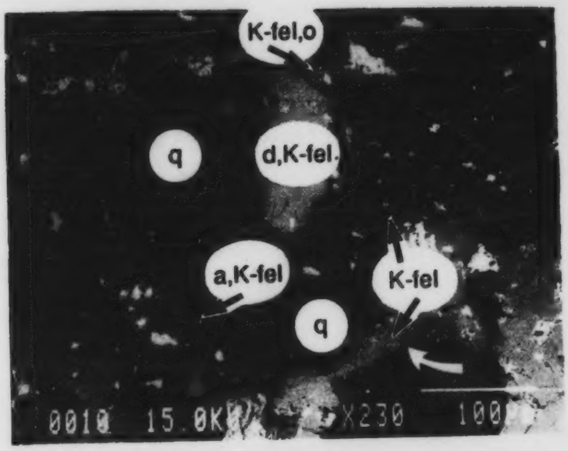

Photo 357.1. Backscattered electron image (BEI) of a dolomitic subarkose (sample 7-63, 1135.4 m). K-fel=potassium feldspar, q=quartz, a=authigenic, d=detrital, o=overgrowth. Note ragged outline of some K-fel as a result of dissolution (arrow).

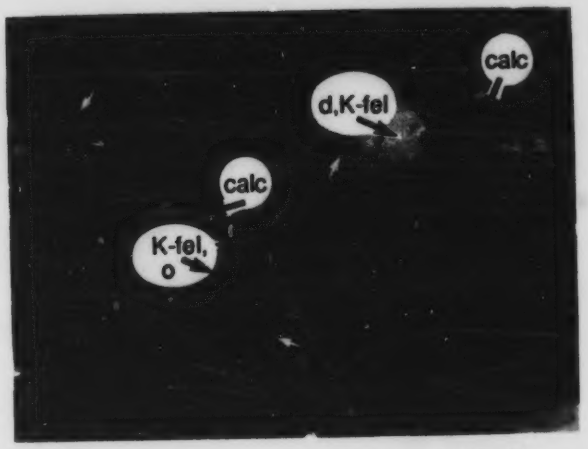

Photo 357.2. Cathodoluminescence photomicrograph of a dolomitic subarkose (sample 32-81, 1068.7 m) showing bright blue luminescing detrital potassium feldspar with non-luminescent overgrowths (white arrows), bright yellow-orange luminescing calcite and orange-red dolomite. Large black areas are pore space. Long dimension of photo is approximately 5 mm. d=dolomite, calc=calcite, other symbols as in Photo 357.1.

quartz sandstones, dolomitic arkoses and sandy dolostones (Longstaffe et al. 1990). In a few instances, the pervasive dolomitization that commonly characterizes carbonate-rich members of this suite has not occurred; instead, sandy limestone is present. The framework grains are predominantly quartz and potassium feldspar. Most grains are subangular to rounded and range in size from 0.25 to 1.5 mm. Plagioclase is essentially nonexistent (less than 1%) and few, if any, rock fragments are present. Clay minerals are mainly of the 10Å variety (illite/ferric, illite/glauconite). Ferroan dolomite is the major cement but quartz and potassium feldspar overgrowths and calcite are also common. Heavy minerals such as pyrite, apatite, tourmaline and rutile are accessory phases. Evaporitic minerals such as gypsum and anhydrite are locally important. Thin section porosity varies from 0 to 30%.

Feldspar

Feldspar in these rocks is almost exclusively potassic ($Or_{86\text{-}100}$). Its abundance (to the virtual exclusion of other feldspars) is a striking feature of these rocks. Potassium feldspar occurs most commonly as detrital grains upon which abundant overgrowths have developed. Some detrital grains are microperthitic. Potassium feldspar overgrowths are not in optical continuity with detrital grains, but are enriched in K and depleted in Ba and Na relative to the detrital substrate (Table 357.1). Potassium feldspar also occurs as euhedral crystals in pore space, as fine-grained matrix and in association with illite (alteration?). Potassium feldspar may also be replaced by dolomite. Some potassium feldspar displays textures typical of dissolution (Photo 357.1). Chemically, most of these varieties have compositions similar to the potassium feldspar overgrowths, but generally the former is richer in Na and poorer in K. Detrital grains can be distinguished from overgrowths and other diagenetic modes of potassium feldspar by their different cathodoluminescent properties. Detrital grains are characterized by varying shades and intensities of blue and purple luminescence while the diagenetic potassium feldspar remains non-luminescent (Photo 357.2). Relict detrital grains of potassium feldspar, which appear totally altered in plane-polarized light, can also be recognized using cathodoluminescence. Diagenetic potassium feldspar has crystallized early in the paragenetic sequence presently preserved in these rocks. Diagenetic potassium feldspar disrupts quartz overgrowths and coats some detrital quartz grains. While more than 1 episode of diagenetic potassium feldspar precipitation has undoubtedly occurred, most potassium feldspar crystallization predates all but initial development of some grain-coating illite (Photo 357.3).

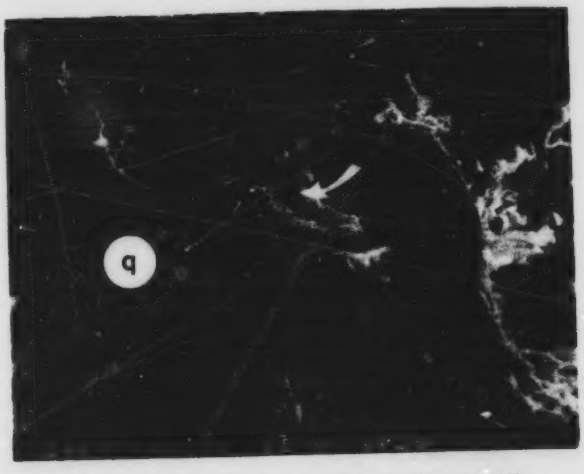

Photo 357.3. Scanning electron photomicrograph of diagenetic illite (arrow) in a dolomitic subarkose (sample 39-146, 1453.0 m). Identification is based on morphology and EDX spectrum. Symbols as in Photo 357.1.

Table 357.1. Summary of Average Chemical Compositions, Minerals from Cambro-Ordovician Rocks, southwestern Ontario

Phase	Core No.*	SiO_2	Al_2O_3	Na_2O	K_2O	CaO	MgO	BaO	SrO	MnO	FeO	TiO_2	Cr_2O_3	F	Cl	Total
Detrital K-feldspar																
OGS-2 (n = 8)	1	63.58	18.21	1.09	14.65	0.00		1.63	0.20							99.36
OGS-8 (n=3)	1	64.25	18.77	1.25	14.46	0.04		1.38	0.28							100.43
OGS-10 (n = 17)	2	65.51	18.29	0.66	15.54	0.03		0.38	0.17							100.57
OGS-14 (n = 6)	2	64.22	18.60	1.14	14.99	0.06		1.04	0.00							100.03
OGS-18 (n = 3)	3	62.66	19.11	1.40	13.65	0.00		3.49	0.13							100.47
OGS-21 (n = 5)	3	64.14	18.72	0.93	15.05	0.03		1.75	0.04							100.65
OGS-22 (n = 8)	3	63.14	19.59	1.03	14.83	0.03		0.89	0.06							99.51
OGS-25 (n = 15)	3	66.51	18.58	0.73	14.92	0.00		0.27	0.26							101.28
OGS-31 (n = 4)	5	65.05	18.76	0.71	15.58	0.00		0.35	0.00							100.45
OGS-32 (n = 4)	5	65.96	18.37	0.44	14.62	0.02		0.26	0.00							99.67
OGS-33 (n = 4)	5	64.50	18.35	0.34	15.70	0.00		0.57	0.00							99.46
OGS-40 (n = 5)	6	65.87	18.48	0.82	14.67	0.03		0.88	0.00							100.75
OGS-46 (n = 5)	6	65.18	18.18	1.14	14.45	0.07		0.28	0.00							99.30
OGS-63 (n = 8)	7	63.24	18.17	0.61	17.12	0.01		0.61	0.00							99.76
K-feldspar overgrowths																
OGS-2 (n = 4)	1	65.59	17.95	0.11	16.76	0.00		0.02	0.11							100.34
OGS-8 (n = 2)	1	66.27	18.22	0.00	16.52	0.00		0.03	0.29							101.22
OGS-18 (n = 3)	3	64.83	18.29	0.04	16.64	0.12		0.02	0.10							100.03
OGS-21 (n = 2)	3	66.14	18.24	0.05	16.88	0.02		0.01	0.00							101.32
OGS-22 (n = 6)	3	64.65	18.93	0.05	16.20	0.05		0.02	0.02							99.91
OGS-31 (n = 5)	5	66.11	18.51	0.03	15.01	0.02		0.00	0.00							99.68
OGS-46 (n = 2)	6	65.81	17.69	0.04	15.07	0.04		0.00	0.00							98.65
OGS-63 (n = 8)	6	65.36	18.04	0.02	19.11	0.00		0.04	0.00							102.57
Euhedral K-feldspar																
OGS-8 (n = 3)	1	65.99	18.21	0.03	16.10	0.01		0.00	0.01							100.35
OGS-18 (n = 3)	3	64.98	18.31	0.67	15.11	0.04		0.40	0.26							99.77
OGS-22 (n = 11)	3	63.97	19.13	0.57	15.86	0.03		0.23	0.01							99.81
Altered K-feldspar																
OGS-14 (n = 5)	2	65.35	18.68	0.63	15.96	0.05		0.26	0.00							100.92
OGS-21(n = 12)	3	65.29	18.48	0.36	15.86	0.02		0.13	0.00							100.13
OGS-22 (n = 4)	3	63.00	19.23	0.40	16.00	0.02		0.17	0.02							98.83
OGS-32 (n =2)	5	66.44	17.14	0.67	12.99	0.00		0.00	0.00							97.24
OGS-33 (n = 5)	5	64.24	19.01	0.15	13.86	0.09		0.12	0.00							97.47
OGS-40 (n = 10)	6	67.30	18.24	0.09	14.93	0.06		0.08	0.00							100.70
OGS-63 (n = 5)	7	64.15	17.88	0.32	19.45	0.01		0.07	0.00							101.88
Matrix K-feldspar																
OGS-8 (n = 3)	1	66.68	18.52	0.49	13.62	0.08		0.15	0.01							99.54
Glauconite																
(n=16)		52.52	11.04	0.04	8.05	0.21	5.56	0.02		0.02	14.75	0.03	0.03	0.75	0.01	92.99
Matrix clay																
OGS-10 (n = 9)	2	49.42	23.19	0.10	7.96	1.05	4.07	0.05		0.03	3.81	0.51	0.00	0.14	0.01	90.34
OGS-14 (n = 9)	2	52.83	21.25	0.11	8.97	1.19	3.26	0.09		0.04	2.85	0.56	0.00	0.00	0.00	91.15
OGS-25 (n = 5)	3	53.98	22.50	0.08	7.82	0.38	3.28	0.00		0.00	3.36	1.48	0.03	0.03	0.03	92.88
OGS-32 (n = 8)	5	44.90	21.65	0.06	6.51	0.32	4.32	0.01		0.00	4.32	0.27	0.00	0.06	0.14	82.56
OGS-33 (n = 4)	5	50.47	25.35	0.04	6.05	0.26	3.59	0.00		0.00	3.51	0.00	0.00	0.00	0.09	89.36
Fe-Mg-rich clay																
OGS-32 (n = 3)	5	26.54	22.70	0.05	0.10	0.04	12.29	0.00		0.00	22.71	0.00	0.00	0.10	0.01	84.54
OGS-33 (n = 2)	5	26.07	21.56	0.00	0.07	0.00	11.95	0.00		0.00	27.86	0.02	0.00	0.28	0.00	87.81
OGS-51 (n = 2)	6	27.33	21.91	0.03	0.13	0.19	15.31	0.00		0.07	20.29	0.01	0.02	0.18	0.04	85.51
Diagenetic Calcite																
Pore filler (n = 24)						54.17	0.54	0.01	0.01	0.64	0.43					55.80
Inclusions in dolomite (n = 4)						55.99	0.79	0.02	0.10	0.58	0.61					58.09
Cores to dolomite rhombs (n = 4)						55.64	0.73	0.00	0.02	0.30	0.20					56.89
Diagenetic Dolomite																
Replacing K-feldspar (n = 6)						30.95	19.26	0.00	0.00	0.33	2.11					52.66
Zoned rhombs, bands >2.5 %Fe (n = 17)						30.02	18.90	0.00	0.00	0.67	3.39					52.98
Zoned rhombs, bands <2.5 %Fe (n = 22)						30.42	20.67	0.00	0.01	0.30	1.31					52.71
Mottled, high Fe areas (n = 18)						29.05	18.48	0.01	0.02	0.98	4.96					53.50
Mottled, low Fe areas (n = 16)						29.99	22.33	0.01	0.00	0.17	0.91					53.41
Rim on calcite cement (n = 3)						30.35	18.69	0.00	0.00	0.92	3.41					53.37

n = number of separate subsamples analyzed.

** See Figure 1 for core locations.*

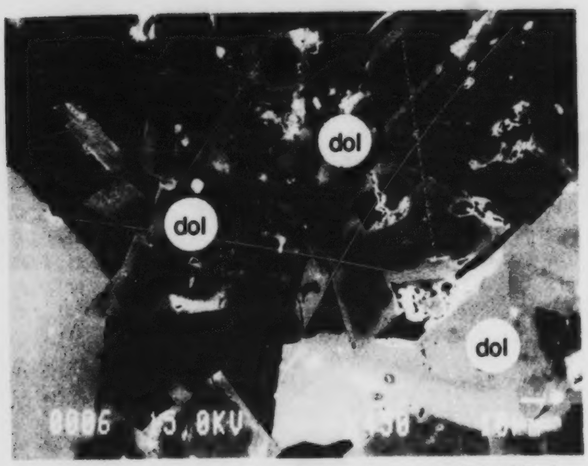

Photo 357.4a. BEI of a dolomitic subarkose (sample 32-81, 1068.7 m) showing fine scale chemical variations in diagenetic dolomite rhombs. Bright zones are Fe-rich while dark zones are Fe-poor, averaging 3.39 and 1.31 wt % FeO, respectively (Table 357.1). Symbols as in Photo 357.2.

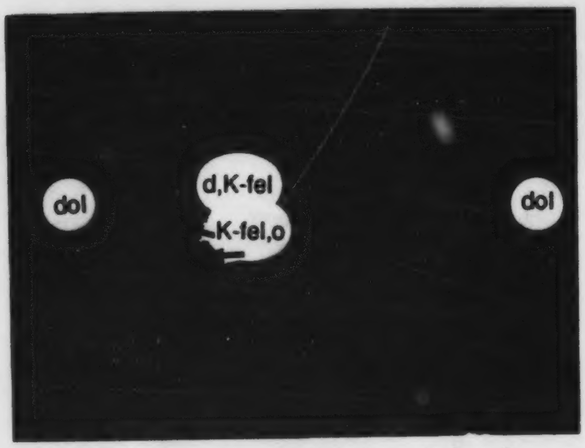

Photo 357.4b. Cathodoluminescence photomicrograph of a sandy dolomite (sample 3-18, 1197.3 m). Dolomite zones display varying shades of red to orange luminescence. Darker zones are interpreted as being enriched in Fe which quenches luminescence. Brighter zones are poorer in Fe. Symbols as in Photo 357.2.

Carbonates

There are 5 recognizable textural varieties of dolomite: 1) dolomite replacement of potassium feldspar, generally Fe-poor (less than 2.5 % FeO); 2) zoned rhombic crystals, with alternating Fe-Mn-rich and Fe-Mn-poor bands on a micrometre scale; 3) pore filling, mottled dolomite, with irregular distribution of high and low Fe-Mn contents on a micrometre scale; 4) dolomite rims of variable Fe-Mn content with calcite cores and 5) pore filling dolomite containing irregularly shaped inclusions of calcite. The chemical variability of the dolomite is summarized in Table 357.1 and the fine scale of chemical variability is readily apparent from BEI and cathodoluminescence images (Photos 357.4a and b). Dolomite crystallization has postdated formation of most other diagenetic phases in these rocks, with the exception of some calcite and late vug- and pit-filling sulphates. Calcite is less abundant than dolomite but in some samples is the only carbonate phase present. It is usually confined to the shallower portions of the cores. A common trend within individual cores is calcite at the top (mainly Ordovician), followed by coexisting calcite and dolomite (Ordovician and some Cambrian) and then dolomite as the only carbonate phase near the bottom (mainly Cambrian). There are 3 textural varieties of calcite: 1) calcite included within pore-filling dolomite; 2) massive pore-filling calcite and 3) calcite cores to dolomite rhombs. The Fe, Mn and Mg contents of all varieties are low (Table 357.1).

Other Phases

Glauconite occurs near the top of the Cambrian section and in the Ordovician samples. Its formation is typical of slow, shallow-marine sedimentation and characterizes Cambro–Ordovician rocks worldwide. Glauconite from these samples has a chemical composition within the reported range for such clay minerals (Velde and Meunier 1987, Table 357.1). Besides early glauconite, illitic clay (including an Fe-rich variety) is also present, filling pores between detrital quartz and feldspar grains. This illitic clay predates formation of some quartz and potassium feldspar overgrowths, and crystallization of all dolomitic and calcitic cements. It is also associated with potassium feldspar alteration and also occurs intermixed with pyrite. The continuity of some quartz overgrowths has been interrupted by crystallization of diagenetic potassium feldspar or illitic clay. Quartz-overgrowth formation predates carbonate cementation.

PARAGENESIS

From the available data, the following paragenetic sequence can be proposed: grain-coating, detrital (?) illite/authigenic glauconite; potassium feldspar overgrowths (± other authigenic potassium feldspar, first stage); quartz overgrowths (± authigenic potassium feldspar, second stage); diagenetic illite; early calcite; dolomite and de-dolomitization/late calcite.

ISOTOPE RESULTS FOR CARBONATE MINERAL

Stable O, C Isotopes

The results of stable oxygen and carbon isotopic analysis of diagenetic carbonates from most lithologic units are summarized in Table 357.2 and Figures 357.2a and b, expressed in the usual d-notation, relative to the standard Peedee belemnite (PDB). Most quartz arenite samples contained insufficient carbonate for analysis.

The majority of Cambrian samples (43 of 63) contain dolomite as their only carbonate phase. These dolomites have

Table 357.2 Isotopic compositions of diagenetic carbonates.

			Bulk Rock Compositions*							****
Sample	**Core No.****	**Dolomite**	**Calcite**	**Quartz**	**K-feldspar**	**$^{87}Sr/^{86}Sr$ carbonate*****	**$\delta^{18}O_{dol}$**	**$\delta^{13}C_{dol}$**	**$\delta^{18}C_{cc}$**	**$\delta^{13}C_{cc}$**
Bulk Rock										
OGS-1	1	0.76	0.13	0.00	0.11	0.70867	-3.75	-4.04	-6.61	-3.30
OGS-3	1	0.49	0.00	0.44	0.07	0.70911	-6.66	0.30		
OGS-4	1	0.97	0.00	0.00	0.00	0.70915	-6.99	-1.03		
OGS-5	1	0.98	0.00	0.00	0.00	0.70916	-6.16	-1.27		
OGS-6	1	0.86	0.00	0.14	0.00	0.70911	-7.00	-1.55		
OGS-7	1	0.66	0.00	0.10	0.24	0.70912	-6.54	-2.54		
OGS-9	2						-1.16	-0.40	-9.94	-2.90
OGS-11	2	0.39	0.01	0.57	0.02	0.70937	-8.12	-2.11		
OGS-12	2	1.00	0.00	0.00	0.00	0.70927	-5.72	-1.25		
OGS-13	2	1.00	0.00	0.00	0.00	0.70919	-5.54	-1.25		
OGS-14	2	0.54	0.00	0.35	0.11	0.70963				
OGS-15-1	2	1.00	0.00	0.00	0.00	0.70959	-6.08	-3.97		
OGS-15-2	2	0.87	0.00	0.00	0.13	0.70956	-6.01	-3.79		
OGS-17	3	0.13	0.87	0.00	0.00	0.70863	-3.08	-0.99	-4.26	-1.51
OGS-18	3	0.26	0.04	0.61	0.08	0.7094	-8.21	-3.18	-9.05	-3.63
OGS-19	3	0.69	0.04	0.23	0.04	0.70883	-2.47	-4.74	-4.04	-4.04
OGS-21	3	0.33	0.00	0.23	0.44	0.70923	-6.17	-3.35		
OGS-26	4	0.68	0.00	0.18	0.04		-7.06	-1.68		
OGS-28	4	0.82	0.00	0.13	0.01		-7.57	-2.08		
OGS-29	4	0.56	0.01	0.38	0.01		-7.57	-1.95		
OGS-36	6	0.36	0.00	0.58	0.04		-8.22	-1.22		
OGS-37	6	0.45	0.00	0.51	0.03		-7.99	-1.26		
OGS-38	6	0.75	0.01	0.21	0.01		-8.20	-1.20		
OGS-39	6	0.84	0.06	0.05	0.01		-8.46	-1.09		
OGS-40	6	0.54	0.02	0.36	0.06		-8.40	-1.22		
OGS-42	6	0.44	0.00	0.50	0.03		-8.05	-1.27		
OGS-43	6	0.18	0.00	0.34	0.37		-8.03	-1.22		
OGS-45	6	0.63	0.00	0.32	0.04		-7.84	-0.60		
OGS-47	6	0.94	0.03	0.01	0.02		-8.32	-0.79		
OGS-51	6	0.37	0.01	0.61	0.01		-7.68	-4.31		
OGS-57	7	0.63	0.00	0.34	0.03		-7.54	-0.20		
OGS-59	7	0.67	0.00	0.14	0.02		-6.91	-1.31		
OGS-60	7	0.90	0.00	0.06	0.04		-6.62	-1.96		
OGS-61	7	0.79	0.02	0.16	0.03		-7.37	-1.82		
OGS-66	8	0.89	0.00	0.06	0.03		-6.40	-2.37		
OGS-67	8	0.34	0.00	0.54	0.12		-7.67	-3.00		
OGS-89	13	0.06	0.82	0.08	0.00		-5.76	-4.44	-4.90	-4.53
OGS-89 R									-4.70	-4.53
OGS-94	13	0.01	0.04	0.89	0.03				-14.66	-2.29
OGS-185	21	0.52	0.24	0.16	0.03		-2.58	-4.82		
OGS-185 R							-2.47	-4.77	-6.63	-4.99
OGS-187	21	0.69	0.00	0.20	0.03		-2.46	-4.64		
OGS-189	21	0.03	0.07	0.69	0.18		-11.75	-5.87	-9.76	-5.60
OGS-106	23	0.05	0.00	0.69	0.21		-7.56	-2.54		
OGS-72	32	0.04	0.89	0.01	0.00		-5.54	-1.91	-4.57	-2.12
OGS-75	32	0.53	0.07	0.33	0.04		-5.21	-1.86	-8.80	-2.40
OGS-76	32	0.41	0.00	0.39	0.17		-6.10	-2.43		
OGS-77	32	0.16	0.08	0.67	0.06		-3.10	-8.03	-10.87	-4.21
OGS-79	32	0.05	0.03	0.84	0.07		-8.69	-2.95	-11.89	-3.42
OGS-81	32	0.35	0.07	0.44	0.10		-5.61	-2.96		
OGS-135	39	0.00	0.92	0.01	0.03				-5.76	-2.30
OGS-135 R									-5.68	-2.44
OGS-136	39	0.14	0.80	0.01	0.01		-6.66	-1.80	-5.70	-1.95
OGS-137	39	0.09	0.83	0.02	0.02		-7.36	-1.72	-5.34	-2.11
OGS-139	39	0.23	0.00	0.42	0.29		-5.73	-1.69		
OGS-140	39	0.37	0.00	0.40	0.13		-6.92	-0.24		

Table 357.2 Continued.

Sample	Core No.**		Bulk Rock Compositions*							****
		Dolomite	Calcite	Quartz	K-feldspar	$^{87}Sr/^{86}Sr$ carbonate***	$\delta^{18}O_{dol}$	$\delta^{13}C_{dol}$	$\delta^{18}C_{cc}$	$\delta^{13}C_{cc}$
Bulk Rock										
OGS-141	39	0.73	0.00	0.19	0.05		-7.12	-0.68		
OGS-142	39	0.72	0.00	0.19	0.05		-7.49	-0.03		
OGS-143	39	0.41	0.00	0.46	0.08		-7.68	-0.34		
OGS-144	39	0.72	0.00	0.17	0.05		-7.23	-0.63		
OGS-145	39	0.63	0.00	0.23	0.07		-6.39	-1.97		
OGS-146	39	0.24	0.00	0.53	0.16		-7.26	-3.11		
OGS-147	39	0.82	0.00	0.10	0.03		-6.34	-1.98		
OGS-148	39	0.79	0.00	0.11	0.03		-7.34	-3.45		
OGS-149	39	0.83	0.00	0.11	0.03		-6.18	-2.58		
OGS-239	43	0.00	0.04	0.94	0.00				-9.58	-1.19
OGS-240	43	0.01	0.13	0.82	0.01				-12.80	-5.41
OGS-241	43	0.02	0.10	0.84	0.02		-11.42	-2.26	-12.13	-3.55
OGS-242	43	0.02	0.11	0.83	0.02		-11.68	-4.29	-12.15	-4.89
OGS-243	43	0.00	0.06	0.03	0.11				-10.80	-7.24
OGS-244	43	0.00	0.27	0.09	0.00				-11.06	-6.83
OGS-244 R									-11.24	-6.75
OGS-115	44	0.18	0.67	0.05	0.02		-6.56	0.53	-5.91	0.24
OGS-116	44	0.06	0.71	0.14	0.04		-6.23	-2.15	-4.75	-2.14
OGS-117	44	0.27	0.26	0.31	0.07		-5.55	-0.38	-5.58	-0.79
OGS-118	44	0.11	0.62	0.14	0.04		-6.00	-1.75	-5.30	-2.30
OGS-119	44	0.10	0.29	0.40	0.08		-5.79	-0.87		
OGS-122	44	0.13	0.22	0.46	0.08		-8.95	-2.04	-6.68	-1.70
OGS-123	44	0.15	0.02	0.74	0.03		-7.82	-3.87	-7.30	-4.95
OGS-125	44	0.01	0.05	0.90	0.01		-12.09	-6.83	-9.76	-7.35
OGS-128	44	0.49	0.02	0.34	0.03		-3.22	-6.88	-4.36	-6.50
OGS-133	44	0.21	0.01	0.72	0.02		-8.44	-7.42	-8.11	-7.53
OGS-197	48	0.55	0.12	0.22	0.03		-3.69	-0.40	-7.56	-0.78
OGS-198	48	0.25	0.17	0.44	0.04		-3.61	0.04	-9.25	-0.46
OGS-199	48	0.00	0.90	0.05	0.00				-6.56	-1.13
OGS-200	48	0.19	0.11	0.56	0.05		-3.50	-0.96	-9.22	-1.41
OGS-201	48	0.18	0.30	0.39	0.05		-5.17	-1.21	-8.67	-1.88
OGS-202	48	0.44	0.23	0.23	0.02		-3.34	-1.28	-9.74	-1.69
OGS-203	48	0.00	0.79	0.09	0.00				-6.17	-4.86
OGS-206	48	0.04	0.04	0.40	0.31		-10.21	-3.27	-9.84	-3.54
OGS-191	60	0.09	0.07	0.70	0.08		-6.67	-4.17	-13.49	-4.13
OGS-261	63	0.19	0.71	0.05	0.00		-5.20	0.27	-6.41	-0.09
OGS-262	63	0.32	0.07	0.33	0.02		-2.18	-0.21		
OGS-263	63	0.41	0.45	0.06	0.00		-4.18	-0.72	-7.63	-0.97
OGS-264	63	0.06	0.06	0.73	0.06		-4.72	-1.01	-11.00	-1.30
OGS-265	63	0.01	0.36	0.51	0.07		-6.85	-2.63	-5.72	-2.90
OGS-266	63	0.00	0.24	0.57	0.08				-6.39	-2.32
OGS-266 R									-6.30	-2.50
OGS-250	70	0.34	0.52	0.06	0.02		-3.93	-3.68	-5.93	-4.63
OGS-250 R							-4.37	-3.62	-5.56	-4.43
OGS-251	70	0.01	0.06	0.80	0.06		-13.13	-2.94	-10.75	-2.42
OGS-251 R	C						-13.35	-2.48	-7.00	2.65
OGS-254	70	0.72	0.03	0.13	0.07		-3.34	-5.38	-4.91	-5.08
OGS-256	70	0.13	0.08	0.45	0.13		-9.05	-7.99		
OGS-256 R							-8.94	-7.28		

** Proportions based on XRD peak heights.*

*** See Figure 1 for core locations.*

**** $^{87}Sr/^{86}Sr$ measured on acid leached fraction.*

***** Isotope values are in PDB.*

R denotes repeat analysis.

C denotes contamination.

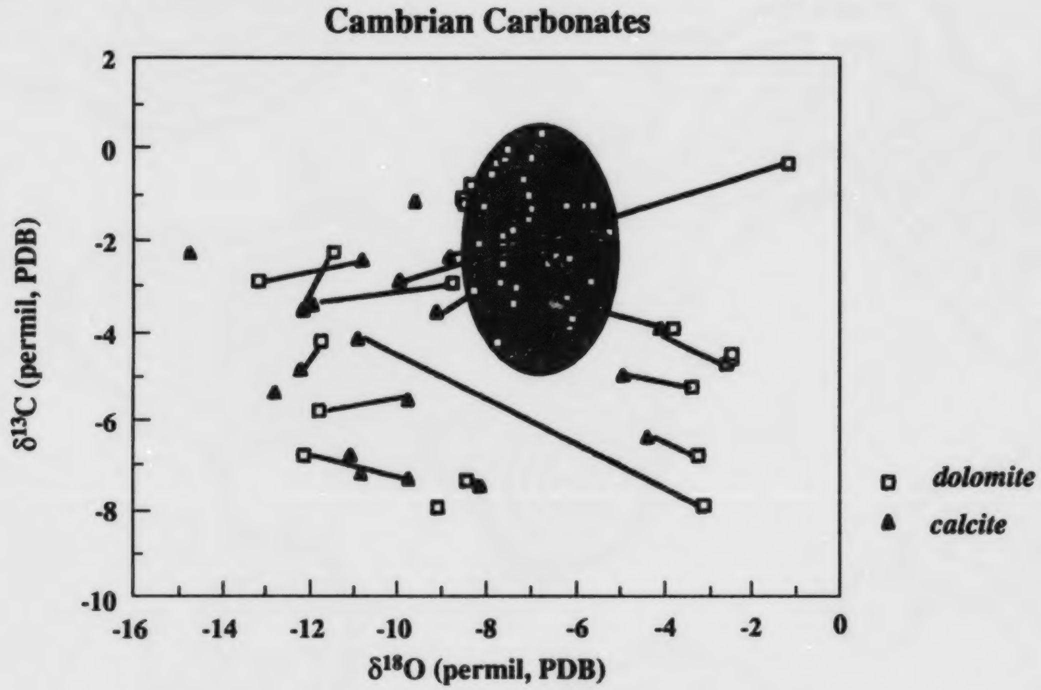

Figure 357.2a. O- and C-isotope compositions of diagenetic carbonates in Cambrian strata. Values for coexisting calcite and dolomite are joined by a line. Stippled area represents the field of Cambrian dolomites with $\delta^{18}O_{average}$=-7.2‰, PDB.

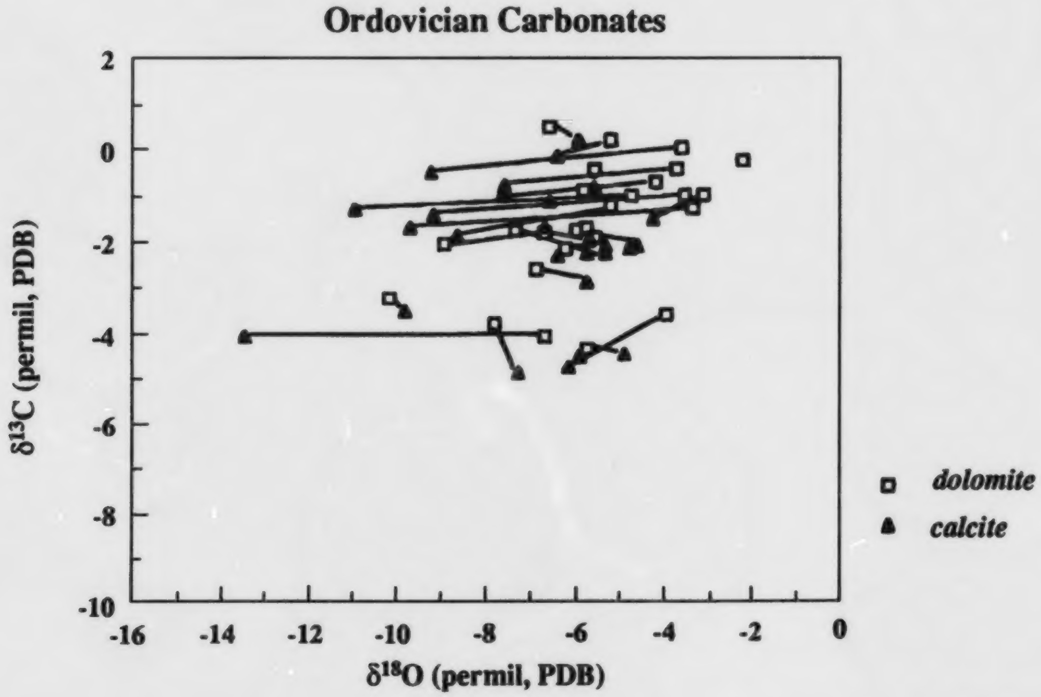

Figure 357.2b. O- and C-isotope compositions of diagenetic carbonates in Ordovician strata. Values for coexisting calcite and dolomite are joined by a line.

a narrow range of $\delta^{18}O$ values, with a mean of -7.2 + 0.8 ‰ (PDB) (*see* Figure 357.2a). There are 13 Cambrian samples which contain both calcite and dolomite and 5 samples contain only calcite. The majority of Ordovician samples (22 of 29) contain mixtures of calcite and dolomite. Of the remaining 7 samples, 4 contain calcite and 3 contain dolomite. Hence, 42% of the carbonate-bearing samples (41 of 97) contained both calcite and dolomite, permitting measurement of the O-isotope fractionation between these phases: $\delta^{18}O_{dolomite}$ - $\delta^{18}O_{calcite} = \Delta^{18}O_{dolomite\text{-}calcite}$ = -2 to 9 ‰ (*see* Table 357.2; Figure 357.2a, b). Most samples have Δ-values within the range commonly reported for coexisting calcite and dolomite (Land 1983) and could have formed at equilibrium. However, O-isotope disequilibrium between dolomite and calcite is clearly indicated by Δ-values as large as 9 ‰ and by samples with $\delta^{18}O_{calcite}$ greater than $\delta^{18}O_{dolomite}$. Within most of the cores, apparent disequilibrum is the exception. For example, only 7 samples, representing 6 different cores, have $\Delta_{dolomite\text{-}calcite}$ greater than 4 ‰. In contrast, most samples with $\delta^{18}O_{calcite}$ greater than $\delta^{18}O_{dolomite}$ (i.e., $\Delta_{dolomite\text{-}calcite}$ less than 0) are confined to 2 specific cores located outside of the Appalachian basin (cores 39 and 44).

Diagenetic carbonate minerals from siliciclastic rock types tend to have lower $\delta^{18}O$ values than intercalated carbonate-rich units. For example, samples OGS-17, OGS-18 and OGS-19, which contain both calcite and dolomite, are closely spaced (less than 4 m) in descending stratigraphic order within 1 core, and hence have experienced a similar burial history. Samples OGS-17 and OGS-19, which contain more than 90% carbonate, have similar dolomite and calcite $\delta^{18}O$ values whereas the $\delta^{18}O$ values of these minerals in sample OGS-18, an arkosic sandstone with only 25% carbonate cement, are approximately 5 ‰ lower (*see* Table 357.2). We suggest that permeability of the carbonate-poor rock types to low-^{18}O meteoric water was greater than in the intercalated, carbonate-rich rocks during this stage of diagenesis, i.e., the arkosic sandstones were better conduits for meteoric water. On a larger scale, Figure 357.3 shows the trend of decreasing ^{18}O of carbonate minerals with total carbonate in the rock. Point counting reveals that porosity also decreases with increasing carbonate.

Sr Isotopes

Sr-isotope analyses for selected dolomite and calcite samples are also listed in Table 357.2. Many of the samples that only contain dolomite have $^{87}Sr/^{86}Sr$ ratios similar to Cambrian seawater (Burke et al. 1982) (Figure 357.4; average = 0.70926). Some samples containing both dolomite and calcite are less radiogenic than the pure dolomite (*see* Table 357.2), suggesting that the calcite has a lower $^{87}Sr/^{86}Sr$ ratio than the dolomite. Such behaviour would be consistent with 1) precipitation from seawater at a later time or 2) alteration by waters which equilibrated with overlaid (Ordovician) carbonates. The $^{87}Sr/^{86}Sr$ values for individual phases could not be determined from the dolomite-calcite mixtures; no simple relationship is apparent. The presence of 2 generations of calcite cement can partially account for the complexity. In addition, there exists some relationship between the $^{87}Sr/^{86}Sr$ ratio of the "carbonate" leachate and the abundance of potassium feldspar in the sample. Carbonate that replaced potassium feldspar may have incorporated radiogenic Sr during this diagenetic process. Alternatively, potassium feldspar may have contributed radiogenic Sr to the "carbonate" leachate during analytical procedures. These possibilities are being investigated.

DISCUSSION

The formation of the unusual and complex potassium feldspar-carbonate diagenetic mineral assemblage has undoubtedly required a special set of physico-chemical conditions. The origin of the potassium feldspar is of particular interest because similar material is widespread throughout Cambro–Ordovician sedimentary rocks of mid-continental North America, and the immediately underlying Precambrian basement (e.g., Stablein and Dapples 1977; Hearn and Sutter 1985; Duffin 1989). Buyce and Friedman (1975) and Russell et al. (1984) suggested that the potassium feldspar precipitated on tidal flats fed by highly alkaline river and groundwaters. Basu (1981) noted that increased potassium feldspar stability and enhanced plagioclase weathering could result from alkaline conditions related to the absence of higher-order land plants in early Phanerozoic time. Marginal seas around the North American supercontinent in Proterozoic and early Phanerozoic time may have become saline through evaporation, and alkaline through restricted circulation, providing a suitable environment for potassium feldspar precipitation. Alternatively, others favour later, tectonically-induced, basin-wide and inter-basin fluid migration (and diagenetic/hydrothermal conditions) to explain the potassic nature of these rocks (Hearn and Sutter 1985; Hearn et al. 1987; Hay et al. 1988; Duffin et al. 1989).

Based on the various petrographic techniques utilized in this study, the potassium feldspar is considered to have formed early in the diagenetic history of these rocks: virtually all diagenetic potassium feldspar predates dolomitization and precipitation of calcite cements. While no isotopic information is presently available for the potassium feldspar (*see* "Future Work"), O and C isotopes and $^{87}Sr/^{86}Sr$ ratios have been measured on all of the diagenetic carbonates. These compositions help to place some constraints on the origin of the potassium feldspar.

The isotopic data suggest that both seawater (or its evolved derivative) and meteoric water have been present in this diagenetic system. Dolomites from the lowest parts of the Cambrian sequence have $\delta^{18}O$ and $^{87}Sr/^{86}Sr$ values compatible with derivation from Cambrian seawater. Calcite-dolomite pairs from upper parts of the Cambrian sequence and from Ordovician samples have $\delta^{18}O$ compositions which bracket the dolomites. The lower O-isotope values imply the involvement of meteoric water while the

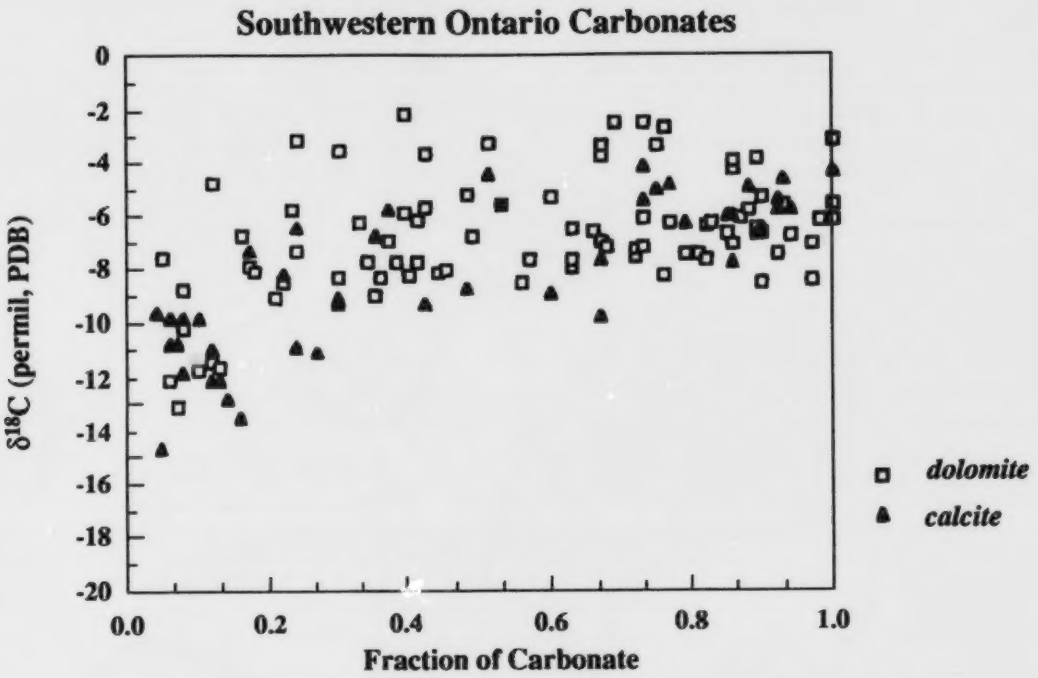

Figure 357.3. O-isotope composition of diagenetic carbonates related to the proportion of carbonate in the sample as determined by XRD. Both calcites and dolomites become enriched in ^{18}O with increasing fraction of carbonate in the sample. Note that on average, $\delta^{18}O_{dolomite}$ is 3 to 4‰ greater than $\delta^{18}O_{calcite}$.

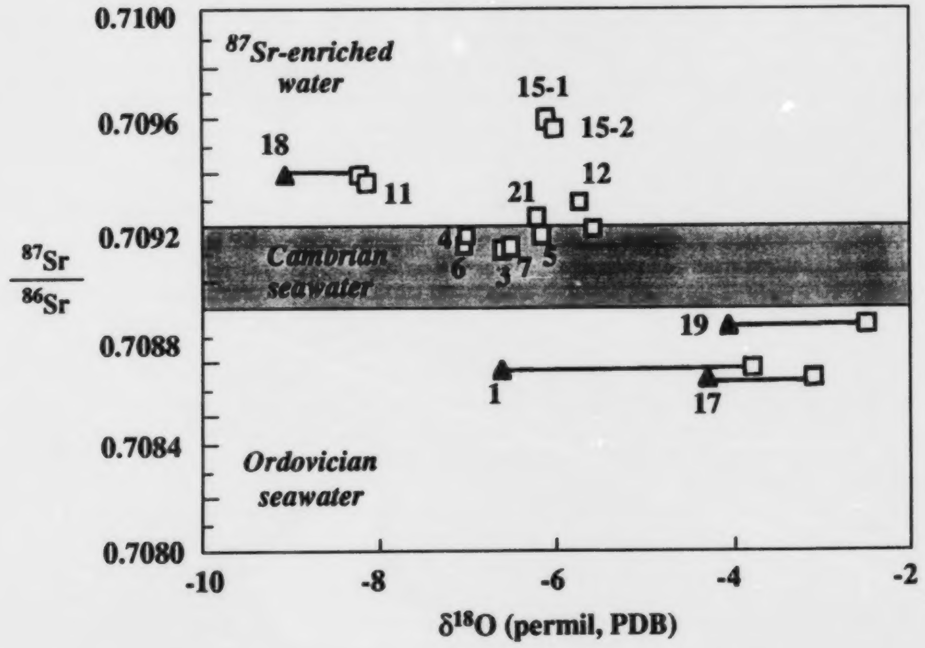

Figure 357.4. $^{87}Sr/^{86}Sr$ vs. $\delta^{18}O$ for diagenetic carbonates. Values for coexisting calcite and dolomite are joined by a line. Number labels correspond to individual samples as listed in Table 357.2. For example, 15-1 is sample OGS-15-1 in the table. Fields of $^{87}Sr/^{86}Sr$ values for Cambrian and Ordovician seawater are from Burke et al. (1982). Triangle = calcite, square=dolomite.

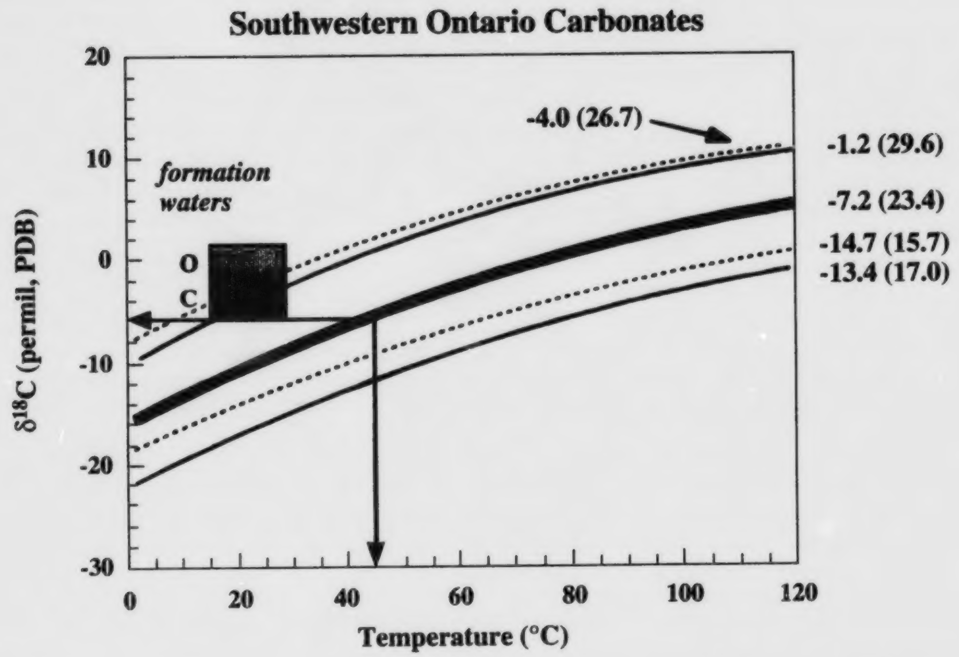

Figure 357.5. δ^{18}O values of water versus temperature (°C) for diagenetic calcite and dolomite from Cambrian and Ordovician units. Curves are shown for the maximum and minimum δ^{18}O values obtained for each phase using the following mineral-water oxygen-isotope fractionation equations: calcite-water, O'Neil et al. (1969) modified by Friedman and O'Neil (1977); dolomite-water, Land (1983). Dashed lines are calcite, solid lines are dolomite. Heavy solid line is the average for Cambrian dolomites from which a temperature of 45°C was calculated for a water composition of -6‰ (SMOW). δ values for carbonates are expressed relative to both PDB and SMOW, the latter in parentheses. Formation water isotopic compositions are from Frape (1989). Formation water temperatures were calculated using a surface temperature of 15°C and a geothermal gradient of 19.2°C/km.

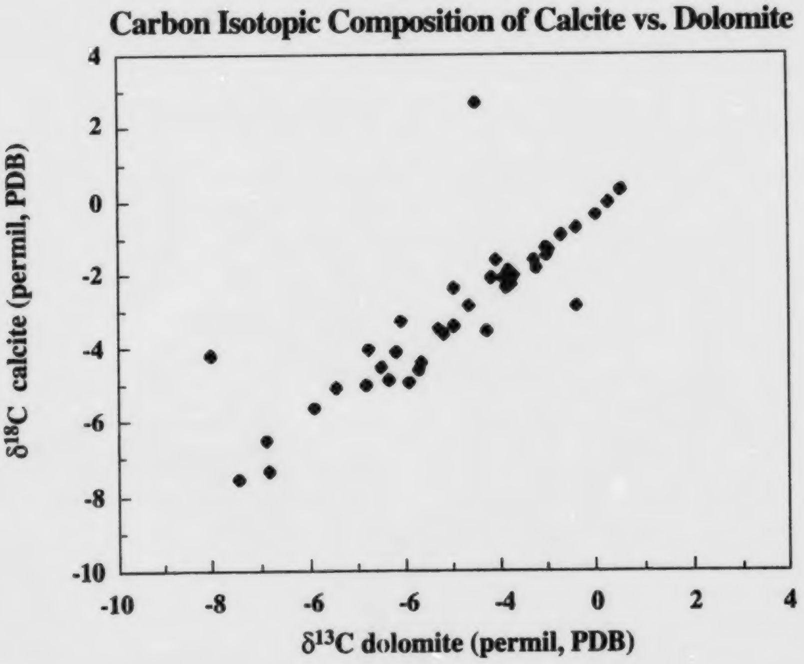

Figure 357.6. δ^{13}C of calcite versus dolomite from Cambrian and Ordovician units. This strong correlation suggests derivation of the calcite from dissolution of dolomite (see text).

higher values may represent a substantial influx of evolved pore waters (possibly brines) which have isotopically equilibrated with overlying carbonate sequences. Available $^{87}Sr/^{86}Sr$ values for the carbonates are consistent with such an interpretation.

Figure 357.5 illustrates the range in $\delta^{18}O$ for dolomite and calcite plotted relative to water $\delta^{18}O$ values and temperature. The O-isotopic compositions of the Cambrian dolostones ($\delta^{18}O = -7.2‰$, PDB) suggest low temperature of formation, i.e., 45°C for a water with $\delta^{18}O = -6‰$ standard mean ocean water (SMOW) (Figure 357.5). Independent evidence suggests that this is not an unreasonable O-isotope composition for Cambrian seawater (Wadleigh and Veizer 1990). These observations would suggest that the earlier diagenetic potassium feldspar crystallized at still lower temperatures.

Figure 357.5 also illustrates the isotopic compositions measured for present formation waters in the Ordovician and Cambrian units (Frape 1990). The most ^{18}O-enriched calcites and dolomites are in apparent isotopic equilibrium with these waters. The calcites are primarily although not exclusively located in strata of Ordovician age, while the dolomites occur in strata of both ages. In contrast, the Cambrian dolomites ($\delta^{18}O=-7.2‰$ PDB) are not in equilibrium with present pore waters.

Figure 357.6 illustrates the strong correlation between the C-isotope compositions of associated calcites and dolomites. The slope is essentially 1 and the correlation coefficient is 0.94. The corresponding O data display no correlation. This behaviour strongly suggests that the calcite has been derived from dolomite dissolution. Petrographic evidence also supports a de-dolomitization episode later in the diagenetic history of the rocks.

SUMMARY

The diagenetic history of Cambro–Ordovician mixed carbonate and clastic rocks from southwestern Ontario is being investigated using mineralogical, geochemical and isotopic methods. The general objectives are 1) to deduce the nature of fluids and temperatures involved in mineral reactions and 2) to relate chemical and isotopic variations in diagenetic minerals to basin-wide phenomena such as changing fluid fluxes, mass transport, burial history, detrital mineralogy and sedimentary facies variations.

The second year of this research has focussed on 1) completion of regional sampling, and mineralogical and geochemical characterization of the Cambrian and Ordovician sandy units and 2) O-, C- and Sr-isotope studies of the diagenetic dolomite and calcite cements.

Stable O, C and $^{87}Sr/^{86}Sr$ isotope results for the diagenetic carbonates suggest that both seawater (or possibly brines) and meteoric water have influenced this diagenetic system. The most ^{18}O-enriched calcites and dolomites are in apparent isotope equilibrium with present formation waters. Cambrian dolomites have $d^{18}O$ and $^{87}Sr/^{86}Sr$ values compatible with derivation from Cambrian seawater. The values are also consistent with low temperature of formation (approximately 45 °C). This suggests that the diagenetic potassium feldspar may have crystallized at still lower temperatures.

ACKNOWLEDGEMENTS

This research was supported by Ontario Geoscience Research Grant 357 to F.J. Longstaffe, R.H. McNutt and S.K. Frape and by Natural Sciences and Engineering Research Council Operating Grant NSERC A7387 to F.J. Longstaffe. We would like to thank T.R. Carter (Ontario Ministry of Natural Resources), R.M. Easton (Ontario Geological Survey) and the Electron Microprobe Laboratory staff (University of Western Ontario) for their assistance in this study.

FUTURE WORK

Additional work planned or in progress includes: 1) separation of glauconite for detailed stable and radiogenic isotope studies (its stable isotopic composition should provide information on early diagenetic pore waters; radiogenic isotope dating of this early diagenesis may be possible); 2) separation of both quartz and potassium feldspar overgrowths for isotopic study (dating, thermal history, fluid composition) and 3) characterization of clay mineralogy throughout the study area.

REFERENCES

Basu, A. 1981. Weathering before the advent of land plants: evidence from unaltered detrital K feldspars in Cambrian–Ordovician arenites; Geology, v.9, p.132–133.

Burke, W.H., Denison, R.E., Hetherington, E.A., Koepnick, R.B., Nelson, N.F. and Otto, J.B. 1982. Variation of seawater $^{87}Sr/^{86}Sr$ throughout Phanerozoic time; Geology, v.10, p.516–519.

Buyce, M.R. and Friedman, G.M. 1975. Significance of authigenic K-feldspar in Cambrian–Ordovician carbonate rocks of the proto-Atlantic shelf in North America; Journal of Sedimentary Petrology, v.45, p.808–821.

Clayton, R.N., Friedman, I., Graf, D.L., Meents, W.F. and Shimp, N.F. 1966. The origin of saline formation waters: 1. Isotopic composition; Journal of Geophysical Research, v.71, p.3869–3882.

Dollar, P.S., Frape, S.K. and McNutt, R.H. 1988. Geochemistry of formation waters, southwestern Ontario, Canada and southern Michigan, U.S.A.: implications for origin and evolution; Ontario Geoscience Grant Program, Final Open File Report.

Duffin, M.E. 1989. Nature and origin of authigenic K-feldspar in Precambrian basement rocks of the North American midcontinent; Geology, v.17, p.765–768.

Duffin, M.E., Lee, M., Klein, G. and Hay, R. 1989. Potassic diagenesis of Cambrian sandstones and Precambrian granitic basement in UPH-3 Deep Hole, upper Mississippi Valley, U.S.A.; Journal of Sedimentary Petrology, v.59, p.848–861.

Folk, R.L. 1968. Petrology of Sedimentary Rocks; Hemphill Publishing Co., Austin, Texas, 182 p.

Frape, S.K. 1990. Chemical aspects of sedimentary basin fluids and diagenesis; *in* Introduction to Diagenesis: Methods and Applications, Short Course, 1990 Eastern Section Meeting, American Association of Petroleum Geologists, p.57–83.

Friedman, I. and O'Neil, J.R. 1977. Compilation of stable isotope fractionation factors of geochemical interest; *in* Data of Geochemistry, 6th ed., United States Geological Survey, Professional Paper 440-KK, 12p.

Fritz, P., Lapcevic, P.A., Miles, M., Frape, S.K., Lawson, D.E. and O'Shea, K.J. 1988. Stable isotopes in sulphate minerals from the Salina Formation in southwestern Ontario; Canadian Journal of Earth Sciences, v.25, p.195–205.

Hay, R.L., Lee, M., Kolata, D.R., Matthews, J.C. and Morton, J.P. 1988. Episodic potassic diagenesis of Ordovician tuffs in the Mississippi Valley area; Geology, v.16, p.743–747.

Hearn, P.P. and Sutter, J.K. 1985. Authigenic potassium feldspar in Cambrian carbonates: evidence of Alleghenian brine migration; Science, v.228, p.1529–1531.

Hearn, P.P., Sutter, J.F. and Belkin, H.E. 1987. Evidence for Late Paleozoic brine migration in Cambrian carbonate rocks of the central and southern Appalachians: implications for Mississippi valley-type sulfide mineralization; Geochimica et Cosmochimica Acta, v.51, p.1323–1334.

Hitchon, B. and Friedman, I. 1969. Geochemistry and origin of formation waters in the western Canada sedimentary basin: 1. Stable isotopes of hydrogen and oxygen; Geochimica et Cosmochimica Acta, v.33, p.1321–1349.

Land, L.S. 1983. The application of stable isotopes to studies of the origin of dolomite and to problems of diagenesis of clastic sediments; *in* Stable Isotopes in Sedimentary Geology, Short Course 10, Society of Economic Paleontologists and Mineralogists, p.4.1–4.22.

Longstaffe, F.J. 1987. Stable isotope studies of diagenetic processes; *in* Stable Isotope Geochemistry of Low Temperature Fluids, Short Course 13, Mineralogical Association of Canada, p.187–257.

——1988. Mineralogical and oxygen-isotope studies of clastic diagenesis: implications for fluid flow in sedimentary basins; *in* Hydrogeology of Sedimentary Basins, Proceedings of the 3rd Annual Canadian/American Conference on Hydrogeology, p.204–220.

——1989. Stable isotopes as tracers in clastic diagenesis; *in* Clastic Diagenesis, Short Course 15, Mineralogical Association of Canada, p. 201–277.

Longstaffe, F.J., Wadleigh, M.A., Frape, S.K. and McNutt, R.H. 1990. Diagenetic evolution of Cambro-Ordovician clastic sedimentary rocks, southwestern Ontario; *in* Geoscience Research Grant Program Summary of Research 1989–1990, Ontario Geological Survey, Miscellaneous Paper 150, p.143–152.

McNutt, R.H., Frape, S.K. and Dollar, P. 1987. A strontium-, oxygen- and hydrogen-isotopic composition of brines, Michigan and Appalachian basins, Ontario and Michigan; Applied Geochemistry, v.2, p.495–506.

O'Neil, J.R., Clayton, R.N. and Mayeda, T.K. 1969. Oxygen isotope fractionation in divalent metal carbonates; Journal of Chemical Physics, v.51, p.5547–5558.

O'Shea, K.J., Miles, M.C., Fritz, P., Frape, S.K. and Lawson, D.E. 1988. Oxygen-18 and carbon-13 in the carbonates of the Salina Formation of southwestern Ontario; Canadian Journal of Earth Sciences, v.25, p.182–194.

Russell, M.J., Hall, A.J., Willan, R.C.R., Allison, I., Anderton, R. and Bowes, G.E. 1984. On the origin of the Aberfeldy celsian + baryte + base-metal deposits, Scotland; *in* Prospecting in Areas of Glaciated Terrain 1984, Institute of Mining and Metallurgy, p.159–170.

Stablein, N.K. and Dapples, E.D. 1977. Feldspars of the Tunnel City Group (Cambrian), western Wisconsin; Journal of Sedimentary Petrology, v.47, p.1512–1538.

Velde, B. and Meunier, A. 1987. Petrological phase equilibria in natural clay systems; *in* Chemistry Monograph 6, p.423–458.

Wadleigh, M.A. and Veizer, J. 1990. Isotope geochemistry of Lower Paleozoic articulate brachiopods; *in* Program with Abstracts, Joint Annual Meeting, Geological Association of Canada–Mineralogical Association of Canada, p.A 136.

Grant 359 Structural Geology and Stratigraphic Correlations in the Midlothian Lake–Peterlong Lake Area, Abitibi Subprovince

---

R.B. Hrabi and H. Helmstaedt

Department of Geological Sciences, Queen's University, Kingston K7L 3N6

The supracrustal Archean rocks of the Midlothian Lake–Peterlong Lake area have been subdivided into five assemblages. Four assemblages are composed of metavolcanic rocks and one, the Midlothian assemblage, is composed of Timiskaming metasedimentary rocks. The pre-Timiskaming metavolcanic rocks are intruded by the Kenogamissi Batholith. The four metavolcanic units have been named after the townships in which they are best developed.

The tholeiitic Beemer assemblage and the overlying calc-alkalic English assemblage are both exposed along the east margin of the Kenogamissi Batholith. The contact between these assemblages is not exposed. The 2727±1.5 Ma age of the English assemblage indicates that it and the underlying Beemer assemblage are the oldest metavolcanic packages in the field area.

The upper contact of the English assemblage is a zone of high strain. The overlying tholeiitic Zavitz–Hutt assemblage is interpreted to have been structurally juxtaposed onto the Beemer assemblage. The age of the Zavitz–Hutt assemblage relative to the English assemblage is not known because they are in structural contact. The old age of the English assemblage compared to the age of most of the metavolcanic rocks from the southern Abitibi Subprovince is taken as evidence that the Zavitz–Hutt assemblage is younger than the English assemblage.

The youngest metavolcanic rocks in the map area belong to the calc-alkalic Halliday assemblage. Its lower contact with the Zavitz–Hutt assemblage is gradational and not marked by any significant zones of high strain. Facing directions in both the Zavitz–Hutt assemblage near the contact and through all of the Halliday assemblage indicate tops to the south. The Halliday assemblage, thus, is interpreted as a south-facing homocline lying conformably or disconformably above the Zavitz–Hutt assemblage.

The stratigraphic relationships proposed here differ from previous correlations. The English and Halliday assemblages were believed to be lateral equivalents and the English assemblage was correlated with significantly younger metavolcanic units elsewhere in the Abitibi Subprovince.

Structural observations in the Midlothian Lake–Peterlong Lake area indicate that the structural history can be divided into five major deformation events:

D1: Development of a narrow zone of high strain at the contact between the calc-alkalic English assemblage and the tholeiitic Zavitz–Hutt assemblage suggesting that the Zavitz–Hutt assemblage was thrust over the English assemblage.

D2: Map-scale folding of the combined Zavitz–Hutt and English package is characterized by east- to northeast-trending axial traces and gently- to moderately-plunging fold axes. An axial-planar foliation is not well-developed.

D3: Deformation associated with the intrusion of the Kenogamissi Batholith. This includes a well-developed foliation in the metavolcanic rocks adjacent to the batholith and a locally-developed crenulation cleavage in previously strained metavolcanic rocks several kilometres from the batholith margin.

D4: Folding of the Timiskaming metasedimentary rocks into an east-trending, asymmetric syncline with no axial planar fabric. However, locally developed spaced cleavage in the metasedimentary rocks along both the north and south contacts with the metavolcanic rocks is interpreted to have formed at this time.

D5: Northeast-trending, steeply-plunging folding resulted in open, map-scale folds and tight, small-scale folds with strong axial-planar foliations. The folds are best expressed in the Timiskaming metasedimentary rocks but the northeast-trending foliation is observed in both the metasedimentary and metavolcanic rocks.

INTRODUCTION

The Midlothian Lake–Peterlong Lake area is located in the southwest corner of the Abitibi greenstone belt, approximately 50 km south of Timmins and 95 km west-southwest of Kirkland Lake (Figure 359.1). The existing geological database was assembled by the Ontario Geological Survey and its predecessors between 1926 and 1984 (Gledhill 1926; Rickaby 1932; Marshall 1947; Abraham 1954; Bright 1970, 1984; Pyke 1978). Two recent geological compilation maps also include the map area (MERQ–OGS 1983; Ontario Geological Survey 1991).

The Archean rocks of the map area have been divided into six assemblages based on similar lithologic associations. Each has been named after the township(s) where it is predominant. The assemblages are described in relative stratigraphic order from oldest to youngest. This order is revised from the previous correlation (MERQ–OGS 1983; Table 359.1). Figure 359.2 illustrates the distribution of supracrustal assemblages and the Kenogamissi Batholith in the Midlothian Lake-Peterlong Lake area.

ASSEMBLAGE DESCRIPTIONS

Beemer Assemblage

This sequence of rocks, located in the Beemer and Semple townships adjacent to the Kenogamissi Batholith, consists of massive to pillowed, Mg-tholeiitic basalt (rock names are based on field criteria originally developed in the Kirkland Lake and Timmins areas (Jensen and Langford 1985; Pyke 1982)). The sequence is folded around protrusions of the batholith, but all facing directions are to the east away from the Kenogamissi Batholith. Near the batholith margin, the metavolcanic rocks are metamorphosed to amphibolite grade, and either the primary structures are strongly flattened, as observed in the horizontal plane, parallel to the batholith margin or a mafic gneiss is developed. The present facing direction of the metavolcanic rocks is largely controlled by reorientation during the intrusion of the Kenogamissi Batholith. The upper contact of the assemblage is either covered by Quaternary glacial deposits or is in intrusive contact with the Muskasenda mafic intrusion.

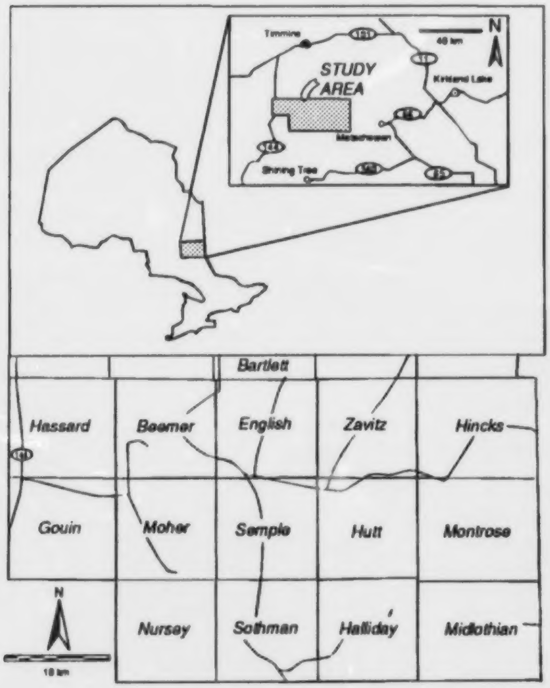

Figure 359.1. Location of study area and townships in study area.

English Assemblage

The rocks of this assemblage are poorly exposed and occupy most of English Township where they overly the Beemer assemblage. They also occur as a thin sequence which extends eastward in the southern part of Zavitz Township. In both areas the rocks are white-weathering, light-green, calc-alkalic intermediate to felsic. In English Township they are tuffs, lapilli tuffs, volcanic breccias and, locally, massive flows. In Zavitz Township, pillowed flows are also present. In addition, discontinuous units of magnetite iron formation are found at several stratigraphic levels and north of the field area in Bartlett Township, a thick unit of ultramafic rock overlies the English assemblage.

Facing directions in the unit are very rare but indicate that the assemblage faces to the southeast in English Township and to the north in the narrow unit in southern Zavitz Township. The Zavitz–Hutt assemblage overlies this package and the contact between them is marked by a narrow, laterally extensive zone of high strain.

A sample from the English assemblage directly north of the field area in Bartlett Township yielded a U–Pb zircon date of 2727±1.5 Ma (Corfu et al. 1989). This is the second oldest date obtained from metavolcanic rocks in the Abitibi greenstone belt in Ontario. The date indicates that the English assemblage is one of the oldest in the map area.

Zavitz–Hutt Assemblage

This assemblage consists of magnesium- and iron-rich tholeiitic pillowed and massive basalt with local units of flow breccia and rare interflow sedimentary rocks. The magnesium- and iron-rich members are interbedded, with units ranging from hundreds of metres to kilometres thick. Some of these thick units of uniform, massive iron-rich tholeiites may be volcanic sills. In addition to these rock types, there is a thin, discontinuous unit of polysutured, carbonate-altered komatiite at the base of the assemblage in east-central English Township.

In Zavitz Township, the unit forms an east-plunging syncline with an east- to northeast-trending axial trace. In

Table 359.1. Previous and revised correlation and stratigraphic order of metavolcanic assemblages in the Midlothian Lake-Peterlong Lake area.

Approximate age	Formation Name (MERQ-OGS 1983)	Assemblage Name (this study)	Revised Stratigraphic Order (this study)
youngest	Middle Fm. of the Tisdale Gp. (Cycle III)	Zavitz-Hutt	Halliday
	Lower Fm. of the Tisdale Gp. (Cycle III)		Zavitz-Hutt
	Upper Fm. (felsic unit) of the Deloro Gp. (Cycle II)	English and Halliday	English
oldest	Upper Fm. (mafic unit) of the Deloro Gp. (Cycle II)	Beemer	Beemer

Note: The dashed line between the English and Zavitz-Hutt assemblages indicates a structural contact. The revised stratigraphic order is only meant to illustrate the relative ages of the metavolcanic assemblages. The assemblages are not correlated with the MERQ-OGS (1983) formations.

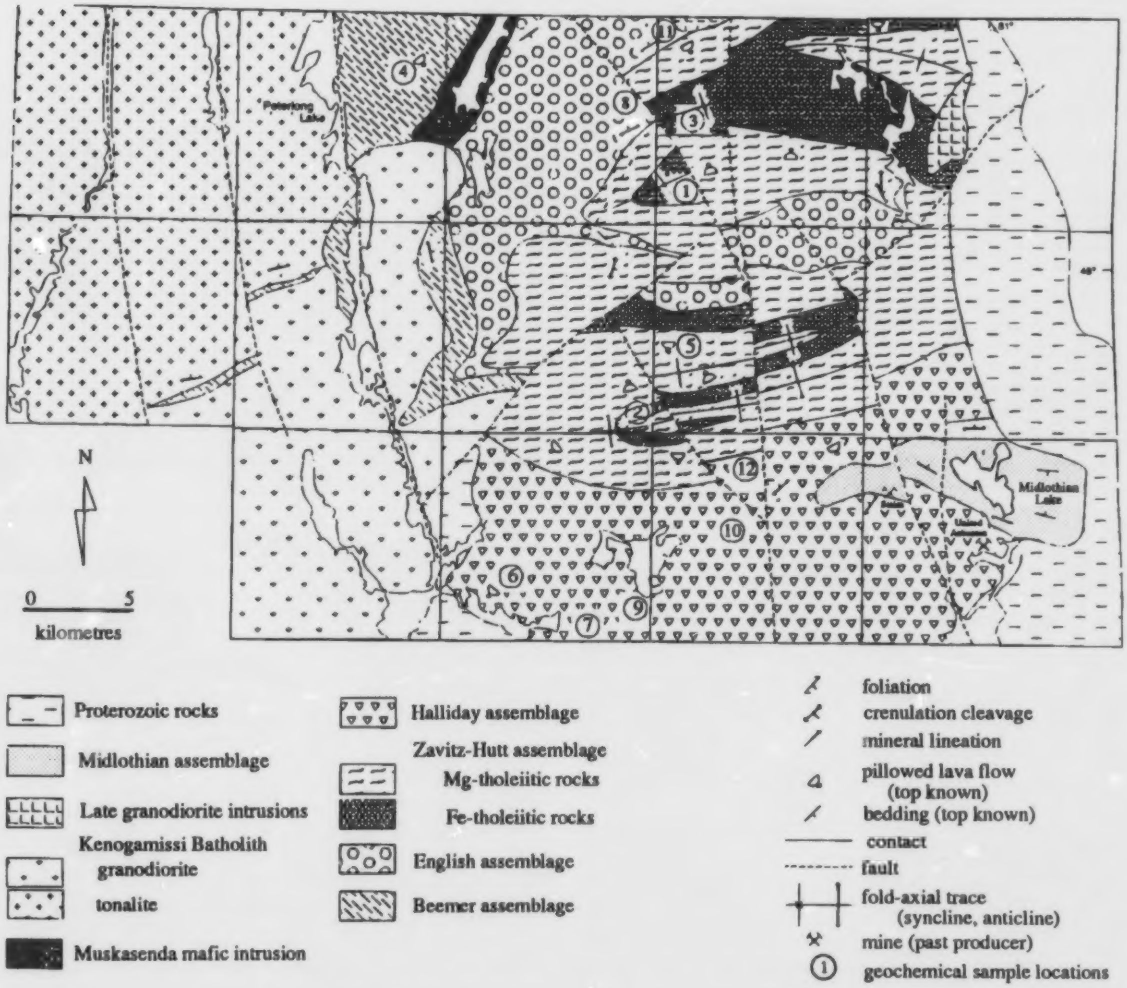
Peterlong Lake
Midlothian Lake
81°
48°
1
2
3
4
5
6
7
8
9
10
11
12
N
0
5
kilometres
Proterozoic rocks
Midlothian assemblage
Late granodiorite intrusions
Kenogamissi Batholith
granodiorite
tonalite
Muskasenda mafic intrusion
Halliday assemblage
Zavitz-Hutt assemblage
Mg-tholeiitic rocks
Fe-tholeiitic rocks
English assemblage
Beemer assemblage
foliation
crenulation cleavage
mineral lineation
pillowed lava flow (top known)
bedding (top known)
contact
fault
fold-axial trace (syncline, anticline)
mine (past producer)
geochemical sample locations

Figure 359.2. Distribution of assemblages within Midlothian Lake–Peterlong Lake area. See Figure 1 for township names.

Semple and Hutt townships, it forms several east- to northeast-trending anticline-syncline pairs. At the southern margin the assemblage faces south and is in stratigraphic contact with the overlying Halliday assemblage.

Halliday Assemblage

The northeastern part of the assemblage, in Midlothian and Montrose townships, consists of calc-alkalic felsic, quartz- and feldspar-phyric tuffs and flows often interlayered with thin beds of mudstone. The central part, in Halliday Township, consists predominantly of calc-alkalic intermediate volcanic breccia to tuffs, massive flows and some hydrothermal or intrusion breccias. The southern part of the Halliday assemblage is composed of pillowed and massive calc-alkalic basalts and andesites. Numerous mafic and ultramafic sills intrude the package in Midlothian Township and along its southern contact. In contrast to the English assemblage, there are no units of iron formation in the Halliday package.

This assemblage has been previously mapped as an anticline (Bright 1970; MERQ–OGS 1983). All reliable younging indicators, however, show that the top is always to the south and suggest that the whole Halliday assemblage is a south-facing homocline. The package is unconformably overlain to the south by Paleoproterozoic sedimentary rocks of the Gowganda Formation.

Midlothian Assemblage

This assemblage is found in Midlothian Township and consists of Timiskaming metasedimentary rocks, similar to those described by Hyde (1980) in the Kirkland Lake area. Common facies include massively-bedded conglomerate, interbedded conglomerate and trough cross-bedded sandstone and interbedded sandstone and mudstone. Conglomerates are heterolithic, poorly-sorted and commonly contain clasts of black chert, quartz, quartz-feldspar porphyry, ultramafic and fuchsite-altered rock in addition to the more common mafic to felsic metavolcanic clasts.

The unit is folded into an upright, asymmetric syncline. The contact of the assemblage with the surrounding metavolcanic rocks is poorly exposed and no clear depositional unconformity was found.

Kenogamissi Batholith

This composite batholith occupies the west half of the map area and is composed of biotite to hornblende tonalite, granodiorite and diorite. None of the phases of the batholith has been dated. Structural relationships, however, indicate that the biotite to hornblende tonalite is the oldest phase and is intruded by the younger granodiorite.

The tonalite is highly strained at the contact with the granodiorite and along much of the contact metavolcanic rocks and iron formation form a narrow, highly-strained unit between the two phases. The wide metamorphic aureole within the adjacent metavolcanic rocks contrasts with the narrow aureole around the Round Lake Batholith, which has been interpreted as a solid-state diapir (Jackson and Harrap 1989).

Geochemistry

Samples with minimal alteration were collected from all the metavolcanic and intrusive assemblages within the map area. These samples are presently being analyzed for major elements, trace elements and rare earth elements by X-ray fluoresence spectroscopy and instrumental neutron activation analysis. These data will be used to substantiate the field subdivision of the rocks and to petrogenetically subdivide the rocks. A preliminary analysis of major elements on a subset of these samples has been completed with the results shown in Table 359.2, sample locations are shown in Figure 359.2. The results plotted on an AFM diagram (Figure 359.3) clearly differentiate the calc-alkalic English and Halliday assemblages from the tholeiitic Beemer and Zavitz–Hutt assemblages. Analysis of all the data may allow individual assemblages to be distinguished by geochemical methods.

Table 359.2. Major element composition of representative samples from metavolcanic assemblages. See Figure 2 for sample locations.

Sample	Rock Type	SiO_2	TiO_2	Al_2O_3	Fe_2O_3	MnO	MgO	CaO	Na_2O	K_2O	P_2O_5	LOI	Total
1	tholeiitic	50.23	1.28	13.69	14.40	0.19	6.57	8.87	2.85	0.82	0.11	0.90	99.91
2	tholeiitic	51.61	2.14	11.17	18.40	0.23	2.65	6.50	3.11	0.34	0.76	2.33	99.24
3	tholeiitic	52.42	1.79	12.18	16.61	0.27	3.34	4.69	5.05	0.36	0.14	2.65	99.50
4	tholeiitic	45.77	0.95	12.75	13.25	0.19	4.82	10.71	1.25	0.04	0.08	9.05	98.86
5	tholeiitic	46.30	0.68	15.97	10.99	0.26	5.45	12.95	1.98	0.08	0.06	5.40	100.12
6	calc-alkalic	64.26	0.61	15.21	5.80	0.06	2.83	4.53	2.69	1.77	0.20	2.21	100.17
7	calc-alkalic	58.33	0.87	16.59	6.70	0.12	4.03	6.10	4.63	0.19	0.17	3.67	101.40
8	calc-alkalic	60.47	0.51	14.16	6.24	0.11	1.83	4.33	3.33	1.54	0.13	5.25	97.90
9	calc-alkalic	60.52	0.60	17.13	6.09	0.08	3.32	6.77	3.13	0.62	0.13	2.52	100.91
10	calc-alkalic	64.73	0.51	14.60	3.80	0.07	1.17	3.39	3.83	2.09	0.15	4.01	98.35
11	calc-alkalic	66.27	0.43	15.89	3.17	0.04	1.87	2.06	6.41	1.01	0.16	1.89	99.20
12	calc-alkalic	73.13	0.19	10.02	2.83	0.10	1.26	2.41	1.28	2.99	0.03	4.70	98.94

Note: All elements in weight percent.

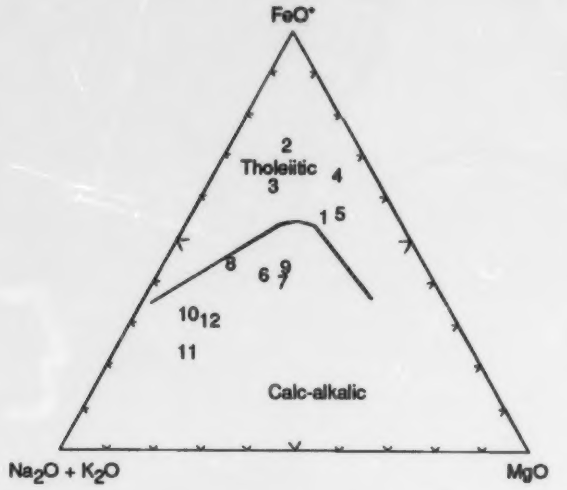

Figure 359.3. AFM diagram of analyses of representative samples from all metavolcanic assemblages. FeO* = Fe_2O_3 * 0.89981. Locations of samples are shown on Figure 2.

STRUCTURAL HISTORY

D1

The earliest deformation seen in the map area is a narrow zone of high strain along the contact between the English and Zavitz–Hutt assemblages which is continuous around the nose of the large syncline in Zavitz Township (Figure 359.2). This zone has been extended as far east as the Zavitz–Hincks township boundary. The deformation fabrics form irregular compositional banding resembling a mafic gneiss (Photo 359.1) and, in the nose of the syncline, a very well-developed, shallowly-dipping penetrative foliation (Photo 359.2). Kinematic indicators in the high strain zone are very rare and consist of variably-plunging, minor S-folds around both limbs of the D2 syncline in Zavitz Township.

D2

The second deformation consists of map-scale folds with east- to northeast-trending axial traces and gently- to moderately-plunging fold axes. Within the folds, foliation patterns can be irregular, but observations do not suggest an early axial planar foliation developed during this folding event. The D1 foliations are folded around the syncline in Zavitz Township (*see* Figure 359.2). The pole to the best fit great circle roughly corresponds to the fold axis of the syncline (*see* Figure 359.4a). Mineral lineations on these foliations have little variation and form a tight cluster (*see* Figure 359.4b). This coincides with the pole to the best-fit great circle to the foliation and indicates that they have been reoriented parallel to the fold axis. The tholeiitic Zavitz–Hutt assemblage was folded at this time whereas the calc-alkalic Halliday assemblage was simply rotated to become a south-facing homocline.

D3

This deformation includes all the structures associated with the intrusion of the Kenogamissi Batholith. Generally, both the tonalite and granodiorite have only weakly developed foliations. However, the tonalite has a very strong fabric locallized only at the contact with the granodiorite, while the granodiorite is only weakly deformed. This deformation indicates that the granodiorite phase is later than the tonalite phase.

Both intrusion phases of the batholith imposed a wide structural and metamorphic aureole on the country rocks, but differentiating the effects of these two phases was not possible. Pre-intrusion structural features can no longer be distinguished near the batholith. Primary volcanic features such as pillows can be recognized sporadically near the contact, but, observed on a horizontal plane, they are strongly flattened. In general,

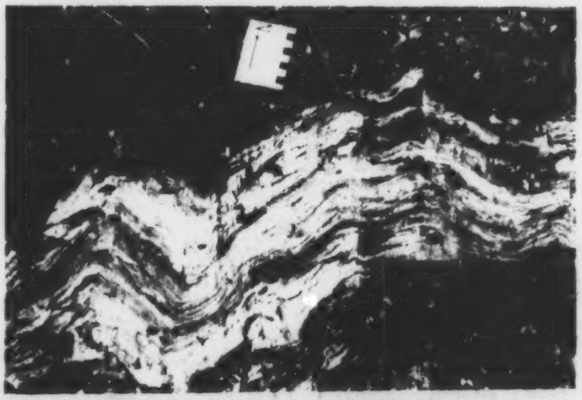

Photograph 359.1. Well-developed compositional banding in metavolcanic rocks at the contact between the English and Zavitz–Hutt assemblages. Photo taken along logging road in northwest Zavitz Township, south of Geikie Pluton.

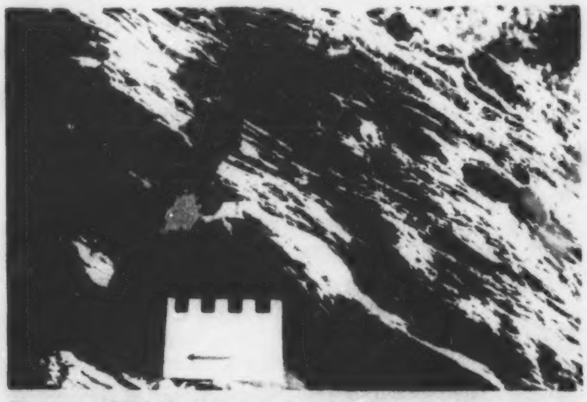

Photograph 359.2. Vertical outcrop face of metavolcanic rock at the contact between the English and Zavitz–Hutt assemblages. Well-developed foliation dips gently to northeast. Photo taken along Papakomeka Road at the English–Semple township boundary.

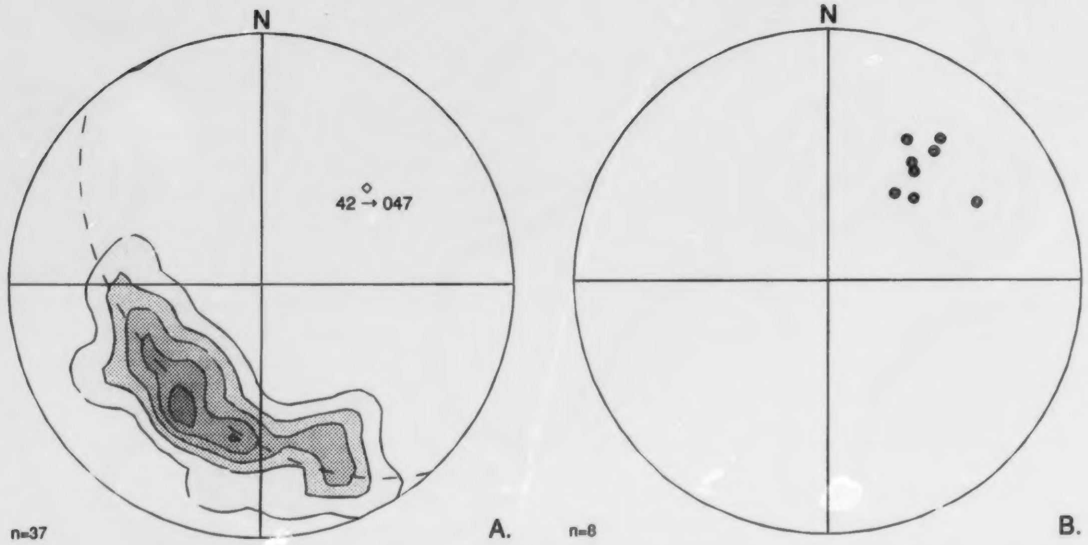

Figure 359.4.a) Contoured equal-area stereonet of poles to D1 foliation. Diamond marks the pole (trend 047°, plunge 42° to the best-fit great circle and represents the D2 fold axis. b) Equal-area stereonet of D1 mineral lineations.

the intrusion of the batholith caused metavolcanic rocks near the batholith margin to be deformed and metamorphosed to amphibolite-grade highly foliated or gneissic rocks.

A strong north-trending crenulation cleavage is also found in mafic and felsic metavolcanic rocks near the English–Zavitz township boundary. The crenulation cleavage is grouped with the D3 deformation event because it cross-cuts opposing limbs of D2 folds, trends parallel to the batholith margin and is consistent with the orientation of foliations in metavolcanic rocks adjacent to the batholith (*see* Figure 359.5).

D4

Following their deposition in Midlothian Township, Timiskaming metasedimentary rocks were folded into an approximately east-trending asymmetric syncline. No axial planar foliation was found in the core of the fold. However, based on alignment of chlorite, sericite or fuchsite, there is, a strong, spaced cleavage, found near both the north and south metasedimentary–metavolcanic contacts. These structures may be due to structural reactivation along the contact during folding. Another effect associated with this deformation event is north-dipping reverse faults in ultramafic intrusions in Midlothian Township.

D5

Several related structures were formed during this deformation event. First, bedding planes within the Timiskaming metasedimentary rocks are openly folded about a steeply-plunging fold axis trending 044° plunging 77° (Figure 359.6). The D4 spaced cleavage is folded about a similar fold axis although the pattern is not as well developed. Second, outcrop-scale, northeast-trending, steeply-plunging folds with tight interlimb angles were observed which have similar orientations as the first structure. These smaller folds are bisected by a strong, anastomosing, closely-spaced axial-planar cleavage. The D5 folds are generally observed only in the metasedimentary section but the cleavage is observed in both metavolcanic and metasedimentary rocks. O'Hanley (1988) studied extensional asbestos veins at the past-producing United Asbestos Mine in Midlothian Township. He concluded that the asbestos veins were formed during a northwest-southeast compression with the ±1 closer to the horizontal than the vertical. This is consistent with formation during the D5 deformation event.

Late Faults

Late north- to northwest-trending brittle faults, with left-lateral separation of up to 6 km, are the last deformation features observed in the map area. These faults have been reactivated in the Proterozoic since they displace Proterozoic Abitibi dykes less than the Archean Kenogamissi Batholith-metavolcanic contact and they have been observed to deform Huronian Gowganda sedimentary rocks to the east of the map area (Powell et al. 1990).

Comparison with Other Structural Studies in Abitibi Subprovince

Several structural studies based in the Matachewan, Timmins and Kirkland Lake area (Powell et al. 1990; Piroshco and

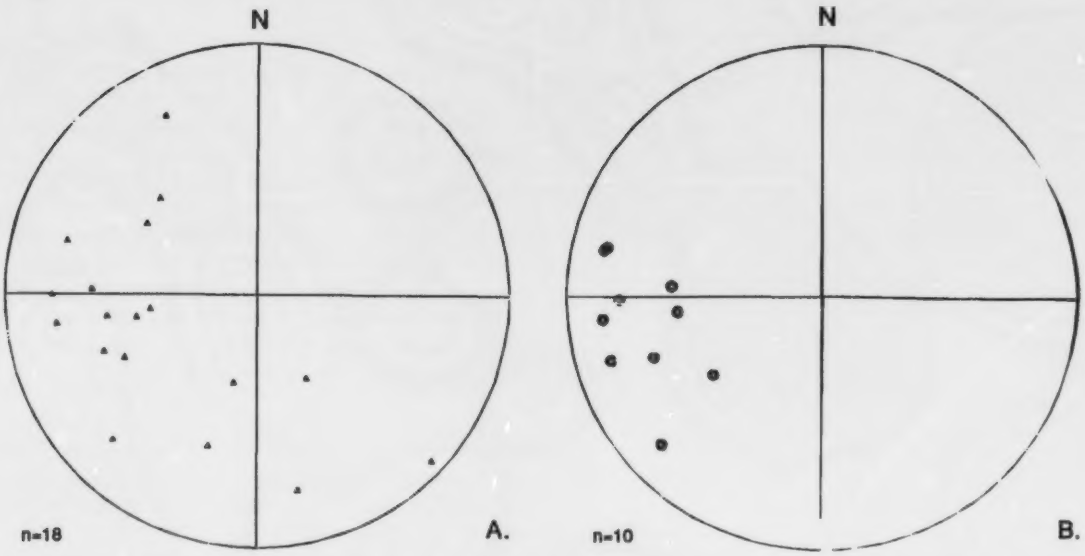

Figure 359.5.a) Equal-area stereonet of poles to D3 foliation in metavolcanic rocks adjacent to Kenogamissi Batholith. Variation in orientation due to syn-intrusion folding around protrusions of the batholith. b) Equal-area stereonet of poles to crenulation cleavage in highly strained metavolcanic rocks several kilometres from Kenogamissi Batholith. The orientation of these foliations are similar to those adjacent to the Kenogamissi Batholith.

Kettles 1988; Hodgson and Hamilton 1989) have recently been completed and have documented similar structural events to this study (Table 359.3).

All the studies recognize pre-Timiskaming deformation events, generally as early folding of the metavolcanic rocks with no associated axial-planar cleavage. In addition, an earlier structural juxtaposition of metavolcanic assemblages is recognized in this study. These early deformation events may be a result of initial tectonic assembly of the Abitibi Subprovince. Specific deformation events related to magmatic intrusion were not observed in the Timmins or Kirkland Lake studies. Later deformation common to all studies includes folding of Timiskaming metasedimentary rocks into upright homoclines or synclines, followed by formation of northeast-trending folds and foliations.

REGIONAL STRATIGRAPHY OF SUPRACRUSTAL ASSEMBLAGES

Previous Stratigraphic Correlations

The only previous attempt at correlation of the metavolcanic rocks in the map area was the MERQ–OGS (1983) Lithostratigraphic Map of the Abitibi Subprovince. This compilation is based on a subdivision of the metavolcanic rocks into four cycles. The upper three cycles are composed of a lower division of ultramafic volcanic rocks, a central division of tholeiitic metavolcanic rocks and an upper division of varied calc-alkalic metavolcanic rocks. The upper two cycles also have an alkalic division at the top of the cycle. The lowest cycle consists only of the upper varied calc-alkalic division. On the MERQ–OGS (1983) map the rocks belonging to the Beemer assemblage were included in a mafic part of the calc-alkalic division of cycle II (Upper Formation of the Deloro Group, *see* Table 359.1). Jensen and Langford (1985) show the Beemer assemblage as part of the tholeiitic division of cycle II (Middle Formation of the Deloro Group). Both the English and Halliday assemblages are included in felsic part of the calc-alkalic division of cycle II (Upper Formation of the Deloro Group). The Zavitz–Hutt assemblage forms both the ultramafic and tholeiitic divisions of cycle III (Lower and Middle Formations of the Tisdale Group). Cycles I and IV are not present in the map area.

Several problems exist with this correlation:

- Initial geochemical data indicate that the Beemer assemblage is tholeiitic, not calc-alkalic;
- The U–Pb date from the English assemblage of 2727±1.5 Ma is significantly older than any other date from the calc-alkalic division of Cycle II;
- There are lithologic differences between the English and Halliday assemblages, most notably the lack of iron formation in the Halliday assemblage, which indicate that these assemblages should not be correlated;
- The contact of the English and Zavitz–Hutt assemblages is very sharp and is marked by a narrow but laterally persistent zone of high strain which follows the contact around a large D2 fold in English and Zavitz township and has been traced to the Zavitz–Hincks township

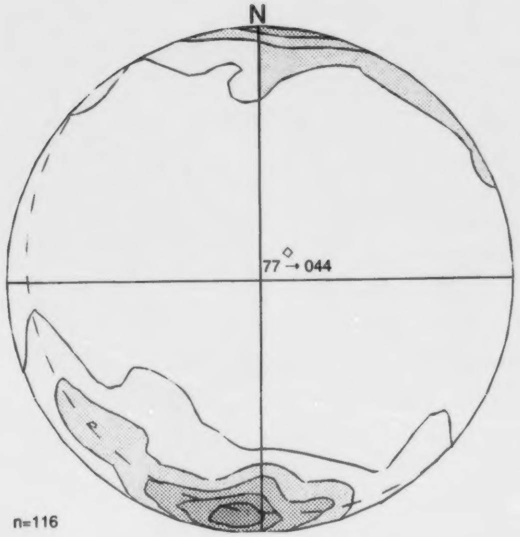

Figure 359.6. Contoured equal-area stereonet of poles to bedding in metasedimentary rocks of the Midlothian assemblage. Diamond marks the pole (trend 044°, plunge 77°) to the best-fit great circle and represents the D5 fold axis.

boundary. Whereas facing directions within the two assemblages do not conflict with each other, the two assemblages are in structural contact, making the original stratigraphic relationship between the two unclear;

- The southern contact of the Zavitz–Hutt assemblage with the Halliday assemblage is gradational and the contact is not marked by any significant zones of high strain. Facing-directions from pillows in the Zavitz–Hutt assemblage immediately north of the contact are to the south. In the Halliday assemblage all facing directions from pillows and sedimentary structures in volcaniclastic rocks are also to the south. These observations suggest that the Halliday assemblage is a south-facing homocline which is younger than the Zavitz–Hutt assemblage.

Revised Stratigraphy of the Map Area

The contact between the Beemer and the English assemblage is not exposed because there is extensive Quaternary glacial cover and a large mafic intrusion that occurs along the contact. With no evidence to contradict its present correlation, the Beemer unit is retained as an older assemblage stratigraphically below the English assemblage. The 2727±1.5 Ma (Corfu et al. 1989) date from the English assemblage and the position of both the English and Beemer packages on the margin of the Kenogamissi Batholith suggest that they are parts of older volcanic belts which have been tectonically uplifted and exposed by the intrusion. Jackson and Fyon (in press) note that this situation is similar to that of the Pacaud assemblage at the margin of the Round Lake Batholith.

The Zavitz–Hutt assemblage is in tectonic contact with the English assemblage. Thrusting of the Zavitz–Hutt assemblage onto the English assemblage is most consistent with the structural observations. The combination of a structural contact and the lack of an age determination from the Zavitz–Hutt assemblage does not further constrain the age of this assemblage. However, considering the old age of the English assemblage compared to the majority of the metavolcanic rocks from the southern Abitibi subprovince, the Zavitz–Hutt assemblage is interpreted to be younger than the English assemblage.

The clear stratigraphic relationship between the Zavitz–Hutt and Halliday assemblage permits the conclusion that the Halliday package is younger than the Zavitz–Hutt unit, lies stratigraphically above it and is the youngest metavolcanic assemblage in the map area.

Stratigraphic Correlations within the Southern Abitibi Subprovince

Based on several criteria, such as U–Pb zircon dating, lithologic associations and magnetic characteristics, Jackson and Fyon (in press) have proposed new correlations of the metavolcanic assemblages within the Abitibi Subprovince. Those from the southern Abitibi Subprovince are summarized in Table 359.4. The map area is included in this compilation. All of the assemblages described in this report are either

Table 359.3. Proposed correlation of deformation events interpreted in the southern Abitibi Subprovince.

this study	**Matachewan Area Powell et al. (1990)**	**Timmins Area Piroshco and Kettles (1988)**	**Kirkland Lake Area Hodgeson and Hamilton (1989)**
D1	–	–	–
D2	Da1	D0	D0
D3	Da2	–	–
D4	Da3	D1	
	Da4	D2	D1
D5	Da5	D3	D2

Table 359.4. Correlation of metavolcanic assemblages in the southern Abitibi Subprovince.

Approximate age age	Assemblage Name	
	within field area	outside of field area
youngest	Midlothian	Timiskaming, Rideout
	Halliday	Skead (2701^{+3}_{-2}), Gauthier
	Bowman (Zavitz–Hutt)	Larder (2705±2)
	Bartlett (2727±1.5) (English)	Eldorado, Boston
oldest	Peterlong (Beemer)	Catherine (2720±?)

Note: Where they differ assemblage names used in this report for the Midlothian Lake–Peterlong Lake area are in brackets. Dates of assemblages from Corfu et al. (1989) except date from Catherine assemblage from Jackson and Fyon (in press). Compiled from Jackson and Fyon (in press).

equivalent to those described by Jackson and Fyon (in press) or form a part of their larger assemblages. In general the lithologic and structural relationships observed in the map area support this new correlation. However, their correlation of the Peterlong (Beemer) assemblage with the Catherine assemblage is problematic. Both these assemblages form "older" metavolcanic groups but, the 2727± 1.5 Ma Bartlett (English) assemblage, which overlies the Peterlong assemblage, is older than the 2720 Ma Catherine assemblage. However, as already mentioned, the Peterlong–Bartlett contact is not exposed and there is the possibility that these assemblages are structurally juxtaposed.

Several similar structural relationships exist between the map area and the metavolcanic rocks south of Kirkland Lake and west of the Round Lake Batholith. South of Kirkland Lake, an unnamed fault juxtaposes the tholeiitic rocks of the Catherine group against the underlying Wabewawa and Pacaud assemblages (Jackson and Harrap 1989). A permissible correlation of the Zavitz–Hutt assemblage is with the Catherine assemblage. The structural relationship with the underlying assemblages is therefore the same for both the Zavitz–Hutt and Catherine assemblages. The contact between the Catherine assemblage and the overlying Skead assemblage exhibits both depositional and deformational features and has been interpreted as a sheared primary contact (Jackson and Harrap 1989). The original depositional nature of this contact is the same as the contact between the Zavitz–Hutt assemblage and the overlying Halliday assemblage in the map area.

ACKNOWLEDGEMENTS

We would like to thank Andy Fyon (Ontario Geological Survey, Sudbury) for assistance throughout this project, staff of Resident Geologists offices in Timmins and Kirkland Lake for all their help during the summer and Bob Foster and Al Grant (Queen's University, Kingston) for the geochemical analyses.

REFERENCES

Abraham, E.M. 1954. Geology of Sothman Township, District of Sudbury; Ontario Department of Mines, v.62, pt.6, 36p.

Bright, E.G. 1970. Geology of Halliday and Midlothian Townships, Districts of Sudbury and Timiskaming; Ontario Department of Mines, Geological Report 79, 33p.

—— 1984. Geology of the Ferrier Lake–Canoeshed Lake Area, District of Sudbury; Ontario Geological Survey, Report 231, 60p.

Corfu, F., Krogh, T.E., Kwok, Y.Y., and Jensen, L.S. 1989. U–Pb zircon geochronology in the southwestern Abitibi greenstone belt, Superior Province; Canadian Journal of Earth Sciences, v.26, p.1747–1763.

Gledhill, T.L. 1926. Grassy River Area, District of Sudbury; Ontario Department of Mines, v.35, pt.6, p.57–76.

Hodgson, C.J. and Hamilton, J.V. 1989. Gold mineralization in the Abitibi greenstone belt: end-stage result of Archean collisional tectonics; *in* The Geology of Gold Deposits: The Perspective in 1988, Economic Geology, Monograph 6, p.86–100.

Hyde, R.S. 1980. Sedimentary facies in the Archean Timiskaming Group and their tectonic implications, Abitibi greenstone belt, northeastern Ontario, Canada; Precambrian Research, v.12, p.161–195.

Jackson S.L. and Harrap, R.M. 1989. Geology of Parts of Pacaud, Catharine, and Southernmost Boston and McElroy Townships; Ontario Geological Survey, Miscellaneous Paper 146, p.125–131.

Jackson, S.L. and Fyon, A.J. in press. The Abitibi Subprovince in Ontario; *in* Geology of Ontario, Ontario Geological Survey, Special Publication Number 4.

Jensen, L.S and Langford, F.F. 1985. Geology and petrogenesis of the Archean Abitibi Belt in the Kirkland Lake area, Ontario; Ontario Geological Survey, Miscellaneous Paper 123, 130p.

Marshall, H.I. 1947. Geology of Midlothian Township, District of Timiskaming; Ontario Department of Mines, v.56, pt.5, 24p.

MERQ–OGS. 1983. Lithostratigraphic map of the Abitibi Sub-Province; Ministère de l'Énergie et des Ressources du Québec – Ontario Geological Survey, DV 83-16, Map 2484, scale 1:500 000.

O'Hanley, D.S. 1988. Field Investigations at the United Asbestos deposit, Midlothian Township, District of Timiskaming; Ontario Geological Survey, Miscellaneous Paper 141, p.219–221.

Ontario Geological Survey. 1991. Bedrock geology of Ontario, east-central sheet; Ontario Geological Survey, Map 2543, scale 1:1 000 000.

Piroshco, D. and Kettles, K. 1988. Geology of Tisdale and north Whitney townships, District of Cochrane; *in* Summary of Field Work and Other Activities 1988, Ontario Geological Survey, Miscellaneous Paper 141, p.197–205.

Powell, W.G., Hodgson, C.J. and Carmichael, D.M. 1990. Tectono-metamorphic Character of the Matachewan Area, Northeast Ontario. Ontario Geological Survey, Miscellaneous Paper 150, p.56–65.

Pyke, D.R. 1978. Geology of the Peterlong Lake Area, Districts of Timiskaming and Sudbury; Ontario Geological Survey, Report 171, 53p.

—— 1982. Geology of the Timmins Area, District of Cochrane; Ontario Geological Survey, Report 219, 141p.

Rickaby, H.C. 1932. Bannockburn Gold Area, District of Timiskaming; Ontario Department of Mines, v.41, pt.2, p.1–24.

Grant 363 Seismotectonic Framework and Microearthquake Monitoring Program in the Western Lake Ontario Region: a Progress Report

A.A. Mohajer, H.C. Halls and R. McGrory

Department of Geology, University of Toronto Erindale Campus, Mississauga, Ontario.

Microseismic monitoring of the Burlington-Hamilton-Niagara area was begun in 1989. After an extensive background noise survey at 30 test sites, the three most favourable locations were selected and a three-station network with digital recording systems, set in the trigger mode of operation, were deployed. Since then, 1500 triggered events have been recorded by this network. The results of the evaluation of this microseismic data show that 95 of the recorded events were not quarry blasts as they occurred at night, 3 events of this group were recorded at more than one station, and events of $M \geq 1$ can be detected at distances up to 50 km. Pattern recognition, timing of the events and response spectra characteristics were used to identify natural events from false triggers and unscheduled blasts during the day time. So far, the project has demonstrated that microseismic monitoring can be conducted in suburban and moderately developed areas, that microearthquakes do occur in southern Ontario and that these events can be detected and discriminated by a properly designed and instrumented seismic network.

INTRODUCTION

Parts of the Canadian Shield, covering central and eastern Canada, are generally known as being among the most stable continental land masses of the world with little concern for earthquake hazards. However, recent large magnitude earthquakes, such as the 1985, Mb6.9 Nahanni and the 1988, Mblg6.5 Saguenay earthquakes, have occurred in "unexpected" areas of the central and eastern Canadian craton. The 1989 Mb6.2 Ungava (Quebec) earthquake produced the first reported surface faulting in eastern North America. Unexpected earthquake locations and recent developments in the multidisciplinary approach to seismotectonic investigations point to the need for studying geology and geophysics and integrating the results with seismicity data. This approach has been followed by compilation of all available geological information and by utilization of a microearthquake monitoring program in order to improve assessment of seismic hazards in southern Ontario.

More than 30 earthquakes ($M<5$) were reported in southwestern Ontario during the 19th and the first half of the 20th centuries. More recently, a series of small magnitude ($M<3.5$) events at the western end of Lake Ontario, around Burlington, in the mid 1970's, an earthquake of M3.4 in July 1987 and two recent ones of M3.3 and M2.2 that occurred beneath Lake Ontario in August 1989, have raised concerns regarding their source parameters and potential to generate future large magnitude events.

In order to confirm seismotectonic relations in the region, a program of microearthquake monitoring was started in April 1989. First an extensive background noise survey at 30 test sites was performed to select the most suitable sites for permanent monitoring of small magnitude microseismic events (Mohajer and Halls 1990). Although the background noise was dominated by industrial activity and heavy traffic in highly developed areas of southern Ontario, a few relatively quiet sites were found which yielded acceptable levels of noise for the intended detection of local microearthquakes (*see* Figure 363.1). This report describes the progress made during the second year of the study.

REGIONAL SETTING

The study area is located at the western end of Lake Ontario in the Burlington-Hamilton-Niagara region (*see* Figure 363.1). The region is underlain by Paleozoic rocks of Ordovician and Silurian age that rest unconformably on a Precambrian basement. These Precambrian rocks are part of the Central Gneiss Belt of the Grenville Province. A thin layer of Quaternary materials overlies the Paleozoic sequence, generally obscuring the bedrock surface. Few major faults have been mapped in the area, but several stress relief features have been identified both onshore (White et al. 1974) and in the bottom of Lake Ontario (Thomas et al., in press). A number of lineaments have been interpreted from remote sensing data and from the total-field aeromagnetic map (Geological Survey of Canada 1987) and are illustrated in Figure 363.1.

A major linear aeromagnetic anomaly, informally named the Niagara–Pickering magnetic lineament, crosses

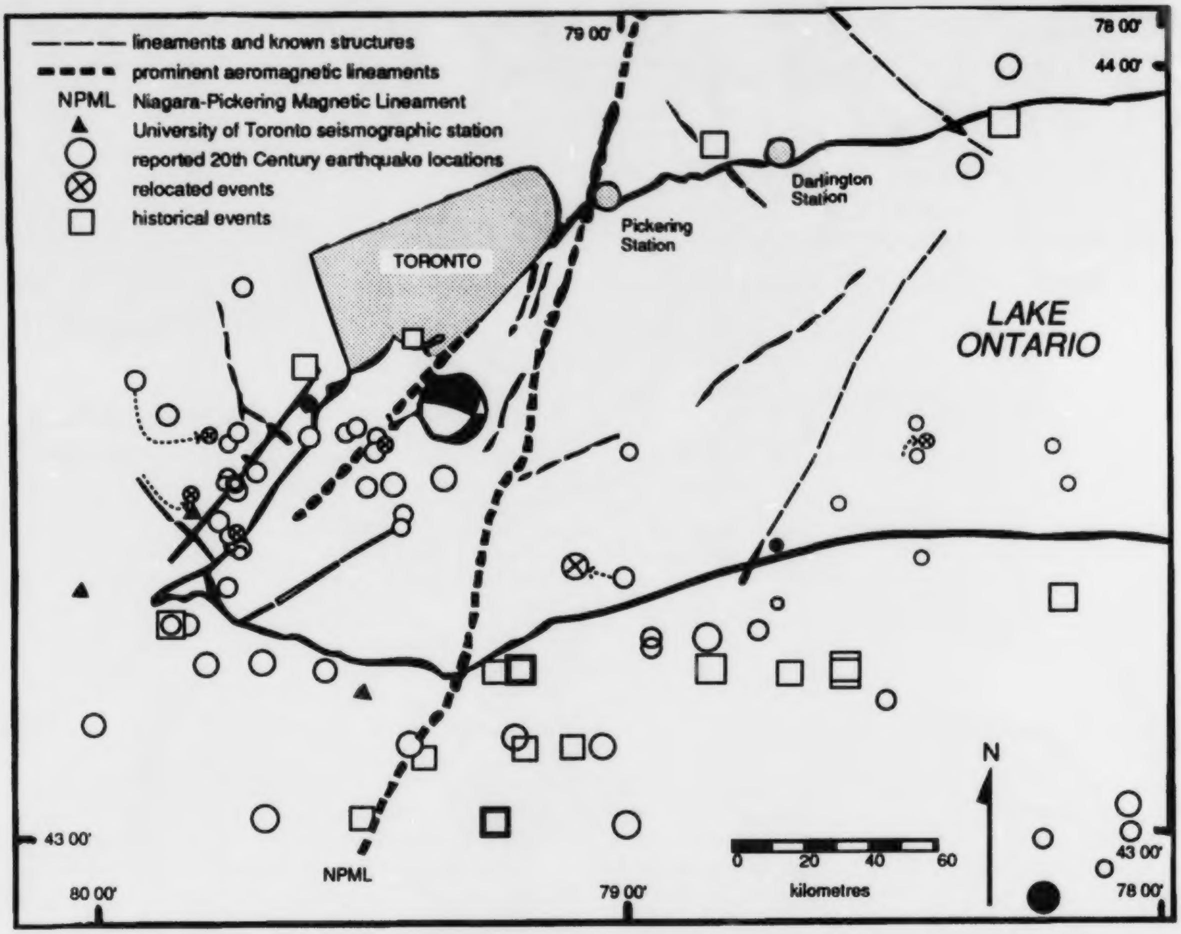
lineaments and known structures
prominent aeromagnetic lineaments
NPML Niagara-Pickering Magnetic Lineament
University of Toronto seismographic station
reported 20th Century earthquake locations
relocated events
historical events
TORONTO
Pickering Station
Darlington Station
LAKE ONTARIO
NPML
79 00'
78 00'
44 00'
43 00'
80 00'
0 20 40 60
kilometres
N

Figure 363.1 A compilation of the well located seismic events of the western Lake Ontario region and locations of the University of Toronto seismographic stations.

the western end of Lake Ontario and passes beneath the north shoreline of the lake just to the east of Toronto. This feature is identified on the Bedrock Geology Map of Ontario (Ontario Geological Survey 1991) as a fault that is traceable in the subsurface and is the southern extension of the Central Metasedimentary Belt Boundary Zone (CMBBZ). The CMBBZ separates the Central Metasedimentary Belt from the Central Gneiss Belt, two subprovinces in the Grenville Province. Hanmer (1988) indicated that the CMBBZ is marked by northwest overthrusting and concluded that it formed as a ductile fault zone about 1060 Ma ago. Minor structures along the zone reflect both the kinematics and the ductile conditions existing during its formation (Hanmer and Ciesielki 1984). Evidence of more recent brittle faulting has been found in the Precambrian rocks and in the Paleozoic strata exposed in the Coboconk Quarry which lies along the trace of the CMBBZ to the east of Lake Simcoe (Wallach and Mohajer 1990).

Thomas et al. (in press) have identified a second prominent aeromagnetic lineament that trends southwest from Toronto toward Hamilton (Burlington-Toronto aeromagnetic lineament) (*see* Figure 363.1). Adams and Basham (1989) proposed a speculative model that extended the St. Lawrence Rift valley through Lake Ontario and across the southern part of the study area (*see* Figure 363.2). This rift model was originally postulated to explain the distribution of major seismic activity in eastern Canada.

ANALYSIS OF THE RECORDED MICROSEISMIC EVENTS

In order to confirm seismotectonic relations in the western Lake Ontario region, a program of microearthquake monitoring was started in April 1989. Suitable sites were selected based on the results of an extensive background noise survey that was conducted in the first year of the study (Mohajer and Halls 1990). A seismographic network consisting of three station with a 40 km aperture has been deployed at the most favourable locations namely, Mt. Nemo (10 km north of Burlington), Rockton (16 km east of Cambridge) and Grimsby (4 km south of

Grimsby town centre, Niagara peninsula). The seismometers were placed directly on the bedrock surface and the digital recording systems were set for the triggered mode of operation.

The results to date show that a total of 1500 triggered events were recorded by this network. Most of the recorded events are quarry blasts or local non-tectonic disturbances, although several natural events have been identified. The detection threshold of the network is capable of distinguishing M≥1 events at distances up to 50 km. These small magnitude earthquakes are presumably more frequent than the larger ones. Nevertheless, the detection of this level of seismicity requires local instrumental coverage, therefore, they are usually undetected by the wider spaced regional networks.

Pattern recognition, timing of the events and response spectra characteristics were used to identify natural events from false triggers and unscheduled quarry blasts. A total of 95 events, which were not quarry blasts, were recorded in the hours between 6 PM and 8 AM (*see examples* Table 363.1). Among this group, 3 triggered events were recorded at more than one station. This means that their magnitude was large enough to be detected at a regional scale and, therefore, it is unlikely that they were false triggers or local disturbances.

A comparison of the power spectra of a known quarry blast with that typical of events occurring late at night or in early morning is illustrated in Figures 363.3 and 363.4. Figure 363.4 also illustrates the relatively rapid drop of amplitude response in the blast power spectrum in comparison with the natural event. It appears that the higher frequency range of the power spectra for quarry blasts decrease more sharply, indicating a lack of energy in high frequency for quarry blasts as compared to earthquakes.

The power spectrum is a combined effect of both source, including primary and secondary wave (scattering) sources, and the recording site. Since the site effect is constant for a single station and the secondary sources are statistically common if the sample area of the coda waves is roughly the same, the observed difference in power spectral shape between quarry blasts and other recorded events (possibly earthquakes) reflects the difference between the two sources. Thus, the difference in power spectra can be used for seismic discrimination between quarry blasts and earthquakes.

It was also observed that the coda decay is significantly higher for quarry blasts than local small magnitude events. This difference, however, disappears for the higher frequencies (e.g. 6 to 12 Hz). This phenomenon may be related to the greater contribution of surface waves to quarry blasts due to the extreme shallowness of their source depth. This suggests

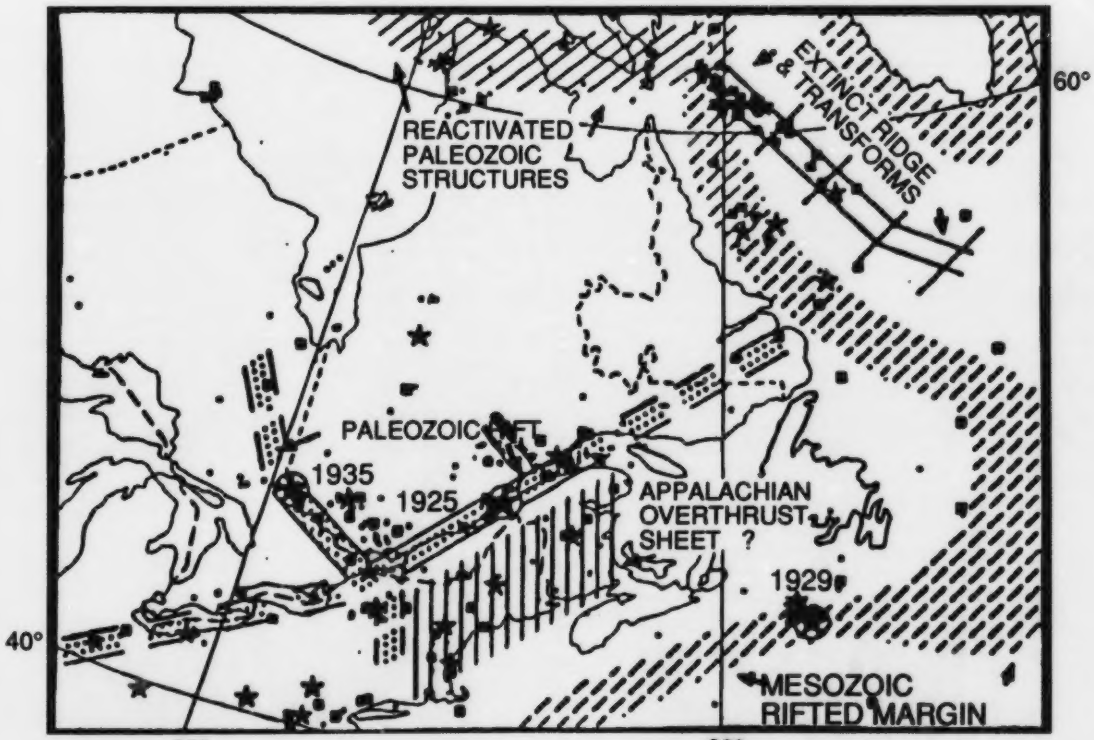

Figure 363.2 Speculative model suggesting extension of the St.Lawrence rift zone across Lake Ontario (after Adams and Basham 1989).

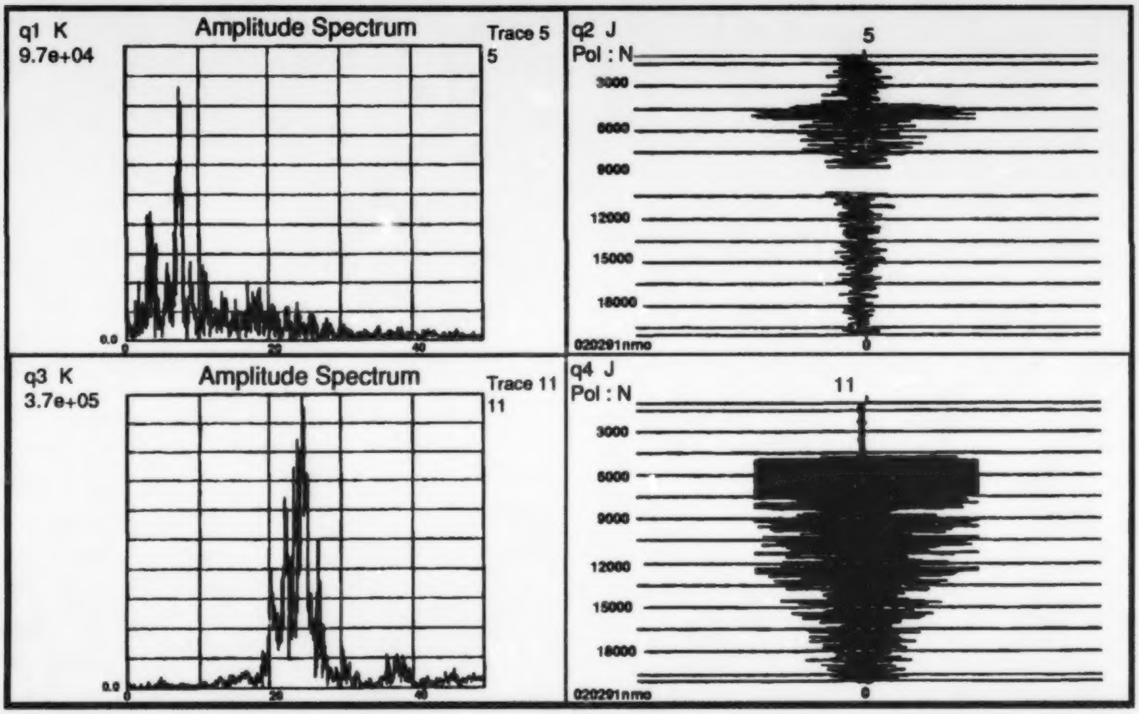

Figure 363.3 Examples of the events recorded in more than one station. Trace 5 is a typical event of Mn=1 (Nuttli or MbLg equivalent to ML, local magnitude scale for eastern North America) recorded at a distance of about 30 km. Trace 11 is a typical quarry blast with equivalent Mn=2.

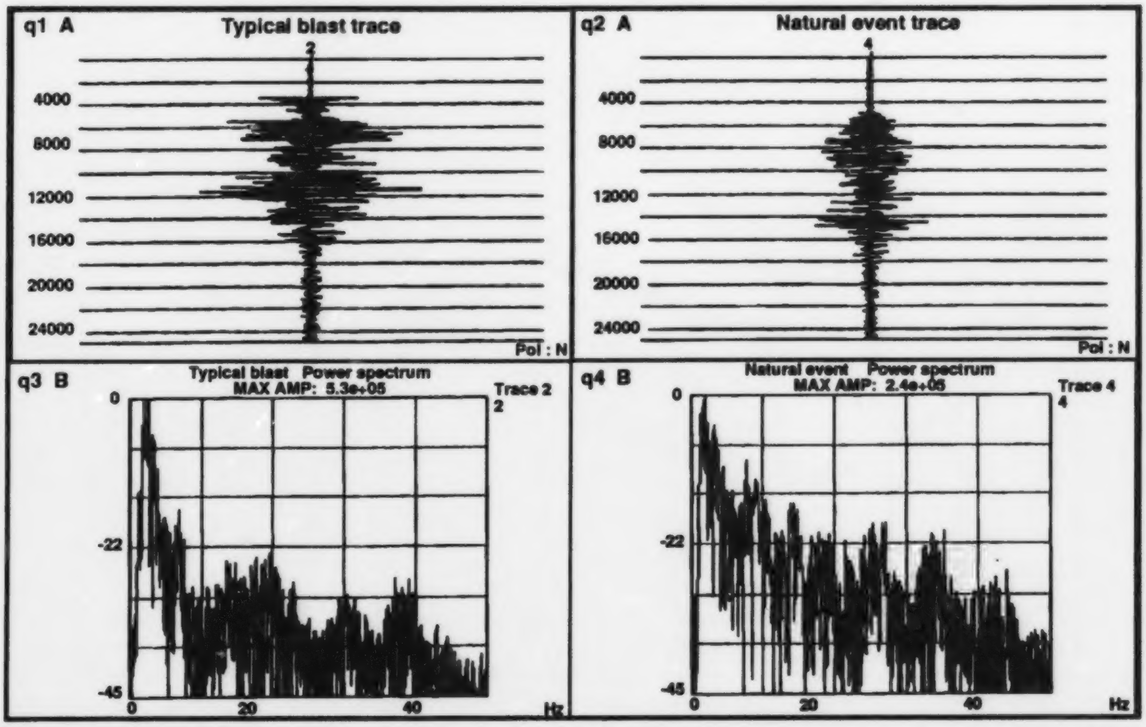

Figure 363.4 Time history and power spectra for two Mn=1 events recorded in Mt. Nemo site. Trace 2 shows a sharp decrease of energy in the higher frequency range for a blast, as compared to a natural event represented by Trace 4 spectrum.

that the coda waves at high frequencies are dominated by the same body waves, probably S waves, for both quarry blasts and earthquakes.

A similar observation between the explosions and a large number of known earthquake events in southern California has also been reported by Su et al. (1991). They were able to establish that the coda decay rate (Qc-1) is significantly higher for quarry blasts than earthquakes for lower frequencies (1.5 to 3 Hz), and that the coda power spectrum of the quarry blasts is significantly different from that of the earthquakes for local events.

DISCUSSION AND CONCLUSIONS

The result of the two year monitoring program in the western Lake Ontario region shows the feasibility of such an undertaking in the developed regions of southern Ontario. It has been demonstrated that even in areas of relatively high background noise (Mohajer and Halls 1990), microearthquakes as small as M≥1 can be detected by utilizing a network of three digital recording systems set in the triggered mode of operation. This project has established the feasibility of microseismic monitoring in areas of high background noise and has motivated the installation of an expanded network of five

Table 363.1 A few examples of the events large enough to be recorded by more than one station during the evening hours, between 13:00 to 22:59 UCT (Universal Co-ordinated Time), outside normal quarry activity hours.

Julian: date	H:	Min:	Sec	Stn.	Code	Traces No.	PRS-4	No.	Dur Sample rate
205:	02:	20:	40	NEMO	0630	06300095.12C	0095	98	100
205:	02:	20:	49	WBUR	0717	07170248.121	0248	50	100
205:	02:	20:	49	WBUR	0717	07170248.221	0248	50	100
205:	02:	20:	49	WBUR	0717	07170248.321	0248	50	100
229:	12:	59:	00	WBUR	168B	168B0248.104	0248	100	100
229:	12:	59:	00	WBUR	168B	168B0248.204	0248	100	100
229:	12:	59:	00	WBUR	168B	168B0248.304	0248	100	100
229:	12:	59:	23	NEMO	168A	168A0095.103	0095	100	100
229:	12:	59:	23	NEMO	168A	168A0095.203	0095	100	100
229:	12:	59:	23	NEMO	168A	168A0095.303	0095	100	100
232:	00:	15:	20	WBUR	168B	168B0248.109	0248	98	100
232:	00:	15:	20	WBUR	168B	168B0248.209	0248	98	100
232:	00:	15:	20	WBUR	168B	168B0248.309	0248	98	100
232:	00:	15:	48	NEMO	168A	168A0095.107	0095	96	100
232:	00:	15:	48	NEMO	168A	168A0095.207	0095	96	100
232:	00:	15:	48	NEMO	168A	168A0095.307	0095	96	100
243:	12:	59:	27	WBUR	828B	828B0248.10C	0248	99	100
243:	12:	59:	27	WBUR	828B	828B0248.20C	0248	99	100
243:	12:	59:	27	WBUR	828B	828B0248.30C	0248	99	100
243:	12:	59:	32	NEMO	828A	828A0095.106	0095	100	100
243:	12:	59:	32	NEMO	828A	828A0095.206	0095	100	100
243:	12:	59:	32	NEMO	828A	828A0095.306	0095	100	100
285:	02:	14:	07	WBUR	108B	108B0248.10E	0248	100	100
285:	02:	14:	07	WBUR	108B	108B0248.20E	0248	100	100
285:	02:	14:	07	WBUR	108B	108B0248.30E	0248	100	100
285:	02:	14:	43	NEMO	108A	108A0095.108	0095	96	100
302:	11:	19:	36	WBUR	020B	020B0248.10F	0248	98	100
302:	11:	19:	36	WBUR	020B	020B0248.20F	0248	98	100
302:	11:	19:	36	WBUR	020B	020B0248.30F	0248	98	100
302:	11:	19:	46	NEMO	025A	025A0095.10A	0095	96	100

seismographic stations in the east and north Toronto region with support from the Atomic Energy Control Board.

Among the 1500 triggered events which were recorded in the western Lake Ontario region, 95 events occurred during the evening hours (6 PM to 8 AM, corresponding to 23 to 13 UTC) and are clearly not the result of local quarry blasts. There are 10 active quarries mostly along the Niagara Escarpment which generate the bulk of the recorded events during the normal working hours. Although the blast schedules are known, several unscheduled isolated blasts have caused additional complications which makes it necessary to attempt a discriminatory procedure for identification of the natural events from the local blasts. It appears that the power spectra shapes can serve as a tool for such discrimination. Also 3 triggered events were recorded at more than one station suggesting a regional rather than local energy source.

In view of the overall seismotectonic environment of southern Ontario, and the scarcity of larger magnitude events, recorded microseismic events will provide necessary information for the assessment of potential seismic hazard. This project has demonstrated that microseismic events do occur in southern Ontario and that they can be detected.

ACKNOWLEDGEMENTS

The writers are grateful to the Ontario Geological Survey for providing the opportunity and funds to perform this interesting study. P. Basham, R. North, J. Adams, and J. A. Drysdale of Geological Survey of Canada were helpful in providing information on the data files and in the loan of instruments. J. Bowlby of Ontario Hydro, and G. McFall of the Ontario Geological Survey provided valuable discussions and information.

REFERENCES

Adams, J. and Basham, P. 1989. The seismicity and tectonics of Eastern Canada; *in* Neotectonics of North America, Geological Society of America, v.CSMV-1, p.127–142.

Geological Survey of Canada 1987. Aeromagnetic total field map, Rochester, Ontario-New York, Geophysical Series Map 7334G, scale 1:250 000.

Hanmer, S.K. 1988. Ductile thrusting at mid-crustal level, southwestern Grenville Province; Canadian Journal of Earth Sciences, v.25, p.1049–1059.

Hanmer, S.K. and Ciesielki, Andre 1984. A structural reconnaissance of the northwest boundary of the Central Metasedimentary Belt, Grenville Province, Ontario and Quebec; *in* Current Research, Part B, Geological Survey of Canada, Paper 84-1B, p.121–131.

Mohajer A.A. and H.C. Halls 1990. A seismotectonic study of the western Lake Ontario Region, Phase 1: a background noise survey; *in* Geoscience Grant Program Summary of Research 1989–1990, Ontario Geological Survey, Miscellaneous Paper 150, p.164–174.

Ontario Geological Survey 1991. Bedrock geology of Ontario, southern sheet; Ontario Geological Survey, Map 2544, scale 1:250 000.

Su, F., Aki, K. and Biswas, N.N. 1991. Discriminating quarry blasts from earthquakes using coda waves; Bulletin of the Seismological Society of America, v.81, p.162–178.

Thomas, R.L., McMillan, R.K., Keyes, D., Bowlby, J.R., Lewis,C.F.M. and Mohajer, A.A. in press. Recent faulting along the St. Lawrence rift system in eastern Lake Ontario.

Wallach J. L. and A. A. Mohajer, 1990. Integrated geoscientific data relevant to assessing seismic hazard in the vicinity of the Darlington and Pickering nuclear power plants; *in* Proceedings, Canadian Geotechnical Conference 1990, p.679–686.

White, O.L., Karrow, P.F. and Macdonald, J.R. 1974. Residual stress relief phenomenon in southern Ontario; *in* Proceedings, 9th Canadian Rock Mechanics Symposium, 1973, p.232–348.

Grant 364 Multiple Fluid-Inclusion Generations in Variably Deformed Quartz: Hollinger–McIntyre and Kerr Addison–Chesterville Archean Gold-Bearing Quartz Vein Systems, Northern Ontario.

D. M. DeR. Channer and E. T. C. Spooner

Department of Geology, Earth Sciences Centre, University of Toronto, Toronto, Ontario.

Fluid inclusions are as much a part of the microstructural evolution of quartz veins as they are a record of the chemistry of ore-forming fluids and other fluids trapped in veins. The apparently complex geometrical patterns defined by fluid inclusions in vein quartz result from the interaction of dislocations with fluid inclusions and vice versa.

A simple but detailed procedure has been developed to study fluid inclusions in ductilely deformed quartz. This involves mapping fluid inclusions on the basis of their microstructural setting and correlating microstructural features with patterns defined by fluid inclusions. Using this procedure sample-specific fluid chronologies have been established which then serve as a basis for comparison within the same sample, between samples on the same mine level, between samples at different mine levels and between samples in different mines.

Results show that: 1) mineralizing fluids at Hollinger–McIntyre and Kerr Addison were low to moderate salinity H_2O-CO_2-NaCl fluids with an average total homogenization temperature of approximately 280°C and with evidence for H_2O-CO_2 phase separation; 2) fluids of this composition were trapped pre-, syn-, and post-deformation and may record a declining temperature with time; 3) paragenetically early phases such as scheelite preserve moderate salinity (approximately 19 equivalent weight % NaCl) aqueous fluids which predate mineralizing fluids; 4) aqueous fluids of variable salinity postdate mineralization; 5) preliminary data suggest that $CH_4/(CH_4+CO_2)$ ratios at Hollinger–McIntyre increase with depth and with lateral distance from the deposit and 6) the variation of quartz microstructure with position within a vein is an important control on which stages of the overall fluid history are preserved and is therefore an important consideration when selecting samples for bulk analysis.

INTRODUCTION

A complete study of large Archean gold-bearing quartz vein ore systems such as the Hollinger–McIntyre and Kerr Addison–Chesterville deposits involves 2 main stages. First, an understanding of the three-dimensional geometry and time-sequence development is obtained by integration of detailed geological mapping and structural analysis with mine-geology level plans (either extant or reconstructed from drill-hole data). The second stage consists of detailed research studies carried out using samples geologically constrained by work done in the first stage. The physical geometry of the Hollinger–McIntyre deposit is well understood owing to a number of studies, some of which are those of Furse (1948), Jones (1948), Burrows and Spooner (1986), Mason and Melnik (1986), Wood, Burrows and Spooner (1986), Wood (1987), and Burrows (1991). The following studies formed the basis for geochemical investigations: (Smith et al. 1984; Wood, Burrows, Thomas and Spooner 1986; Wood 1987; Burrows 1991). The physical geometry of the Kerr Addison deposit was poorly known until the comprehensive study of Smith et al. (1990).

An important subdivision within the second stage of investigations is fluid-inclusion geochemistry. Fluid inclusions associated with gold mineralization at Hollinger–McIntyre were studied by Smith et al. (1984) and Wood, Burrows, Thomas and Spooner (1986). In these studies the main characteristics of the ore-bearing fluid (i.e., CO_2-rich, low to moderate salinity, variable CH_4 levels in the CO_2) were recognized; in addition, Wood et al. recognized the occurrence of sporadic phase separation as a probable cause of gold precipitation in some areas of the deposit and Wood (1987) recognized the occurrence of secondary, lower-homogenization-temperature aqueous inclusions. However, some fundamental questions require further study and arise from the observations that the fluid-inclusion-bearing vein quartz shows varying degrees of ductile deformation and that the geometrical distribution of fluid inclusions can appear to be very complicated.

Some of these questions are:

1. How does quartz microstructure vary with position within a vein and what are the implications for preservation of fluid inclusions, especially primary fluid inclusions?

2. What is a good procedure for the systematic study of fluid inclusions in ductilely deformed vein quartz so that sample-specific fluid chronologies can be identified?

3. How can deformational features be useful in building up sample specific chronologies of fluid events?

4. How has the deformation affected fluid-inclusion contents?

5. Having defined sample specific fluid chronologies, how do these chronologies compare with those for samples from the same level, from different levels, from the same vein over different levels and from samples contained in different host rocks? What are the three-dimensional trends in fluid composition in comparison with the three-dimensional physical geometry of the deposits?

All these questions will be partially addressed in this paper. Firstly, the microstructural textures of the veins are described. This is an important introduction to the textural classification of fluid inclusions which is based on their microstructural occurrence. The fluid-mapping procedure which is subsequently described is based on this textural classification. The results obtained using this procedure will be discussed in terms of 1) the effects of deformation on fluid inclusion contents, 2) a mechanism for formation of the observed fluid-inclusion geometries, 3) their geological implications and 4) their implications for the bulk fluid-inclusion analysis of approximately 1 g quartz samples for volatiles and ionic constituents of the aqueous phase (Channer et at. 1990).

Most of the data has been obtained using samples from Hollinger–McIntyre but preliminary data are also reported for a sample from the 4014-foot level of the Kerr Addison deposit. Consequently all observations and data refer to Hollinger–McIntyre unless Kerr Addison is specifically mentioned. Because of the relatively small number of samples studied to date, some of the following generalizations may be modified in the future.

QUARTZ MICROSTRUCTURE

The highly variable and often complex outcrop scale morphologies of veins at Hollinger–McIntyre are well described in references previously given. Burrows (1991) discusses the controls on vein morphology and orientation (e.g., rock type, hydrofracturing, theoretical shear-fracture orientations, zones of structural dilatancy). The gold-bearing quartz veins at Hollinger–McIntyre and Kerr Addison are interpreted to have formed synchronously with shear-zone development (Smith et al. 1990; Burrows 1991).

Primary Textures

Veins commonly contain primary depositional textures, such as the following.

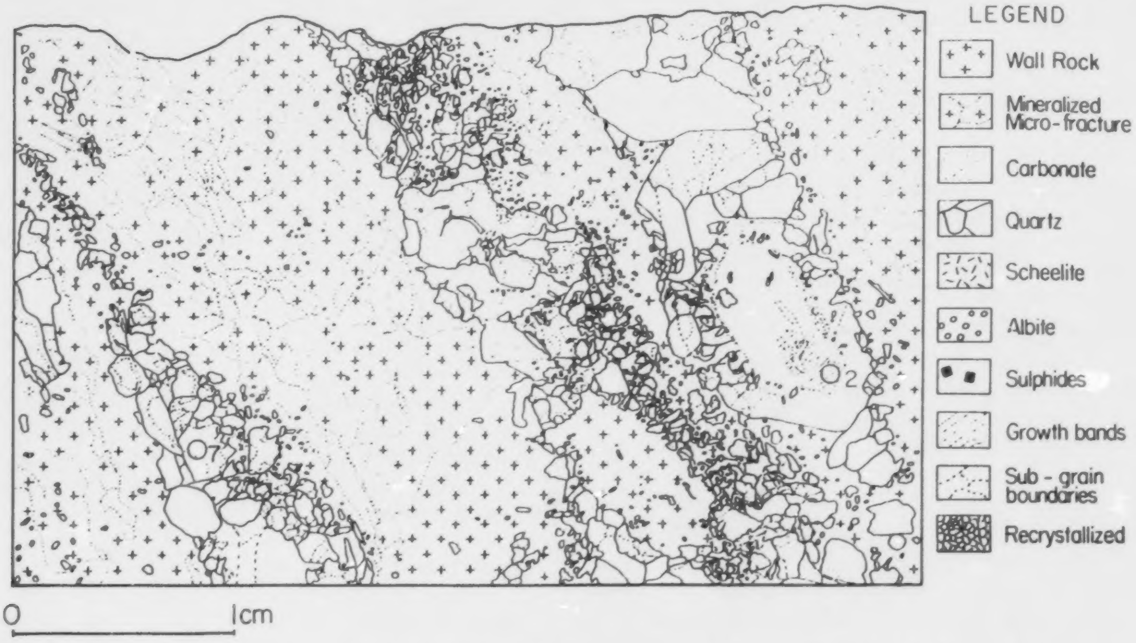

Figure 364.1. Line drawing of fluid inclusion section, sample KA15. The drawing was made by tracing over a 8.5 inch by 11 inch colour lasercopy of a whole-section slide photograph. The figure illustrates quartz and wall-rock micro-textures, especially primary growth textures. Circled areas (locations 2 and 7) were mapped for fluid-inclusion work. The legend applies to Figures 364.1, 2, 4a, 5, 7a, and 9.

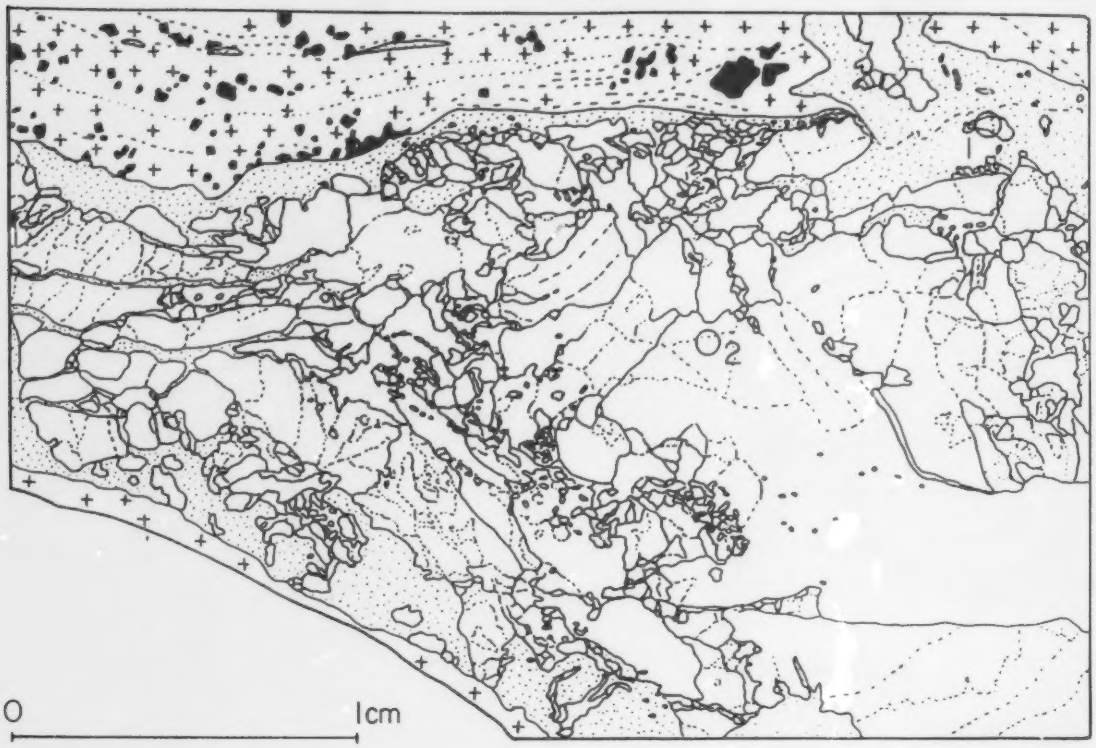

Figure 364.2. Line drawing of fluid-inclusion section TSPN-2. Drawing procedure as for 364.1. The vein is at most 3 cm wide but because of thickness changes along its length it displays many of the microstructural and textural changes described in the text for vein centres to vein margins. Circled areas (locations 1 and 2) refer to fluid-inclusion mapped areas as described in the text.

1. Early paragenetic phases such as albite and scheelite may form euhedral crystals projecting into veins from vein walls.

2. Ankerite commonly forms a fringe of fine- to medium-grained crystals along vein walls.

3. Free gold may occur close to the carbonate fringe at vein margins.

4. Fragments of wall rock can be seen in various stages of detachment from vein margins. These fragments act as crystallization sites and may be fringed by carbonate or albite.

Usually, however, the primary textures have been modified to some extent by ductile and brittle deformation. This is especially true of quartz which almost never retains primary growth textures. The sample from Kerr Addison used in this study is, however, a rare exception. Figure 364.1 illustrates quartz and wall-rock textures in an approximately 5 by 3 cm fluid-inclusion section of sample KA15 from the 4014-foot level, 631/2 stope, Kerr Addison Mine. The sample comes from a stage 3 "cherty siliceous break" vein (Smith et al. 1990) which is mineralized and syn-deformational but formed prior to main-stage gold veins. Figure 364.1 shows 3 sub-parallel quartz veinlets separated by wall-rock seams of comparable thickness. The wall rock consists of an original talc-carbonate altered ultramafic rock being replaced along fractures by pyrite-chalcopyrite-?petzite-rutile-carbonate-quartz. The quartz shows quite variable grain size and degree of deformation. Most large crystals are relatively undeformed with minor sub-grain development. Some recrystallization has occurred at grain margins. A prominent crystal has well-preserved primary growth textures. The crystal contains 2 zones, an inner euhedral, pseudo-hexagonal zone with an outline defined by inclusions of carbonate (and minor fuchsite) and an outer subhedral, but still recognizably hexagonal, zone which in most places is in contact with the wall rock. Most of the microstructural modifications to this crystal have occurred along the long sides of the crystal in the outer zone. The wall-rock boundary and the line of solid inclusions between the inner and outer zones apparently have exerted an influence on the location of sub-grains and recrystallized grains. The lower part of the quartz crystal contains growth bands defined by alternating solid, inclusion-rich and inclusion-poor bands. The innermost growth bands have been offset and separated by a zone of recrystallization but the outermost growth bands, while offset, have not been separated. The

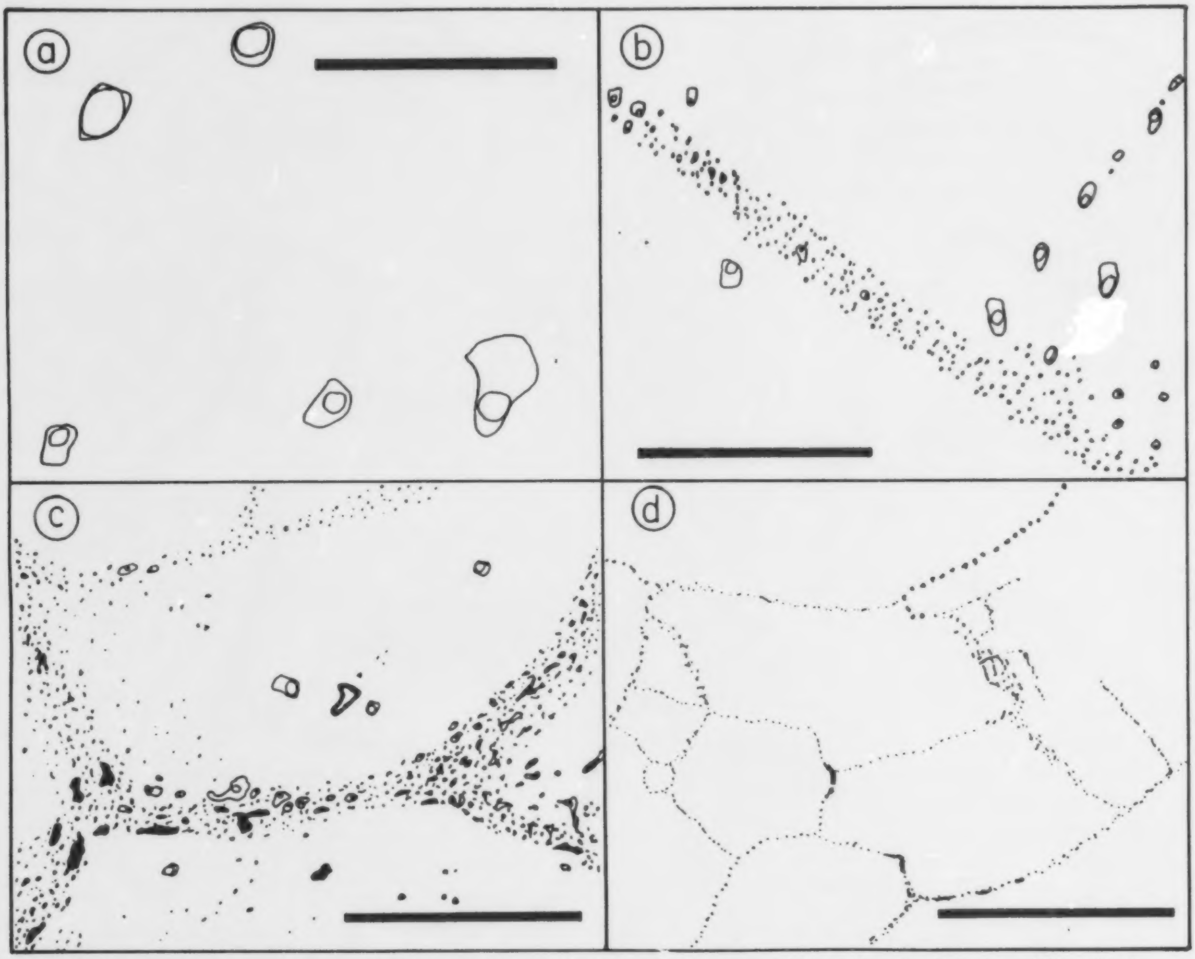

Figure 364.3. The different textural settings of fluid inclusions in variably deformed vein quartz; scale bar 100mm for a), b), c), and 200mm for d): a) isolated fluid inclusions in undeformed or low-strain quartz; b) inclusions on healed fractures with an early, "mature" fracture cut by a later, "immature" fracture; c) fluid inclusions within an anastomosing sub-grain boundary network, note that both liquid rich inclusions and darkened vapour-rich inclusions are present; d) small bubbles along high-angle grain boundaries in recrystallized quartz.

margin of the inner zone is continuous and straight in this region. These observations can be interpreted in terms of passive crystal growth, interrupted by a discrete, ductile deformational event and followed by continued growth. The discovery of primary crystal growth textures in syn-deformational veins is important evidence that, despite microstructural modification, primary textures can survive. Other examples of euhedral quartz crystals occur on a smaller scale in Figure 364.1 (i.e., the crystal-containing location 7).

Textures from Vein Centres to Vein Margins

Figure 364.2 shows a 2 to 3 cm thick quartz-carbonate vein in pyritized wall rock. The vein shows pinch and swell along its length. The wider end shows some of the features typical of vein centres while the thin end shows more recrystallization, elongation of grains parallel to the vein wall and smearing out of ankerite. In the vein centre quartz grains are up to 1 cm in size and are equant to elongate in shape. Grain interiors may contain zones of discontinuous undulatory extinction and sub-grains are commonly developed either in crystal margins or throughout the whole crystal. Sub-grains are usually 1 to 2 mm in size and are either prismatic or equant in shape. Grain boundaries are characterized by narrow zones of dynamic recrystallization: this feature, combined with other features such as the sub-grains in crystal margins and discontinuous undulatory extinction in crystal interiors, produces an incipient "core and mantle" texture (Burrows et al. 1979). Some grains contain discrete bands of dynamic recrystallization cutting right through the crystal although the orientations of these bands vary in adjacent crystals. Ankerite, although rare in vein centres, is usually smeared out along crystal boundaries while at vein edges it can retain a more primary morphology. In vein margins quartz crystals are generally less than 1 cm in size and are more variable in shape. The discrete recrystallization bands

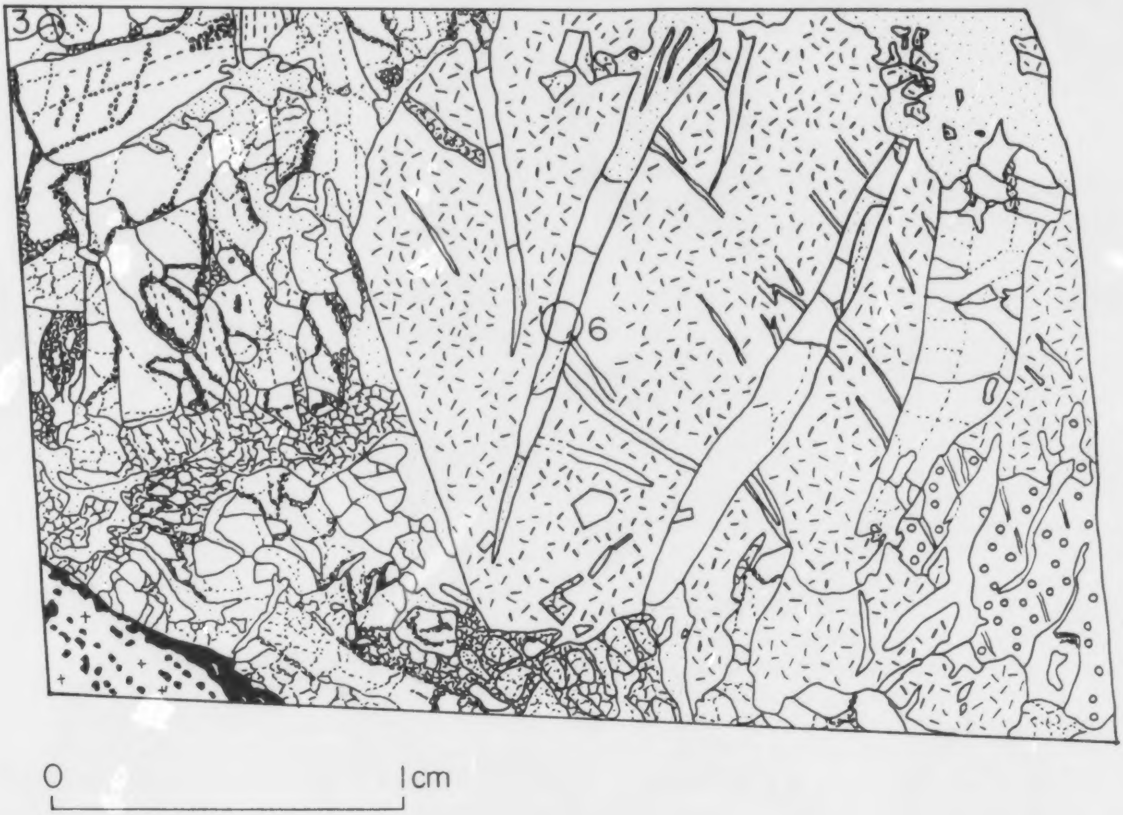

Figure 364.4a. Line drawing of fluid-inclusion section TSP33-5a; drawing procedure as for 364.1. The quartz microstructure is complex and appears to show 2 distinct episodes of quartz growth and deformation. The latter episode is related to tensional fracturing of the scheelite. Circled areas (locations 3 and 6) refer to fluid-inclusion mapped areas as described in the text.

described previously are more common in vein margins: larger grains have a more pronounced "core and mantle" texture while smaller grains are commonly recrystallized to clear, irregularly shaped grains. Within carbonate at the vein margin and especially in protected re-entrants, low-strain quartz can be preserved (i.e., location 1 in Figure 364.2).

The microstructure of the vein quartz suggests that the crystals have undergone work hardening (White 1971, 1973) owing to the applied stress and that they have attempted to relieve the accumulated strain energy by a combination of dynamic recovery and dynamic recrystallization. Quartz microstructure appears to show general variations according to position within a vein. Vein centres contain relatively uniform quartz grain size and the microstructure is dominated by networks of equant sub-grains within crystals. Vein margins have a more variable microstructure with both low-strain and dynamically recrystallized quartz occurring. In general, vein centres, especially those of thick veins, appear to be dominated by dynamic recovery (i.e., a stable sub-grain structure develops) whilst towards vein margins and in thin veins dynamic recrystallization becomes more important as a means of recovery. Vein centres approximate to monomineralic zones where the only stress heterogeneities arise from variations in crystal size, shape, and orientation. Vein margins, however, are more likely to contain extremes in stress gradients owing to variable mineralogy, detached wall-rock fragments, and anisotropies such as the vein/wall rock contact. Consequently in vein margins one can observe both primary, low-strain quartz and totally recrystallized quartz.

Textural Settings of Fluid Inclusions

Fluid inclusions occur in 4 main textural settings in the variably deformed quartz (*see* Figure 364.3) based on their microstructural associations. Isolated fluid inclusions (Figure 364.3a) are not related to linear or microstructural features; they appear to be randomly distributed or alternatively associated with primary crystallization features such as growth bands (e.g., Kerr Addison sample). They would be classified as primary with respect to formation of their host mineral according to the criteria of Roedder (1984). Inclusions on healed fractures (Figure 364.3b) form linear features which show varying degrees of

TABLE 364.1. SUMMARY OF MICROTHERMOMETRIC DATA: TSP 33-5a (location 6).

No.	Occurrence	Type	Tm(CO_2) (°C)	ρ(CO_2) (g/cc)	NaCl (eq.wt%)	Th (°C)	Homog. to L or V	No. of meas.
1a	P, sch	H_2O-CO_2-NaCl	-56.3	0.6	1.7	d		5
1b	P, sch	H_2O-NaCl			18.6	d		1
2	HF, sch	H_2O-NaCl			15 - 22	170 - 257	L	4
3	P, qz	H_2O-CO_2-NaCl	-56.4	0.86	0.41 - 7	258 - 365	L/V	5
4	HF/SGB	H_2O-CO_2-NaCl	-56.4	0.7	6.4	100 - 263	L	17
5	HF	H_2O-CO_2-NaCl	nd	nd	8.4	130 - 223	L	7
6a	SEC	H_2O-NaCl			6.4	139	L	8
6b	SEC	H_2O-NaCl			19.4	133	L	12

Notes: Numbers in first column refer to numbers on Figure 364.4b.
Abbreviations used in all tables: P = primary, ISO = isolated, probably primary, CLU = cluster, probably primary, HF = healed fracture, SGB = sub-grain boundary, HGB = high-angle grain boundary, SEC = secondary, nd = not determined, d = decrepitated, L = liquid, V = vapour, CRIT = critical.

healing (Lemmleyn and Kliya 1960; Smith and Evans 1984) and which may or may not crosscut crystal boundaries or microstructural features. Inclusions associated with sub-grain boundaries (Figure 364.3c) typically define curved and anastomosing features in which inclusions often have low shape factors (Sterner and Bodnar 1989) and may be darkened owing to leakage of H_2O with consequent increase of the vapour to liquid ratio. However, liquid rich inclusions may also be present. Inclusions in high-angle grain boundaries between recrystallized quartz grains (Figure 364.3d) are typically small (less than 1mm) and dark owing to disaggregation of larger inclusions and loss of most fluid along the grain boundaries.

Vein quartz from Hollinger–McIntyre and Kerr Addison typically contains great numbers of fluid inclusions which give the quartz a "peppery" appearance in thin section. The textural classification of fluid inclusions based on their microstructural associations is the basis of the procedure for determining sample-specific fluid chronologies to be described below. When the fluid inclusions are viewed from this microstructural perspective, the importance of sample location relative to position within the vein becomes clear

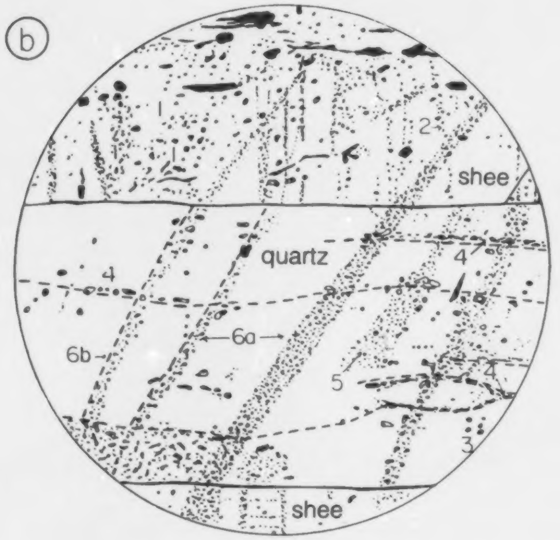

Figure 364.4b. Fluid inclusion/microstructural map for location 6, TSP33-5a; diameter 1.76 mm. The location is within a quartz-filled fracture within scheelite (Shee). Successive stages of fluid introduction are numbered sequentially and also refer to numbers of fluid stages in Table 364.1. Optical strain features (i.e., sub-grain boundaries) are shown as heavy dashed lines in this and subsequent figures of this type. In this figure the correlation of stage 4 with sub-grain boundaries is clear.

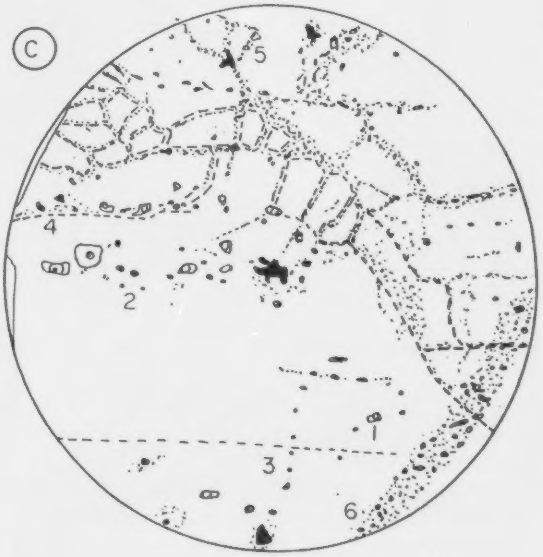

Figure 364.4c. Fluid inclusion/microstructural map for location 3, TSP33-5a; diameter 0.7 mm. This shows isolated (stage 1) and healed fracture (stages 2 and 3) fluid inclusions in second-stage quartz which is in contact with sub-grain-dominated earlier quartz along a zone of recrystallization.

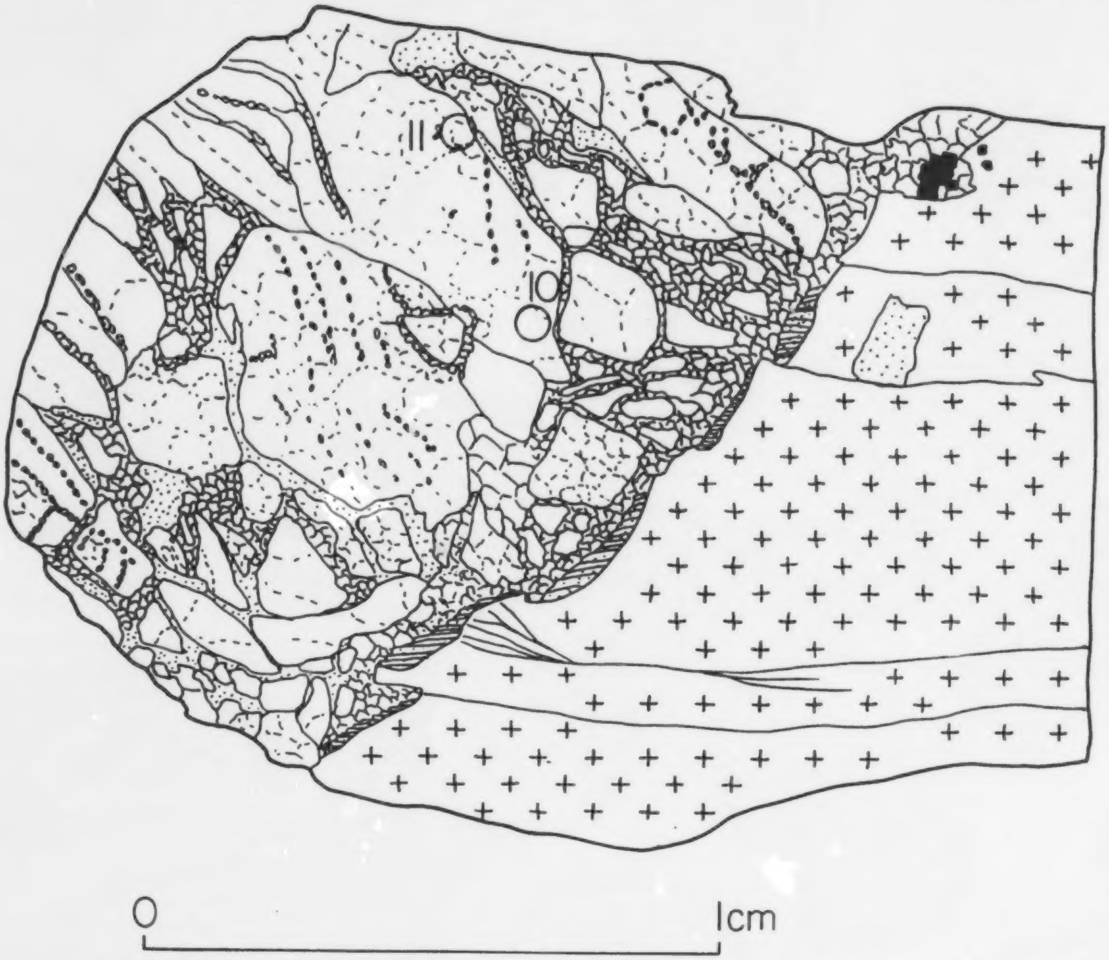

Figure 364.5. Line drawing of fluid-inclusion section TSP33-1; drawing procedure as for 364.1. In this thin vein dynamic recrystallization has modified much of the quartz. Core and mantle texture is well developed. Note the deformed fringe of carbonate crystals against the wall rock.

since different stages of fluid history within a vein may be preserved in different parts of the vein (i.e., low strain areas may preserve early, primary fluids while recrystallized areas may contain only late fluids).

PROCEDURE FOR FLUID-INCLUSION MAPPING

A crossed-polars colour slide is made of the whole fluid-inclusion section. This slide is then used to make either a colour laser copy or a colour print for use as a base map. With a tracing-paper overlay on the base map petrographic and microstructural features are noted (e.g., Figure 364.1). Also, areas suitable for fluid-inclusion mapping are located. These areas are circular and, depending on the magnification used, have diameters of 1.76 or 0.76 mm. A minimum of 3 maps is made for each section. The sections are 100 mm thick and so the map is a two-dimensional representation of the three-dimensional fluid-inclusion geometry. On a copy of the original map all the microstructural features are marked. On another copy the different fluid events as distinguished on textural grounds are colour coded for comparison with other areas. Another copy is used during microthermometry when each inclusion measured is given a reference number.

RESULTS

Results will be presented in the following sections: 1) determination of a sample specific fluid chronology, 2) comparison of fluid chronologies for different samples on the same mine level, 3) horizontal trends in fluid chemistry, 4) vertical trends in fluid chemistry and 5) preliminary data for fluid composition at the 4014-foot level in the Kerr Addison Mine.

TABLE 364.2. SUMMARY OF MICROTHERMOMETRIC DATA: TSP 33-5a (location 3).

No.	Occurrence	Type	Tm(CO_2) (°C)	ρ(CO_2) (g/cc)	NaCl (eq.wt%)	Th (°C)	Homog. to L or V	No. of meas.
1	ISO	H_2O-CO_2-NaCl	-56.5	0.81	3.38	d		1
2	HF	H_2O-CO_2-NaCl	-56.6	0.58 - 0.80	2.42 - 4.51	271 - 299	CRIT/V	13
3	HF	H_2O-CO_2-NaCl	-56.6	0.80	3.19	173 -196	L	3
4	SGB	H_2O-CO_2-NaCl	-56.6	0.56 - 0.71	2.81 - 3.76	271 - 306	V	4
5	HGB	H_2O-CO_2-NaCl	-56.5	0.69	nd	nd		1
6	SEC	H_2O-NaCl			16.9 - 19.6	86 -133	L	4

Notes: Numbers in first column refer to Figure 364.4c.

Sample-Specific Fluid Chronology

Sample TSP33-5a comes from a thin (approximately 5 cm wide) vein steeply dipping to the south in #33 Pit of the Hollinger Mine. It consists of scheelite-albite-quartz-carbonate-pyrite - Au and is hosted in altered mafic metavolcanic rocks. The microtextures are shown in Figure 364.4a. The quartz shows a wide range of microstructural features: in some areas (adjacent to wall rock) the quartz has a sub-grain dominated microstructure with dynamic recrystallization at grain boundaries and in bands cutting through grains. The recrystallized grains usually have grain sizes comparable to those of the sub-grains. Typically this quartz is "peppery" in appearance and many fluid inclusions occur along sub-grain or high-angle grain boundaries. In other areas (vein centre) the quartz appears to be clean, with low internal strain and small numbers of well-formed and preserved fluid inclusions; it is often associated with zones of recrystallization and has a range of grain sizes. These crystals may have formed by dynamic recrystallization combined with fluid-assisted grain growth. The scheelite contains tensional fractures which are infilled with quartz and carbonate. An area (marked on Figure 364.4a as location 6) including 1 of these fractures was selected for fluid-inclusion mapping since the scheelite is paragenetically early while the quartz is later in the sequence. The fluid-inclusion map for location 6 is shown in Figure 364.4b with the microstructural features also depicted to illustrate which fluid stages are associated with microstructural features. The numbers on the diagram identify successive stages of trapped fluids in chronological order. Microthermometric data are summarized in Table 364.1.

The earliest fluid inclusions (stage 1) are primary inclusions in scheelite and appear to be of 2 types, a low-salinity, H_2O-CO_2 type (1a) and a moderate-salinity (18.6 equivalent weight % NaCl) aqueous type (1b). Stage 2 occurs on healed fractures which are clearly truncated at the contact with the quartz-filled fracture. The fluid in stage 2 is similar to 1b in salinity and homogenizes to the liquid in the range 170 to 257°C. Fluid stage 3 is trapped as primary inclusions with respect to quartz in the fractures: it contains H_2O with a low but variable salinity (0.41 to 7 equivalent weight % NaCl) and pure CO_2. Homogenization is both to liquid and vapour in the range 258 to 365°C. Fluid stages 4 and 5 have similar chemistries to fluid 3 but occur on healed fractures and have lower ranges of homogenization temperatures (100 to 263°C) to the liquid only. The healed fractures containing fluid 4 are fluid 5 crosscut sub-grain boundaries (*see* Figure 364.4b). The latest fluid events (6a and 6b, Figure 364.4b) occur in poorly-healed fractures which crosscut all grain boundaries but which are associated with elongate sub-grain boundaries defining zones of discontinuous undulatory extinction. These fluids show trail specific salinities (i.e., 6.4 equivalent weight % NaCl for 6a and 19.4 equivalent weight % NaCl for 6b but similar homogenization temperatures (135 to 140°C).

Several important points arise from these data.

1. Moderate- to high-salinity aqueous fluids were present both at the earliest stages of vein formation and after vein formation.
2. H_2O-CO_2-NaCl fluid inclusions predate deformation (fluid 1a), formed syn-deformationally (fluids 3 and 4), and also postdate deformation (fluid 5); they also record a decline in temperature with time.
3. Fluid 3 shows evidence for H_2O-CO_2 phase separation.

An area of second-stage quartz (location 3 in Figure 364.4a) was also mapped (Figure 364.4c). The lower part of the map contains a second-stage, low-strain quartz crystal with a small number of well-developed inclusions in isolated (stage 1) and healed fracture (stage 2, 3) settings. The margins of the crystal have sub-grain boundary associated inclusions (stage 4) while the crystal centre is low strain with 1 zone of discontinuous undulatory extinction. The upper part of the map shows sub-grain dominated quartz and the boundary between the 2 types of quartz is a zone of recrystallization (stage 5 fluids). Late secondary fluids (stage 6) crosscut all other features. The microthermometric data are summarized in Table 364.2. It can be seen by comparison with Table 364.1 that fluids in location 3 correlate with fluids in location 6 in the following way: $1_3 = 3_6$, 2_3 and $4_3 = 4_6$, $3_3 = 5_6$, $6_3 = 6b_6$. This correlation suggests that the fracturing event which formed the quartz-filled fractures in the scheelite was the same event which promoted new quartz growth in the quartz matrix. In this sample, therefore, the vein quartz preserves only main stage and later fluid stages while earlier fluid stages must be looked for in earlier paragenetic phases.

Comparison of Fluid Chronologies for Different Samples on the Same Mine Level

In addition to the sample described above 2 other samples from the Hollinger surface pits were studied. One (TSP33-1) was also from #33 Pit and consists of a thin (approximately 2 cm wide), moderately dipping vein hosted in a mafic breccia unit. The other (TSPN-2) was from a thin vein in mafic metavolcanic rocks at the contact with the Pearl Lake Porphyry. The microtextures of TSP-N2 have already been described (*see* Figure 364.2 and relevant text). Fluid inclusions were mapped for 2 areas, location 1 in low-strain quartz within carbonate in the vein margin and location 2 in sub-grain-dominated quartz in the vein centre. Location 1 contains fluid inclusions in 3 textural settings: isolated or in small clusters, on short, linear healed fractures or as late secondary trails crosscutting grain boundaries. The quartz contains some sub-grain boundaries but not all of these are associated with healed fractures. Location 2 contains a similar chronology but in this case early fluid inclusions are contained in areas bounded by sinuous, anastomosing fluid-inclusion trails associated with sub-grain boundaries. In sample TSP33-1 the vein quartz has well-developed core and mantle texture (*see* Figure 364.5) and, in addition, bands of recrystallization are common. Quartz crystal interiors are sub-grain dominated. Locations 10 and 11 were studied from this sample. Location 10 contains a fluid-inclusion geometry dominated by curvilinear healed fractures. Rare, isolated fluid inclusions occur between these healed fractures. In this case the healed fractures do not correlate with optical strain features although all contain irregular and darkened fluid inclusions which have clearly been affected by deformation. Location 11 is a small area of lower strain containing rare isolated inclusions and a late secondary trail of aqueous fluids.

Histograms of $TmCO_2$, salinity, CO_2 density, and total homogenization temperature are shown in Figures 364.6a, b, c, and d, respectively, H_2O-CO_2-$NaCl$ fluids in each of the 3 samples and for the 3 textural settings, primary (P), healed fracture (HF), and sub-grain boundary (SGB). For all samples and all textural settings the CO_2 is pure with only inclusions in TSP-N2 showing a slight depression of the CO_2 melting point. Primary inclusions from all samples show a similar range of salinities while HF and SGB inclusions show some tendency for an increasing dispersion of salinities. The CO_2 density range is quite wide, from 0.55 to 0.82 g/cc, but the range for 1 sample and textural type is the same as for all samples and all textural types. Total homogenization temperatures cluster between 265 and 290°C for P inclusions while the range is greater for HF and SGB inclusions.

Late aqueous inclusions for the 3 samples are compared in Figure 364.6e. Homogenization temperatures form a cluster between 115 and 155°C while salinities seem to be sample specific and even trail specific as shown in Table 364.1 for fluid types 6a and 6b.

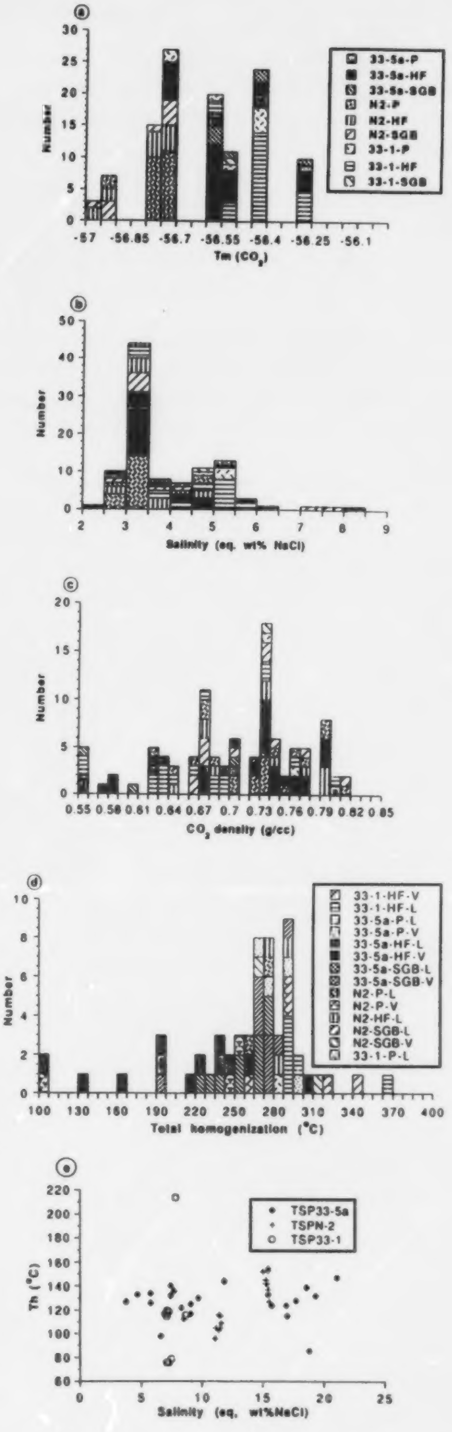

Figure 364.6. Comparison of microthermometric data for 3 samples from the Timmins (formerly Hollinger) surface pits, TSP33-5a, TSPN-2, TSP33-1. Abbreviations for textural classification of fluid inclusions, P = isolated or primary, HF = healed fracture, SGB = sub-grain boundary; L and V = liquid or vapour phase homogenization respectively. The legend in a) applies also to b) and c): a) $TmCO_2$, b) Salinity, c)CO_2, d) Th, e) Th vs. salinity for aqueous secondary inclusions.

The following points can be made.

1. These data are in good agreement with those of Wood, Burrows, Thomas and Spooner (1986) with regard to the composition and range of homogenization temperatures for main-stage H_2O-CO_2-NaCl fluids.

2. The CO_2-bearing fluids appear to show little compositional change with time within a sample and do not exhibit extreme compositional changes because of deformation, apart from an increase in salinity in some cases.

3. All textural types of fluid inclusions may show liquid and vapour homogenization but only in the P and HF types can this be taken as evidence in favour of phase separation; in the SGB type this feature is the result of deformation.

4. The sample-specific fluid-inclusion chronologies established for vein quartz in each of the 3 samples are similar.

Horizontal Trends in Fluid Chemistry

A sample from a barren vein 1.5 km north of the Hollinger Mine was studied for comparison with the samples from the surface pits within the ore deposit. The sample (89-655-1) is from the central portion of a vein approximately 0.5 m wide which has a quartz-pyrite-ankerite? mineral assemblage. The quartz forms 3 to 10 mm grains (*see* Figure 364.7a) which are mostly relatively undeformed, showing areas of discontinuous undulatory extinction; in some crystals more advanced sub-grain formation has occurred. Areas of dynamic recrystallization do occur but are limited to grain boundaries and some discrete bands. Fluid inclusions were mapped for 2 areas, location 1 in low-strain quartz (Figure 364.7b) and location 2 in recrystallized quartz (Figure 364.7c). The low-strain area contains a now familiar fluid chronology with P, HF, SGB and late secondary fluid inclusions. The recrystallized area contains isolated inclusions (Prext—stage 1) and HF inclusions (stage 2) within recrystallized quartz grains which have bubbles defining high-angle grain boundaries (stage 3). Late aqueous secondary inclusions crosscut recrystallized grains. The microthermometric data are summarized in Table 364.3.

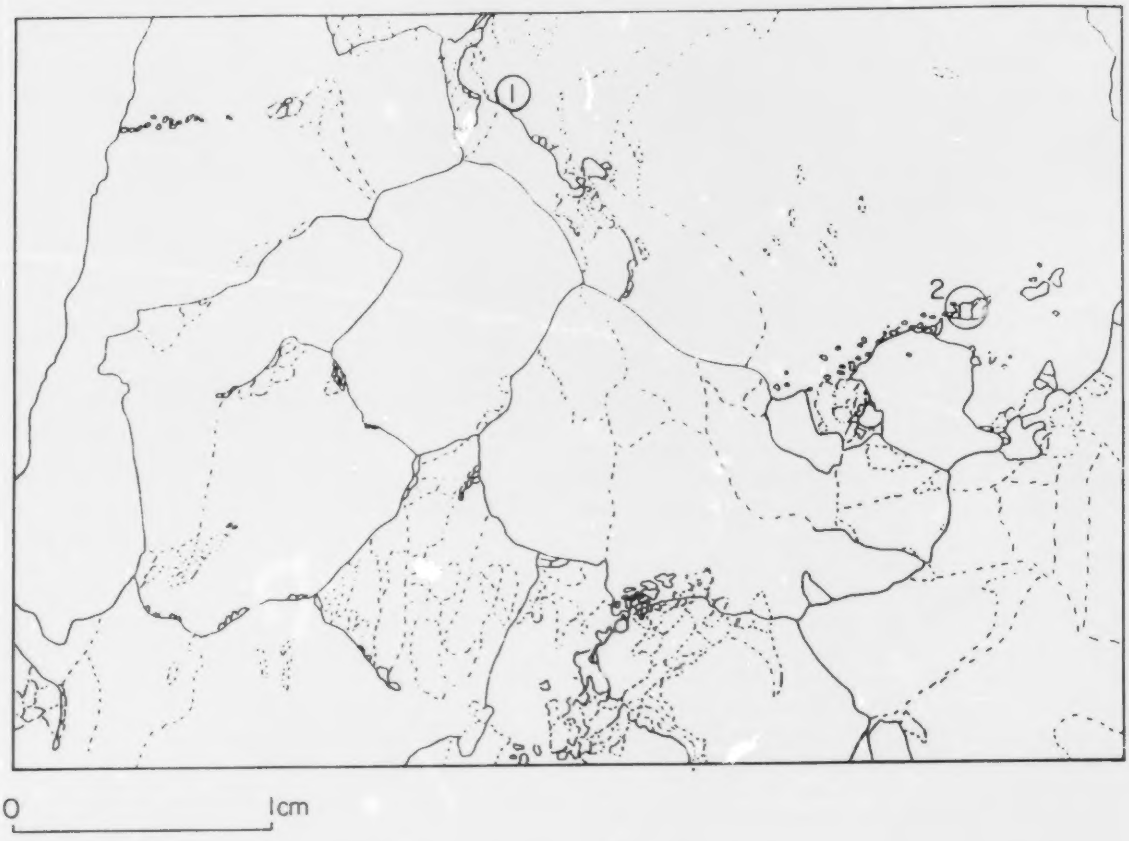

Figure 364.7a. Line drawing of fluid-inclusion section 89-655-1; drawing procedure as for 364.1. This sample is from a thick (approximately 0.5 m) vein and contains relatively large and mostly undeformed crystals. Deformed crystals have a sub-grain-dominated microstructure with minor areas of recrystallization.

TABLE 364.3. SUMMARY OF MICROTHERMOMETRIC DATA: 89-655-1 (locations 1 and 2).

No.	Occurrence	Type	Tm(CO_2) (°C)	ρ(CO_2) (g/cc)	NaCl (eq.wt%)	Th (°C)	Homog. to L/V	No. of meas.
Location 1								
1	P	H_2O-CO_2-CH_4-NaCl	-57.7	-0.3 - 18.8 (L)	10.4	239-302	L	10
2	HF	H_2O-CO_2-CH_4-NaCl	-58.0	19.4 (L)	10.3	248-284	L	5
3	HF/SGB	H_2O-CO_2-CH_4-NaCl	-57.1	20.0 (L)	1.8 - 10.0	118-385	L/V	14
4	SEC	H_2O-NaCl			(17.6wt%)	144	L	8
Location 2								
1	Prext	H_2O-CO_2-NaCl	-56.8	0.75	(0.93 - 8.61wt%)	125-465	L/V	23
2	HF	H_2O-CO_2-NaCl	nd	nd	nd	351	CRIT	2
3	HGB	H_2O-CO_2-NaCl	nd	nd	nd	393	L	1
4	SEC	H_2O-NaCl			nd	108	L	2

Notes: Numbers in first column refer to Figures 364.7b and 7c, locations 1 and 2, respectively.

A clear trend which emerges from Table 364.3 is that in going from P to HF to SGB inclusions in location 1 to Prext in location 2 the dispersion of total homogenization temperatures increases with both SGB and Prext inclusions showing liquid- and vapour-phase homogenization (*see* also Figure 364.8). This trend is similar to that indicated by Figure 364.6d and suggests that 1 characteristic feature of progressive deformation is increasing dispersion of homogenization temperatures together with introduction of both liquid- and vapour-phase homogenization. The CO_2 melting point is variably depressed, probably because of CH_4, in all textural settings. The relatively high CH_4 levels in the CO_2 contrast with the pure CO_2 found in samples from the Timmins surface pits (compare with Figure 364.6a). The aqueous secondary fluids are, however, comparable in terms of salinity and homogenization temperature to those found in samples within the ore deposit.

Vertical Trends in Fluid Chemistry

A sample from a deep level (4550 feet) of the Hollinger Mine has been studied. This sample is from the Geological

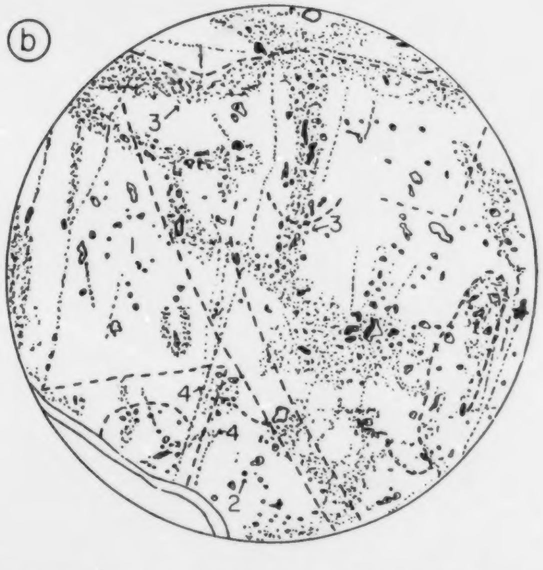

Figure 364.7b. Fluid inclusion/microstructural map for location 1, sample 89-655-1; diameter 1.76 mm. Isolated inclusions (stage 1) and short-healed fractures (stage 2) are bounded by sinuous healed fractures (stage 3) only some of which are associated with sub-grain boundaries. Late aqueous fluids (stage 4) crosscut all other features.

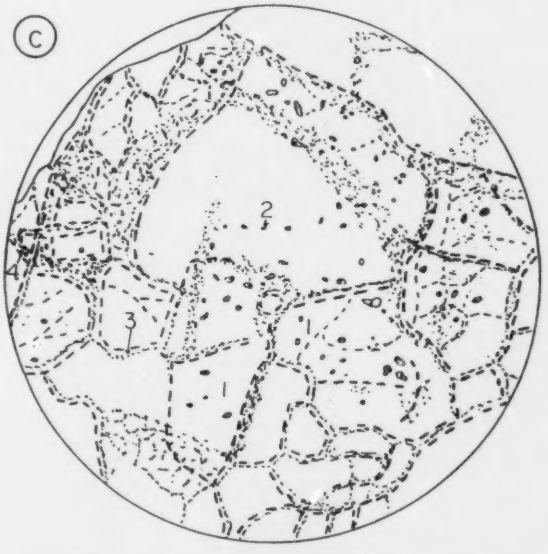

Figure 364.7c. Fluid inclusion/microstructural map for location 2, sample 89-655-1; diameter 0.7 mm. This area has a polygonal pattern of inclusions along high-angle grain boundaries (stage 3). A number of isolated inclusions (stage 1) and HF inclusions (stage 2) occur within recrystallized grains. Late aqueous fluids (stage 4) crosscut high-angle grain boundaries.

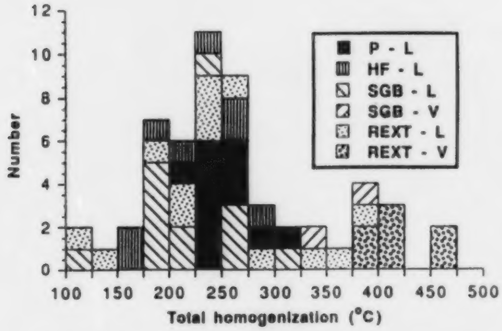

Figure 364.8. Histogram of Th values for sample 89-655-1, locations 1 and 2. Stage 4 aqueous fluids are not shown.

Survey of Canada collection (catalogue number 065525). The sample is analogous to TSP33-5a in that it consists of scheelite-quartz-carbonate with the scheelite having fractures infilled with quartz, carbonate and muscovite (*see* Figure 364.9). The sample comes from 59 vein which is hosted in mafic volcanic rocks just south of the Pearl Lake Porphyry. Locations 9 and 11 within quartz-filled fractures were mapped and are illustrated in Figure 364.10a and b where it can be seen that most of the inclusions are secondary (stage 2 in location 9 and 3, 4 in location 11). However, small clusters (stage 1 in both locations) and healed fractures (stage 2 in location 11) containing earlier fluids are preserved. Microthermometric data are summarized in Table 364.4 for both areas.

Primary inclusions and those on short healed fractures are CO_2 dominated with no visible H_2O. CO_2 melting points are well depressed with a range from -58.0 to -61.7°C. Two types of aqueous secondary fluids were measured, a low salinity (3.97 equivalent. weight % NaCl) type and a moderate salinity (16 to 27 equivalent weight % NaCl + $CaCl_2$) type; both types homogenized at similar temperatures. A new type of secondary fluid (stage 4 in location 11) consists of supercritical CH_4 at room temperature: this fluid occurs as late, secondary trails which crosscut all other fluid events.

Preliminary Data for Fluid Composition at the 4014-Foot Level in the Kerr Addison Mine

Details of location and micro-textures have been given for this sample in the section on quartz microtextures. Microthermometry has been carried out on 2 mapped areas, both of which

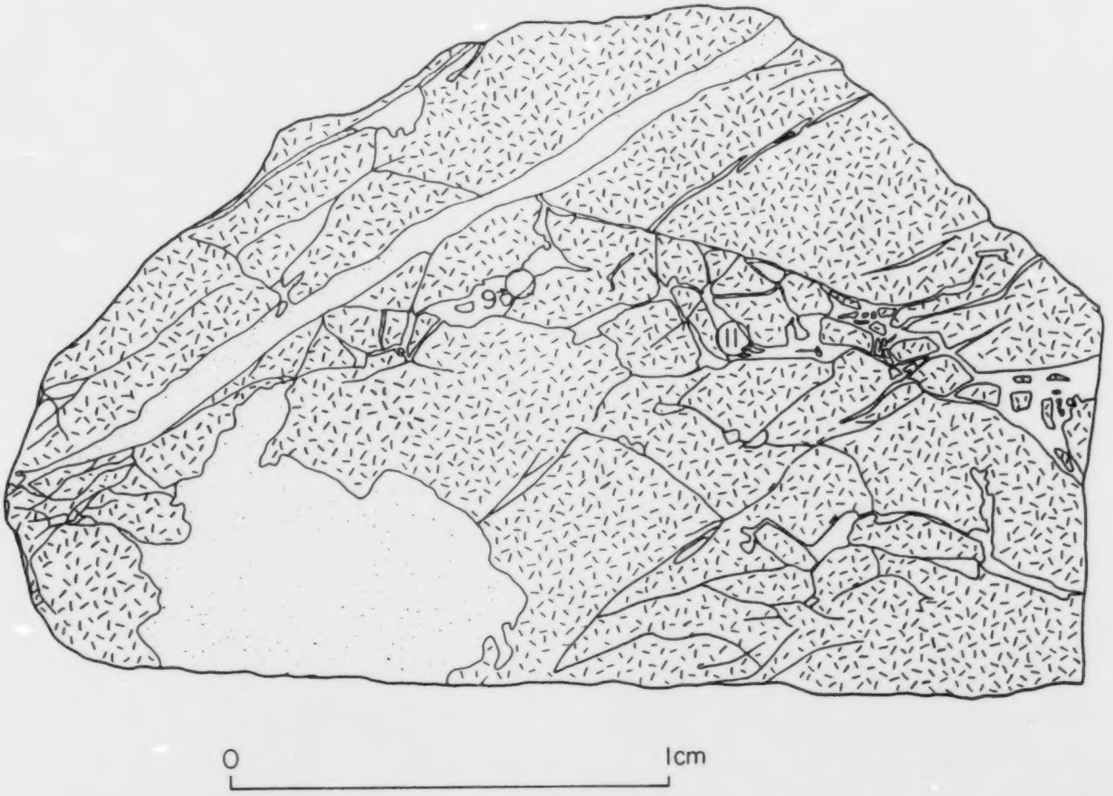

Figure 364.9. Line drawing of fluid-inclusion section H4550-1; drawing procedure as for 364.1. This shows a scheelite crystal with a network of brittle fractures infilled by quartz-carbonate-(muscovite).

TABLE 364.4. SUMMARY OF MICROTHERMOMETRIC DATA: H4550-1 (loc 9 and 11).

Location 9 No.	Occurrence	Type	Tm(CO_2) (°C)	Th(CO_2) (°C)	Salinity (wt% Na + Ca)	Th (°C)	Homog. to L/V	No. of meas.
1	ISO	CO_2-CH_4	-60.1	7.3 (L)				8
2	SEC	H_2O-NaCl-$CaCl_2$			16 - 27	128	L	20
Location 11								
1	CLU	CO_2-CH_4	-60.8	-4.7 (L)				5
2	HF	CO_2-CH_4	-60.2	-1.2 (L)				4
3	SEC	H_2O-NaCl			3.97	113	L	6
4	SEC	CH_4			–	84.8	L/V	8

Notes: Numbers in first column refer to Figures 364.10a and 364.10b, locations 9 and 11, respectively.

occur within primary quartz crystals. These areas (locations 2 and 7) are identified on Figure 364.1 and the fluid-inclusion maps are shown in Figure 364.11. In location 2 (Figure 364.11a) growth zones are clearly visible and inclusions occur in primary (stage 1) and pseudo-secondary settings (stages 2 and 3). In location 7 (Figure 364.11b) the same textural settings occur but visible growth zones are not displayed. Microthermometric results are shown in Table 364.5.

In all cases the CO_2 is pure (-56.6 to -56.9°C) and the salinity of the aqueous phase is low (3.8 to 4.5 equivalent weight % NaCl). The CO_2 density is quite high (0.79 to 0.97 g/cc) which explains the fact that most inclusions are two-phase at room temperature. Most inclusions decrepitated between 200 and 300°C but the homogenization temperatures obtained for stage 1 fluid inclusions suggest a range of 220 to 332°C with homogenization to both liquid and vapour phases. The latest stage (3 in both locations 2 and 7) of CO_2-bearing inclusions on healed fractures has lower temperatures (132 to 225°C) but similar salinities (4.0 to 4.7 equivalent weight % NaCl). Late secondary trails contain very small inclusions whose composition has not yet been determined.

DISCUSSION

Effects of Deformation on Fluid Inclusion Contents

The effects of deformation on fluid-inclusion contents as

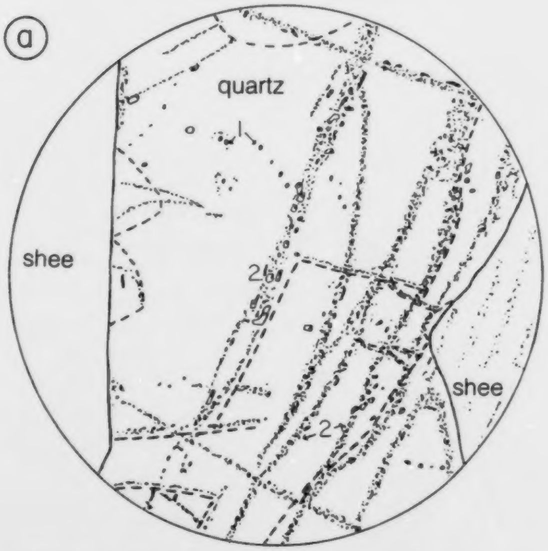

Figure 364.10a. Fluid inclusion/microstructural map for location 9, H4550-1; diameter 0.7 mm. The location is within a quartz-filled fracture in scheelite. Isolated fluid inclusions (stage 1) are rare, as are short healed fractures. Most inclusions occur on late secondary trails (stage 2) and are predominantly saline aqueous fluids.

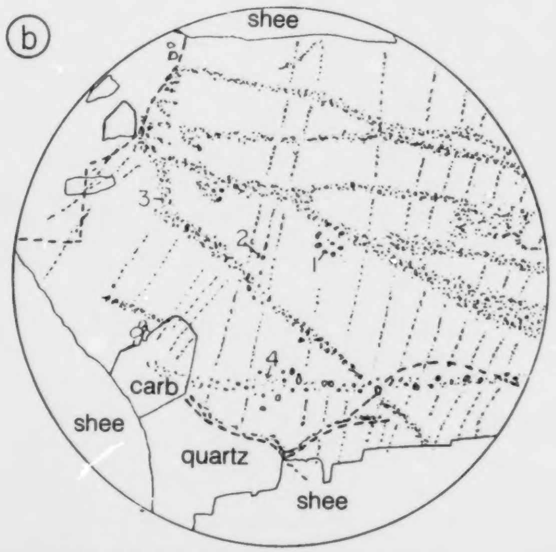

Figure 364.10b. Fluid inclusion / microstructural map for location 11, H4550-1; diameter 0.7 mm. The location is within a quartz filled fracture in scheelite. This area contains early clusters (stage 1) and HF inclusions (stage 2). There are 2 types of secondary fluid: low-salinity aqueous (stage 3) and fairly pure CH_4 (stage 4).

TABLE 364.5. SUMMARY OF MICROTHERMOMETRIC DATA: KA15 (locations 2 and 7).

No.	Occurrence	Type	Tm(CO_2) (°C)	ρ(CO_2) (g/cc)	Salinity (wt% NaCl)	Th (°C)	Homog. to L/V	No. of meas.
Location 2								
1	ISO	H_2O-CO_2-NaCl	-56.6 to -56.7	0.79 - 0.92	3.8	d		12
2	HF	H_2O-CO_2-NaCl	-56.6 to -56.7	0.86 - 0.92	4.1	283(1)	V	10
3	HF	H_2O-CO_2-NaCl	nd	nd	4.7	132	L	1
Location 7								
1	CLU	H_2O-CO_2-NaCl	-56.9 to -56.7	0.83 - 0.97	4.51	220 - 332(3)	L/V	22
2	HF	H_2O-CO_2-NaCl	-56.9 to -56.7	0.89 - 0.98	nd(2)	185(3)	L	16
3	HF	H_2O-CO_2-NaCl	-56.8	0.80 - 0.87	3.97	135 - 225(3)	L	2

Notes: (1) n = 1 for Th values, all other inclusions decrepitated in the range 200 to 300°C, (2) salinity nd since all Tm(cl) > Th(CO_2), range of Tm(cl) is 7.1 - 9.0°C, (3) for Th values n = 5 for stage 1, n=1 for stage 2, n = 2 for stage 3. Numbers in first column refer to Figures 364.11a and 364.11b, locations 2 and 7, respectively.

observed in this study are as follows.

1. The sinuous fluid inclusion trails are frequently associated with sub-grain boundaries and contain both vapour-rich and liquid-rich inclusions which homogenize to vapour and liquid, respectively, over a greater temperature range than do the primary inclusions (e.g., *see* Figures 364.6d and 364.8); in Figure 364.6d this behaviour is not so obvious since the range of Th values for primary and HF inclusions is also quite large.

2. $TmCO_2$: in sample 89-655-1 the CO_2 is more pure in SGB-associated inclusions and in inclusions in the recrystallized quartz as compared with the primary inclusions. This, however, is not likely to be a result of deformation since another area of primary inclusions gave the same range of CO_2 melting points as was found in undeformed and deformed textural settings in locations 1 and 2. Hence the CO_2 in this sample contains variable amounts of dissolved CH_4 irrespective of textural location.

3. CO_2 density: the range of values is as great for SGB-associated inclusions as it is for primary and HF inclusions (*see* Figure 364.6c), mainly because both phase separation and deformation cause variable CO_2 densities in inclusions.

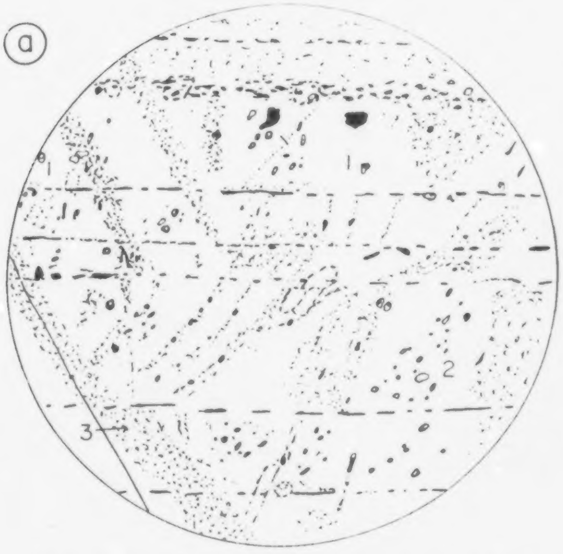

Figure 364.11a. Fluid inclusion / microstructural map for location 2, KA15; diameter 0.7 mm. Horizontal growth bands contain isolated fluid inclusions (stage 1) between them; also short healed fractures (stage 2) cross 1 or 2 growth bands. Late aqueous trails cut across all features (stage 3).

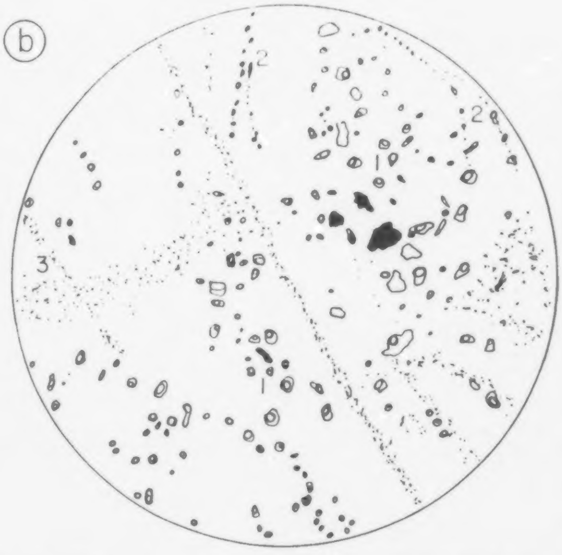

Figure 364.11b. Fluid inclusion/microstructural map for location 7, KA15; diameter 0.7 mm. Clear quartz with many isolated / cluster (stage 1) inclusions or inclusions on short healed fractures (stages 2 and 3).

4. Salinity: there is a suggestion (*see* Figure 364.6b) that the range increases to higher values for inclusions in sub-grain boundaries but this requires more data to be validated.

These observations and measurements can be compared with those of Kerrich (1976) and Noble (1982), both of whom discuss the effects of deformation on Th values relative to primary inclusions in undeformed quartz. In a study on syntectonic vein quartz Kerrich (1976) found that in recrystallized quartz crystals adjacent to undeformed crystals the number of fluid inclusions had decreased, and vapour-to-liquid ratios and homogenization temperatures had increased for the remaining inclusions. Noble (1982), also studying syn-deformational vein quartz, found that homogenization temperatures were dispersed to both higher and lower values for inclusions in strained quartz (both sub-grain dominated and recrystallized). Results from this study are most consistent with those of Noble (1982) since the same dispersion to high- and low-Th values was found. Assuming constant inclusion volumes higher Th values are caused by preferential leakage of liquid H_2O relative to vapour while lower Th values result from addition of H_2O. In the following section we suggest that both leakage and addition of H_2O are possible when inclusions are forming in a syn-tectonic environment.

Interaction of Fluid Inclusions and Dislocations in Quartz

Results show that fluids were being introduced to veins synchronously with bulk vein deformation. In this section we use published information on the interaction between dislocations and inclusions in quartz to suggest processes by which the observed geometrical patterns of fluid inclusions may be obtained.

Dislocations have been shown to be fundamental to the creep of quartz and the dislocation structures associated with work hardening and recovery have been well documented (e.g., White 1973); these dislocation structures have also been correlated with optical strain features. The interaction of inclusions with dislocations during deformation has been well studied, mainly for solid inclusions but also concerning bubbles (White 1973; Knipe and White 1978; McLaren et al. 1983; McLaren et al. 1989). Dislocations generally surmount elastically-hard solid inclusions by climb, but a fluid inclusion appears to the dislocation as a free surface (i.e., analogous to the dislocation arriving at a free crystal surface) and so the section of the dislocation which intersects the fluid inclusion is lost. Dislocations are therefore attracted to fluid inclusions since they will have a lower energy within them than without. This would suggest that dislocations can become attached to liquid inclusions in quartz. Knipe and White (1978) found that bubble size and separation were the main determinants of whether dislocation migration was free or hindered by pinning of dislocations at inclusions. Calculations using their data for typical fluid inclusion sizes show that inclusion spacings of approximately 4 mm or greater are required for free dislocation movement. The implication is that primary inclusions separated by greater than 4 mm will not hinder dislocation movement, whereas inclusions on healed fractures with smaller spacings may act as traps for dislocations and therefore be directly involved in the microstructural development of the quartz.

By consideration of the events occurring within a simple vein as it is forming, it can be seen why the observed inclusion geometries and relationships with microstructural features occur. Opening of a fracture occurs within the active shear zone in response to factors such as fluid overpressure or favourable orientation relative to the principal stress distribution. Fluid enters the fracture and begins to alter the wall rock. Crystallization proceeds from the walls inwards and "primary" fluid inclusions may be trapped in growing minerals. Depending on the balance between fluid pressure in the vein and lithostatic pressure "ambient" fluids in the wall rock may flow into the vein margin and be trapped as primary or pseudo-secondary inclusions in early paragenetic phases (e.g., scheelite). When solid continuity is made across the vein, the quartz begins to deform. Both dislocations and inclusions of whatever type will move under the external stress field. At the same time shear stresses or local fluid overpressure from trapped fluid pockets will cause fracturing. Fluid enters the fracture which then begins to heal and ultimately traps a "secondary" trail of fluid inclusions the compositions of which are essentially the same as those of the primary inclusions. This fluid inclusion trail becomes involved at once in the continual microstructural development, especially since the fracturing event itself may create dislocations (Fitzgerald et al. 1991) and because the inclusions on the fracture may be closely spaced so that they can trap dislocations. As any one area of quartz is deformed it undergoes work hardening owing to dislocation multiplication and then it attempts to relieve the accumulated strain energy by organizing the dislocations (i.e., by recovery) into patterns optically visible as sub-grains or recrystallized grains. In the presence of significant H_2O a sub-grain recovery structure is favoured while under drier conditions recrystallization is favoured (Hobbs 1968). In fluid-rich areas of the vein inclusions held at the sub-grain boundaries, or dragged into them, can either leak or actually receive water via water-saturated dislocations (Bakker and Jansen 1990). This would give the observed trends in homogenization temperatures observed in this study and by Noble (1982). In quartz undergoing recrystallization, mobile high angle grain boundaries destroy most inclusions whose contents are lost along the grain boundaries; in this situation leakage is to be expected in remaining inclusions but not addition of H_2O. This is what was found by Kerrich (1976) in his study of quartz affected mainly by recrystallization.

From the above discussion a correlation of fluid-inclusion trails with microstructural features is inevitable: either migrating fluid inclusions are trapped in recovery structures or closely-spaced fluid inclusions on healed fractures pin dislocations which then organize themselves into a recovery structure. Regarding vein formation as a dynamic system involving numerous variables it is possible to see how apparently complex fluid-inclusion geometries can be produced. The heterogeneous strain distribution within the quartz vein will then result in different stages of this dynamic process, including primary textures and fluid inclusions, being preserved.

Geological Implications

Results from detailed fluid-inclusion mapping and microthermometry have shown that low salinity, H_2O-CO_2-NaCl fluids similar to those found in previous studies of Hollinger–McIntyre and other Archean gold-bearing quartz vein ore deposits (e.g., Smith et al. 1984; Ho et al. 1985; Wood, Burrows, Thomas and Spooner 1986; Robert and Kelly 1987; Walsh et al. 1988) are present in the Hollinger–McIntyre and Kerr Addison deposits. An important new finding, however, is that these fluids have been shown to have been trapped at different stages relative to the deformation of the veins, with most of the fluid trapping occurring syn-deformationally. This is consistent with the structural observations of Wood, Burrows and Spooner (1986), Smith et al. (1990), and Burrows (1991) on the timing of vein emplacement relative to deformation. Results given above for sample specific chronologies show that these inclusions record decreasing temperature with time (i.e., TSP33-5a locations 3 and 6, KA15 locations 2 and 7). The early fluids may also show evidence for phase separation while later fluids do not show this.

Samples from the Hollinger Mine containing early paragenetic mineral phases (i.e., scheelite) show evidence for the presence of aqueous fluids at the same time as mineralization. Similar results were obtained by Burrows (1991) for the Lamaque Mine using paragenetically early tourmaline. Early aqueous fluids could be either ambient fluids present in the wall rock or they could represent an early, pre-mineralization pulse of fluid flow through the shear zone. The time gap between mineralization and formation of late secondary aqueous fluids or even later CH_4 fluids has not been constrained. There are several possibilities for the origin of these late aqueous fluids including: 1) ambient crustal fluids present in and around the shear zone into which mineralizing fluids were introduced; i.e., the same fluids as the early aqueous fluids; 2) spent hydrothermal fluids which have recirculated back into the system having lost most of their CO_2, (this is a less likely possibility owing to the salinity difference between the aqueous fluids and the mineralizing fluids) or 3) the late saline fluids and late CH_4 fluids found in the deep Hollinger sample having similar composition of shield brines.

Preliminary results from samples outside the Hollinger Mine and from a deep level within the mine show that primary fluids in both cases are enriched in CH_4 relative to primary fluids in surface pit samples. High $CH_4/(CH_4 + CO_2)$ ratios were also found in deep samples (1500-, 1800-, and 2700-foot levels) by gas chromatographic analysis (Spooner et al. 1987). Also, Smith et al. (1984) and Spooner et al. (1987) found high levels of dissolved CH_4 specifically in samples from veins hosted in graphitic-schist horizons. These data indicate that some three-dimensional variations in fluid chemistry may occur. In contrast, the CO_2 from the deep Kerr Addison sample is pure which suggests that elevated CH_4 levels with increasing depth are not a ubiquitous feature of Archean gold systems. However, the existence of this trend in one of the largest known deposits of its kind is cause enough for further evaluation. There is strong evidence that the nature of the host rock plays an important role: the Kerr Addison sample has an ultramafic host while the Hollinger samples were all from mafic volcanic host rocks. The presence of carbonaceous interflow horizons and of carbonaceous material dispersed within volcanic flows is well documented in the Hollinger–McIntyre mine and also within the flow ore at the Kerr Addison Mine. In addition, petrographic observations on a quartz-carbonate sample from the 2700-foot level at Hollinger showed small flecks of graphite occurring at the interface between the carbonate and the quartz (*see* Figure 364.12). This texture was also observed by Keys (1938) in his observations on Hollinger vein material. Petrographic evidence thus supports the possibility that the presence of graphite may be an important control on fluid chemistry in Hollinger–McIntyre. Also Smith et al. (1984) calculated that the mineralizing fluids should have been in equilibrium with graphite. The effect of graphite on fluid composition will depend on the degree of interaction of the fluid with graphitic material. Further analyses should reveal if this effect leads to local fluctuations in fluid composition or whether the original deep fluid was already affected by graphite.

Implications for Bulk Fluid Inclusion Volatile/Cation/Anion Analysis

The procedure which has been described above and the results which have been obtained have important implications for sample selection for bulk fluid-inclusion analysis (e.g. Channer et at. 1990). The relative degree of deformation of the sample is important since a sample with a lot of dynamic recrystallization may have lost most early fluids, but may be a good sample for analyzing late, secondary aqueous fluids. Relatively undeformed samples may be better candidates for analyzing primary fluids although the dilution effect of later trapped fluids has to be assessed. The procedure identifies the number of fluid events in a sample and the degree of compositional variation between them: this is important both as an aid to sample selection and also in data interpretation.

CONCLUSIONS

1. A simple procedure has been established to map fluid inclusions in deformed quartz on the basis of their textural setting and to establish their relations with microstructural features. As a result of this procedure it has been established that microstructural features can be used as relative timing tools in establishing sample specific chronologies.

2. Mineralizing fluids in gold bearing quartz veins at Hollinger–McIntyre and at Kerr Addison have been shown to be H_2O-CO_2-NaCl fluids similar to those found in other studies of similar deposits. Sample specific chronologies show that these fluids were introduced syn-deformationally. There appears to be little compositional variation with time for the mineralizing fluids, but in some cases a decline of temperature can be measured.

3. The importance of microstructural variation within a vein has been established as a factor to be considered in fluid-inclusion studies. For example, the sample from Kerr Addison showed evidence both for preservation of primary growth textures and for syn-deformational crystal growth; this sample contained well-preserved, primary fluid inclusions. In sample TSP33-5a the fluid chronology in quartz fractures in scheelite correlated with the chronology for second-stage vein quartz, while inclusions in scheelite preserve earlier stages of the fluid history of the vein. In TSPN-2 an area from low strain quartz in the vein margin had a similar fluid chronology to an area from the sub-grain-dominated vein centre. Hence in some cases a complex fluid history may be obtained while in others a similar history of events is obtained from different parts of the vein.

4. The most obvious effect of deformation on fluid-inclusion contents is to cause leakage. This is shown by increased vapour to liquid ratios and darkening of inclusions (Wilkins and Barkas 1978). Also H_2O may be added to inclusions resulting in lower homogenization temperatures. Both leakage and addition of water can occur for inclusions in quartz in an actively deforming and fluid-bearing vein in which recovery is dominated by sub-grain formation (i.e., this study and Noble 1982). Under drier conditions recovery is dominated by recrystallization and in this situation leakage occurs but not water addition. There is a suggestion that there is a salinity increase in inclusions which have leaked.

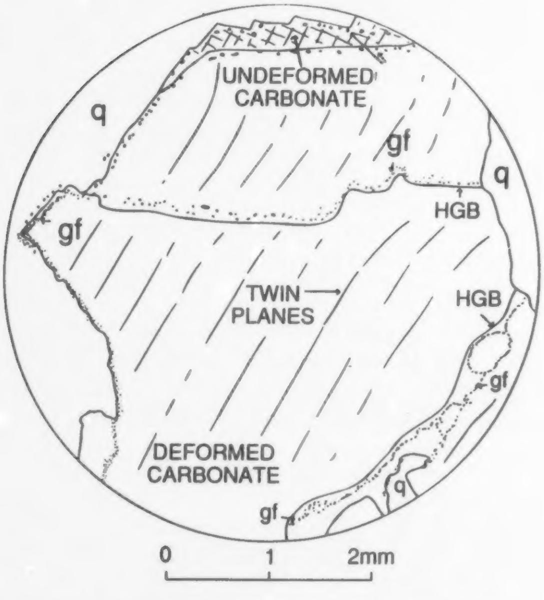

Figure 364.12. Diagram of graphite (gf) occurring at the interface between carbonate and quartz, and also in zones where the carbonate has been recrystallized along fractures and in places infilled by quartz. Sample 27-S157, Hollinger Mine, 2750-foot level, 95 vein.

5. Preliminary data for three-dimensional variations in fluid composition suggest that in Hollinger–McIntyre the $CH_4/(CH_4 + CO_2)$ ratio may increase laterally and with depth. The geometry of this trend and the role of graphite as a cause are being evaluated. The lack of this trend at Kerr Addison suggests that the nature of the host rock is also important. At the same mine level samples from similar host rocks have fluid chronologies and compositions which compare well.

6. This detailed fluid inclusion/microstructural analytical procedure is a necessary pre-requisite to bulk fluid-inclusion analysis using techniques and procedures described in Channer et al. (1990).

ACKNOWLEDGMENTS

This research is supported by Ontario Geoscience Research Grant 364 to E.T.C. Spooner. We thank the Geological Survey of Canada for providing sample H4550-1 (GSC 065525). We also thank individuals K. Gorra for photographic work, G. Taylor for preparing fluid-inclusion sections, and A. E. Camacho for assistance with drafting. D.M.DeR.Channer gratefully acknowledges receipt of a Canadian Rhodes Scholars Foundation Scholarship and a NATO Overseas Studentship.

REFERENCES

Bakker, R.J. and Jansen, J.B.H. 1990. Preferential water leakage from fluid inclusions by means of mobile dislocations; Nature (London), Physical Science, v.345, p.58–60.

Burrows, D.R. and Spooner, E.T.C. 1986. The McIntyre Cu-Au deposit, Timmins, Ontario, Canada; *in* Proceedings of Gold '86, an International Symposium on the Geology of Gold, p.23–39.

Burrows, D.R. 1991. Relationships between Archean lode gold quartz vein deposits and igneous intrusions in the Timmins and Val-d'Or areas, Abitibi Subprovince, Canada; unpublished PhD thesis, University of Toronto, Toronto, Ontario, 198p.

Burrows, S., Humphreys, J. and White, S.H. 1979. Dynamic recrystallization: a comparison between magnesium and quartz; Bulletin of Mineralogy, v.102, p.75–79.

Channer, D.M.DeR., Bray, C.J. and Spooner, E.T.C. 1990. Multi-species (~30) fluid inclusion cation/anion/volatile analysis (ion/gas chromatography; ICP-AES) applied to the Hollinger–McIntyre and Kerr Addison Archean gold-bearing quartz vein systems; Ontario Mines and Minerals Symposium, Program with Abstracts, p.21.

Fitzgerald, J.D., Boland, J.N., McLaren, A.C., Ord, A. and Hobbs, B.E. 1991. Microstructures in water-weakened single crystals of quartz; Journal of Geophysical Research, v.96, no.B2, p.2139–2155.

Furse, G.D. 1948. McIntyre Mine; *in* Structural geology of Canadian ore deposit, Canadian Institute of Mining and Metallurgy, p.482–496.

Ho, S.E., Groves, D.I. and Phillips, G.N. 1985. Fluid inclusions as indicators of the nature and source of ore fluids and ore depositional conditions for Archean gold deposits of the Yilgarn block, Western Australia; Transactions of the Geological Society of South Africa, v.88, p.149–158.

Hobbs, B.E. 1968. Recrystallization of single crystals of quartz; Tectonophysics, v.6, p.353–401.

Jones, W.A. 1948. Hollinger Mine; *in* Structural geology of Canadian ore deposits, Canadian Institute of Mining and Metallurgy, p.464–481.

Kerrich, R. 1976. Some effects of tectonic recrystallization on fluid inclusions in vein quartz; Contributions to Mineralogy and Petrolology, v.59, p.195–202.

Keys, M.R. 1938. A comparative study of the mineralogy of the auriferous quartz veins encountered in the Hollinger Mine, Porcupine district, Ontario; unpublished MSc thesis, Queen's University, Kingston, Ontario, 55p.

Knipe, R.J. and White, S.H. 1978. On the deformation of quartz containing bubbles; Journal of the Geological Society of London, v.135, p.313–316.

Lemmleyn, G.G., and Kliya, M.O. 1960. Distinctive features of the healing of a crack in a crystal under conditions of declining temperature; International Geology Review, v.2, p.125–128.

Mason, R. and Melnik, N. 1986. The anatomy of an Archean gold system—The McIntyre–Hollinger complex at Timmins, Ontario, Canada; *in* Proceedings of Gold '86, an International Symposium on the Geology of Gold, p.40–55.

McLaren, A.C., Cook, R.F., Hyde, S.T. and Tobin, R.C. 1983. The mechanisms of the formation and growth of water bubbles and associated dislocation loops in synthetic quartz; Phys. Chem. Minerals, v.9, p.79–94.

McLaren, A.C., FitzGerald, J.D. and Gerretsen, J. 1989, Dislocation nucleation and multiplication in synthetic quartz: relevance to water weakening; Phys. Chem. Minerals, v.16, p.465–482.

Noble, S.N. 1982. Petrology and fluid inclusion study of W-Mo mineralization of the Logtung deposit, South-central Yukon territory; unpublished MSc thesis, University of Toronto, Toronto, Ontario, 286p.

Robert, F. and Kelly, W.C. 1987. Ore-forming fluids in Archean gold-bearing quartz veins at the Sigma Mine, Abitibi greenstone belt, Quebec, Canada; Economic Geology, v.82, p.1464–1482.

Roedder, E. 1984. Fluid inclusions; Reviews in Mineralogy, Mineralogical Society of America, v.12, 646p.

Smith, T.J., Cloke, P.L. and Kesler, S.E. 1984. Geochemistry of fluid inclusions from the McIntyre–Hollinger gold deposit, Timmins, Ontario, Canada; Economic Geology, v.79, p.1265–1285.

Smith, D.L. and Evans, B. 1984. Diffusional crack healing in quartz; Journal of Geophysical Research, v.89, p.4125–4135.

Smith, J.P., Spooner, E.T.C., Broughton, D.W. and Ploeger, F.R. 1990. Grant 364. The Kerr Addison–Chesterville Archean Gold-Quartz vein system, Virginiatown: Time sequence and associated mafic "albitite" dike swarm; *in* Geoscience Research Grant Program Summary of Research 1989–1990, Ontario Geological Survey, Miscellaneous Paper 150, p.175–199.

Spooner, E.T.C., Bray, C.J., Wood, P.C., Burrows, D.R. and Callan, N.J. 1987. Grant 236. gold-bearing quartz vein and Cu-Au-Ag-Mo-anhydrite mineralization, Hollinger–McIntyre mines, Timmins, Ontario: $\delta^{13}C$ values (McIntyre), fluid-inclusion gas chemistry, Pressure (depth) estimation, and H_2O-CO_2 phase separation as a precipitation and dilation mechanism; *in* Geoscience Research Grant Program Summary of Research 1986–1987, Ontario Geological Survey, Miscellaneous Paper 136, p.35–56.

Sterner, S.M. and Bodnar, R.J. 1989. Synthetic fluid inclusions—VII. Re-equilibration of fluid inclusions in quartz during laboratory simulated metamorphic burial and uplift; Journal of Metamorphic Geology, v.7, p.243–260.

Walsh, J.F., Kesler, S.E., Duff, D. and Cloke, P.L. 1988. Fluid inclusion geochemistry of high grade, vein hosted gold ore at the Pamour Mine, Porcupine Camp, Ontario; Economic Geology, v.83, p.1347–1367.

White, S.H. 1971. Natural creep deformation of quartzites; Nature (London), Physical Science, v.234, p.175–177.

White, S.H. 1973. The dislocation structures responsible for the optical effects in some naturally deformed quartzites; Journal of Materials Science, v.8, p.490–499.

Wilkins, R.W.T. and Barkas, J.P. 1978. Fluid inclusions, deformation, and recrystallization in granite tectonites; Contributions to Mineralogy and Petrology, v.65, p. 293–299.

Wood, P.C. 1987. The Hollinger–McIntyre gold-bearing quartz vein system, Timmins, Ontario: geological characteristics, fluid properties, and light stable isotope geochemistry; unpublished MSc thesis, University of Toronto, Toronto, Ontario, 288p. Also available as Ontario Geological Survey Open File Report 5756, 1991, 289p.

Wood, P.C., Burrows, D.R. and Spooner, E.T.C. 1986. Grant 236. gold-bearing quartz vein and intrusion hosted Cu-Au-Ag-Mo mineralization, Hollinger–McIntyre mines, Timmins, Ontario: Geological characteristics, structural examination, igneous and hydrothermal alteration geochemistry, and light stable isotope geochemistry; *in* Geoscience Research Grant Program Summary of Research, 1985–1986, Ontario Geological Survey, Miscellaneous Paper 130, p.115–137.

Wood, P.C., Burrows, D.R., Thomas, A.V. and Spooner, E.T.C. 1986. The Hollinger–McIntyre gold-bearing quartz vein system, Timmins, Ontario, Canada; Geologic characteristics, fluid properties, and light stable isotope geochemistry data; *in* Proceedings of Gold '86, an International Symposium on the Geology of Gold, p.56–80.

Grant 370 New Information on Tectonic Relations among the Parry Sound, Seguin and Rosseau Domains

R.I. Macfie and J.M. Dixon

Department of Geological Sciences, Queen's University, Kingston, Ontario.

Mapping of the region of the triple junction between the Parry Sound domain, the Rosseau domain and the Seguin domain of the southwestern part of the Central Gneiss Belt (Ontario Grenville) demonstrates that rocks of the Parry Sound domain have been thrust westward to northwestward over the Rosseau domain, and rocks of the Seguin domain have been thrust northwestward over the Parry Sound domain. However, the steeply dipping boundary between the northwesternmost part of the Seguin domain and the Parry Sound domain is complex. It appears to have been modified by a significant component of northwest-southeast flattening caused by local compression of the northwestern Seguin domain against a ramp-like perturbation in its basal shear zone. Major splays cutting the Parry Sound domain, rooted in the shear zone beneath Seguin domain, may have formed during this compressional deformation.

Minor gold anomalies have been detected in samples of "Seguin Falls gneiss", a unit of possible supracrustal origin which was previously suggested as a target for gold exploration.

INTRODUCTION

The southwestern part of the Grenville Province in Ontario has been divided by Davidson and co-workers (Davidson and Morgan 1981; Davidson et al. 1982; Culshaw et al. 1983) into a number of lithotectonic domains characterized by contrasting rock types, metamorphic grade and structural style. These domains are separated by major ductile deformation zones, and it has been inferred that the domains are erosional remnants of mid-crustal tectonic slices emplaced during northwest-directed thrusting during the Grenvillian orogeny (ca. 1160 to 970 Ma, Rivers et al. 1989). The study area of this project (Figure 370.1) includes a complex triple junction where three of these domains intersect in a manner suggestive of sandwiching of a granulite facies sheet (Parry Sound domain) between amphibolite facies sheets (Rosseau and Seguin domains) with contrasting lithostructural characteristics (Macfie and Dixon 1990a).

This study, now in its second year, has been designed in part to elucidate the tectonic history of this part of the Central Gneiss Belt. The initial goals of the project were to examine the validity of the domainal subdivision and to test the general model of northwest-directed thrusting of tectonic sheets in the middle or deep crust. Northwest-directed thrusting within the Grenville Province has been demonstrated in many places, but the relatively complex model which Davidson and co-workers published following reconnaissance mapping in the area around Parry Sound, Ontario (Davidson et al. 1982; Culshaw et al. 1983), continues to be tested (e.g., Nadeau *in* Davidson et al. 1985; Culshaw et al. 1990). The study area of the present project comprises an important, but hitherto unmapped, part of the type area for the tectonic model of Davidson and co-workers. The study area was chosen in part because the traces of major deformation zones, well-expressed as topographic lineaments, are visible with striking clarity on air photographs and topographic maps (e.g., the shaded topographic map NTS 31 E/SW Edition 5, 1965). Such topographic lineaments provide reliable indicators of the locations of major deformation zones, and were used by Davidson and co-workers as a framework for their tectonic model for the southwestern Central Gneiss Belt. Work to date on this project has confirmed their model in its broadest aspects, in that their lithotectonic domains are recognizable and are bounded by deformation zones showing evidence of predominantly northwest-directed ductile flow (Macfie and Dixon 1990a).

However, we have found evidence that the tectonic history is more complicated than previously suspected.

Another goal of the project is the evaluation of the economic mineral potential of the area. The study area includes part of the Parry Sound domain, within which previous workers have identified numerous mineral occurrences (Hewitt 1967; Garland and Villard 1990) and an abundance of possible metavolcanic rocks, making the domain an apparently favourable target for exploration. However, although marble, semi-pelitic metasediment and quartzite occur sporadically within the Parry Sound domain, what some workers have considered to be metavolcanic and stratified metasedimentary rocks have been shown to be tectonites (e.g., Davidson and Morgan 1981), and a re-examination of the true nature and origin of the Parry Sound "greenstone belt" (Villard 1980) has become necessary from the point of view of mineral exploration. Work to date demonstrates the existence, at least within the study area of this project, of a considerable amount of metasupracrustal rock, some of possible volcanic or proximally-resedimented volcanic origin.

Preliminary conclusions following the first year of work on this project were presented by Macfie and Dixon (1990a). This report presents new data and further conclusions following the second field season and a further eight months of laboratory work.

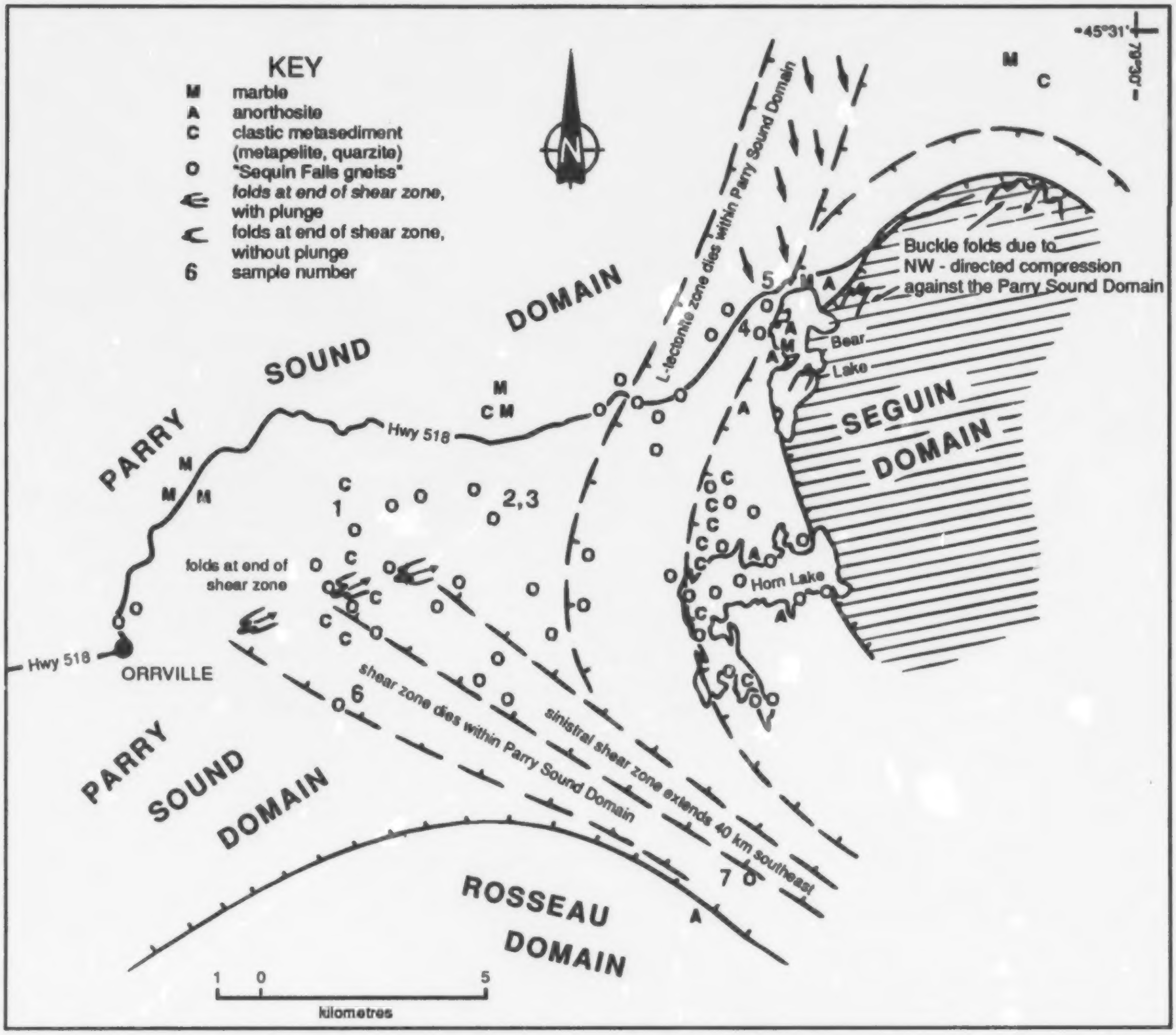
KEY
M marble
A anorthosite
C clastic metasediment (metapelite, quartzite)
O "Sequin Falls gneiss"
folds at end of shear zone, with plunge
folds at end of shear zone, without plunge
6 sample number
N
45°31'
79°30'
L-tectonite zone dies within Parry Sound Domain
Buckle folds due to NW - directed compression against the Parry Sound Domain
Bear Lake
SEGUIN DOMAIN
PARRY SOUND DOMAIN
Hwy 518
Hwy 518
ORRVILLE
folds at end of shear zone
Horn Lake
2,3
1
4
5
6
7
shear zone dies within Parry Sound Domain
sinistral shear zone extends 40 km southeast
PARRY SOUND DOMAIN
ROSSEAU DOMAIN
1 0 5
kilometres

Figure 370.1. Simplified geology of the study area. Heavy solid lines are domain boundaries. Dashed lines represent major deformation zones. Ticks indicate dips of major features. Numbered locations correspond to sample numbers in Table 370.1. For more detailed maps of the geology of the area see Macfie and Dixon, 1990a,b.

Ongoing work includes a thermobarometric study, now in its preliminary stage, aimed at acquiring an improved understanding of the magnitude of displacements associated with emplacement of the lithotectonic domains. U–Pb geochronological work is planned as part of the Lithoprobe Abitibi–Grenville research program.

GEOLOGY OF THE STUDY AREA

The general geology of the area was described by Macfie and Dixon (1990a). Briefly, in this area the Parry Sound domain consists predominantly of intermediate to mafic orthogneiss and gneiss of indeterminate origin. Metagabbro is common, as is granitoid gneiss. Gneiss of unequivocal supracrustal origin occurs sporadically, and includes metapelite, quartzite and marble. Other rock of probable supracrustal origin is widespread, including grey intermediate gneiss that contains distinctive calc-silicate boudins and that at one location shows unusual layering and grain-size variation which do not appear to be tectonic or igneous in origin. The significance of this gneiss is discussed in detail in Macfie and Dixon (1990a). The Parry Sound domain shows abundant evidence of having been subjected to granulite facies temperature conditions, although retrogression of granulite facies assemblages to amphibolite facies has affected all rocks in the Parry Sound domain to a greater or lesser degree.

Both the Seguin domain and the Rosseau domain contain a greater proportion of granitoid rocks and a much lower proportion of mafic rocks than does the Parry Sound domain. The part of the Rosseau domain included in the study area consists mostly of relatively homogeneous, poorly layered, highly migmatitic granitoid orthogneiss with conspicuous hornblende porphyroblasts in leucosome veins. The Seguin domain, on the other hand, consists of more heterogeneous, well layered, less migmatitic gneisses of unknown protolith. Neither domain shows evidence of granulite facies metamorphism within the study area, although evidence of such is observed within both approximately 20 km to the southeast (Davidson et al. 1982).

Internally, the three lithotectonic domains have notably different structural styles. Structure in the Parry Sound domain is lobate at the kilometre scale, with tectonic layering wrapping around bodies of gabbro and orthogneiss. Except near its bounding deformation zones, outcrop-scale fold closures are rarely observed, but stereographic analysis of poles to layering indicates the presence of large-scale folds with southeast-plunging axes (Macfie and Dixon 1990a). Layering in the Seguin domain is much more regularly disposed, and oriented approximately parallel to the boundary of the domain. Layering in the migmatites of Rosseau domain is poorly defined and is generally shallow dipping, except near the domain boundary where gneisses become tectonoclastic. Overall, the three lithotectonic domains are distinguished in the field on the basis of a combination of compositional, metamorphic and structural characteristics.

The Parry Sound domain and the Seguin and Rosseau domains are bounded by wide ductile deformation zones. Evidence of northwest directed thrusting of the Parry Sound domain over the Rosseau domain, and of the Seguin domain over both, is abundant (Macfie and Dixon 1990a), but detailed mapping and new data following the eastward expansion of the study area provide evidence of a more complex tectonic history.

NEW OBSERVATIONS

Parry Sound Domain – Seguin Domain Boundary

The boundary between the Parry Sound domain and the Seguin domain has been found to lie even further to the east than was thought following the first season of field work (Macfie and Dixon 1990a). At that time it was determined that the boundary of the Seguin domain defined by Davidson et al. (1982) was incorrectly placed at the northwesternmost end of the domain. Davidson et al. (1982) had located the boundary along a prominent topographic lineament which was the trace of a major ductile deformation zone. This deformation zone extends approximately 60 km to the southeast, and along most of its length is known to be the southwest margin of the Seguin domain (Davidson et al. 1982). However, Macfie and Dixon (1990a) recognized that at its northwest end this deformation zone terminated within the Parry Sound domain (Figure 370.1) and thus could not be a boundary zone along its entire length. The northwest boundary of the Seguin domain was revised to a location approximately 10 km to the east, at a 3 km wide lineament zone rooted in the longer deformation zone referred to above. This lineament zone is the most prominent such feature in the area and the east dipping deformation zone it represents defined what appeared to be a logical termination for the synformal lobate Seguin domain. Its arcuate trace truncated structures typical of the interior of the Parry Sound domain, and the intensity of deformation as inferred from lineament density on air photographs decreased markedly to its east and west. Therefore, it was interpreted as a wide ductile deformation zone separating a thrust sheet (Seguin domain) from its structural basement (Parry Sound domain).

Certain problems arose, however, from this placement. The new boundary lay at the eastern edge of the study area and the geology to the east, in what had originally been considered the interior of the Seguin domain, was poorly known. It became apparent that much of the rock both within the prominent lineament zone and for approximately 1 km to the east resembled more highly deformed equivalents of the epidote-pod, calc-silicate-bearing grey gneiss typical of the Parry Sound domain in this region. Furthermore, a number of outcrops of strained anorthosite, a rock type occurring along many important tectonic breaks in the southwest Central Gneiss Belt (Davidson 1986), were observed to the east of the proposed boundary lineament zone. Therefore it was decided early in the second field season of the project to expand the study area eastward and to map the boundary in greater detail in order to examine more closely the transition from the Seguin domain to the Parry Sound domain.

It is now apparent that the most prominent zone of topographic lineaments does not represent a deformation zone separating the Seguin domain from its structural basement. Instead it is a zone of high strain imposed upon rocks in the margin of the Parry Sound domain. New evidence permits the precise definition of a boundary which reliably separates the Parry Sound domain and the Seguin domain on the basis of lithological contrast.

The revised boundary (Figure 370.1) is mappable as a distinct compositional break separating an extensive area of migmatitic granitoid gneisses of unknown origin, typical of the Seguin domain, from the more heterogeneous grey and mafic gneisses of the Parry Sound domain. A unit of homogeneous pink medium-grained alaskitic gneiss occurs in the marginal Seguin domain along much of the east side of the boundary, and contains what appear to be segments of mafic dikes (Photo 370.1). These presumed dikes are folded and in places are boudinaged, but segments are laterally extensive and retain morphological characteristics typical of dikes, including what may be apophyses. Such recognizable dikes are not observed in the Parry Sound domain within the study area. Equally importantly, rock types which are distinctive and characteristic of the Parry Sound domain, including the gneiss that contains calc-silicate pods described above, anorthosite, marble and quartzite, occur immediately adjacent to the west side of the lithological transition but are not observed to the east of it (Figure 370.1).

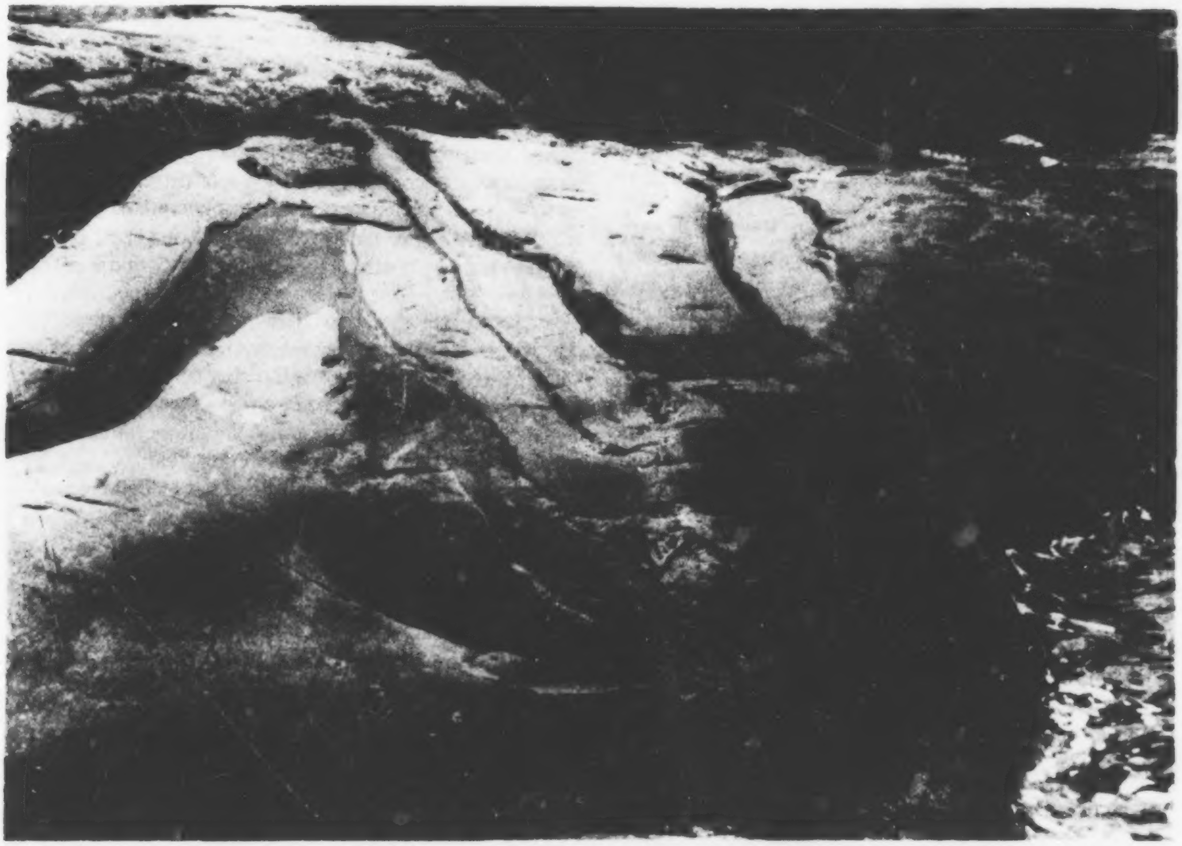

Photo 370.1. Buckled mafic dike segments in pink alaskitic migmatite of northwesternmost Seguin domain, adjacent to the domain boundary; Bear Lake. Width of view in foreground is approximately 2 m.

The lithological boundary, therefore, separates areas of contrasting geology. However, if the domains are remnants of thrust sheets they must be separated by zones or surfaces of dislocation that should be recognizable on the basis of tectonite fabrics. This is demonstrable along much of the Seguin domain boundary—the southwestern boundary of the domain is predominantly a zone of northwest-striking sinistral shear separating the Seguin domain from the very different rocks of the Rosseau domain, the structural basement. However, along the northwestern "front" of Seguin domain the domain boundary is structurally cryptic. It occurs within a 10 km wide zone of tectonites derived from the margins of both the Parry Sound domain and the Seguin domain, but it does not show evidence of relatively higher strain as would be expected of a zone of major dislocation by thrusting. Nor does it present evidence of simple shear such as would be expected of an unmodified thrust surface. Except for minor areas of tectonically mixed rocks, the lithological boundary appears to be a simple compositional break within a wide zone of tectonites.

It is probable that the compositional break between the Parry Sound domain and the northwesternmost Seguin domain represents the basal shear zone of a Seguin–Moon River thrust sheet which has been structurally modified by subsequent east-west compression. The southwestern margin of Seguin domain, which is a ductile shear zone more than 40 km in length, exhibits abundant evidence of northwest directed simple shear and a large amount of strain. This indicates considerable displacement of the Seguin–Moon River thrust sheet. The general morphology of the northwestern front of Seguin domain suggests that the shear zone beneath the Seguin domain here had a ramp-like geometry. This ramp-like structure may have developed as a local perturbation in the basal shear zone as a consequence of the thrusting of the Seguin domain over the less ductile granulites of the Parry Sound domain. However, this area lacks the asymmetric fabric elements that would have developed during northwestward displacement by simple shear. For example, gneisses contain abundant symmetrical, and no rotated asymmetrical, porphyroclasts. Likewise, C-S fabrics and shear bands, easily found in the southwest marginal shear zone, have not been observed at the northwestern front of the Seguin domain. Nonetheless, the great width of the tectonite zone in the area of the ramp-like structure suggests a considerable amount of strain, manifested largely as transposed tectonic layering, a strongly developed stretching lineation, and boudinaged gneissic layering and pegmatite dikes.

There are indications that much of this strain is the result of northwest-southeast flattening caused by a significant component of northwest directed pure shear, perhaps effected by compression due to drag on the ramp-like structure (cf. Berger and Johnson 1980) during continued northwest displacement of the Seguin domain. Flattening is indicated by conspicuous buckle folding, into boundary parallel orientations, of mafic dikes in the margin of the Seguin domain (Photo 370.1), and apparent folding of the lithological boundary itself (Figure 370.1). The latter occurs at the northern corner of the Seguin domain, where the boundary zone bends in a moderately tight arc opening to the south. Within the bend, layering at outcrop scale is folded with south plunging fold axes and S and Z parasitic folds are compatible with buckling of the boundary during southeast-northwest horizontal shortening. This horizontal shortening may have steepened the ramp-like northwestern end of the Seguin domain and overprinted the earlier formed asymmetric fabric elements developed during thrusting on the ramp. Flattening during local horizontal shortening could also account for the great width of the boundary parallel zone of transposed gneisses between the Parry Sound domain and the northwesternmost Seguin domain.

The model of southeast-northwest compression against a local steeply dipping part of the shear zone between the Seguin and Parry Sound domains may also account for two previously unexplained features in the underlying Parry Sound domain. In the western part of the study area, within the Parry Sound domain, rocks are less retrogressed from granulite facies and less migmatitic, and therefore were probably more rigid than rocks immediately adjacent to the bounding deformation zone. In this area there occur minor (less than 1 m wide) shear zones cutting older tectonic layering. Some show components of dextral, and others sinistral, displacement, usually with a significant component of dip-slip movement. Such shear zones are much less common, or absent, even further west in the interior of the Parry Sound domain (cf. McRoberts et al. 1988). They could be members of conjugate shear pairs resulting from compression and failure of rocks of the Parry Sound domain west of the ramp-like structure in the basal shear zone of the Seguin domain. Some biotite bearing rocks in this area exhibit a weak northeast-striking foliation which transects older tectonic layering. This orientation is unusual for foliation in the study area in general, where the latest foliations are usually southeast-striking (Macfie and Dixon 1990a). This northeast foliation may have been locally imposed on the Parry Sound domain as a result of northwest-directed compression against the ramp-like structure in the basal shear zone of Seguin domain.

A wide zone of north-striking transposed gneissosity, rooted in the deformation zone at the northwestern front of the Seguin domain, appears to die out within the Parry Sound domain north of the study area (Figure 370.1). It contains a high proportion of L-tectonite, with lineations plunging nearly due south. The occurrence of significant amounts of L-tectonite and the remarkably consistent orientation of the lineations are unique to this zone. It probably developed as a result of local constriction in the arcuate ramp-like structure now exposed at the northwestern front of the Seguin domain, during southeast-northwest compression against the irregular basement topography of the Parry Sound domain. The fact that this deformation zone terminates within the Parry Sound domain (metamorphic orthopyroxene and distinctive rock types including quartzite and marble occur on both sides of it) and the fact that lineations are consistently south plunging and not fanned, demonstrate that this deformation zone is not simply a folded part of the thrust surface beneath the Seguin domain. It is, instead, a zone of ductile strain within the margin of the Parry Sound domain, with at least a late history of local north directed movement.

The southwestern boundary of the Seguin domain is readily apparent, for a distance of approximately 40 km, as a prominent topographic lineament. However, this lineament terminates within the Parry Sound domain (Figure 370.1), west of the ramp-like structure at the front of Seguin domain. The deformation zone which it represents ends in outcrop-scale folds with northeast plunging axes. The most likely explanation for this structure is that the portion of the shear zone that cuts into the Parry Sound domain is a footwall splay formed beneath the ramp-like structure in the basal shear zone of the Seguin domain. However, it is not a single plane of failure. Instead it is a broad zone of folding and ductile flow with open folds at its tip and along its structural base, and with progressively tighter folds and greater transposition and mylonitization towards its root. It would appear that progressive movement on the splay, possibly synchronous with southeast-northwest compression against the ramp-like structure at the front of Seguin domain, was taken up by widening of the splay, rather than by forward advance of its tip as would be expected in upper-crustal fold and thrust belts.

Macfie and Dixon (1990a) described a zone of granulite gneiss extending to the southeast between the Rosseau and Seguin domains, continuous with similar granulite gneisses of the interior Parry Sound domain. It appears to be a septum of rock of the Parry Sound domain squeezed between the structural basement (Rosseau domain) and the overlying Seguin domain thrust sheet. It is now evident that although the zone of gneisses showing evidence of granulite facies is approximately 600 m wide (Macfie and Dixon 1990a), a further 6 km of rock of the Parry Sound domain separates the Rosseau and Seguin domains in the study area (Figure 370.1). It is still not known how far rocks of the Parry Sound domain extend to the southeast; granulite gneisses occur approximately on-strike with the "septum" approximately 7 km to the southeast near Skeleton Lake, but it is not known whether they are derived from rocks of the Parry Sound domain. On the basis of gravity modelling, Lindia et al. (1983) suggested that the Parry Sound domain continues in the subsurface for approximately 20 km beneath the Seguin domain.

Tectonic activity continued along the boundary deformation zone of Seguin domain after its emplacement by northwest directed thrusting. In the margin of the Parry Sound domain beneath the southwestern end of the Seguin domain shear folds and flow structures in migmatite gneiss with syn- and post-tectonic leucosome (Photo 370.2) indicate southeast directed normal-sense displacement, perhaps due

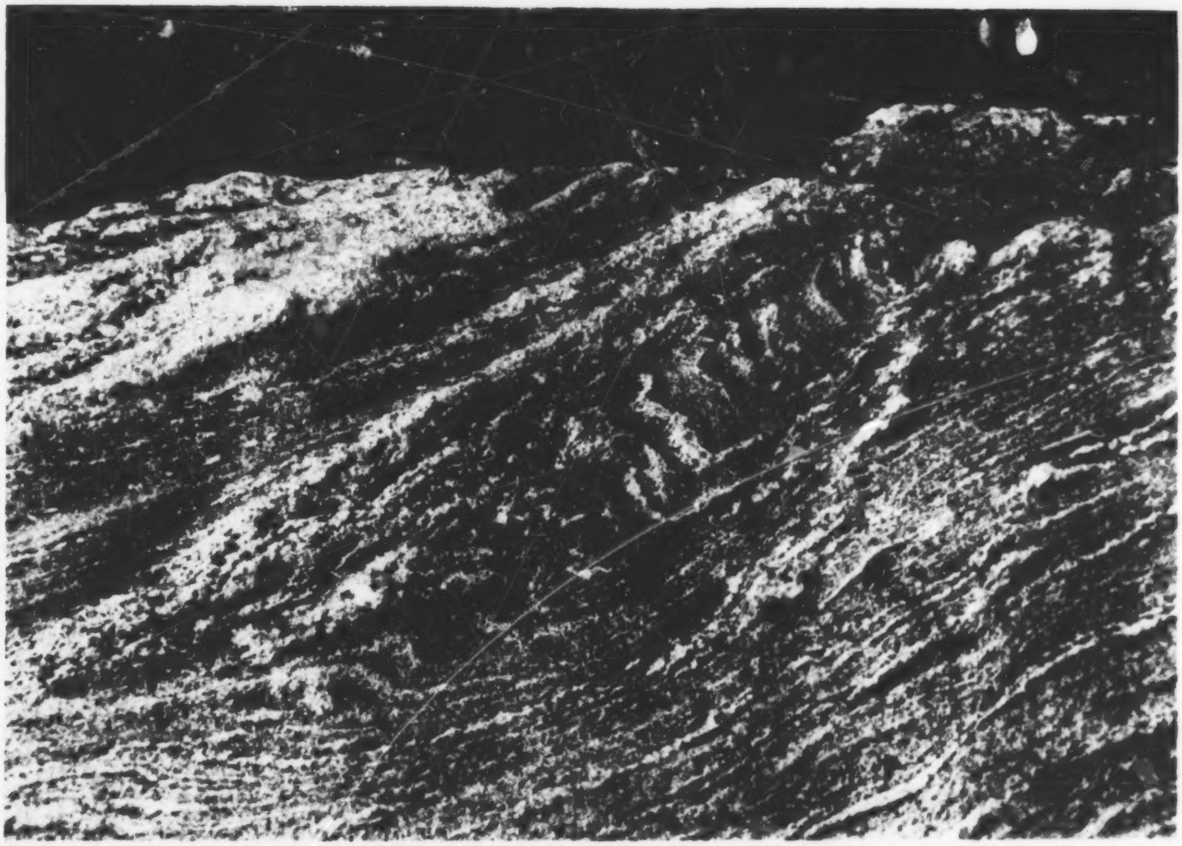

Photo 370.2. Dextral flow structure indicative of late southeast- directed, normal-sense displacement in migmatite from the margin of Parry Sound domain adjacent to the boundary with Seguin domain; Horn Lake. Pencil at right is 14 cm in length.

to local or regional gravitational readjustment following crustal thickening. Later sinistral displacement occurred on minor (typically 1 m in length) east striking, steeply dipping shear zones (Photo 370.3) which occur sporadically in the migmatite gneisses throughout the deformation zone between the Parry Sound and Rosseau domains. This sinistral displacement also occurred at high temperature—the shear zones invariably contain leucosome.

The Distribution of Rocks of Supracrustal Origin

The area within the Parry Sound domain that is known to be underlain by supracrustal and probable supracrustal rocks has been considerably enlarged in the course of mapping in 1990. New outcrops of marble, quartzite and metapelitic rocks have been discovered, including a band of quartzite at least 30 m wide. However, these rocks of undoubted supracrustal origin occur only sporadically (Figure 370.1). Much more widespread (Figure 370.1) is calc-silicate gneiss (containing several percent epidote, sphene, and scapolite) and gneiss containing up to 10% calc-silicate boudins which consist of 90 to 99% epidote, with lesser scapolite, quartz, and orange garnet. In places this gneiss shows unusual layering not readily explicable as a purely tectonic feature. For reasons described in detail in Macfie and Dixon (1990a), this unit, informally named the Seguin Falls gneiss, is thought to be of probable supracrustal, and possible volcaniclastic, origin. New field data and preliminary geochemical analyses further support this hypothesis.

First, there is a strong spatial association between this unit and rocks that are of unambiguous supracrustal origin. It occurs in common association with heterogeneous metapelite, rusty feldspathic and quartzose rocks with metapelitic bands, and banded calc-silicate/quartzose rocks. In contrast, the calc-silicate boudins have not been found in gneiss of obvious plutonic origin.

Second, REE spectra (Figure 370.2) for three rocks of the unit (selected from an area with layering most likely to be derived from primary bedding) are clearly distinct from the spectrum for a typical dioritic orthogneiss of the sort underlying much of the map area, although all of these rocks have similar major element chemistry. It is evident that the gneiss which contains calc-silicate pods is chemically distinct from at least some otherwise similar orthogneiss, within what was once considered a sea of grey gneiss.

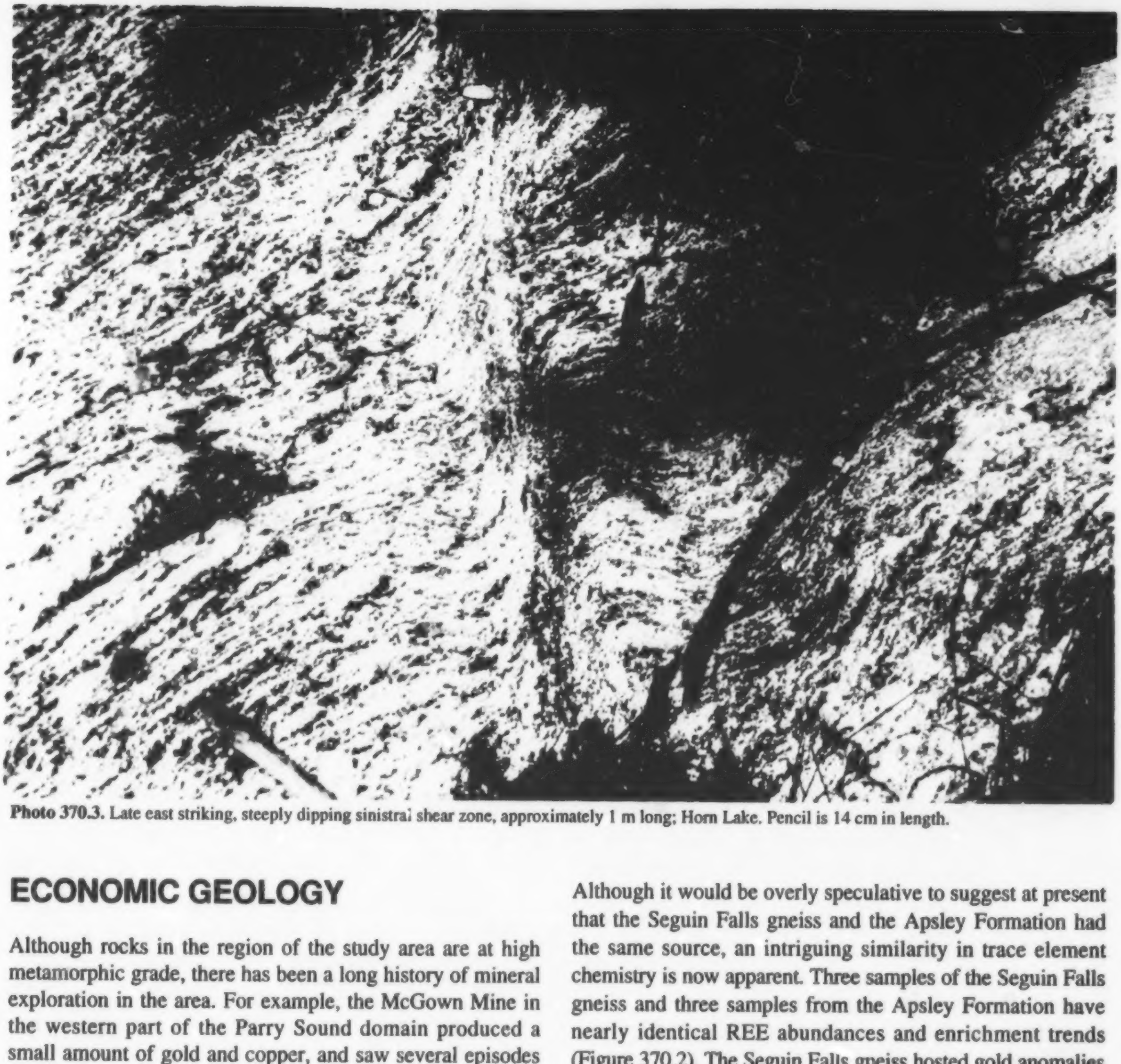

Photo 370.3. Late east striking, steeply dipping sinistral shear zone, approximately 1 m long; Horn Lake. Pencil is 14 cm in length.

ECONOMIC GEOLOGY

Although rocks in the region of the study area are at high metamorphic grade, there has been a long history of mineral exploration in the area. For example, the McGown Mine in the western part of the Parry Sound domain produced a small amount of gold and copper, and saw several episodes of exploratory work between 1894 and 1965 (Garland and Villard 1990). Mineralization in the Parry Sound domain is generally concentrated in a zone structurally above the basal shear zone of the domain (Garland et al. 1989). On the basis of gravity anomaly modelling (Lindia et al. 1983) the domain is believed to be a klippe, such that its basal shear zone crops out on both its western and eastern sides. The zone of mineralization seen along its western margin may therefore also appear at its eastern side, where the study area of the current project is located.

Based on field evidence, Macfie and Dixon (1990a) drew an analogy between the "Seguin Falls gneiss" of the study area of this project and the Apsley Formation of the Elzevir terrane. The Apsley Formation is a turbiditic metasedimentary sequence of probable volcaniclastic origin, which has been recommended as a target for gold and base metal exploration (Easton 1986). Although it would be overly speculative to suggest at present that the Seguin Falls gneiss and the Apsley Formation had the same source, an intriguing similarity in trace element chemistry is now apparent. Three samples of the Seguin Falls gneiss and three samples from the Apsley Formation have nearly identical REE abundances and enrichment trends (Figure 370.2). The Seguin Falls gneiss hosted gold anomalies according to the map of Hewitt (1967), and Macfie and Dixon (1990a) suggested that, with its easily recognized calc-silicate boudins, it might be a practical target for gold exploration. Selected samples have now been analyzed for Au by Instrumental Neutron Activation Analysis and the results are interesting. Of the seven most promising samples of various rock types from across the study area (Figure 370.1), only two contain Au at concentrations above the detection limit of 5 ppb (Table 370.1). Both are from occurrences of Seguin Falls gneiss. One (SR-44) is from a rusty pyrite-rich quartz vein in a shear zone, and the other (SR-283B) is from a pyrite-rich gossan. Gold contents are low (24 and 7 ppb Au respectively), but anomalous relative to unmineralized samples of the Seguin Falls gneiss and other gossans sampled from the study area. The Seguin Falls gneiss is the best target for mineral prospecting found in the area to date.

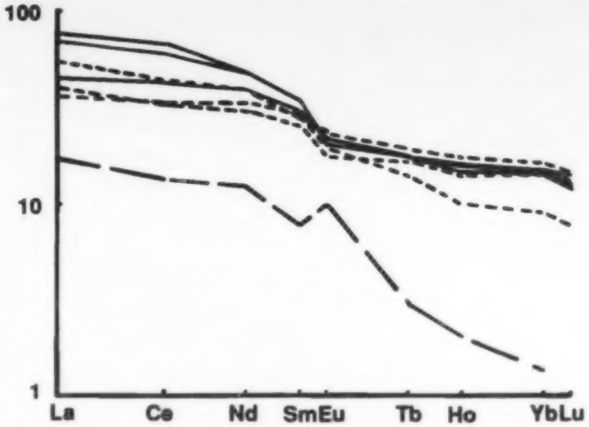

Figure 370.2. Chondrite-normalized REE spectra from three samples of Seguin Falls gneiss (solid lines), three samples of Apsley Formation of Elzevir terrane (short dashes) and a sample of dioritic orthogneiss typical of the study area (long dashes).

Other discoveries of potential economic interest include new occurrences of marble and a layer of quartzite at least 30 m wide, all found within the Parry Sound domain. Such rock types are of interest as sources of industrial minerals, but occurrences in the study area of this project are small, sporadic and not of high purity. Accessible but small (less than 500 m wide across strike) bodies of regularly jointed pink granitoid gneiss, possibly of interest as facing stone, have also been mapped out.

CONCLUSIONS

Kinematic indicators and stretching lineations demonstrate that the crustal slices represented in the study area by the Parry Sound domain and the Seguin domain were emplaced as west- to northwest-directed thrust sheets. However, the deformation zone between the Parry Sound domain and the northwesternmost part of the Seguin domain, which has a ramp-like geometry and probably was initially a local perturbation in the basal shear zone of the Seguin–Moon River thrust sheet that carried part of the thrust sheet over the more rigid rocks of the Parry Sound domain, appears to have been subsequently modified by a significant component of horizontal west- or northwest-directed compression against the Parry Sound domain.

Later tectonic activity evident in the region of the northwest Seguin domain—Parry Sound domain boundary includes high-grade, normal-sense, southeast-directed displacement and late sinistral displacement on steeply dipping, east striking minor shear zones.

Minor gold anomalies have been identified within the "Seguin Falls gneiss", a readily identifiable and extensive unit of probable supracrustal origin which has previously been suggested as a target for gold prospecting (Macfie and Dixon 1990a).

ACKNOWLEDGMENTS

This project is funded by a Geoscience Research Grant to J.M. Dixon. R.I. Macfie was supported by an Ontario Graduate Scholarship. R.M. Easton of the Ontario Geological Survey is thanked for obtaining REE analyses of samples from the study area and for providing REE data for samples of the Apsley Formation. Hugh Jennings provided excellent assistance in the field.

REFERENCES

Berger, P. and Johnson, A.M. 1980. First-order analysis of deformation of a thrust sheet moving over a ramp; Tectonophysics, v.70, p.T9–T24.

Culshaw, N., Corrigan, D., Ketchum, J. and Wallace, P. 1990. Georgian Bay geological synthesis: Twelve Mile Bay to Port Severn, Grenville Province of Ontario; *in* Current Research, Part C, Geological Survey of Canada, Paper 90-1C, p.107–112.

Table 370.1. Concentration of gold in selected samples from the study area. Instrumental neutron activation analyses performed by Bondar–Clegg.

Key	Sample	Au, ppb	Description
1.	RM 444C	<5	Rusty metapelitic gneiss, muscovite, sillimanite and pyrite-bearing.
2.	RM 676B	<5	Grey intermediate gneiss of the "Seguin Falls gneiss" unit.
3.	RM 676C	<5	Grey intermediate gneiss of the "Seguin Falls gneiss" unit.
4.	SR 034	<5	Pyrite-bearing gossan in quartzofeldspathic gneiss.
5.	SR 044	24	Pyrite and chalcopyrite-bearing quartz vein in shear zone in "Seguin Falls gneiss" unit.
6.	SR 283B	7	Pyrite-bearing gossan in "Seguin Falls gneiss" unit.
7.	SR 497	<5	Pyrite-bearing gossan in quartzofeldspathic gneiss.
	QGRM21	<5	Queen's University standard, expected value 2 ppb.
	QGRM22	57	Queen's University standard, expected value 45 ppb.

Key numbers refer to numbered locations in Figure 370.1.

Culshaw, N.G., Davidson, A. and Nadeau, L. 1983. Structural Subdivisions of the Grenville Province in the Parry Sound–Algonquin region, Ontario; *in* Current Research, Part B, Geological Survey of Canada, Paper 83-1B, p.243–252.

Davidson, A. 1986. New Interpretations in the Southwestern Grenville Province; *in* The Grenville Province, Geological Association of Canada, Special Paper 31, p.61–74.

Davidson, A., Culshaw, N. and Nadeau, L. 1982. A Tectono-metamorphic Framework for part of the Grenville Province, Parry Sound Region, Ontario; *in* Current Research, Part A, Geological Survey of Canada, Paper 82-1A, p.175–190.

Davidson, A. and Morgan, W.C. 1981. Preliminary Notes on the Geology East of Georgian Bay, Grenville Structural Province, Ontario; *in* Current Research, Part A, Geological Survey of Canada, Paper 81-1A, p.291–298.

Davidson, A., Nadeau, L., Grant, S.M. and Pryer, L.L. 1985. Studies in the Grenville Province of Ontario; *in* Current Research, Part A, Geological Survey of Canada, Paper 85-1A, p.463–483.

Easton, R.M. 1986. Paleoenvironment and Facies of the Apsley Formation, Peterborough County; *in* Summary of Field Work and Other Activities 1986, Ontario Geological Survey, Miscellaneous Paper 132, p.141–151.

Garland, M.I. and Villard, D. 1990. Algonquin Resident Geologist's District—1990; *in* Report of Activities 1990, Resident Geologists, Ontario Geological Survey, Miscellaneous Paper 152, p.3–29.

Garland, M.I., Villard, D.J. and Marmont, C. 1989. Algonquin Resident Geologist's District—1988; *in* Report of Activities 1989, Regional and Resident Geologists; Ontario Geological Survey, Miscellaneous Paper 142, p.347–353.

Hewitt, D.F. 1967. Geology and Mineral Deposits of the Parry Sound–Huntsville Area; Ontario Geological Survey, Geological Report 52, 65p.

Lindia, F.M., Thomas, M.D. and Davidson, A. 1983. Geological Significance of Bouguer Gravity Anomalies in the Region of Parry Sound Domain, Grenville Province, Ontario; *in* Current Research, Part B, Geological Survey of Canada, Paper 83-1B, p.261–266.

Macfie, R.I. and Dixon, J.M. 1990a. Tectonic relations among Parry Sound domain and Seguin and Rosseau subdomains; *in* Geoscience Research Grant Program, Summary of Research 1989–1990, Ontario Geological Survey, Miscellaneous Paper 150, p.200–212.

—— 1990b. Tectonic relations among Parry Sound domain and Seguin and Rosseau subdomains; *in* Lithoprobe Abitibi–Grenville Workshop Report III, p.81–84.

McRoberts, G., Macfie, R.I. and Hammar, J. 1988. Geology of the Manitouwabing Lake Area, District of Parry Sound; *in* Summary of Field Work and Other Activities 1988, Ontario Geological Survey, Miscellaneous Paper 141, p.309–314.

Rivers, T., Martignole, J., Gower, C.F. and Davidson, A. 1989. New tectonic divisions of the Grenville Province, southeast Canadian shield; Tectonics, v.8, p.63–84.

Villard, D.J. 1980. 1979 Report of the Algonquin Regional Mineral Resource Coordinator; *in* Annual Report of the Regional and Resident Geologists 1979, Ontario Geological Survey, Miscellaneous Paper 91, p.117–112.

Grant 375 Sedimentary Evolution in the Michipicoten Greenstone Belt, Wawa Subprovince, Superior Province

R.J. Rice and J.A. Donaldson

Ottawa–Carleton Geoscience Centre, Department of Earth Sciences, Carleton University, Ottawa

Variably deformed Dore metasediments in the southern, middle and northern metasedimentary belts within the Michipicoten greenstone belt record differences in depositional environment which reflect significant variations in paleogeography.

Sedimentation in the southern metasedimentary belt was synchronous with the youngest volcanic episode (2.7 Ga) and may have predated deposition of Dore metasediments elsewhere by roughly 15 to 20 Ma. A deep marine environment, characterized by turbidity currents, debris flows and associated felsic pyroclastic volcanism, is inferred for most of these metasediments. The deep marine setting was interrupted once by a period of uplift and fluvial deposition.

Deposition in the middle and northern metasedimentary belts may have been coeval. Turbidite-submarine fan and siliciclastic shelf environments are preserved in the northern region of the middle metasedimentary belt. In the western region of the northern metasedimentary belt, marine felsic pyroclastic volcanism dominated but was interrupted once by uplift and probable fluvial deposition. The presence of pyroclastic lithofacies in this region suggests that the youngest volcanic episode in the Michipicoten greenstone belt lasted about 20 Ma. In the eastern region of the northern belt, Dore metasediments are best interpreted as fluvial, with some felsic pyroclastic input suggesting a period of subaerial exposure possibly equivalent to that recorded in the west.

INTRODUCTION

The Wawa Subprovince, which extends from the Vermilion region of Minnesota to the Kapuskasing structural zone of Ontario (Card 1990), is bordered to the north by the Quetico Subprovince, and to the south by the Southern Province (Ontario Geological Survey 1991a).

The Michipicoten greenstone belt, the largest supracrustal belt within the Wawa Subprovince, is composed principally of metavolcanic rocks and a relatively small percentage of metasedimentary rocks (Card 1990).

Geochronological work in the Michipicoten greenstone belt and adjacent areas (Turek et al. 1982, 1984, 1988, 1990; Sullivan et al. 1985; Frarey and Krogh 1986) indicates that volcanism and associated sedimentation occurred in the roughly 200 Ma period between 2.9 and 2.7 Ga (continuous volcanism and sedimentation is not implied) with subsequent major deformation and metamorphism occurring in a roughly 50 Ma period between 2.7 and 2.65 Ga (Card 1990, figure 3). The supracrustal sequence has attained greenschist to lower amphibolite facies regional metamorphic grade (Studemeister 1983; Card 1990, figure 8).

An overall objective of this project is to document the sedimentary evolution of the latest pre-deformation period of the Michipicoten greenstone belt and to relate this evolution to economic mineralization. Two approaches have been utilized: 1) "Sections" ("Section" is used here to indicate a conformable stratigraphic succession uninterrupted by faults which could cause juxtapositioning of units of unrelated paleogeographic setting. The presence of folds in the "sections" effects only unit thicknesses, and does not juxtapose unrelated units.) of the Dore metasediments have been examined, and depositional settings inferred in five areas (Shark Lake, Arliss Lake, Kapimchigama–Radford lakes, Kabenung Lake and Troupe Lake) representing portions of three discrete, smaller belts of metasediments (southern, middle, northern) within the Michipicoten greenstone belt (Figure 375.1). 2) Samples of the metasediments have been collected to petrographically evaluate their provenance, and the tectonic setting of the latest pre-deformation period.

PREVIOUS WORK

General

Numerous gold-related studies have been carried out in the Michipicoten region. These include early work by Gledhill (1927), Moore (1931), and Frohberg (1935), and more recent work by Heather and Arias (1987), Heather and Buck (1988), and Heather et al. (1988). Results of early mapping by Bruce (1940a, 1940b) were incorporated into the initial regional geological compilation map produced by Goodwin (1963). Two succeeding geological compilation maps have included the Michipicoten greenstone belt (Milne et al. 1971; Ontario Geological Survey, 1991b). Township mapping has been completed at a scale of 1 inch to 1/4 mile by Sage

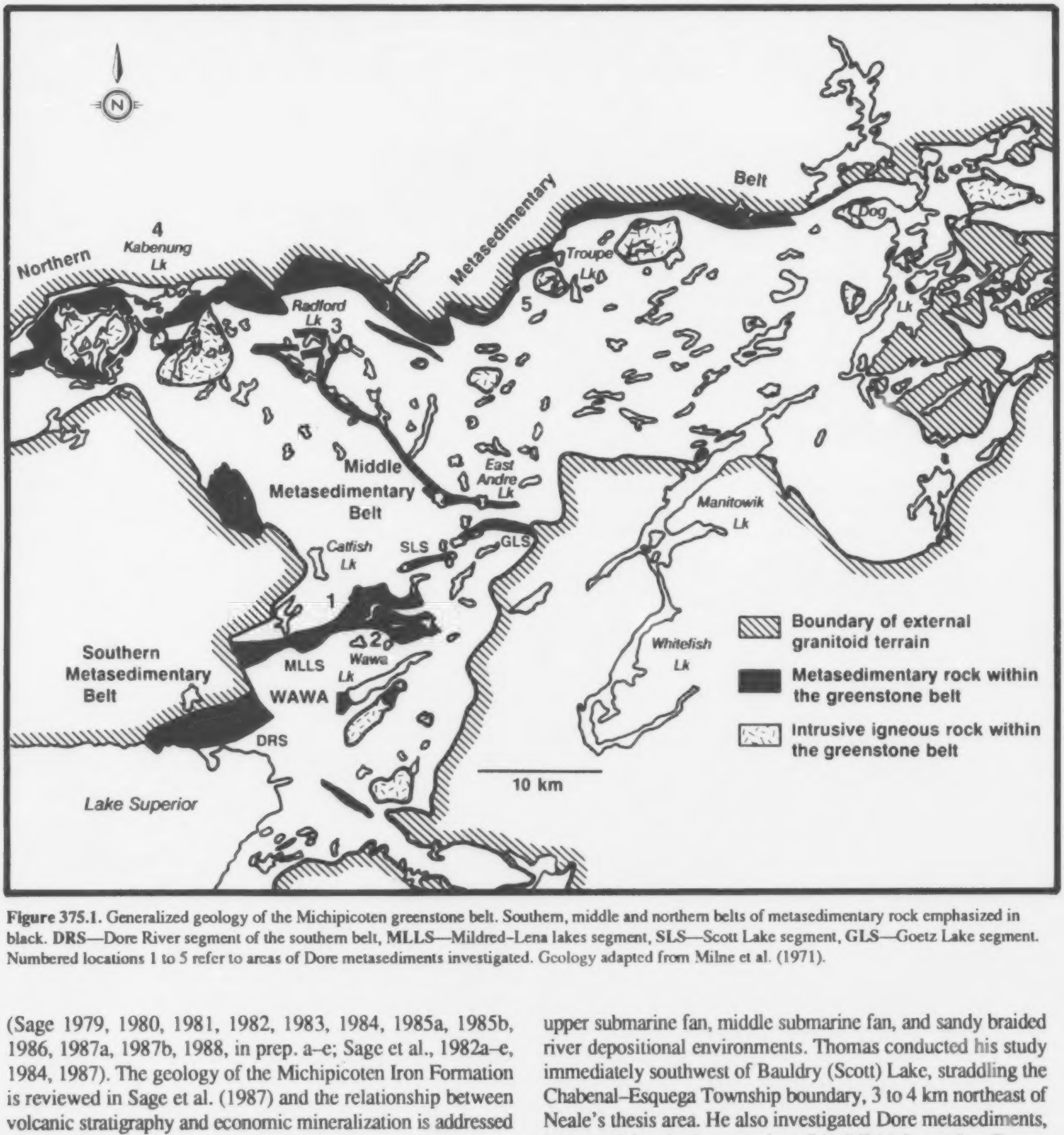
N
Northern
4
Kabenung Lk
Metasedimentary
Belt
Radford Lk
3
Troupe Lk
5
Dog Lk
Middle Metasedimentary Belt
East Andre Lk
Manitowik Lk
Catfish Lk
SLS
GLS
1
2
Southern Metasedimentary Belt
MLLS
Wawa Lk
WAWA
DRS
Whitefish Lk
Lake Superior
10 km
Boundary of external granitoid terrain
Metasedimentary rock within the greenstone belt
Intrusive igneous rock within the greenstone belt

Figure 375.1. Generalized geology of the Michipicoten greenstone belt. Southern, middle and northern belts of metasedimentary rock emphasized in black. DRS—Dore River segment of the southern belt, MLLS—Mildred-Lena lakes segment, SLS—Scott Lake segment, GLS—Goetz Lake segment. Numbered locations 1 to 5 refer to areas of Dore metasediments investigated. Geology adapted from Milne et al. (1971).

(Sage 1979, 1980, 1981, 1982, 1983, 1984, 1985a, 1985b, 1986, 1987a, 1987b, 1988, in prep. a–e; Sage et al., 1982a–e, 1984, 1987). The geology of the Michipicoten Iron Formation is reviewed in Sage et al. (1987) and the relationship between volcanic stratigraphy and economic mineralization is addressed in Sage (1987b).

Sedimentological

Previous sedimentological work in the Michipicoten greenstone belt is restricted to a reconnaissance evaluation by Ojakangas (1983) and Bachelor of Science theses by Neale (1981) and Thomas (1984). Neale studied Dore metasediments overlying the Helen–Eleanor portions of the Michipicoten Iron Range immediately west of Lena Lake in Chabenal Township. In this study Neale defined four sedimentary facies interpreted to represent, in ascending stratigraphic order, subaerial mass flow, upper submarine fan, middle submarine fan, and sandy braided river depositional environments. Thomas conducted his study immediately southwest of Bauldry (Scott) Lake, straddling the Chabenal–Esquega Township boundary, 3 to 4 km northeast of Neale's thesis area. He also investigated Dore metasediments, here overlying the Lucy portion of the Michipicoten Iron Range. Thomas (1984) defined eight facies, and three facies associations interpreted to represent, in ascending stratigraphic order, submarine fan-basinal or alluvial fan-lacustrine, submarine fan, and fluvial-alluvial fan depositional environments.

STRUCTURAL SETTING

Recent structural work in the Michipicoten greenstone belt has been conducted by Shrady (1988, 1991), McGill and Shrady (1986) and Arias and Helmstaedt (1989, 1990a, 1990b). These and earlier structural studies are reviewed in Arias and Helmstaedt (1989).

McGill and Shrady (1986) recently completed the first detailed structural studies of metasedimentary rocks in the Michipicoten greenstone belt by studying areas lying, respectively, immediately west and east of the Algoma Central Railway tracks in central Chabenal Township. Their deformation history for this region involves early kilometre-scale recumbent folding and associated thrusting with later northwest and northeast oriented folding, pervasive shearing, and late faulting.

A regional structural study is currently being completed by Arias and Helmstaedt (1990b) in the central and east-central region of the Michipicoten greenstone belt designed to complement the detailed work of McGill and Shrady. Their work suggests a regional-scale, south verging, recumbent nappe structure which has been refolded about generally east-trending axes with associated imbricate thrusts (Arias and Helmstaedt 1990b, figure 343.4). This regional-scale structural interpretation in the central area of the belt corresponds closely to the deformation sequence proposed for the southwestern region of the belt by McGill and Shrady (1986). Much of the outcrop pattern of Dore metasediments in the Michipicoten greenstone belt can be explained with this fold and thrust belt model, suggesting that the Dore strata may have formed a single belt-wide clastic sequence.

STRATIGRAPHIC SETTING

Logan (1863) and Coleman and Wilmott (1902) proposed the earliest stratigraphic terminology for metasediments in the Michipicoten greenstone belt. The former suggested that the name "Dore" be applied to a thick oligomictic orthoconglomerate containing clasts that can exceed 265 mm (boulder; descriptive terminology from this project) observed at the mouth of the Dore River in what is now southern Bostwick Township; the latter proposed the term "Eleanor slates" for finer-grained clastic metasediments in the Lena and Mildred lakes area of what is now eastern Chabenal Township (Neale 1981). Subsequent usage has resulted in the name "Dore" being applied to all exposures of clastic metasediments thought to cap a third volcanic "cycle" (see concluding paragraph of this section regarding usage of "cycle" to describe the mafic-felsic volcanic sequences) in the Michipicoten greenstone belt regardless of grain size. Usage has not been rigorous however, because Neale (1981) referred to the Dore metasediments as a group, whereas Thomas (1984) referred to them as a formation. The latter is appropriate because the Michipicoten Group (Goodwin 1962) was defined as containing these metasediments. Two lines of evidence bear on the question of whether the Dore metasediments can be considered a single deformed succession: 1) As mentioned above, there is a similarity of structural style between the southern and middle sedimentary belts, and much of the outcrop pattern of the metasediments can be explained with the fold and thrust belt model of Arias and Helmstaedt (1990b). 2) Isotopic ages of 2698±2 (magmatic zircon from igneous clast in Dore conglomerate), 2682±3 (detrital zircon from matrix of arenite), and 2680±3 Ma (detrital zircon from matrix of arenite; F. Corfu, Jack Satterly Geochronology Laboratories, Royal Ontario Museum, personal communications, 1991) obtained from Dore metasediments in the Mildred–Lena lakes segment of the southern metasedimentary belt, the northwestern extremity of the middle metasedimentary belt, and the Iris Lake area of the northern metasedimentary belt, respectively, suggest that sedimentation in the southern belt could be 15 to 20 Ma older than in the middle and northern belts. Whereas the structural model supports the contention that the Dore metasediments are a single succession, the isotopic data can be interpreted to indicate: 1) that the succession is a single, but diachronous, unit across the Michipicoten greenstone belt and/or 2) that the succession is a single unit with source regions of differing age or 3) that it consists of two separate successions (F. Corfu, personal communication, 1991). Assuming that the age difference is real (this may not be true because the younger dates were obtained from detrital zircons), the first and second interpretations are favoured herein because they provide a simpler explanation. The petrographic study planned for the Dore metasediments as part of this project should provide detrital composition information with which to evaluate the likelihood of multiple source regions, albeit without information on their relative ages.

The stratigraphy of the Michipicoten greenstone belt has been addressed principally by Goodwin (1962), Attoh (1980), Sage et al. (1987), and Arias and Helmstaedt (1990b). The lithologic succession representative of the volcanic strata of the belt is best observed in the central portion of the Goetz Lake segment of the southern metasedimentary belt which includes the Josephine portion of the Michipicoten Iron Range (*see* Figure 375.1). The stratigraphy of the Michipicoten greenstone belt has been reviewed recently by Arias and Helmstaedt (1990b).

Cyclic volcanic stratigraphy initially proposed by Goodwin (1962) and Attoh (1980) was confirmed by Sage (1986) and Sage et al. (1987) on the basis of mapping and geochemistry, as well as geochronology by Turek et al. (1982, 1984), Sullivan et al. (1985), and Frarey and Krogh (1986). The geochronological work indicated ages of about 2.75 and 2.7 Ga for the first and second "cycles", with the youngest third "cycle" not dated. Turek et al. (1988) defined a still older volcanic "cycle" at about 2.9 Ga which resulted in four volcanic "cycles" being proposed for the Michipicoten greenstone belt.

The most recent modifications to the volcanic stratigraphy of the Michipicoten greenstone belt comes from Arias and Helmstaedt (1990b) based on field relations in the Goetz Lake segment (this paper's nomenclature) of the southern metasedimentary belt. Their modifications are: 1) the contact between the Dore metasediments and the overlying mafic to intermediate volcanics of the fourth "cycle" is tectonic (thrust) rather than depositional; the fourth "cycle" is, therefore, interpreted to be a structural repetition of the base of the third "cycle". 2) the Dore metasediments, now the youngest supracrustal rocks in the Michipicoten greenstone belt, are considered to unconformably overlie the mafic to intermediate volcanic base of the third "cycle" and are therefore not part of it.

The stratigraphic modifications of Arias and Helmstaedt (1990b) are important to any sedimentological study of the Michipicoten greenstone belt because they provide a structurally realistic stratigraphic framework within which to work. These modifications accentuate the importance of determining the true nature of major lithologic contacts in the Michipicoten greenstone belt, as well as for Archean supracrustal sequences in general. The observations of Arias and Helmstaedt (1990b) indicate the need for caution in assuming cyclic, genetic relationships between felsic and mafic volcanic rocks, because the nature of many major lithologic contacts is largely undetermined, and also because only the felsic portions of volcanic "cycles" are dated. For this report the term "cycle" is placed in quotation marks to reflect this consideration.

REGIONAL SEDIMENTARY GEOLOGY

Metasedimentary rocks in the Michipicoten greenstone belt occur in three distinct smaller belts, which for the purpose of this project are informally termed southern, middle, and northern belts (*see* Figure 375.1). The southern belt is partitioned into four segments by the late north- to northwest-trending faults discussed above. For this project, from east to west these segments are informally referred to as Goetz Lake, Scott Lake, Mildred–Lena lakes, and Dore River (*see* Figure 375.1). The middle belt is affected by late faults only in its northwestern extremity, where it is partitioned into west and east segments which were not otherwise named for this project. Although the northern belt is affected by the late faults, it exists more or less continuously along the northern boundary of the Michipicoten greenstone belt with external granitoid rocks (*see* Figure 375.1).

Northern Metasedimentary Belt

Troupe Lake Region

A single, small exposure of conglomerate and arenite metasediment was examined in the eastern end of the northern metasedimentary belt (location 5, Figure 375.1) in central south Dunphy Township, approximately 2 km west of the southwestern extremity of Troupe Lake. The conglomerate is grey to white weathering and oligomictic (quartzofeldspathic igneous clasts), containing 20 to 30% clasts stretched into parallelism with a prominent near vertical foliation. In the subhorizontal outcrop surface, clasts have a maximum dimension of 25 cm, with a stretching ratio ranging from 3:1 to 4:1. Clasts are embedded in a coarse- to very coarse-grained metaquartzite matrix. No primary structures are preserved.

An exposed contact between the conglomerate and grey to white weathering, medium-grained metaquartzite is depositional and gradational. The metaquartzite displays numerous laminae of yellow-brown pelitic detritus parallel to the foliation, and contains sparse quartzofeldspathic clasts up to 3 cm, deformed up to a ratio of 2:1 in the foliation plane. As in the conglomerate, no primary features are preserved. A 1.1 m horizon of quartz-phyric tuff that is interstratified with the metaquartzite displays primary stratification parallel to the foliation.

The size of clasts and matrix in the conglomerate indicates a high energy environment, possibly fluvial. In this context, the transitional contact with the metaquartzite could indicate maintenance of the same depositional setting, which might also suggest that the felsic pyroclastic unit interstratified with the metaquartzite was subaerial.

Kabenung Lake Region

A second location in the northern metasedimentary belt was examined at Kabenung Lake, in the western end of the belt (location 4, Figure 375.1). The geology of this area has been mapped by Sage (1987a, 1988). Lakeshore exposures of felsic pyroclastics were examined around islands and along the southern shoreline of the lake straddling the Knicely–Dahl Township boundary (*see* Figure 375.2). Bedding in the lakeshore outcrops dip near vertically and locally are slightly overturned, facing consistently south to southwest. Abundant primary features are preserved, and the strata contain a well-developed near vertical foliation parallel to primary stratification. No fold closures were observed.

Tuff, lapillistone and volcaniclasitc conglomerates are exposed around the lake. Tuff and finer-grained lapillistone, interpreted as subaqueous pyroclastic fall deposits, are the prominent volcanogenic metasediment. These rock types are commonly interstratified on a scale of tens of centimetres to metres in individual outcrops, with the proportion of each varying with location. The lapillistone commonly weathers pale grey-brown, and is of similar colour on fresh surfaces. Abundant clasts in the lapillistone are commonly 1 to 2 cm, but can be up to 15 cm where flattened parallel to foliation, as seen in subhorizontal outcrop surfaces. These clasts are of three predominant compositional types: 1) quartz porphyry (apparent stretching ratio of 4 or 5:1); 2) dark grey quartz-phyric tuff (10 to 15:1); 3) tuff (10 to 15:1). Tuff units weather pale green-grey and are grey on fresh surfaces. They occur as either non-stratified or faintly stratified (laminated to very thinly bedded) horizons and frequently contain isolated quartz porphyry clasts up to 2 cm. Primary features common in both rock types may be attributed to a variable combination of volcaniclastic depositional processes and water reworking. Individual outcrops thus represent a variable mixture of pyroclastic and epiclastic sediment (classification as per Cas and Wright 1987). The most common primary feature attributable to volcaniclastic processes is normal grading varying from several centimetres to several tens of centimetres

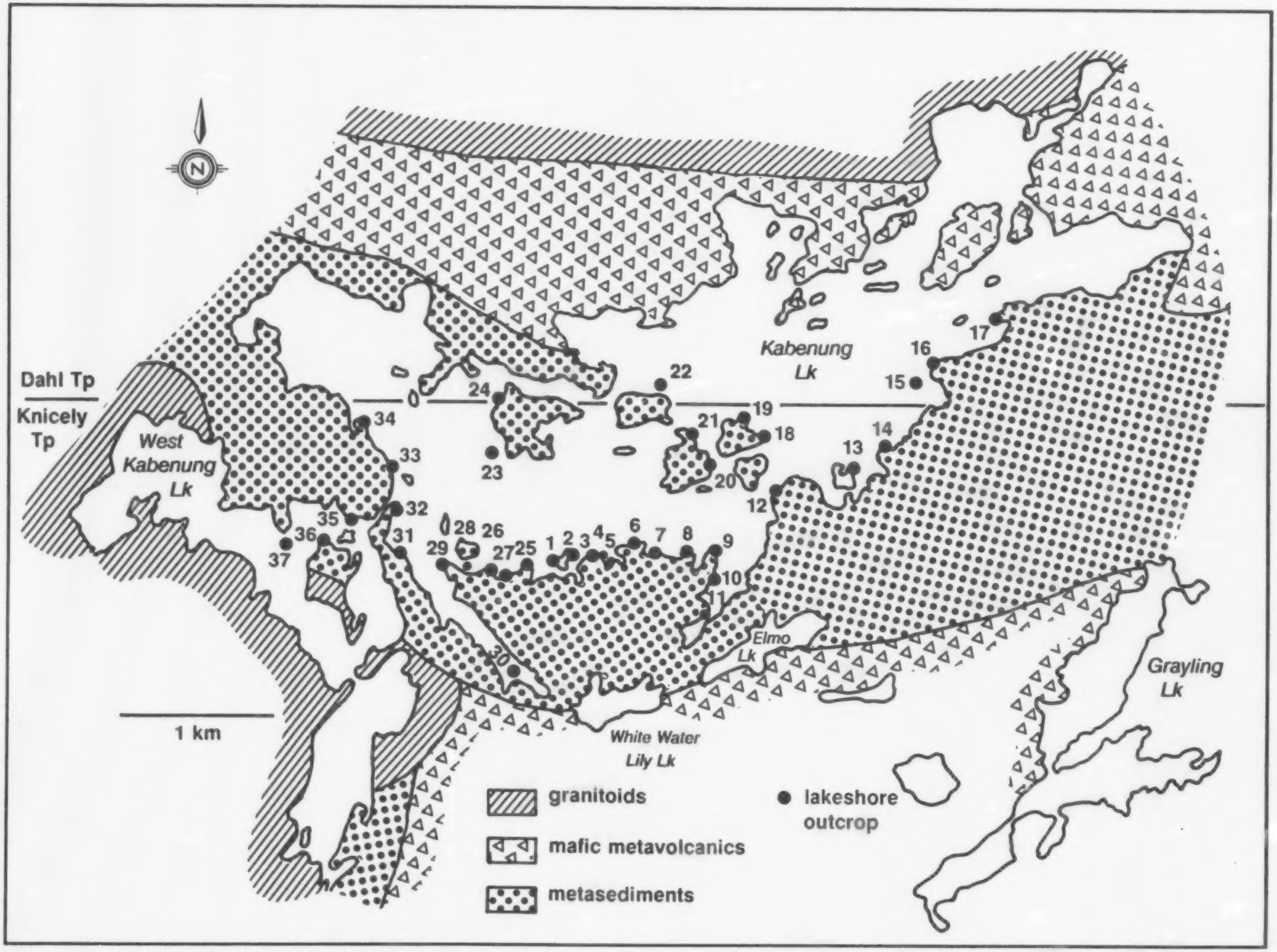
N
Dahl Tp
Knicely Tp
West Kabenung Lk
Kabenung Lk
Elmo Lk
White Water Lily Lk
Grayling Lk
1 km
1
2
3
4
5
6
7
8
9
10
11
12
13
14
15
16
17
18
19
20
21
22
23
24
25
26
27
28
29
30
31
32
33
34
35
36
37
granitoids
mafic metavolcanics
metasediments
lakeshore outcrop

Figure 375.2. Local geology and locations of lakeshore outcrop examined on Kabenung Lake in the central northern metasedimentary belt (area 4, Figure 375.1). Geology from Sage (in press—Knicely Township.) and from Milne et al. (1971—Dahl Township).

in thickness. Frequently, the finer-grained tops of fall deposits consists of darker coloured tephra. Common indicators of reworking, restricted to the upper portions of individual fall units, include rip-up clasts of dark coloured tephra, ripple cross-lamination, and more rarely cross-stratification in sets up to several tens of centimetres in thickness. Both tuff and lapillistone may contain several centimetre-thick layers of darker brown-weathering, non-stratified, silty sediment differing in appearance from the finer-grained, dark coloured tephra and not obviously depositionally related to the surrounding pyroclastic sediment (no grading). These horizons are interpreted as background sedimentation of hemipelagic detritus representing breaks in volcaniclastic deposition.

Volcaniclastic conglomerate is a common, but relatively less prominent, rock type at Kabenung Lake. The volcaniclastic conglomerate weathers green-grey to grey and is grey on fresh surface. Clasts represent about 80% of the rock with the remainder a reworked pale green-grey to grey, silty matrix. The clasts are highly flattened subhorizontally parallel to the dominant foliation, reaching up to 50 cm in the outcrop plane. Four clast types are common: 1) quartz porphyry (stretched 3 to 4:1); 2) non-phyric tuff (10 to 12:1); 3) non-phyric finer tuff (6 to 8:1) 4) dark grey, quartz and feldspar phyric tuff (10 to 12:1). The conglomerate locally contains 20 to 30 cm thick interstratified layers of finer-grained lapillistone, locally displaying indications of reworking, but the conglomerate lacks primary features. Based on the variety of clast types, and the evidence of reworking in the interstratified lapillistone, the conglomerate is interpreted as the product of erosion of a lithified volcanic sequence.

A non-volcaniclastic conglomerate, estimated to be 100 m thick, occurs at several localities on the southwestern shore of the lake (stations 26 to 28, Figure 375.2). Clasts in this conglomerate are highly attenuated parallel to the prominent near vertical foliation and consist of recrystallized white-weathering metachert, mafic metavolcanic, and oxide iron formation, including some banded iron formation, in decreasing order of abundance. The degree of deformation precludes a meaningful estimate of the clast to matrix ratio and has destroyed any primary features. The conglomerate is considered to be a fluvial deposit of local provenance, derived by uplift and erosion of oxide-facies iron formation to the southeast in the Elmo–White Water Lily lakes region (Sage 1988).

Middle Metasedimentary Belt

Kapimchigama—Radford Lakes Region

The middle metasedimentary belt was examined at its northwestern end in the Kapimchigama–Radford lakes region (location 3, Figure 375.1; Figure 375.3). The geology of the area has been investigated by Sage (in prep. d,e) and the deformation sequence delineated in Arias and Helmstaedt (1989, figure 343.4). Arias and Helmstaedt (1989) define a regional fold (F_2) closure, roughly conforming to the configuration of Radford Lake, which plunges northwest and youngs southeast. This fold appears to be an inverted syncline with a northwest-trending axis positioned roughly halfway up the western shoreline of Kapimchigama Lake (vicinity of station 8, Figure 375.3).

Two lithofacies assemblages are present at this location: 1) a highly silicified and locally highly carbonatized interstratified metagreywacke and pelite succession and 2) a succession of metaquartzite with only minor pelite (Photo 375.1). The former is rusty dark grey-weathering and present only at the southern end of Kapimchigama Lake (station 2, Figure 375.3). Metagreywacke units range in thickness from several centimetres to several metres, and only rarely preserve primary features which are limited to ripple cross-lamination. Beds of dark grey- to black-weathering pelite range from several centimetres to several tens of centimetres in thickness, and locally display rippled upper contacts with metagreywacke. This lithofacies assemblage represents repetitive turbidity current deposition.

The metaquartzite and pelite lithofacies assemblage was observed along the western shoreline of Kapimchigama Lake, as well as the southern shore of Radford Lake, representing the core region of the large F_2 fold (stations 2-19, Figure 375.3).

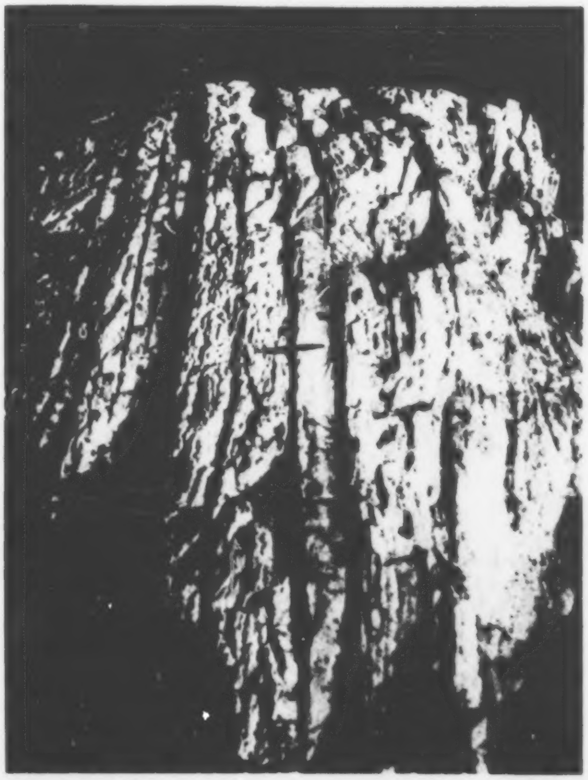

Photo 375.1. White-weathering metaquartzite with thinly interstratified (cms) pelite horizons arranged in thin fining-upward "cycles", Radford Lake, northern middle metasedimentary belt (area 4, Figure 375.1). The metaquartzite displays basal lags and rippled tops. Pencil scale at photo centre. Facing direction right.

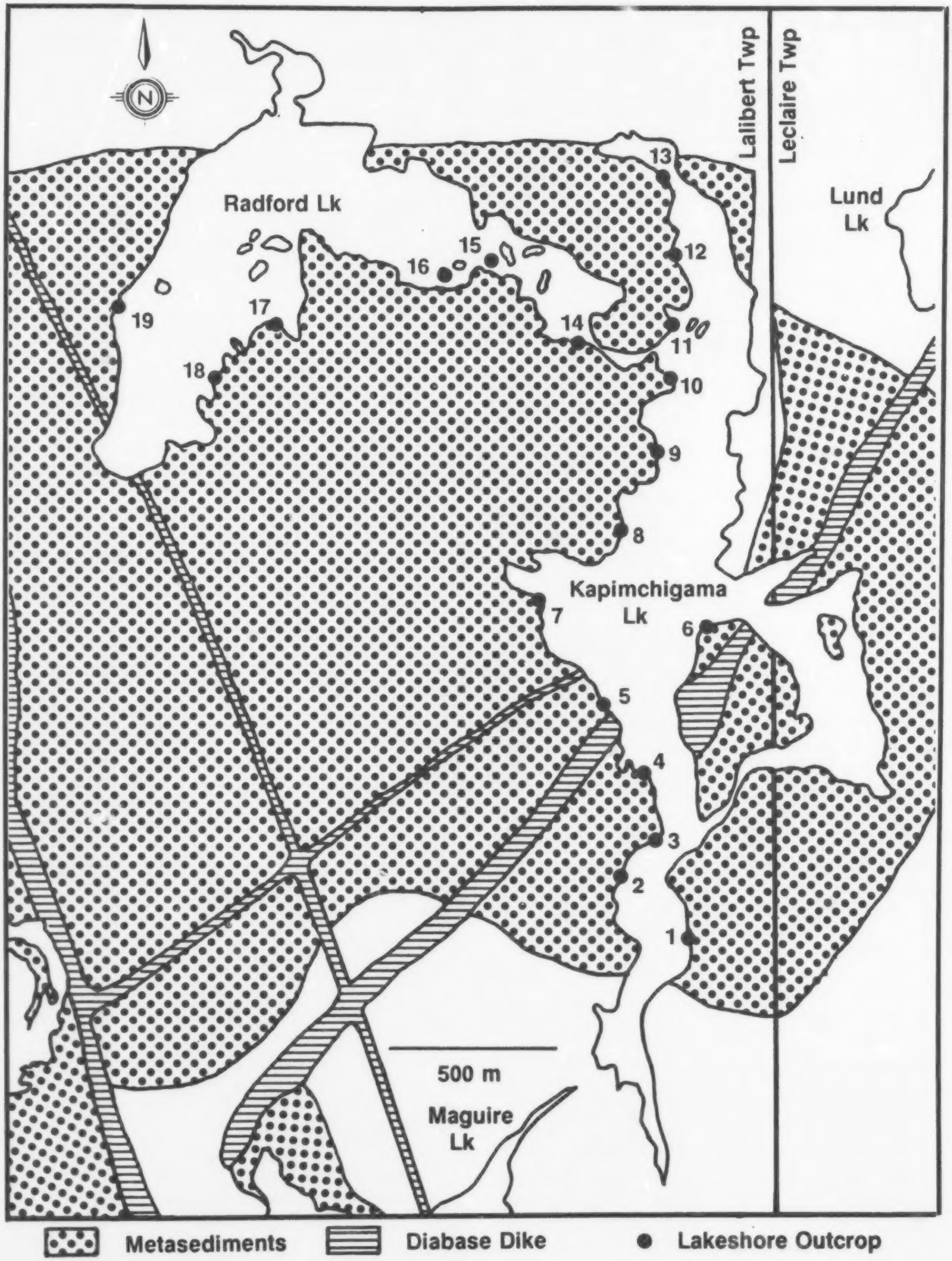
N
Lalibert Twp
Leclaire Twp
Radford Lk
Lund Lk
Kapimchigama Lk
Maguire Lk
500 m
1
2
3
4
5
6
7
8
9
10
11
12
13
14
15
16
17
18
19
Metasediments
Diabase Dike
Lakeshore Outcrop

Figure 375.3. Local geology and locations of lakeshore outcrop examined on Kapimchigama and Radford lakes at the northern extremity of the middle metasedimentary belt (area 3, Figure 375.1). Geology from Sage (1985a—Leclaire Township; and in press—Lalibert Township).

Metaquartzite is grey- to white-weathering, dominantly medium- to coarse-grained, and in places displays primary structures in beds varying from several centimetres to several metres in thickness. Pelite interstratified with the metaquartzite is pale brown- to green-grey-weathering and displays no primary features other than ripple cross-lamination in beds up to 5 cm thick. Primary features recognizable in the metaquartzite are limited to normal grading, ripple cross-lamination, and occasional small scour surfaces. At the southern end of Kapimchigama Lake, near the contact with underlying metagreywacke turbidites (contact not observed), the metaquartzite-pelite assemblage displays a thinly interstratified, coarse to fine repetitive stratification style interpreted as the product of waning turbidity currents. This style of stratification changes abruptly northward along the western shore of Kapimchigama Lake and remains consistent along the southern shore of Radford Lake. The new stratification style consists of amalgamated fining-upward units of metaquartzite, usually tens of centimetres to several metres thick, but only locally displaying the primary features mentioned above. Some underlying metaquartzite units are capped by non-stratified to ripple cross-laminated pelite units several centimetres thick, but more typically, pelite interlayers are absent, and erosional contacts separate contiguous metaquartzite units. This style of stratification is well displayed on a small island in Radford Lake (*see* Photo 375.1). The compositional maturity of the metaquartzite and the fact that it overlies an underlying metagreywacke turbidite sequence suggests that it could represent a prograded siliciclastic shelf deposit. Although the primary features observed are not diagnostic of a shelf environment, the normally graded and rippled metaquartzite units capped by rippled pelite readily fit descriptions of storm deposits recognized on modern shelves. In this context, the turbidite style of stratification observed in the metaquartzite near the southern end of Kapimchigama Lake could be interpreted to represent shelf margin-upper slope deposits, with greater compositional maturity due to the detritus being derived from the adjacent shelf.

Southern Metasedimentary Belt

Arliss Lake Region

The Arliss Lake region is located in central Chabenal Township in the eastern half of the Mildred–Lena lakes segment of the southern metasedimentary belt (location 2, Figure 375.1). The regional geology of Chabenal Township has been reported in Sage (in prep. a) and Sage et al. (1982a). For this report, the Arliss Lake region refers specifically to the region bounded to the west by the Algoma Central Railroad track, north and east by an abandoned spur of this railroad leading past Lena Lake, and south by Arliss Lake (*see* Figure 375.4). This region has been mapped in considerable detail by McGill and Shrady (1986) for the purpose of determining its deformation sequence. Their mapping has shown that the clastic metasedimentary rocks are divisible into a number of discrete packages separated by inferred thrust faults formed early in the deformation history of the Michipicoten greenstone belt in association with regional scale recumbent isoclinal folding. The location of these early thrusts is shown on Figure 375.4 along with the position of 7 sections (2-1 to 2-7, corresponding to Figures 375.5 to 375.11, respectively) constructed between these thrusts across this region. Figures 375.5 to 375.11 designate the bounding thrusts as lithological package boundaries numbered as 5 through 0, inclusive, representing a south to north progression across this region (*see* Figure 375.4). The rocks have a near vertical attitude, are highly fractured due to pervasive shearing interpreted as a late element of the deformation sequence (McGill and Shrady 1986), and are generally difficult to study due to a black weathering rind formed from emissions of the Helen iron mine sinter plant. Some rock types in this region are comparable to those reported below in the Shark Lake region, but in general the lithological diversity here exceeds that of the Shark Lake region.

Section 2-1 (Figure 375.5) is 60 m thick and bounded between the north shoreline of Arliss Lake and lithological package boundary 5. It consists of two lithofacies interpreted as representing a single lithofacies assemblage. This lithofacies assemblage comprises dark grey- to dark brown-weathering, fine- to medium-grained, metagreywacke and dark grey-weathering pelite. These lithofacies occur either regularly and thinly interstratified (centimetre to tens of centimetres) or in units dominated by thick metagreywacke units with only minor pelite interbeds. Primary features are limited to faint stratification and/or ripple cross-lamination and normal grading. Both styles of interstratification are interpreted as turbidite deposition, representing different positions relative to active channel areas on a submarine fan.

Section 2-2 (Figure 375.6) is 180 m thick and bounded between lithological package boundaries 5 and 4. Four metasedimentary lithofacies are identified and interpreted as representing two lithofacies assemblages. The four lithofacies are: 1) dark grey-weathering pelite, 2) dark grey- to dark brown-weathering. fine-grained, metagreywacke, 3) grey- to brown-weathering, very fine- to very coarse-grained feldspathic psammite, and 3) dark grey- to dark brown-weathering, very fine- to fine-grained, quartz-rich psammite. The metagreywacke occurs as either thin- to thick-bedded units up to several tens of metres thick or thinly interstratified with pelite on a scale of centimetres to several tens of centimetres and arranged in fining-upward couplets. Together they compose one of the lithofacies assemblages and are interpreted to represent turbidite deposition at different locations on a submarine fan. The second lithofacies assemblage consists of the feldspathic and quartz-rich psammite. Parts of these lithofacies are non-stratified to well-bedded, with the former displaying few primary structures other than a few ripple cross-laminations and normal grading. However, the latter displays abundant large-scale trough cross-stratification and dewatering and other soft-sediment deformation features. In addition, mudcracks interpreted as indicating desiccation have been reported from a clastic lithofacies likely correlative with this unit in the Scott Lake region (Thomas 1984). Both lithofacies are interpreted as constituting a subaerial stream

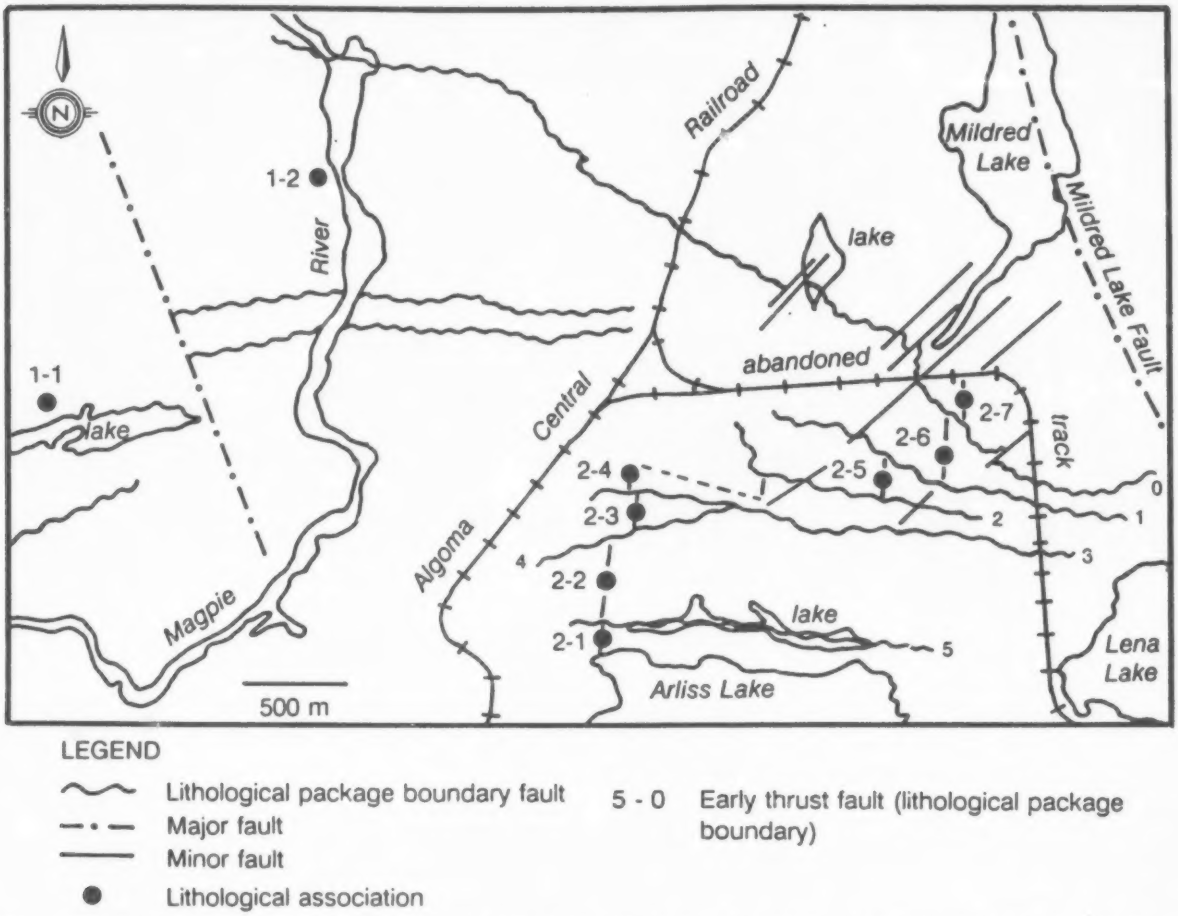
N
1-1
lake
1-2
River
Magpie
500 m
Railroad
Algoma
Central
abandoned
track
lake
Mildred Lake
Mildred Lake Fault
2-1
2-2
2-3
2-4
2-5
2-6
2-7
0
1
2
3
4
5
lake
Arliss Lake
Lena Lake
LEGEND
Lithological package boundary fault
Major fault
Minor fault
Lithological association
5 - 0 Early thrust fault (lithological package boundary)

Figure 375.4. Section location relative to early faults in areas 1 (Shark Lake (informal name) area) and 2 (Arliss Lake area) of the Mildred–Lena lakes segment of the southern metasedimentary belt. Refer to Figure 375.1 for their position within the Michipicoten belt. Geology omitted for clarity. Adapted from Figure 2 of McGill and Shrady (1986).

flow lithofacies assemblage. The inclusion of the feldspathic psammite in this assemblage is tentative, because this lithofacies could have accumulated in a submarine fan setting.

Section 2-3 (Figure 375.7) is 160 m thick and constrained between lithological package boundaries 4 and 3. Four lithofacies are distinguished: 1) dark grey-weathering pelite, 2) dark grey- to dark brown-weathering metagreywacke, 3) pale to dark brown-weathering feldspathic psammite with minor interstratified polymictic orthoconglometrate, and 4) grey- to brown-weathering, fine- to medium-grained, quartz-rich psammite. They are interpreted to constitute at least one, and possibly two, lithofacies assemblages. A turbidite assemblage consists of largely non-stratified pelite, feldspathic psammite with minor conglomerate, and metagreywacke. The latter lithofacies is non-stratified to faintly stratified (usually thinly bedded), and occurs either in isolation or as the coarser bases of fining-upward couplets, up to several tens of centimetres thick, representing partial Bouma sequences. Other than stratification, primary features in the metagreywacke are limited to sparse ripple cross-lamination and normal grading. The feldspathic psammite is largely non-stratified to faintly laminated or thinly bedded, and displays no primary features other than local normal grading and ripple cross-lamination. Its stratigraphic juxtaposition immediately overlying a thick pelite suggests that inclusion in the turbidite assemblage is reasonable. The increased compositional maturity of the quartz-rich psammite could indicate increased sorting in a higher energy, perhaps more channel-proximal, region of a submarine fan system. Alternatively, it could indicate a significant change in depositional environment, with primary structures supporting this change destroyed by pervasive shearing. The former interpretation is favoured herein.

Section 2-4 (Figure 375.8) is 340 m thick and bounded between lithological package boundaries 3 and 2. Five lithofacies are identified: 1 and 2) pale yellow- to grey-brown-weathering coarse tuff and fine lapillistone, both of which locally display indications of reworking; 3) dark grey-weathering pelite; 4) dark grey- to grey-brown-weathering, very fine- to very coarse-grained, metagreywacke; and 5) pale grey-brown-weathering, very fine- to very coarse-grained, quartz-rich psammite. Two

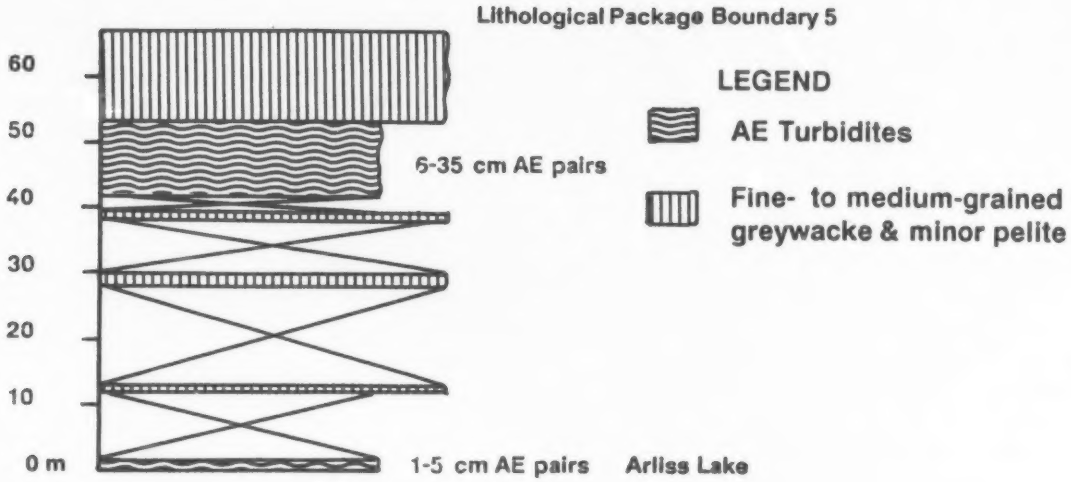
Lithological Package Boundary 5
60
50
40
30
20
10
0 m
6-35 cm AE pairs
1-5 cm AE pairs
Arliss Lake
LEGEND
AE Turbidites
Fine- to medium-grained greywacke & minor pelite

Figure 375.5. Section 2-1, Arliss Lake region. Refer to Figure 375.4 for location in the southern metasedimentary belt and Figure 375.1. for position of area 2 in the Michipicoten greenstone belt. For Figures 375.5–375.13 covered intervals in the "sections" are indicated by "X". Other than this figure where fold closures are absent, "X" is not intended to impart a sense of true stratigraphic thickness as minor closures may not have been recognized.

lithofacies assemblages representing a turbidite-submarine fan (turbidite deposition on a submarine fan) and a marine felsic pyroclastic depositional setting are present in this section; some section units are a combination of these assemblages. The turbidite assemblage consists of pelite, metagreywacke and the quartz-rich psammite lithofacies. Pelite is non-stratified to locally ripple cross-laminated, and occurs as either isolated units or beds thinly interstratified with the other lithofacies. Thin fining-upward couplets of pelite and metagreywacke represent partial (AE) Bouma sequences. Both the metagreywacke and the quartz-rich psammite are commonly non-stratified or display only rare normal grading and ripple cross-lamination. This could, in part, be due to intense shearing. The increased compositional maturity of the quartz-rich psammite is again interpreted to indicate increased sorting in a more channel-proximal, higher energy position on a submarine fan system, perhaps within an active channel region. Coarse tuff and fine lapillistone, commonly well stratified and locally reworked, constitute the felsic volcaniclastic assemblage. Primary features are restricted to normal grading, and a marine setting is assumed due to their intimate stratigraphic association with the turbidite-submarine fan assemblage.

Section 2-5 (Figure 375.9) is 240 m thick and is constrained between lithological package boundaries 2 and 1. Five lithofacies compose this section: 1) dark grey-weathering pelite; 2) dark grey-brown-weathering metagreywacke; 3) pale grey-weathering, very fine- to coarse-grained, quartz-rich psammite; 4) pale brown-weathering, volcaniclastic conglomerate (0.2 to 25 cm clasts); and 5) brown-weathering, siltstone-clast (0.4 to 64 cm) conglomerate. As for the previous section, a turbidite and a felsic pyroclastic lithofacies assemblage are identified. The latter is represented solely by the volcaniclastic conglomerate which: 1) lacks primary features; 2) has interstratified horizons of quartz-rich psammite; and 3) is dominated by volcanic clasts (porphyry, tuff) with rare granitic pebbles. These features suggest that it is a reworked lithofacies, and its stratigraphic association with the turbidite-submarine fan assemblage discussed subsequently suggest a marine setting. The turbidite assemblage includes the remaining lithofacies occurring as either isolated units or interstratified. Metagreywacke and pelite occur in intervals of thin partial Bouma sequences (AE, ACE) in the base and top portion of the section. Lithofacies in this assemblage are largely non-stratified with only occasional faint stratification, normal grading, and ripple cross-lamination. As for the previous section, the paucity of primary features can be attributed to shearing. The regional association of the turbidite assemblage with pillowed mafic metavolcanics suggests a submarine fan depositional setting is a reasonable interpertation. The quartz-rich psammite is interpreted as in sections 2-3 and 2-4, and the siltstone clast conglomerate interstratified with this lithofacies at the 90 m level is suggested to represent bank erosion.

Section 2-6 (Figure 375.10) is 200 m thick and bounded by lithological package boundaries 1 and 0. Five lithofacies compose this section: 1 and 2) pale yellow- to grey-brown-weathering tuff and lapillistone; 3) dark grey-weathering pelite; 4) dark grey-brown-weathering, fine- to medium-grained, metagreywacke; and 5) grey-weathering, coarse-grained, quartz-rich psammite. As in sections 2-4 and 2-5, felsic pyroclastic and turbidite-submarine fan lithofacies assemblages

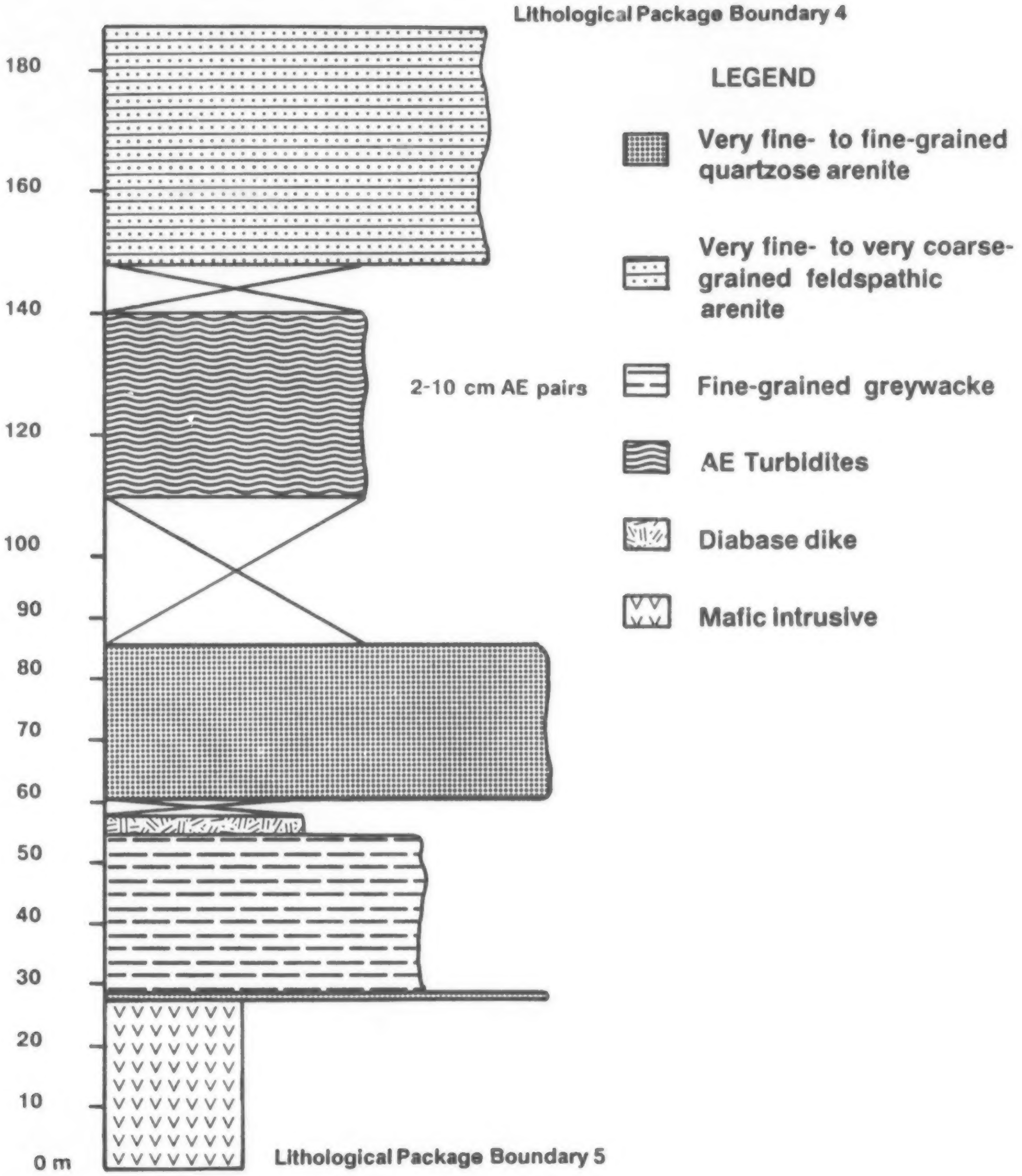
Lithological Package Boundary 4
LEGEND
Very fine- to fine-grained quartzose arenite
Very fine- to very coarse-grained feldspathic arenite
Fine-grained greywacke
AE Turbidites
Diabase dike
Mafic intrusive
2-10 cm AE pairs
180
160
140
120
100
90
80
70
60
50
40
30
20
10
0 m
Lithological Package Boundary 5

Figure 375.6. Section 2-2, Arliss Lake region. Refer to Figure 375.4 for location in the southern metasedimentary belt.

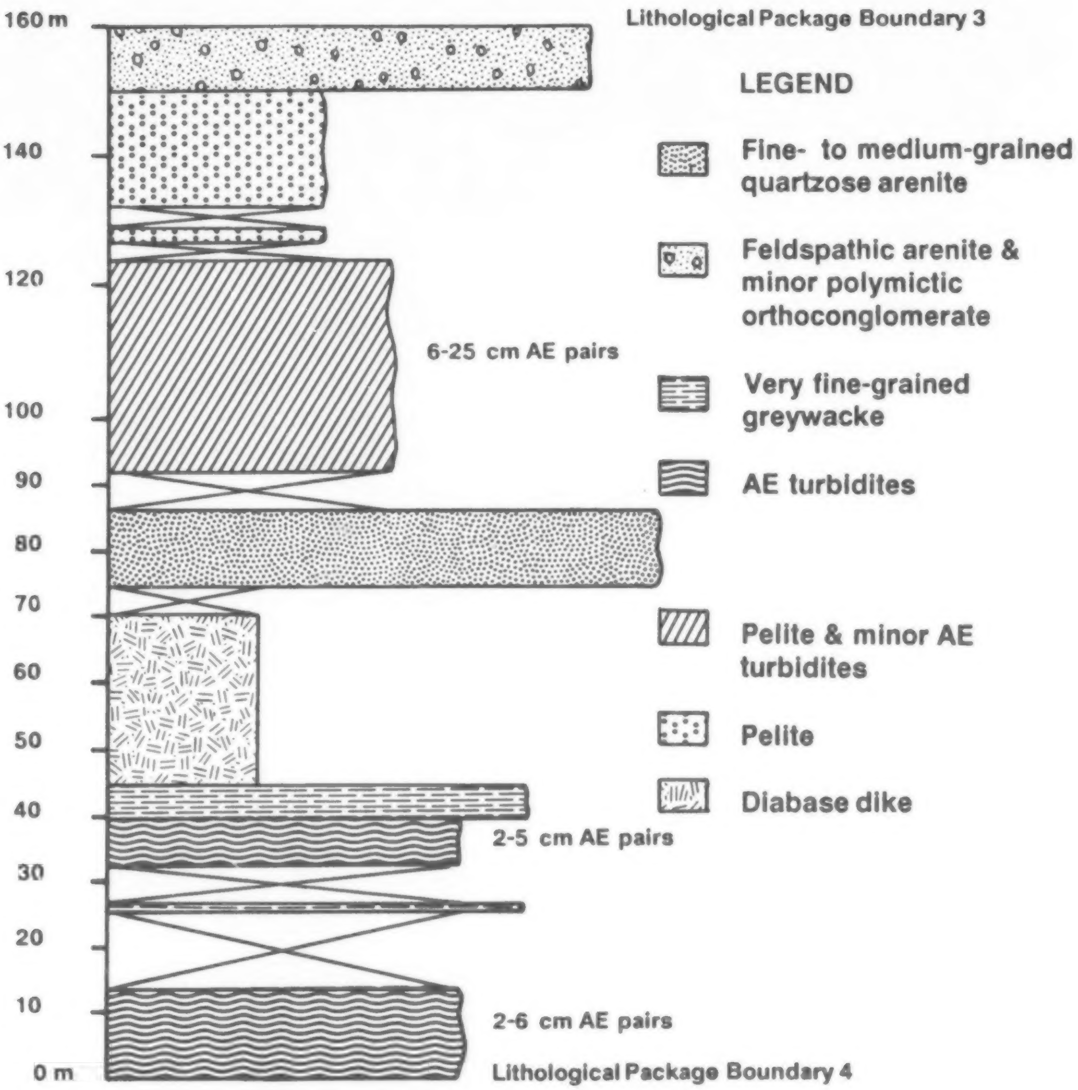
160 m
140
120
100
90
80
70
60
50
40
30
20
10
0 m
Lithological Package Boundary 3
LEGEND
Fine- to medium-grained quartzose arenite
Feldspathic arenite & minor polymictic orthoconglomerate
Very fine-grained greywacke
AE turbidites
Pelite & minor AE turbidites
Pelite
Diabase dike
6-25 cm AE pairs
2-5 cm AE pairs
2-6 cm AE pairs
Lithological Package Boundary 4

Figure 375.7. Section 2-3, Arliss Lake region. Refer to Figure 375.4 for location in the southern metasedimentary belt.

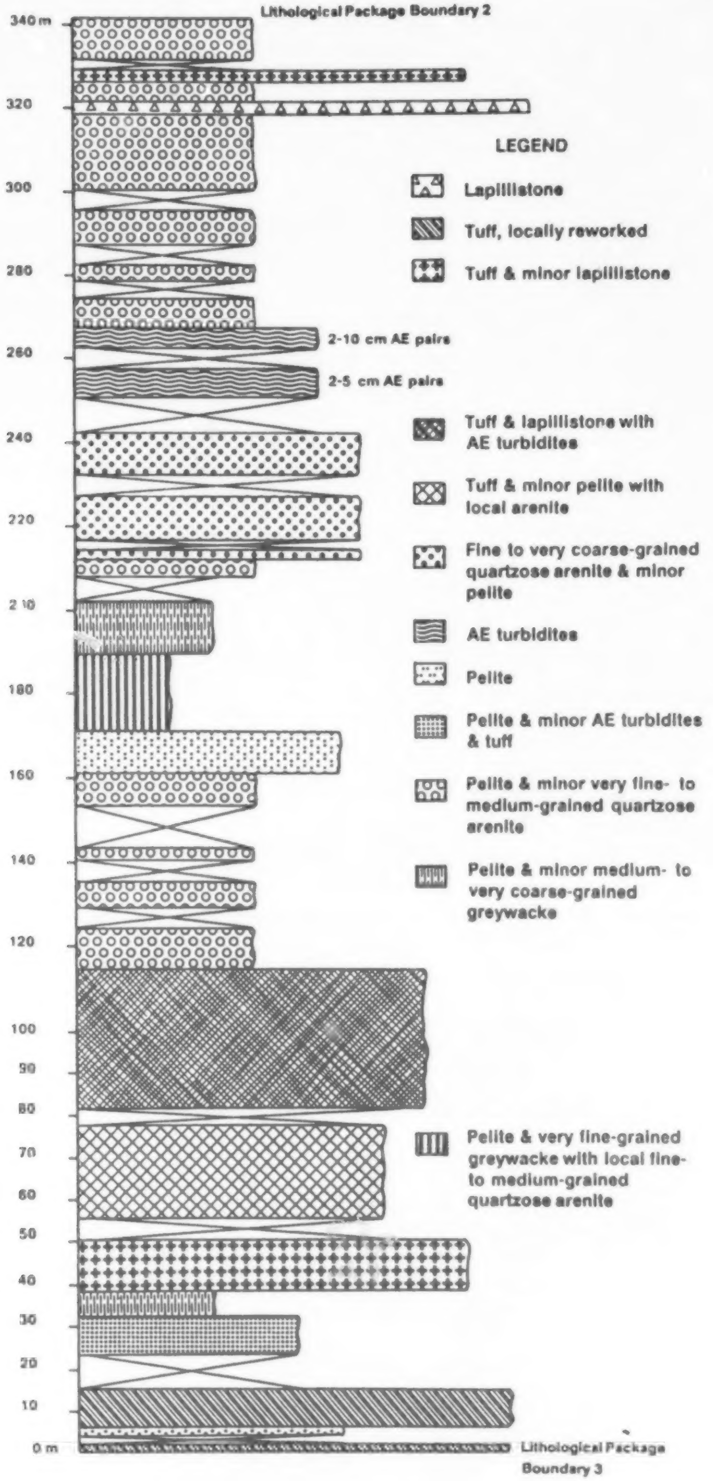
Lithological Package Boundary 2
340 m
320
300
280
260
240
220
200
180
160
140
120
100
90
80
70
60
50
40
30
20
10
0 m
2-10 cm AE pairs
2-5 cm AE pairs
Lithological Package Boundary 3
LEGEND
Lapillistone
Tuff, locally reworked
Tuff & minor lapillistone
Tuff & lapillistone with AE turbidites
Tuff & minor pelite with local arenite
Fine to very coarse-grained quartzose arenite & minor pelite
AE turbidites
Pelite
Pelite & minor AE turbidites & tuff
Pelite & minor very fine- to medium-grained quartzose arenite
Pelite & minor medium- to very coarse-grained greywacke
Pelite & very fine-grained greywacke with local fine- to medium-grained quartzose arenite

Figure 375.8. Section 2-4, Arliss Lake region. Refer to Figure 375.4 for location in the southern metasedimentary belt.

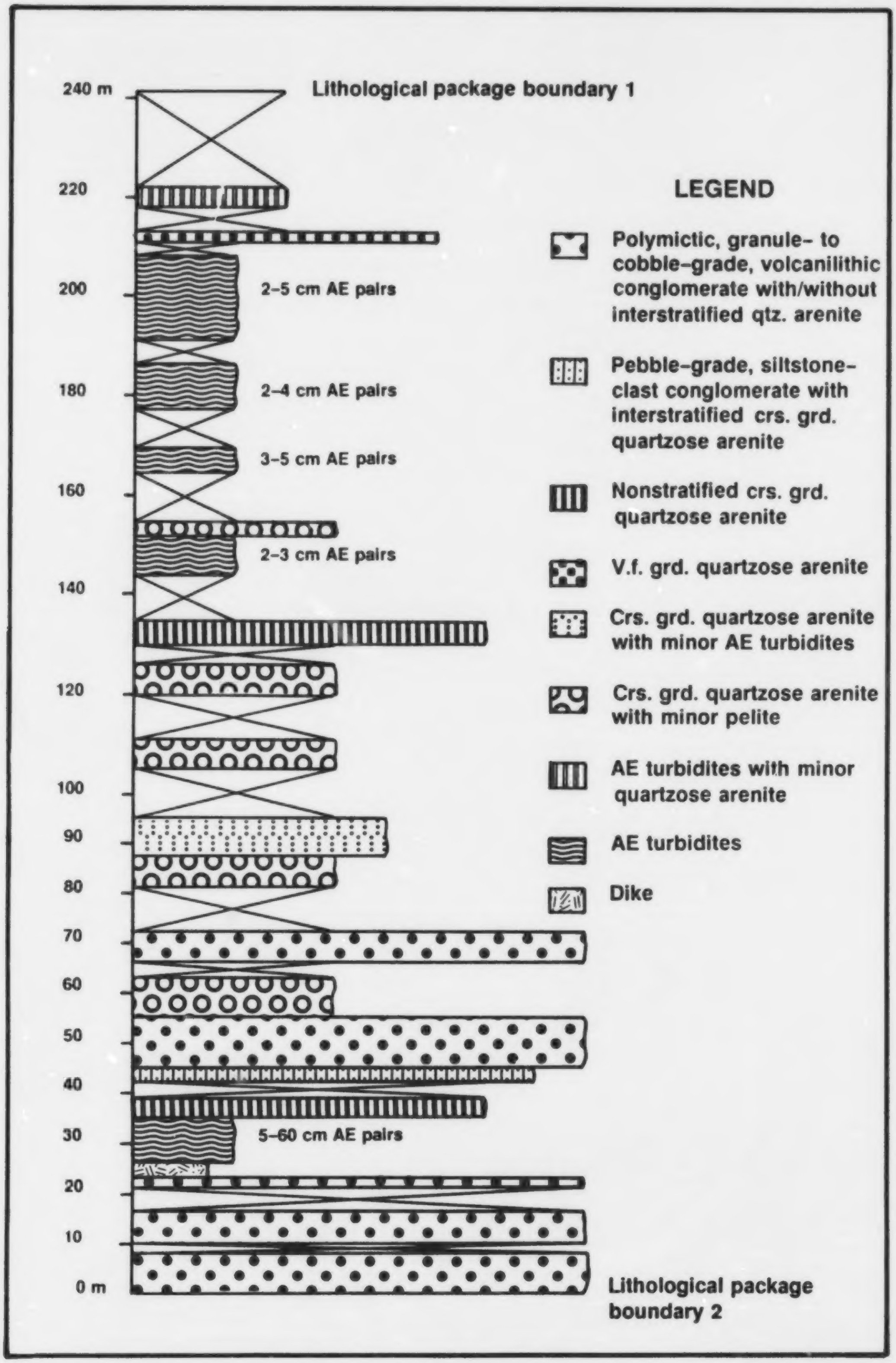
240 m
Lithological package boundary 1
220
200
180
160
140
120
100
90
80
70
60
50
40
30
20
10
0 m
2-5 cm AE pairs
2-4 cm AE pairs
3-5 cm AE pairs
2-3 cm AE pairs
5-60 cm AE pairs
Lithological package boundary 2
LEGEND
Polymictic, granule- to cobble-grade, volcanilithic conglomerate with/without interstratified qtz. arenite
Pebble-grade, siltstone-clast conglomerate with interstratified crs. grd. quartzose arenite
Nonstratified crs. grd. quartzose arenite
V.f. grd. quartzose arenite
Crs. grd. quartzose arenite with minor AE turbidites
Crs. grd. quartzose arenite with minor pelite
AE turbidites with minor quartzose arenite
AE turbidites
Dike

Figure 375.9. Section 2-5, Arliss Lake region. Refer to Figure 375.4 for location in the southern metasedimentary belt.

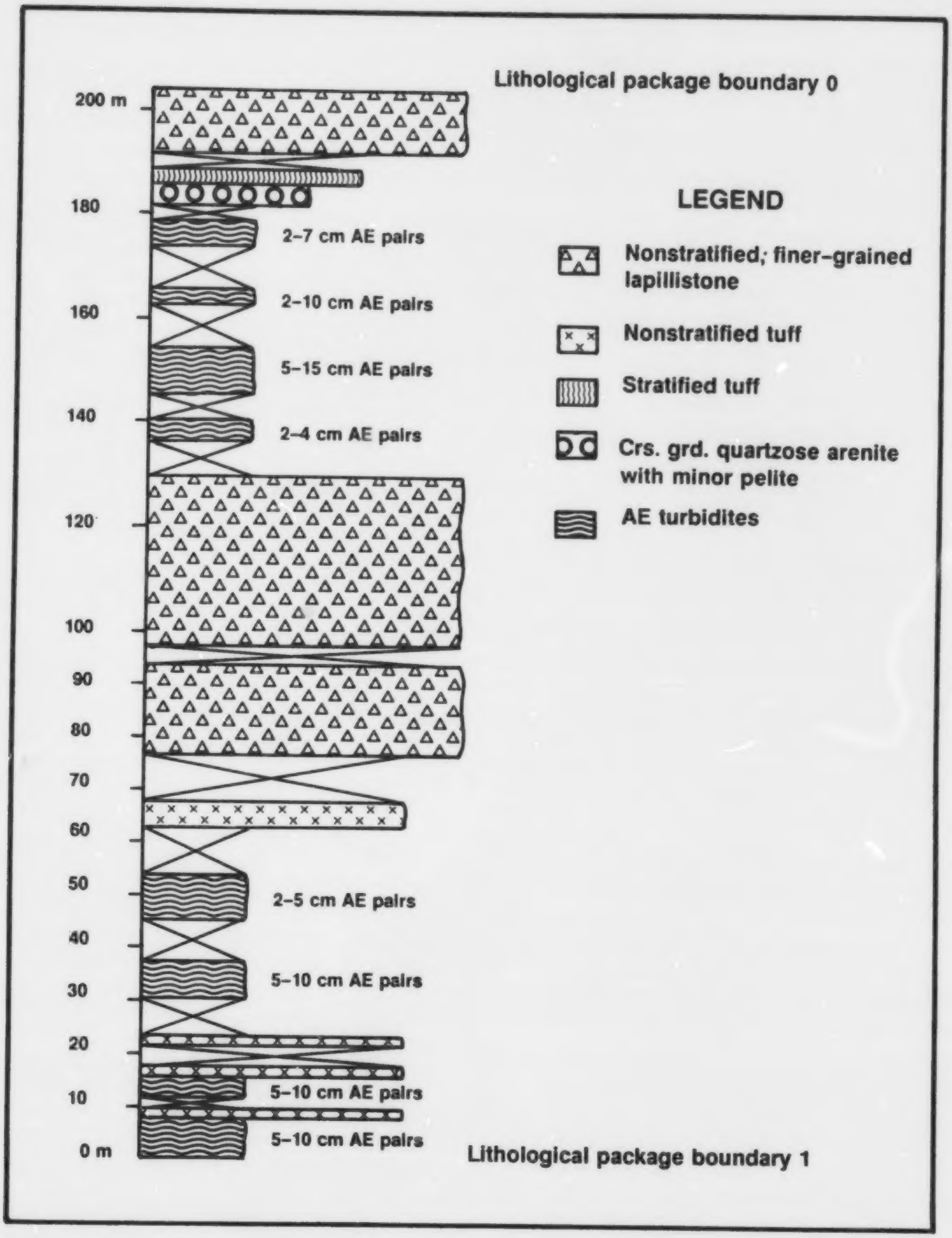
Lithological package boundary 0
200 m
180
2-7 cm AE pairs
160
2-10 cm AE pairs
5-15 cm AE pairs
140
2-4 cm AE pairs
120
100
90
80
70
60
50
2-5 cm AE pairs
40
30
5-10 cm AE pairs
20
10
5-10 cm AE pairs
0 m
5-10 cm AE pairs
Lithological package boundary 1
LEGEND
Nonstratified; finer-grained lapillistone
Nonstratified tuff
Stratified tuff
Crs. grd. quartzose arenite with minor pelite
AE turbidites

Figure 375.10. Section 2-6, Arliss Lake region. Refer to Figure 375.4 for location in the southern metasedimentary belt.

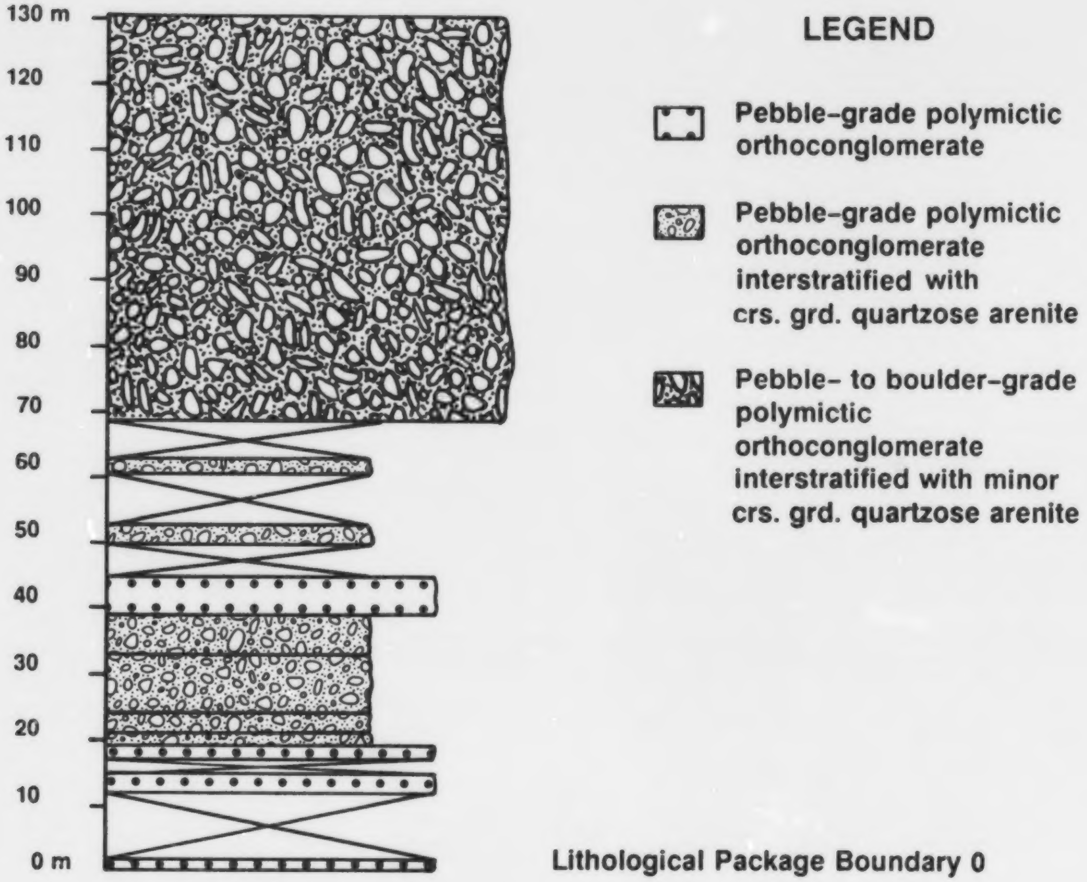
130 m
120
110
100
90
80
70
60
50
40
30
20
10
0 m
LEGEND
Pebble-grade polymictic orthoconglomerate
Pebble-grade polymictic orthoconglomerate interstratified with crs. grd. quartzose arenite
Pebble- to boulder-grade polymictic orthoconglomerate interstratified with minor crs. grd. quartzose arenite
Lithological Package Boundary 0

Figure 375.11. Section 2-7, Arliss Lake region. Refer to Figure 375.4 for location in the southern metasedimentary belt.

are defined, both representing deep marine sedimentation. The former consists of non-stratified to stratified (thinly bedded) tuff and non-stratified lapillistone. Tuff units commonly display normally graded horizons up to several tens of centimetres thick, but otherwise lack primary features. Rare isolated quartz porphyry clasts to about 1 cm occur in the lapillistone. The turbidite-submarine fan lithofacies assemblage consists of pelite and metagreywacke interstratified in thin partial Bouma sequences, or as units of quartz-rich psammite with thin pelite horizons.

Section 2-7 (Figure 375.11) is constrained between lithological package boundary 0 and the abandoned railway spur leading past Lena Lake, and is 130 m thick. Two lithofacies, pebble- to boulder-size polymictic conglomerate and a quartz-rich psammite compose the section defining a single lithofacies assemblage. The conglomerate weathers a rusty pale brown and displays no primary fabric other than occasional horizons of psammite which crudely defines bedding. It consists of about 50% clasts ranging from well rounded to angular which are poorly sorted and include the following rock types: quartz porphyry, tuff and pelite. Additionally, rare undeformed turbidite clasts occur in finer-grained units. Interstitial areas contain coarse-grained, quartz-rich psammite. Non-stratified to normally graded lenses of this lithofacies, up to 5 to 10 cm thick and several tens of centimetres to several metres in lateral extent, occur occasionally throughout the conglomerate defining bedding. The clast size, very poor sorting, and lack of fabric other than sparse psammite lenses suggests that the conglomerate represents debris flow deposition, with the psammite lenses constituting reworking of debris flow surfaces. Direct evidence indicating either a marine or subaerial depositional setting for this lithofacies assemblage is lacking. However, in the context of the deep marine felsic volcanic and submarine fan setting proposed for most lithofacies assemblages in the Arliss Lake region, a marine interpretation constitutes a simpler geologic scenario, and mass flows could easily be generated on the slopes of marine volcanic piles. This contrasts with Neale (1981) who proposed a debris flow interpretation, but suggested that it was subaerial.

In summary, the Arliss Lake region consists predominantly of lithofacies deposited in a deep marine setting characterized by felsic pyroclastic volcanism and submarine fan turbidity current deposition. One lithofacies assemblage in the region can be reasonably interpreted as fluvial.

Shark Lake Region

The Shark Lake region, also located in central Chabenal Township, is the second area examined in the Mildred–Lena lakes segment of the southern metasedimentary belt (location 1, Figure 375.1), and is located roughly 2 km west of the Arliss Lake region. The name "Shark Lake" was informally attached to a prominent lake in this region by Shrady (Shrady, personal communication, 1990) immediately south of which detailed structural studies were conducted. Two sections (1-1, 1-2) were examined in this region (*see* Figure 375.4), the former (*see* Figure 375.12) located in a small outcrop area immediately north of Shark Lake but outside the structural study area of Shrady (1988, 1991), and the latter (*see* Figure 375.13) located across a small outcrop area on the west bank of the Magpie River, roughly 500 m south of the Magpie River dam.

Major structural discontinuities, such as faults, are absent from section 1-1, and close examination of abundant normally graded units indicated no change in younging direction throughout its 360 m thickness. Cleavage-free folds, which are common early structural features in many Archean greenstone belts, can thus be considered absent and the section perceived as a true stratigraphic section with reliable unit thicknesses. A prominent near-vertical northeast-trending foliation is variably well displayed throughout the section depending on rock type, and is subparallel to bedding which dips at a moderate to high angle and youngs to the southeast.

Six lithofacies (*see* Figure 375.12) composing two lithofacies assemblages of roughly equivalent prominence are identified in this section. One lithofacies assemblage consists of volcaniclastic conglomerate, lapillistone, tuff and the reworked equivalent of the latter two lithofacies. Volcaniclastic conglomerate weathers a pale rusty-brown, lacks primary stratification, and is restricted to the lower 120 m of the section in units up to 5 m in thickness (Photo 375.2). Clasts which represent about 60% of the lithofacies, are very poorly sorted, and are of two compositional types: 1) white-weathering, well rounded to angular, quartz porphyry dominates with clasts up to 1 to 2 m in the outcrop plane with an apparent stretching ratio of no more than 2:1. 2) grey-weathering, dominantly sub-angular, well-bedded, quartz and feldspar-phyric tuff to finer-grained lapillistone up to several tens of centimetres in the outcrop plane. Interstitial areas in the volcaniclastic conglomerate consist of coarse tuff to finer lapillistone. The size and restricted composition of the clasts composing the conglomerate suggest that it represents the primary accumulation of pyroclastic debris and might therefore be considered a volcanic breccia. A subaqueous marine setting is presumed on the basis of the regional association with mafic metavolcanics. Tuff and lapillistone commonly are interstratified at a scale of several tens of centimetres to several metres throughout the section, and are more abundant than the conglomerate. Both lithofacies weather pale brown-grey, can be non-stratified or well stratified (very thinly to thinly bedded), and display primary features such as normal grading and ripple cross-lamination. Isolated, grey tuff clasts common in both lithofacies are stretched to about 0.5 to 1 cm in the outcrop plane. Primary features indicative of reworking of these lithofacies, such as rip-up clasts and cross-stratification, occur occasionally in units in the upper 100 m of the section. A marine felsic pyroclastic environment with only occasional reworking of deposits characterizes the depositional setting of this lithofacies assemblage. The restriction of conglomerate to the basal portion of the section could indicate closer proximity to the eruptive centre.

Photo 375.2. Boulder-grade polymictic volcanogenic conglomerate at section 1-1, Shark Lake area, southern metasedimentary belt (area 1, Figure 375.1; Figure 375.4). Clasts are dominantly quartz-feldspar porphyry with minor fine-grained volcaniclastic clasts. Facing direction left. Width of outcrop foreground 2 m.

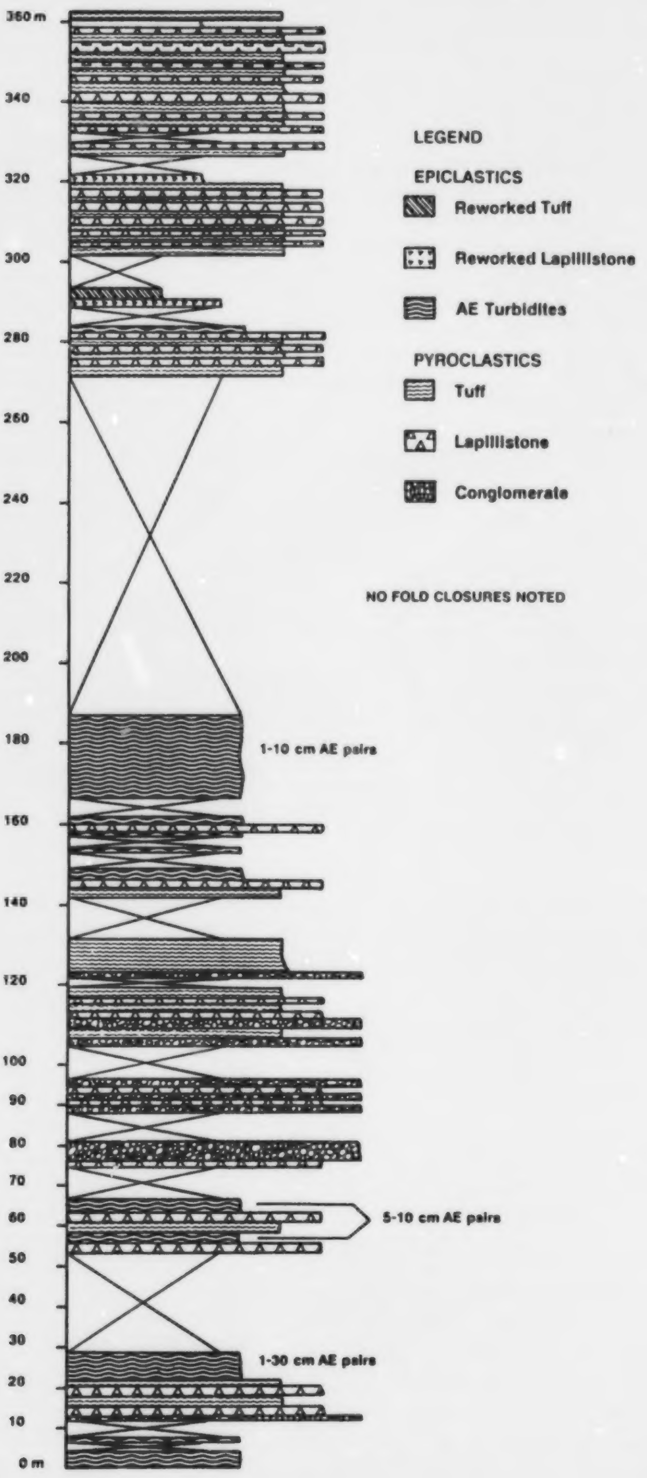
360 m
340
320
300
280
260
240
220
200
180
160
140
120
100
90
80
70
60
50
40
30
20
10
0 m
LEGEND
EPICLASTICS
Reworked Tuff
Reworked Lapillistone
AE Turbidites
PYROCLASTICS
Tuff
Lapillistone
Conglomerate
NO FOLD CLOSURES NOTED
1-10 cm AE pairs
5-10 cm AE pairs
1-30 cm AE pairs

Figure 375.12. Section 1-1, Shark Lake region. Refer to Figure 375.4 for location in the southern metasedimentary belt and Figure 375.1 for position of area 1 in the Michipicoten greenstone belt.

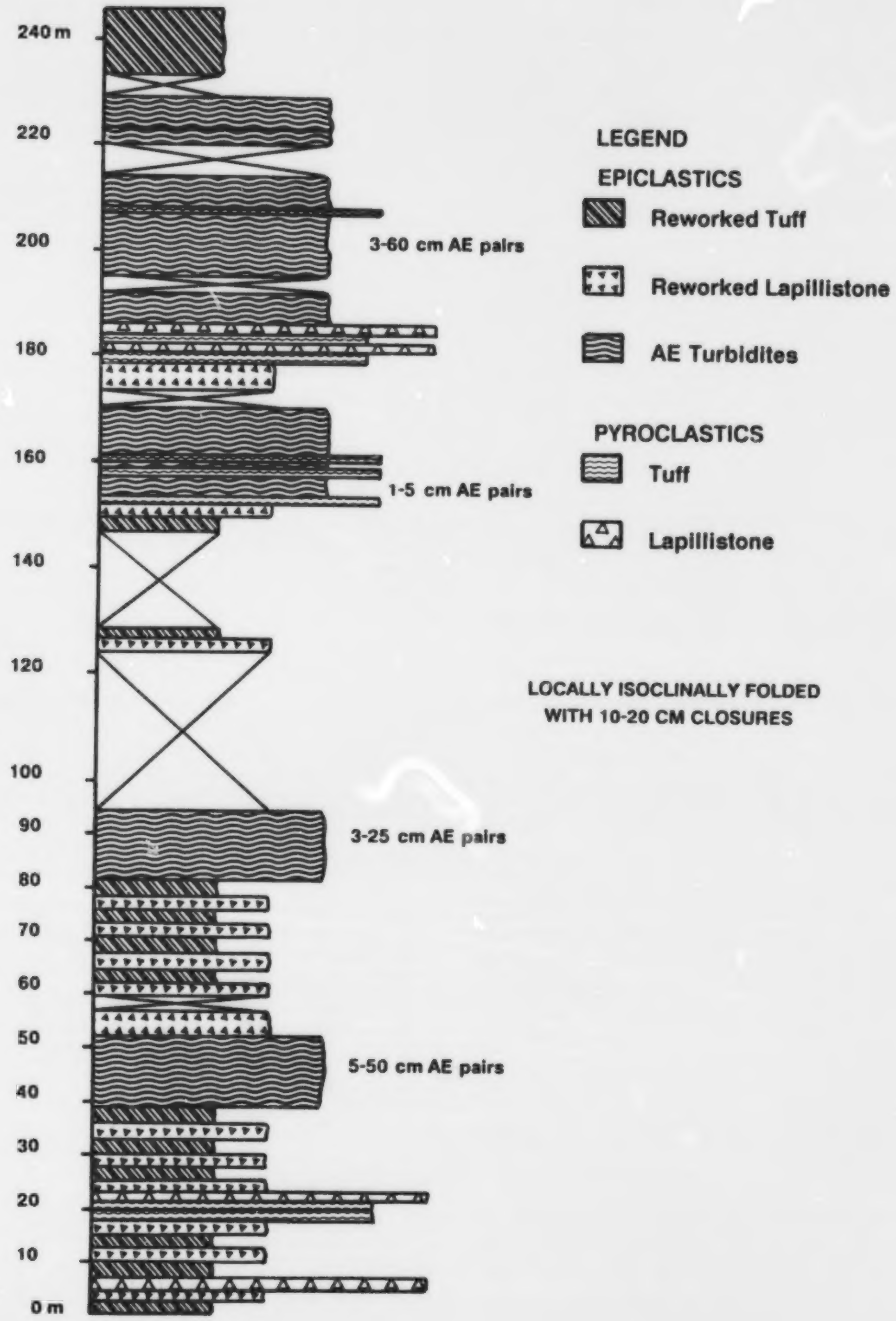
240 m
220
200
180
160
140
120
100
90
80
70
60
50
40
30
20
10
0 m
3-60 cm AE pairs
1-5 cm AE pairs
3-25 cm AE pairs
5-50 cm AE pairs
LEGEND
EPICLASTICS
Reworked Tuff
Reworked Lapillistone
AE Turbidites
PYROCLASTICS
Tuff
Lapillistone
LOCALLY ISOCLINALLY FOLDED
WITH 10-20 CM CLOSURES

Figure 375.13. Section 1-2, Shark Lake region. Refer to Figure 375.4 for location in the southern metasedimentary belt.

A second lithofacies assemblage consists of dark brown- to dark grey-weathering, regularly and thinly interstratified metagreywacke and pelite and is largely restricted to the lower half of the section in units varying from several metres to about 12 m in thickness. The lighter coloured metagreywacke is fine- to medium-grained, occurs in units several centimetres to several metres in thickness, and can be either non-stratified or faintly bedded. Primary features are limited to normal grading and occasional ripple cross-lamination. Pelite units, representing the finer-grained cap of a fining-upward pair, are commonly one to several tens of centimetres in thickness and either non-stratified or faintly stratified, with some ripple cross-lamination. The metagreywacke and pelite pairs represent repetitive turbidity current deposition, with the coarser-grained bases likely representing reworking of finer-grained unconsolidated pyroclastic detritus. The pelitic tops may represent a mixture of reworked, unconsolidated, ash-size tephra and non-volcanic hemipelagic detritus. The restriction of the turbidite lithofacies to the same part of the section containing the volcanic breccia would logically indicate greater instability in a more vent-proximal setting.

In summary, the lithofacies sequence preserved in section 1-1 indicates a marine environment characterized by felsic pyroclastic volcanism interrupted throughout its early history by numerous inactive periods during which time sedimentation was restricted to turbidity current activity.

A late northwest-trending fault sinistrally offsets the region of section 1-2 from that of section 1-1 (*see* Figure 375.4). This section differs from section 1-1 in that local isoclinal folding with 10 to 20 cm closures was recognized on the basis of younging directions of normally graded units, indicating that unit thicknesses are not depositional. However, because thrusting is absent in the section, the stratigraphic units are related, and a single paleogeographic setting can be inferred for the section. The prominent younging direction throughout the section is toward the southeast. Five lithofacies, composing two lithofacies assemblages, are identified in the section (*see* Figure 375.13). The assemblages are similar to those in section 1-1, with the exception of the absence of volcaniclastic conglomerate from the felsic pyroclastic assemblage. Descriptions and interpretations assigned to assemblages are identical to that proposed for section 1-1. General features of the section which serve to distinguish the depositional setting from that preserved in section 1-1 are: 1) volcaniclastic conglomerate is absent; 2) in general, reworking of pyroclastics is more evident, and these units are more common in the basal half of the section; 3) turbidites are concentrated in the top half of the section.

Considered cumulatively, these differences indicate that although a marine felsic pyroclastic environment is represented by both sections, section 1-2 differs in the following ways: 1) the absence of volcaniclastic conglomerate suggests deposition distal to a vent; 2) the overall increase in reworking could indicate either an increase in ambient energy conditions due to shifting marine currents or increased shocking of the sediment pile associated with volcanic tremors; the abundance of reworked units in the basal portion indicates that whatever the mechanism it occurred more frequently during this period; 3) the concentration of turbidite units in the upper portion of the section suggests a waning of volcanic activity so that only turbidite sedimentation occurred.

REGIONAL VARIATION IN DORE SUCCESSION PALEOGEOGRAPHY

Table 375.1 summarizes the lithofacies assemblages identified for each region with their corresponding depositional interpretations. It suggests significant areal differences in paleogeographic setting in the Dore metasedimentary succession.

1. Deposition began in the southern metasedimentary belt likely coeval with the youngest stage of volcanism, and was characterized principally by deep marine felsic pyroclastic and turbidity current sedimentation. An interstratified fluvial lithofacies in this belt indicates that a period of uplift and erosion interrupted an otherwise deep marine setting.

2. Deposition of Dore clastics may have been roughly coeval in the middle and northern metasedimentary belts, and 15 to 20 Ma after the onset of sedimentation in the southern belt. In the Kapimchigama – Radford lakes region representing the northern end of the middle metasedimentary belt, sedimentation progressed from a deep to shallow marine sedimentary environment, with no indication of syndepositional volcanism. Essentially contemporaneous sedimentation at Kabenung Lake in the western portion of the northern metasedimentary belt occurred in a significantly different paleogeographic setting, in which predominantly deep marine felsic pyroclastic sedimentation occurred, perhaps interrupted by a single period of uplift and erosion as indicated by the probable fluvial lithofacies. The presence of felsic pyroclastic lithofacies suggests that the youngest volcanic period in the Michipicoten greenstone belt lasted about 20 Ma, based on the isotopic age of northern belt metasediments from the Iris Lake area. Alternatively, a fourth period of volcanism should be considered for the region. A period of uplift, and felsic pyroclastic as well as fluvial sedimentation, perhaps contemporaneous, is also proposed for the Troupe Lake region in the eastern area of the northern metasedimentary belt.

FUTURE WORK

Additional fieldwork in the Michipicoten greenstone belt will focus on the Dore River segment and the Mildred Lake region of the Mildred–Lena lakes segment of the southern metasedimentary belt, as well as the West Andre – East Andre lakes area, representing the southern end of the middle metasedimentary belt.

Table 375.1. Regional comparison of depositional environment in the Dore metasedimentary succession, Michipicoten greenstone belt.

Metasedimentary Belt	Region	Lithofacies Assemblage
Southern	Shark Lake	marine felsic pyroclastic; turbidite-submarine fan
	Arliss Lake	marine felsic pyroclasitc; turbidite-submarine fan; fluvial; marine debris flow
Middle	Radford–Kapimchigama lakes	turbidite-submarine fan; siliciclastic shelf
Northern	Kabenung Lake	marine felsic pyroclastic; fluvial
	Troupe Lake	fluvial; subaerial felsic pyroclastic

Laboratory work during the remainder of the year will concentrate on establishing a compositional database for the Dore metasediments through comprehensive petrographic studies and XRF analyses.

ACKNOWLEDGEMENTS

Research for this study has been funded by Ontario Geoscience Research Grant 375. This report on the sedimentary evolution of the Michipicoten greenstone belt in the region of Wawa constitutes part of a larger study of the sedimentary evolution of the Abitibi greenstone belt involving J.A. Donaldson (principal investigator), R.J. Rice (post-doctoral fellow—Wawa region), and P. Born (Ph.D. candidate—Timmins region). W. Mueller of the Université du Québec à Chicoutimi has collaborated with this project through his own research in the Duparquet region of the Abitibi in the province of Quebec. Additional funds were provided by NSERC Operating Grant A5536, and a President's Grant (GR-5) from Carleton University.

Dr. Ron Sage, Precambrian Geology Section, Ontario Geological Survey, Toronto, conceived the Wawa portion of the Abitibi project and provided considerable advice. Delio Tortosa and staff of the Resident Geologist's Office, Wawa provided invaluable assistance throughout the field season. Dr. Tom Morris, Engineering and Terrain Geology Section, Ontario Geological Survey, Sudbury, unselfishly offered critical field assistance throughout the summer. Jennifer Bourke was the field assistant for RJR.

REFERENCES

Arias, Z.G. and Helmstaedt, H. 1989. Structural evolution of central and east-central Michipicoten (Wawa) greenstone belt, Superior Province; *in* Geoscience Research Grant Program 1988–1989, Summary of Research, Ontario Geological Survey, Miscellaneous Paper 143, p.210–226.

—— 1990a. Early thrust faults in the Archean Michipicoten greenstone belt, Superior Province, central Ontario; *in* Program with Abstracts, Geological Association of Canada–Mineralogical Association of Canada, Joint Annual Meeting, v.15, p.4.

—— 1990b. Structural evolution of the Michipicoten (Wawa) greenstone belt, Superior Province: Evidence for an Archean fold and thrust belt; *in* Geoscience Research Grant Program 1989–1990, Summary of Research, Ontario Geological Survey, Miscellaneous Paper 150, p.107–114.

Attoh, K. 1980. Stratigraphic relations of the volcanic-sedimentary successions in the Wawa greenstone belt, Ontario; *in* Current Research, Part A, Geological Survey of Canada, Paper 80-1A, p.101–106.

Bruce, E.L. 1940a. Goudreau–Lochalsh Area, District of Algoma, Ontario; Ontario Department of Mines, Map 49G, scale 1:31 680 or 1 inch to 1/2 mile.

—— 1940b. Geology of the Goudreau–Lochalsh Area; Ontario Department of Mines, Annual Report, v.49, pt.3, p.1–50.

Card, K.D. 1990. A review of the Superior Province of the Canadian Shield, a product of Archean accretion; Precambrian Research, v.48, p.99–156.

Cas, R.A.F. and Wright, J.V. 1987. Volcanic successions, modern and ancient; Allen and Unwin, London, 528p.

Coleman, A.P. and Wilmott, A.B. 1902. The Michipicoten iron ranges; University of Toronto Studies, Geological Series, v.2, 83p.

Frarey, M.J. and Krogh, T.E. 1986. U–Pb zircon ages of late internal plutons of the Abitibi and eastern Wawa subprovinces, Ontario and Quebec; *in* Current Research, Part A, Geological Survey of Canada, Paper 86-1A, p.43–48.

Frohberg, H. 1935. The ore deposits of the Michipicoten area; Ontario Department of Mines, Annual Report, v.44, pt.8, p.39–83.

Gledhill, T.L. 1927. Michipicoten gold area, District of Algoma; Ontario Department of Mines, Annual Report, v.36, pt.2, p.1–49.

Goodwin, A.M. 1962. Structure, stratigraphy and origin of iron formations, Michipicoten area, Algoma District, Ontario, Canada; Geological Society of America Bulletin, v.73, p.561–586.

—— 1963. Michipicoten area compilation sheet; Ontario Department of Mines, Geological Series, Preliminary Map P. 184, scale 1:126 720.

Heather, K.B. and Arias, Z.G. 1987. The geological setting of gold mineralization in the Goudreau–Lochalsh area, District of Algoma; *in* Summary of Field Work and Other Activities, 1987, Ontario Geological Survey, Miscellaneous Paper 137, p.155–162.

Heather, K.B. and Buck, S. 1988. The geological and structural setting of gold mineralization in the Missanabie–Renabie District of the Michipicoten Greenstone Belt, Wawa, Ontario; *in* Summary of Field Work and Other Activities, 1988, Ontario Geological Survey, Miscellaneous Paper 141, p.257–270.

Heather, K.B., Arias, Z.G. and Sage, R.P. 1988. The geological setting of gold in the Wawa gold camp, Ontario, Canada; *in* Bicentennial Gold '88, Extended Abstracts Poster Programme, v.1, Geological Society of Australia Incorporated, p.20–22

Logan, W.E. 1863. Geology of Canada; Geological Survey of Canada, Report Progress to 1863, p.53–55.

McGill, G.E. and Shrady, C.H. 1986. Evidence for a complex Archean deformational history, southwestern Michipicoten greenstone belt, Ontario; Journal of Geophysical Research, v.91, no.B13, p.E281–E289.

Milne, V.G., Giblin, P.E., Bennett, G., Thurston, P.C., Wolfe, W.J., Giguere, J.F., Leahy, E.J. and Rupert, R.J. 1971. Manitouwadge–Wawa sheet, Ontario Department of Mines, Geological Compilation Series, Map 2220, scale 1:253 440.

Moore, E.S. 1931. Goudreau and Michipicoten gold areas, District of Algoma; Ontario Department of Mines, Annual Report, v.40, pt.4, p.1–54.

Neale, K.L. 1981. Sedimentology, petrography, and depositional environment of Dore sediments above the Helen–Eleanor Iron Range, Wawa, Ontario: unpublished Bachelor of Science thesis, McMaster University, Hamilton, Ontario, 54p.

Ojakangas, R.W. 1983. Clastic sedimentary rocks of the Michipicoten volcanic-sedimentary belt, Wawa, Ontario; *in* Workshop on a Cross Section of Archean Crust, Lunar and Planetary Institute, Houston, LPI Technical Report 83–03, p.66–68.

Ontario Geological Survey 1991a. Bedrock geology of Ontario, explanatory notes and legend; Ontario Geological Survey, Map 2545.

—— 1991b. Bedrock geology of Ontario, east-central sheet; Ontario Geological Survey, Map 2543, scale 1:1 000 000.

Sage, R.P. 1979. Wawa Area, District of Algoma; *in* Summary of Field Work, 1979, Ontario Geological Survey, Miscellaneous Paper 90, p.48–53.

—— 1980. Wawa Area, District of Algoma; *in* Summary of Field Work, 1980, Ontario Geological Survey, Miscellaneous Paper 96, p.47–50.

—— 1981. Josephine Area, District of Algoma; *in* Summary of Field Work, 1981, Ontario Geological Survey, Miscellaneous Paper 100, p.37–40.

—— 1982. Josephine Area, District of Algoma; *in* Summary of Field Work, 1982, Ontario Geological Survey, Miscellaneous Paper 106, p.28–33.

—— 1983. Josephine Area, District of Algoma; *in* Summary of Field Work, 1983, Ontario Geological Survey, Miscellaneous Paper 116, p.45–49.

—— 1984. Josephine–Goudreau Area, District of Algoma; *in* Summary of Field Work, 1984, Ontario Geological Survey, Miscellaneous Paper 119, p.56–63.

—— 1985a. Precambrian geology of Leclaire Township, District of Algoma; Ontario Geological Survey, Geological Series, Preliminary Map P.2636, scale 1:15 840.

—— 1985b. Goudreau–Lochalsh Area, District of Algoma; *in* Summary of Field Work and Other Activities, 1985, Ontario Geological Survey, Miscellaneous Paper 126, p.90–94.

—— 1986. Stratigraphic correlation in the Wawa area; *in* Volcanology and mineral deposits, Ontario Geological Survey, Miscellaneous Paper 129, p.62–68.

—— 1987a. Geology of the Goudreau–Lochalsh and Kabenung Lake Areas, District of Algoma; *in* Summary of Field Work and Other Activities, 1987, Ontario Geological Survey, Miscellaneous Paper 137, p.134–137.

—— 1987b. Preliminary interpretation of the relationship between economic mineralization and volcanic stratigraphy in the Wawa area; Ontario Geological Survey, Miscellaneous Paper 100, p.41–44.

—— 1988. Geology of the Kabenung Lake Area, District of Algoma; *in* Summary of Field Work and Other Activities, 1988, Ontario Geological Survey, Miscellaneous Paper 141, p.242–248.

—— in preparation a. Geology of Chabenal, Esquega, Lastheels and McMurray Townships, District of Algoma; Ontario Geological Survey, Open File Report 5586.

—— in preparation b. Geology of Abotossaway, Corbiere, Leclaire and Musquash Townships, District of Algoma; Ontario Geological Survey, Open File Report 5587.

—— in preparation c. Geology of Aguonie, Bird, Finan and Jacobson Townships, District of Algoma; Ontario Geological Survey, Open File Report 5588.

—— in preparation d. Geology of Killins, Knicely and Lalibert townships, District of Algoma; Ontario Geological Survey, Open File Report 5589.

—— in preparation e. Precambrian geology of Lalibert Township, District of Algoma; Ontario Geological Survey, Geological Series, Preliminary Map, scale 1:15 840.

Sage, R.P., Rebic, Z., Abercrombie, S., Neale, K., MacMillan, D., England, D. and Calvert, T. 1982a. Precambrian geology of Chabanel Township, District of Algoma; Ontario Geological Survey, Geological Series, Preliminary Map P.2439, scale 1:15 840.

Sage, R.P., Rebic, Z., Abercrombie, S., Neale, K., MacMillan, D. and Calvert, T. 1982b. Precambrian geology of Esquega Township, Wawa area, District of Algoma; Ontario Geological Survey, Geological Series, Preliminary Map P.2440, scale 1:15 840.

Sage, R.P., Sawitsky, E., Turner, J., Leeselleuer, P. and Sagle, E. 1982c. Precambrian geology of McMurray Township, Wawa area, District of Algoma; Ontario Geological Survey, Geological Series, Preliminary Map P.2441, scale 1:15 840.

—— 1982d. Precambrian geology of Lastheels Township, Wawa area, District of Algoma; Ontario Geological Survey, Geological Series, Preliminary Map P.2442, scale 1:15 840.

Sage, R.P., England, D., Calvert, T., Oudkerk, G., Worona, R. and Kosciusko, K. 1982e. Precambrian geology of Musquash Township, District of Algoma; Ontario Geological Survey, Geological Series, Preliminary Map P.2569, scale 1:15 840.

Sage, R.P., Calvert, T., Epstein, R., England, D., Kosciusko, K., Worona, R., Oudkerk, J., Inasi, J., Lockwood, M. and Thomas, D. 1984. Precambrian geology of Corbiere Township, District of Algoma; Ontario Geological Survey, Geological Series, Preliminary Map P.2607, scale 1:15 840.

Sage, R.P., Thorpe, R. and Berdusco, E. 1987. Field trip guidebook—geology and stratigraphy of the Michipicoten iron formation; 33rd Annual Meeting, Institute on Lake Superior Geology, v.33, pt.3, 93p.

Shrady, C.H. 1988. Structural interpretation of the Michipicoten greenstone belt, Ontario; *in* Program with Abstracts, Joint Annual Meeting, Geological Association of Canada-Mineralogical Association of Canada, v.13, p.112.

—— 1991. Deformation history of, and the study of strain applied to, the Michipicoten Greenstone Belt near Wawa, Ontario; unpublished Ph.D. thesis, University of Massachusetts, Amherst, 346 p.

Studemeister, P.A. 1983. The greenschist facies of an Archean assemblage near Wawa, Ontario; Canadian Journal of Earth Sciences, v.20, p.1409–1420.

Sullivan, R.W., Sage, R.P. and Card, K.D. 1985. U–Pb zircon age of the Jubilee stock in the Michipicoten greenstone belt near Wawa, Ontario; *in* Current Research, Part B, Geological Survey of Canada, Paper 85-1B, p.361–365.

Thomas, D.A. 1984. Stratigraphy, lithology, petrography, and depositional environments of the Dore sediments proximal to the Lucy Iron Range, Wawa, Ontario; unpublished Bachelor of Science thesis, Carleton University, Ottawa, Ontario, 37p.

Turek, A., Smith, P.E. and Van Schmus, W.R. 1982. Rb–Sr and U–Pb ages of volcanism and granite emplacement in the Michipicoten belt — Wawa, Ontario; Canadian Journal of Earth Sciences, v.19, p.1608–1626.

—— 1984. U–Pb zircon ages and the evolution of the Michipicoten plutonic-volcanic terrane of the Superior Province, Ontario; Canadian Journal of Earth Sciences, v.21, p.457–464.

Turek, A., Van Schmus, W.R. and Sage, R.P. 1988. Extended volcanism in the Michipicoten greenstone belt, Wawa, Ontario; *in* Program with Abstracts, Joint Annual Meeting, Geological Association of Canada-Canadian Mineralogical Association of Canada, v.13, p.127.

Turek, A., Keller, R. and Van Schmus, W.R. 1990. U–Pb zircon ages of volcanism and plutonism in the Mishibishu greenstone belt near Wawa, Ontario; Canadian Journal of Earth Sciences, v.27, p.649–656.

Grant 382 The Role of the Crust as a Source of PGE in the Sudbury Nickel Deposit: Re/Os Isotope Evidence

---

A.P. Dickin

Department of Geology, McMaster University, Hamilton, Ontario.

Osmium isotope and Sm/Nd geochronology data are presented for Archean and Proterozoic country rocks of the Sudbury Intrusive Complex (SIC). These results are used to calculate the osmium isotope composition of the country rocks at the time of emplacement of the SIC. Published initial osmium compositions of sulphide ores from mines widely spaced around the complex are compared with the country rock data. Ores which are not thought to have been disturbed by younger events yield relatively homogenous ^{187}Os/^{188}Os ratios of 0.54 to 0.60 at 1.85 Ga. They lie within the spectrum of isotopic growth lines displayed by the country rocks, which have ^{187}Os/^{188}Os ratios between 0.50 and 1.11 at 1.85 Ga. Because osmium is a platinum group element (PGE), these results imply that the sulphide ores and related PGE of the SIC can have an entirely crustal source without a mantle derived contribution. This conclusion is consistent with published Nd isotope data for the complex, and supports the meteorite impact hypothesis, since impact is an effective means of melting the vast quantity of crustal rocks necessary to generate the SIC. The extraction of PGE from this silicate melt by a nickel sulphide liquid is analogous to the laboratory fire assay procedure.

INTRODUCTION

The Sudbury Intrusive Complex (SIC) is the world's largest nickel source. It consists of a stratified gabbroic pluton, called the Main Mass, which is overlain by the Onaping tuff and underlain by a "Contact Sublayer" of brecciated country rock, quartz norite and Fe-Ni-Cu-PGE sulphide ore. The SIC was intruded at 1.85 Ga (Krogh et al. 1984) along the boundary between the Archean basement to the northwest and the overlying Early Proterozoic (Huronian) platform sediments to the southeast (*see* Figure 382.1).

Various features of Sudbury geology, such as the widespread distribution of brecciated rock outside the complex, the presence of shatter cones in the footwall rocks, and the lopolith form of the SIC were used by Dietz (1964) to argue for a meteorite impact origin for the complex. Peredery (1972) developed this model further by proposing that the Onaping tuff was a fallback breccia generated by the impact. The impact model, the alternative endogenic model, and the geology and geochemistry of the complex were reviewed in detail in an Ontario Geological Survey special volume edited by Pye et al. (1984).

Faggart et al. (1985) presented Nd isotope data for the silicate rocks of the SIC, which showed that they contained a remarkably strong crustal signature, with an epsilon value of -7.5 ±1 at 1.85 Ga. Faggart et al. (1985) argued that this result could be explained by an exclusively crustal origin for the SIC, which provided strong evidence for an impact origin of the complex. However, because Nd is a lithophile element, this evidence cannot be reliably extrapolated to deduce such an origin for the chalcophile elements in the nickel-bearing sulphide ores of the complex.

The Re/Os isotope system can shed a unique light on the origin of the sulphide ores of the SIC because both elements have a chalcophile affinity, yet they display very different partition coefficients between crustal and mantle reservoirs. The parent element, Re, is strongly partitioned into evolved magmas, such as those which form the crust, while the daughter, Os, is preferentially retained in the mantle.

^{187}Re decays by beta emission to ^{187}Os with a decay constant of 1.64×10^{-11} yr^{-1} (Lindner et al. 1989), corresponding to a half-life of 4.23×10^{10} yr. Given this long half-life, the mantle displays only slow growth of ^{187}Os with time, but the high Re/Os ratio of crustal rocks ensures rapid ^{187}Os production. Hence the two reservoirs develop very different Os isotope ratios over geological time, making the Re/Os method a powerful tracer for distinguishing mantle derived and crustal components in magmas and ores.

This paper presents new osmium isotope analyses of crustal units in the vicinity of Sudbury, for comparison with osmium isotope analyses of Sudbury ores from four different nickel mines (Beneteau et al. 1991; Richardson et al. 1990; Walker et al. 1991). Because osmium is one of the platinum group elements (PGE), it can be used as a tracer for the behavior of the whole group of six similar elements in order to determine their origin.

The crustal rocks selected for analysis included two high grade metamorphic rocks from the Levack gneisses (Superior Province), northwest of the SIC, and two metasedimentary samples from the McKim and Copper Cliff formations of the Huronian supergroup (Southern Province; *see* Figure 382.1). Sm/Nd analyses were performed to date the crustal extraction

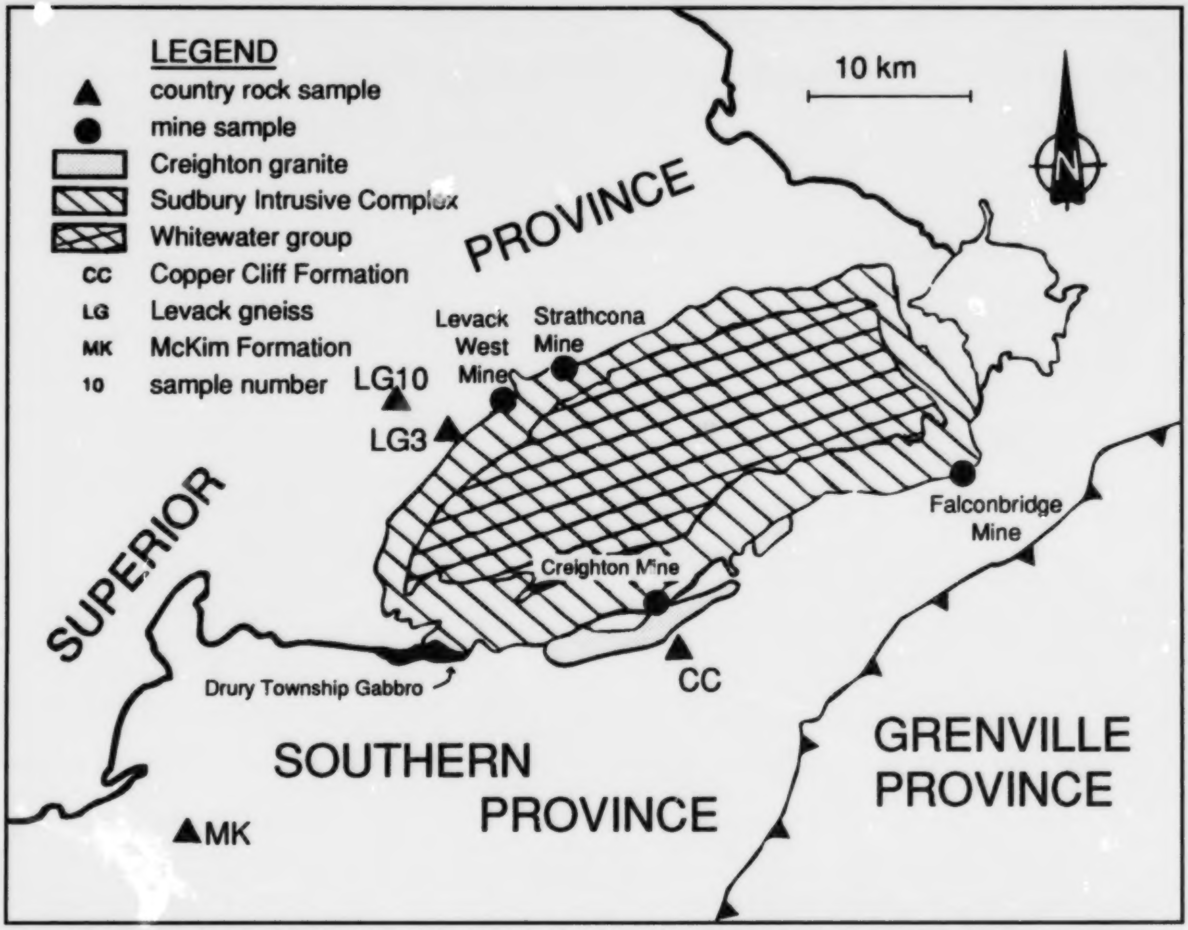
LEGEND
▲ country rock sample
● mine sample
Creighton granite
Sudbury Intrusive Complex
Whitewater group
CC Copper Cliff Formation
LG Levack gneiss
MK McKim Formation
10 sample number
10 km
N
PROVINCE
SUPERIOR
Levack West Mine
Strathcona Mine
LG10
LG3
Falconbridge Mine
Creighton Mine
Drury Township Gabbro
CC
SOUTHERN PROVINCE
GRENVILLE PROVINCE
MK

Figure 382.1. Geological setting of the ring-shaped Sudbury Intrusive Complex relative to the Superior, Southern and Grenville provinces. Locations of both country rock and mine samples are shown.

age of the samples, and hence to determine their osmium isotope evolution over time. In this way an attempt is made to characterise the osmium isotope composition of crustal rocks which might have given rise to the SIC, and thereby to constrain the sources of PGE and other metals in the Sudbury sulphide ores.

ANALYTICAL METHODS

The high ionisation potential of osmium has precluded its analysis by conventional (positive) thermal ion mass spectrometry (TIMS). However, inductively coupled plasma-mass spectrometry (ICP-MS) represents a viable tool for osmium isotope analysis, since the high temperature of the ICP provides a suitable ion source, while quadrupole mass analysis provides sufficient analytical precision to tackle the present study.

Following Russ et al. (1987), osmium was distilled directly into the carrier argon gas supply of the ICP-MS. Isotopic abundances are quoted relative to ^{188}Os rather than ^{186}Os, since the latter is a small peak subject to tungsten interference and is also the daughter product of the rare, long-lived, unstable isotope ^{190}Pt. Data in this report can be converted to ratios against ^{186}Os by multiplying by 0.12, assuming that ^{190}Pt decay is insignificant.

Re and Os concentrations were determined using a mixed ^{185}Re-^{190}Os spike which was incorporated in solid solution in a nickel sulphide matrix (Dickin et al. 1988). This material was prepared by co-precipitating Ni-Re-Os sulphides in aqueous solution with thioacetamide. Trace Re-Os spikes were combined in aqueous solution with ultra-pure reagents: 10g $NiNO_3$-$6H_2O$, 10g Na_2CO_3, 3g thioacetamide and 3g ammonium acetate. After buffering with ammonia to pH 9, the solution was heated overnight at ca. 100°C. After drying, the resulting sulphide precipitate was further diluted with carbonyl nickel in a fire assay. The resulting 20g button was crushed to a powder for use. The isotopic composition of this solid solution spike was determined by Richardson et al. (1989), who found its composition to be within error of the Oak Ridge specification, indicating that the "solid spike" preparation blank was negligible.

Osmium in country rock samples was pre-concentrated by nickel sulphide fire assay using 54g rock, 18g Na_2CO_3, 36g $Na_2B_4O_7$, 1g silica, 2g carbonyl nickel, 1g sulphur and ca. 2 mg of solid spike, heated to 1000°C for 16 hours. The resulting button was dissolved in warm nitric acid.

Osmium isotope analyses were performed on a Sciex Elan operated at 1.4 kw power and 1.2 l/minute sampler gas supply. Five positions were measured across the rounded top of each peak, using a ten second peak switching cycle. After dumping of raw count rates off line, the data were processed in a manner similar to conventional TIMS analysis (time interpolation, background subtraction, peak ratioing, interference correction, statistical processing). However, due to the low mass resolution of the ICP-MS (ca. 250), half-mass positions are not sufficiently free of peak tail to be used as baseline/background. For osmium analysis this is not a problem, since the distillation process normally separates Os from Ta, W, Re and Pt, such that mass positions 181, 183, 185 and 194 can be used collectively to form a good impression of interference-free electronic background.

Both osmium isotope dilution (I.D.) and isotope ratio (I.R.) analyses were performed in the same run, and the data were corrected for fractionation and spike interference using an iterative solution.

Instrumental memory effects are the largest source of potential blank during Os isotope analysis by ICP-MS. To avoid these problems, the complete analytical system (distillation apparatus, tubing and torch) was changed after each sample. A blank (reagent only) run was always made before each analysis to test the success of these measures. However, the most sensitive monitor of memory effects was the analysis of each run in blocks of 5 scans. Any long-term drift of spike/natural isotope ratios during a run was taken as possible evidence of memory, and the data rejected. An upper estimate of total procedural blank is represented by a complete fire assay and total process blank for osmium of 37 picograms. On a fire assay sample of 50g, this represents a maximum of 2% of sample osmium. No blank corrections were therefore made. Further analytical details are reviewed by Richardson et al. (1990).

Sm/Nd analysis was performed using established techniques. After dissolution using HF and HNO_3, samples were split and one aliquot spiked with a mixed ^{150}Nd-^{149}Sm spike. Analysis by this technique yielded Sm/Nd = 0.2280 ± 2 for BCR-1. Standard cation and reverse phase column separation methods were used. Nd isotope analyses were performed on a VG isomass 354 mass spectrometer at McMaster using double filaments and a 4 collector peak switching algorithm, and were normalised to a $^{146}Nd/^{144}Nd$ ratio of 0.7219. An average value of 0.51185 ± 2 (2 sigma population) was determined for the La Jolla standard. Average within run precision on samples was ± .000012 (2σ). The analytical uncertainty on each model age totals about 20 Ma (2σ). This does not include the geological uncertainties of the choice of mantle model and the possibility of mixed provenance.

RESULTS

Osmium isotope ratios and osmium contents of crustal units are presented in Table 382.1. Precision on $^{187}Os/^{188}Os$ ratios was ± 3% (2σ) on three of the samples analysed in this study, but only ± 10% on LG3 (*see* Table 382.1), due to its lower osmium content. Measurement of $^{189}Os/^{188}Os$ ratios demonstrates excellent reproducibility and accuracy for the three more osmium-rich samples, relative to an accepted value of 1.21. LG3, however, displays correspondingly poorer accuracy for this ratio as well.

At the low osmium abundances observed it would be hard to obtain precise Re/Os ratios in order to age correct country rock compositions to 1.85 Ga for comparison with the Sudbury ores. Therefore Sm/Nd data was used (Table 382.2) to determine the time of crustal extraction of the material from the depleted mantle of DePaolo (1981). One can then approximate the osmium isotope growth lines of the samples by assuming closed-system development of Re/Os in the samples since extraction from the mantle reservoir, whose osmium signature is known (Figure 382.2). The Mississagi quartzite (MS9) was used for additional dating control of the Huronian samples but not analysed for Os because too low a concentration was anticipated.

DISCUSSION AND CONCLUSIONS

Analysis of sulphide ores from the Creighton, Falconbridge East and Levack West mines has yielded initial $^{187}Os/^{188}Os$ ratios of 0.60, 0.54 and 0.56 respectively for samples interpreted as undisturbed since the formation of the Sudbury Intrusive Complex (*see* Table 382.1; Richardson et al. 1990; Beneteau et al. 1991; Walker et al. 1991). A higher initial $^{187}Os/^{188}Os$ ratio of 0.91 was determined by Walker et al. (1991) from Strathcona, but some ores in this mine are thought to have been disturbed by later hydrothermal overprinting, so it is possible that this high initial ratio was not an original feature.

Walker et al. (1991) argued that the isotopic heterogeneity between Levack and Strathcona was evidence for derivation of osmium in the sulphide ores from two or more sources, a model also proposed by Beneteau et al. (1991). However, relative to the crustal units analysed in this study, osmium initial ratios from Creighton, Falconbridge and Levack, show a remarkable degree of homogeneity, and fall within the crustal envelope (0.5 to 1.11 at 1.85 Ga). Therefore, it would appear that osmium and other PGE in the Sudbury ores can probably be derived entirely from crustal sources, just as Faggart et al. (1985) proposed crustal derivation of Nd in the silicate rocks.

Dietz (1964) originally proposed that the silicate rocks of the SIC represent an impact melt sheet. This model has been recently supported by Grieve (1991) on the basis of comparison with other impact sites. Because this model implies melting of

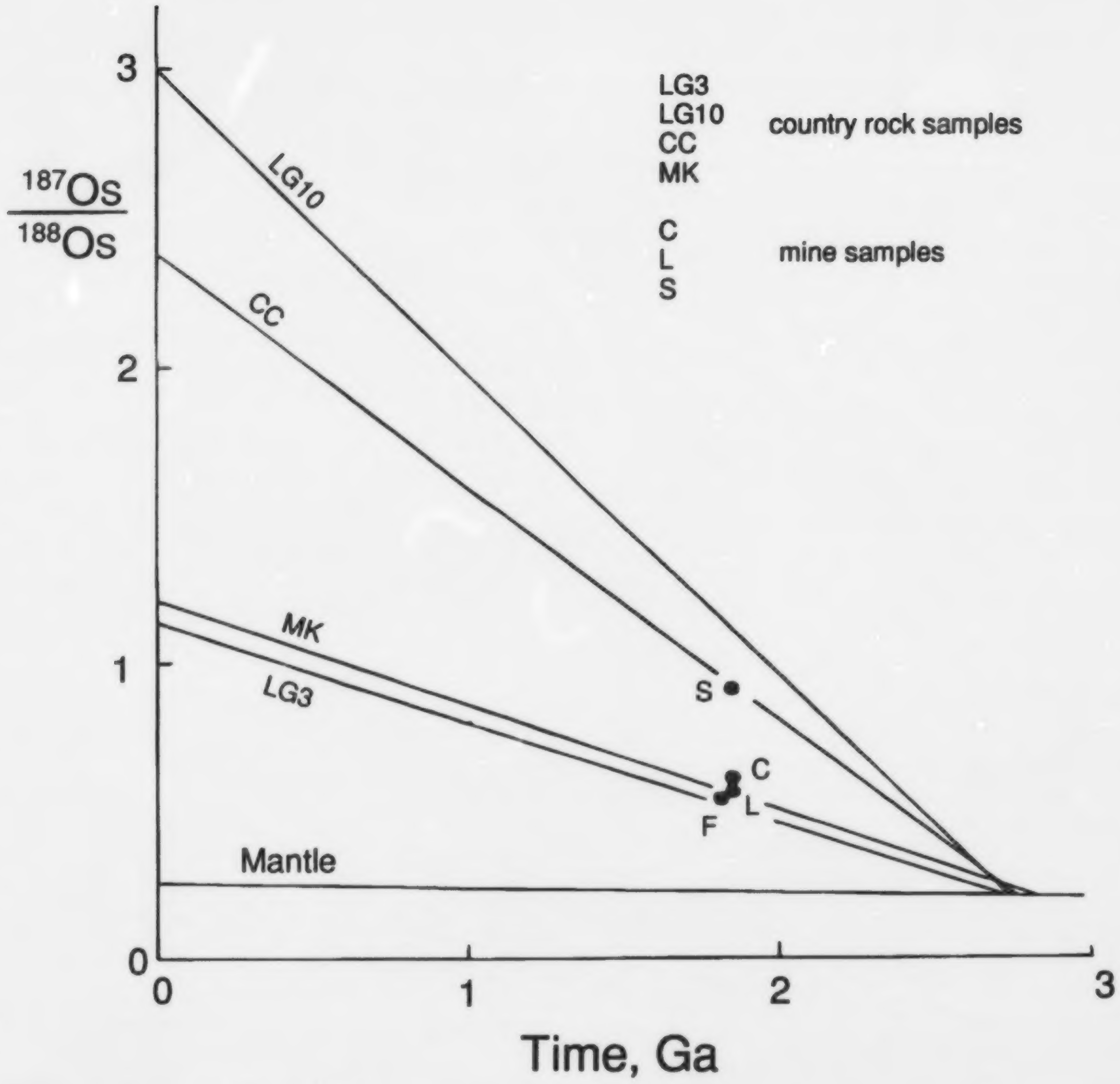

Figure 382.2. Compositions of Sudbury sulphide ores and analysed crustal units which may have acted as osmium sources, plotted on a diagram of $^{187}Os/^{188}Os$ isotope evolution against time.

the earth's surface, it can explain why osmium in the sulphide ores can have a 100% crustal signature.

Sulphide ores at the Creighton mine have Os contents of 100-400 ppb (Richardson el al. 1990). In comparison with the Os contents of crustal units presented here, this implies an enrichment of osmium in the ores relative to country rocks of up to three orders of magnitude. However, this is well within the range of sulphide/silicate distribution coefficients measured for other PGE (eg. Stone et al. 1990).

While the above evidence suggests that the Sudbury PGE are crustal in origin, the source of the sulphide melt itself remains unclear. Dietz (1964) suggested that the sulphide ores represent meteoritic material, but this model has not been widely accepted. They could represent an aggregation of pre-existing sulphide phases from melted country rocks, or be derived from a small component of mantle derived melt, generated in association with the impact by decompression melting.

Prevec and Baadsgaard (1991) have reported an ion microprobe U/Pb age of 1854 ± 14 Ma for a small metagabbro-anorthosite just to the west of the Sudbury structure, in Drury Township (*see* Figure 382.1). This result indicates that basic magmas were present in the crust at the time of the Sudbury event. Such melts could have been released into the crust by an impact event, but their greater density might well have prevented effective mixing with the proposed overlying impact melt.

Table 382.1. Re/Os data for country rocks near Sudbury

Sample number	Rock unit	Os ppb	$\frac{^{189}Os}{^{188}Os}$	$\frac{^{187}Os}{^{188}Os}$	2σ%	$\frac{^{187}Os}{^{188}Os_{1.85}}$
Country rock samples						
LG3	Levack gneiss	0.05	1.06	1.12	10	0.50
LG10	Levack gneiss	0.30	1.19	3.00	3	1.11
MK	McKim Fmn.	0.27	1.24	1.21	3	0.55
CC1	Copper Cliff Fmn	0.20	1.21	2.25	3	0.89
MS9	Mississagi Fmn.	n.d.	n.d.	n.d.	–	n.d.
Sulphide ore samples						
C	Creighton Mine (Richardson el al.1990)					
F	Falconbridge East (Beneteau el al. 1991)					0.60
L	Levack West (Walker et al. 1991)					0.54
S	Strathcona (Walker el al. 1991)					0.56
						0.91

n.d.= not determined

Table 382.2. Sm/Nd data for country rock samples near Sudbury

Sample Number	Nd ppm	Sm ppm	$\frac{^{147}Sm}{^{144}Nd}$	$\frac{^{143}Nd}{^{144}Nd}$	TDM Ga	ε Nd 1.85
LG3	28.36	4.40	.0938	.510903	2.74	- 9.5
LG10	28.60	4.003	.0846	.510740	2.74	-10.5
MK	34.42	6.282	.1084	.511105	2.83	- 9.0
CC1	54.26	9.170	.1021	.511030	2.77	- 9.0
MS	3.15	0.538	.1031	.511098	2.70	- 7.9

Whatever the origin of the sulphide melt, it was probably in contact with the crystallizing silicate magma of the SIC for considerable time, during which PGE could be partitioned from the bulk crustal melt into the sulphide phase in a process analogous to a nickel sulphide fire assay.

This model is currently being tested by Pb isotope analysis of the same samples of country rock and sulphide ore discussed in this report.

ACKNOWLEDGEMENTS

The results reported in this paper were obtained as a result of funding by the Ministry of Northern Development and Mines Ontario Geoscience Research Grant Program. Re/Os analysis of Sudbury ores at McMaster was supported by an NSERC Strategic Grant.

REFERENCES

Beneteau, S.B., Richardson, J.M., Dickin, A.P., McNutt, R.H. and Coates, J. 1991. Re-Os isotopic systematics of the Falconbridge East mine, Sudbury, Ontario, Canada; *in* Program with Abstracts, Geological Association of Canada-Mineralogical Association of Canada, v.16, p.A10.

DePaolo, D.J. 1981. Neodymium isotopes in the Colorado Front Range and crust-mantle evolution in the Proterozoic; Nature, v.291, p.193-196.

Dietz, R.S. 1964. Sudbury structure as an astrobleme; Journal of Geology, v.72, p.412-434.

Dickin, A.P., Richardson, J.M. and McNutt, R.H. 1988. A "solid spike" method for Re-Os analysis of acid-resistant minerals enriched in platinum-group elements (PGE); Chemical Geology, v.70, p.179.

Faggart, B.E., Basu, A.R. and Tatsumoto, M. 1985. Origin of the Sudbury Complex by meteoritic impact: neodymium isotope evidence; Science, v.230, p.436-439.

Grieve, R.A.F. 1991. The Sudbury Igneous Complex: an impact melt sheet; *in* Program with Abstracts, Geological Association of Canada-Mineralogical Association of Canada, v.16, p.A48.

Krogh, T.E., Davis, D.W. and Corfu, F. 1984. Precise U-Pb zircon and badeleyite ages from the Sudbury area; *in* The geology and ore deposits of the Sudbury Structure, Ontario Geological Survey, Special Publication, v.1, p.431-447.

Lindner, M., Leitch, D.A., Russ, G.P., Bazan, J.M. and Borg, R.J. 1989. Direct determination of the half-life of ^{187}Re; Geochimica et Cosmochimica Acta, v.53, p.1597-1606.

Peredery, W.V. 1972. The origin of rocks at the base of the Onaping Formation, Sudbury, Ontario; unpublished PhD thesis, University of Toronto, Toronto, Ontario, 366p.

Prevec, S.A. and Baadsgaard, H. 1991. Ion-microprobe U-Pb zircon age constraints on crustal evolution from Late Archean to Mid-Proterozoic gabbro-anorthosites and granites, Central Ontario; *in* Program with Abstracts, Geological Association of Canada-Mineralogical Association of Canada, v.16, p.A102.

Pye, E.G., Naldrett, A.J. and Giblin, P.E. eds. 1984. The geology and ore deposits of the Sudbury Structure; Ontario Geological Survey, Special Publication, v.1, 603p.

Richardson, J.M., Dickin, A.P., McNutt, R.H., McAndrew, J.I. and Beneteau, S.B. 1989. Optimisation of ICP-MS analyses of a rhenium-osmium spike in solid solution; Journal of Analytical Atomic Spectrometry, v.4, p.465-471.

Richardson, J., Dickin, A.P. and McNutt, R.H. 1990. Re-Os isotope ratio determinations by ICP-MS: a review of analytical techniques and geological applications; *in* Plasma source mass spectrometry, Royal Society of Chemistry, Special Publication, no.85, p.120-144.

Russ, G.P., Bazan, J.M. and Date, A.R. 1987. Osmium isotopic ratio measurements by inductively coupled plasma mass spectrometry; Analytical Chemistry, v.59, p.984-89.

Stone, W.E., Crocket, J.H. and Fleet, M.E. 1990. Partitioning of palladium, iridium, platinum, and gold between sulfide liquid and basalt melt at 1200°C; Geochimica et Cosmochimica Acta, v.54, p.2341-2344.

Walker, R.J., Morgan, J.W., Naldrett, A.J. and Li, C. 1991. Re-Os isotopic systematics of Ni-Cu sulfide ores, Sudbury Igneous Complex, Ontario: evidence for a major crustal component; *in* Program with Abstracts, Geological Association of Canada-Mineralogical Association of Canada, v.16, p.A130.

Grant 384 Geochronology of Hydrothermal Alteration around Volcanic-Hosted Massive Sulphide Deposits in the Superior Province

E.S. Schandl[1,2], D.W. Davis[2], M.P. Gorton[1] and H.A. Wasteneys[2]

[1]Department of Geology, University of Toronto, Toronto, Ontario.
[2]Department of Mineralogy, Royal Ontario Museum, Toronto, Ontario.

U-Pb geochronology of hydrothermal monazite and rutile in the alteration zones of the Winston Lake, Geco and Kidd Creek massive sulfide deposits indicates that the present alteration assemblages consisting of sericite ± biotite + chlorite around the orebodies postdate mineralization by approximately 50 to 70 million years. The monazite fractions define ages of 2659 ± 3 Ma from Kidd Creek (age of the rhyolite host is 2717 ± 2 Ma); 2677 ± 1 Ma from Winston Lake (age of the host rock is 2723 ± 2 Ma) and 2661 ± 1 Ma from the Geco Mine. The rutile age from Kidd Creek, although imprecisely defined at 2663 ± 28 Ma, agrees with the monazite whereas that from Winston Lake at 2651 $^{+6}/_{-4}$ Ma is about 25 million years younger than the monazite.

These ages suggest an association of the alteration assemblages with regional metamorphism and possibly with a post-metamorphic hydrothermal episode. Extensive mobilization of light rare earth elements (LREE), displaying in some alteration zones 2000 times chondritic concentrations, was contemporaneous with late alteration and not with ore deposition. The replacement of syngenetic alteration assemblages around the three Archean massive sulfide deposits during later metamorphic/hydrothermal episodes suggests that in using a chlorite-sericite alteration halo as a guide to mineralization, potential exploration targets lacking in these alteration assemblages may be overlooked.

INTRODUCTION

This report documents a high-precision, U-Pb geochronological study of monazite and rutile from three Archean massive sulfide deposits: the Winston Lake and Geco mines in the Wawa Subprovince and the Kidd Creek Mine in the Abitibi Subprovince (*see* Figure 384.1). The study was undertaken in order to establish the age of hydrothermal alteration associated with the ore. Our objectives are: 1) to determine if the sericite + biotite + chlorite alteration around the orebodies represents a late metasomatic overprint on syngenetic mineralization as suggested by preliminary data from the Kidd Creek deposit (Schandl et al. 1990); 2) to establish the textural relationship between monazite, rutile and the alteration mineral assemblages and 3) to identify the alteration associated with the remobilization of rare earth elements (REE). The Geco and Winston Lake deposits were selected for this study because chlorite + biotite in their alteration zones contain an abundance of hydrothermal monazite suitable for precise U-Pb geochronology. Kidd Creek was re-evaluated using monazite and rutile from the altered rhyolite to determine more precisely the age of alteration (cf. Schandl et al. 1990). Previously analysed rutile (Schandl et al. 1990) was collected from the Hemingway property, whereas those reported here were collected from 2500 feet below surface in the stratigraphic footwall of the North orebody at Kidd Creek.

According to the classification of Morton and Franklin (1987), both Geco and the Winston Lake deposits are representative of the so-called Noranda-type massive sulfides, whereas Kidd Creek represents a Mattabi-type massive sulfide deposit. The Noranda-type deposits characteristically have a well-defined chloritic (Mg-rich) core and sericitic margins, and are typically lacking in carbonates, whereas in the Mattabi-type deposit, carbonate alteration is significant and chloritic (Fe-rich) and sericitic alteration is spatially less well defined. Regional metamorphism to amphibolite grade at Geco and Winston Lake and greenschist grade at Kidd Creek has caused ambiguity in the relationship of the ore to the present alteration assemblages.

The currently accepted model for volcanogenic massive sulfide deposits (Morton and Franklin 1987) suggests that ore-forming processes are intimately associated with pervasive hydrothermal alteration of the host rock to chloritic core and sericitic marginal assemblages (Morton and Franklin 1987). In the Superior Province, however, extensive chloritic and sericitic alteration assemblages are not unique to massive sulfide deposits, but also form halos around Archean gold deposits. The U-Pb age of rutile and titanite associated with the alteration assemblages in gold deposits in the Abitibi Subprovince ranges from 2600 to 2672 Ma (Corfu and Muir 1989; Wong et al. 1991; Jemielita et al. 1990). They are broadly comparable to the age of rutile (2624 ± 62 Ma; Schandl et al. 1990) and fuchsite (2618 ± 8 Ma; Smith et al. 1991) from the Kidd volcanic complex. The felsic volcanic rocks hosting the syngenetic

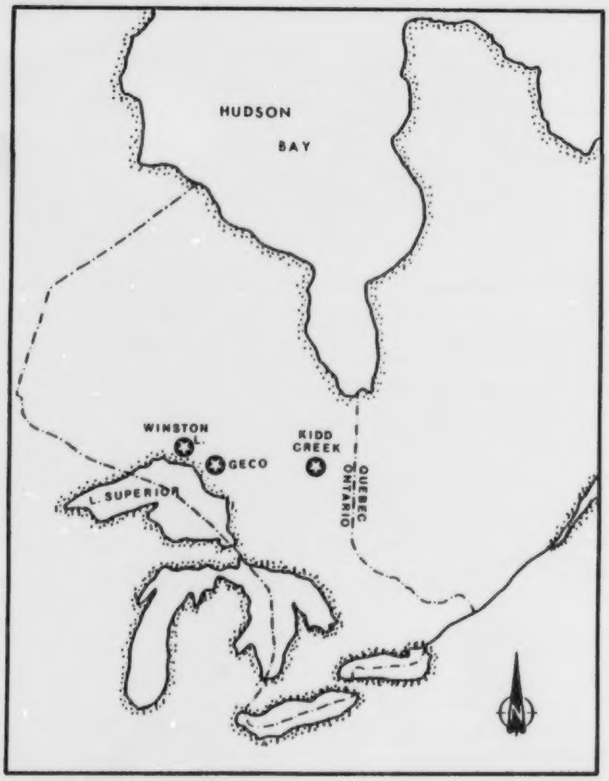

Figure 384.1. Location map.

massive sulfide orebodies at Kidd Creek, dated at 2717 ± 2 Ma (Barrie and Davis 1990) are significantly older than the minerals forming the alteration assemblage around the deposit, suggesting that the present alteration assemblage around Kidd Creek was not contemporaneous with the deposition of the massive sulfides.

Geological Setting

The Geco Mine (Noranda Minerals Inc.) is located just east of the town of Manitouwadge in the Thunder Bay mining district, Ontario. This Cu-Zn deposit occurs in highly deformed metavolcanic and metasedimentary rocks of Archean age (Friesen et al. 1982). The ore is contained within a "sericite schist" underlaid by the "granite gneiss" group, interpreted to be mafic to intermediate volcanic rocks, and overlain by the "grey gneiss" group, interpreted as metasediments intercalated with intermediate volcanic rocks.

The Winston Lake deposit (Minnova Inc.) is located about 20 km west of the town of Schreiber, Ontario and 145 km northeast of Thunder Bay. This Archean massive sulfide deposit occurs at the top of the Winston Lake calc-alkaline felsic volcanic sequence (Morrison and Sim 1989) which is composed of felsic volcanoclastic rocks and flows intercalated with mafic flows and sediments. The ore is in contact partly with altered mafic flows and partly with a volcanoclastic unit, called the "clotted rhyolite" (Morrison and Sim 1989). Both the Geco and Winston Lake deposits have been overprinted by amphibolite-grade metamorphism.

The Kidd Creek deposit (Falconbridge Ltd.) in the Abitibi Subprovince is located 27 km north of Timmins, Ontario. The massive sulfide occurs in rhyolitic volcanoclastic rocks of Archean age (Walker and Mannard 1974; Coad 1985) which in places are intercalated with komatiitic peridotite. The deposit is overprinted by greenschist-facies metamorphism.

MINERALOGY AND TEXTURE OF THE MAJOR ROCK TYPES

Accessory hydrothermal monazite, xenotime and rutile (identified by electron microprobe analysis and X-ray diffraction) are associated with the present alteration assemblages around the orebodies. Although rutile has been previously described from other massive sulfide deposits such as the Ducktown, Tennessee (Nesbitt and Kelly 1980), the Musoshi stratiform copper deposit in Zaire (Richards et al. 1988) and from Kidd Creek (Schandl 1989; Schandl et al. 1990), monazite and its yttrium-rich equivalent xenotime have not been identified, to our knowledge, in massive sulfide deposits.

Monazite is a phosphate of LREE containing predominantly Ce and variable proportions of La, Nd, Sm, Eu, and Th. Xenotime is an yttrium-rich phosphate containing variable proportions of heavy REE. The 2 phosphates are optically similar and indistinguishable in the study samples because of their small size. Thus the description of monazite is applicable to xenotime. Monazite grains have relatively high relief and birefringence similar to, although somewhat lower than, zircon. The average grain size at Geco and Winston Lake is 100 to 200 µm, but at Kidd Creek, it is generally less than 30 µm (*see* Photos 384.1a, 384.1b and 384.2). The color ranges from pale brown to very light yellow, and the minerals are non-pleochroic. Some larger grains have oval and/or subrounded shape (Photo 384.1a) while others are anhedral; the smaller grains are subrounded and have ragged, uneven grain boundaries (Photo 384.2). The most characteristic feature is a dark pleochroic halo in the host mineral around individual grains due to radiation damage caused by the decay of uranium in the monazite. These monazites and their halos are easily mistaken for zircons. The alteration minerals associated with monazite are mostly biotite and chlorite at Winston Lake, biotite at Geco Mine and mostly chlorite at Kidd Creek. Fine-grained, stubby or acicular rutile is commonly associated with monazite at all three deposits.

At Geco Mine the major rock types identified by Friesen et al. (1982) are "granite gneiss", "sericite schist" and "grey gneiss". The granite gneiss consists of variable proportions of biotite, hornblende, sillimanite and anthophyllite; the sericite-biotite schist which hosts the ore consists mostly of quartz and muscovite with trace amounts of biotite, sillimanite, garnet and magnetite and the grey gneiss consists of quartz,

Photo 384.1a. Monazite grains with pleochroic halo in biotite in the biotite schist, Geco mine. Bar = 0.5 mm. Ppl.

Photo 384.1b. Anhedral and subrounded monazite grains in the biotite-chlorite alteration zone of the mafic flow at Winston Lake Mine. Bar =0.5 mm. Ppl.

feldspars and biotite. Further subdivisions within each section include mafic and silicic units (Friesen et al. 1982). Apparently, the anthophyllite-cordierite-garnet alteration at the base of the stratigraphic pile extends for several kilometers outside the mine, although it is limited to a few meters in thickness. A description of the mineralogy of various rock types can be found in Friesen et al. (1982).

Additional petrographic work was necessary to establish the paragenetic sequence of minerals in the various rock types, in order to constrain the alteration associated with accessory minerals used for geochronology in this study. There were 5 major rock types collected for the alteration study, including the anthophyllite-cordierite-garnet gneiss, sericite schist, pegmatitic felsic dyke, biotite schist and grey gneiss. Petrographic observations are summarized as follows:

1. Feldspars are rare in the sericite schist and in the anthophyllite-cordierite-garnet assemblage, but are abundant in the grey gneiss and in the biotite schist.

2. Quartz-feldspar grain boundaries in the grey gneiss are relatively smooth, some form 120° triple junctions, suggesting textural equilibrium, in contrast to the ragged, uneven and embayed grain boundaries of quartz in the sericite schist.

3. Biotite overprints muscovite in all of the sericite schists studied (*see* Photo 384.3).

4. Biotite is absent from the anthophyllite-cordierite-garnet rocks collected for this study.

The paragenetic sequence of alteration minerals in the sericite schist is as follows: 1) recrystallization of the rock to quartz and coarse-grained muscovite (contemporaneous with or predating deformation) and 2) formation of biotite, monazite and xenotime and the remobilization of the ore (poikilitically includes muscovite, *see* Photo 384.4). The paucity of biotite observed in the anthophyllite-cordierite-garnet rock suggests that this unit was impermeable to late fluids and/or that the potassium content of the precursor was very low.

The "pegmatitic felsic dyke" (mine term) consists of very coarse-grained quartz and feldspars. Muscovite is interstitial to the feldspars and all minerals show evidence of minor

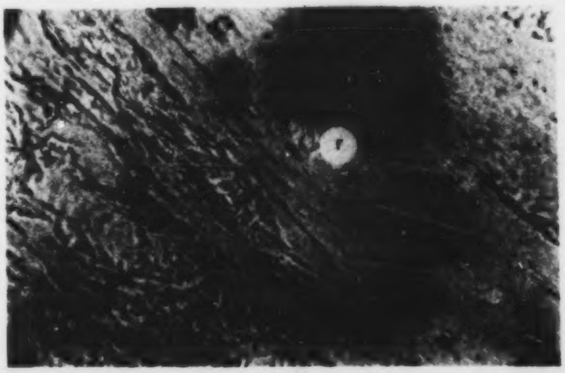

Photo 384.2. Monazite grain with pleochroic halo and rutile (r) in chlorite vein, Kidd Creek Mine. bar = 50 um. Ppl.

Photo 384.3. Biotite (b) poikilitically encloses muscovite (m) in sericite schist, Geco Mine. Bar = 1 mm. Ppl.

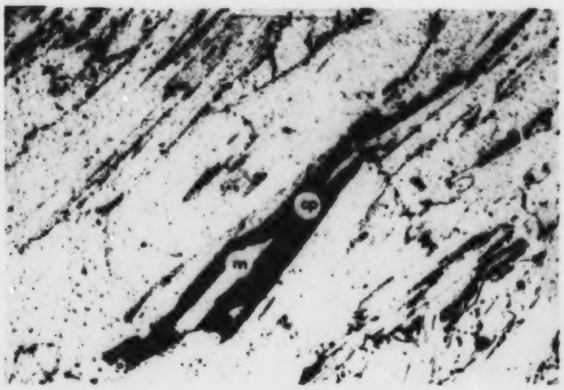

Photo 384.4. Chalcopyrite (cp) poikilitically encloses muscovite (m) in sericite schist, Geco Mine. Bar = 1 mm. Ppl.

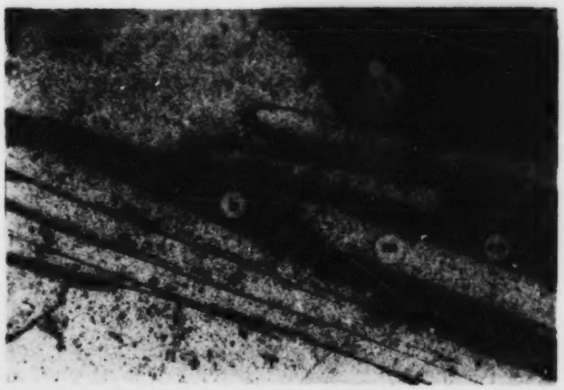

Photo 384.5. Chalcopyrite (cp) and biotite (b) in fractured muscovite (m) in the sericite schist, Geco Mine. Concentric pleochroic halos in biotite (upper right corner) indicates the presence of fine-grained monazite. Bar = 0.5. mm. Ppl.

deformation. Biotite and late-stage metasomatic alteration minerals are absent from the dyke.

Textures and minerals in the schist and in the gneiss suggests that the ore was remobilized, based on the assumption that the massive ore was pre-metamorphic. Pyrite, pyrrhotite and chalcopyrite occur in stringers and some are partially replaced by sphalerite. Fractures in large muscovite grains (up to 7 mm) within the schist are infilled by sulphides (*see* Photo 384.5), whereas quartz, feldspar and mica are poikilitically enclosed by amoeba-textured pyrite in the gneiss. The sulfide-rich biotite schist in the 4/2 copper zone was thought by Friesen et al. (1982) to represent the ore-fluid passage. As petrographic observations in this study indicate that biotite postdates muscovite in the sericite schist, and probably represents a later hydrothermal/metasomatic episode, we suggest that the "ore fluid passage" of Friesen et al. (1982) describes the path of a late potassium-rich fluid that remobilized the ore. Thus, petrographic observations suggest that sulfide remobilization was contemporaneous with crystallization of biotite, monazite and xenotime.

Monazite and rutile are accessory phases in the biotite-rich alteration zone. Most monazite grains are characterized by wide pleochroic halos in the enclosing biotite. Because monazite and rutile appear to have crystallized contemporaneously with biotite, the U-Pb age of these accessory phases is the age of the last hydrothermal episode, as well as the time of REE and ore remobilization.

At Winston Lake, three major rock types were studied: the so-called "clotted rhyolite" (CLR) (*see* Photo 384.6), the "chlorite rock" (CL) (*see* Photo 384.7) and a thin metasedimentary unit. The CLR is a felsic volcanoclastic unit consisting of medium- to coarse-grained quartz, biotite, minor albite, cordierite, sericite and chlorite. The presence of coarse quartz aggregates locally suggests the recrystallization of earlier quartz phenocrysts. The abundance of zircon in the

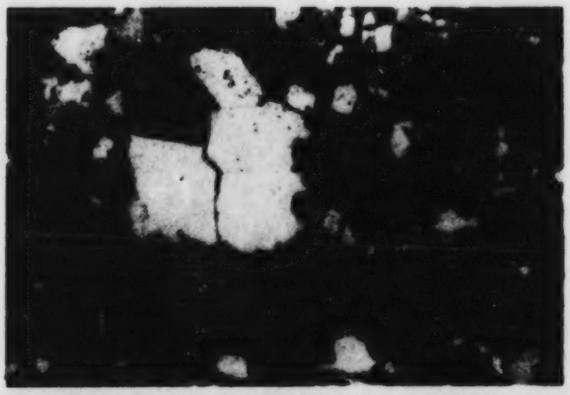

Photo 384.6. "Clotted rhyolite", Winston Lake: recrystallized large quartz phenocryst in fine-grained matrix of quartz, minor albite and biotite. Bar = 0.5 mm. Crossed polars.

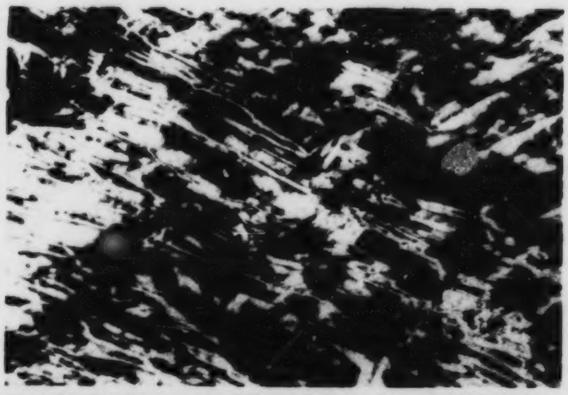

Photo 384.7. "Chlorite rock", Winston Lake: replacement of biotite by chlorite in fractures and between grain boundaries. Bar = 0.5 mm. Crossed polars.

Photo 384.8. Monazite in biotite in the "chlorite rock" at Winston Lake. Bar = 0.5 mm. Ppl.

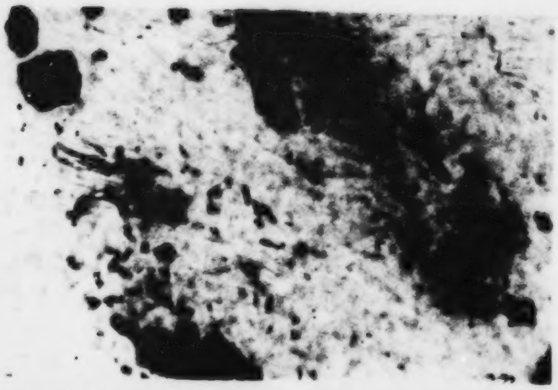

Photo 384.9. Fine-grained rutile aggregates in the "chlorite rock" at Winston Lake. Bar = 0.3 mm. Ppl.

CLR supports a porphyritic felsic volcanic precursor. Intercalated within the CLR units, the mafic units (CL) consist of biotite, chlorite and some anthophyllite. A thin subunit on the topmost section of CL is distinguishable by mineralogy, texture and whole-rock chemistry. Relict slump structures, recrystallized spherule-shaped concretions (up to cm size) and major, trace and REE chemistry of the whole rock suggests that this subunit is most likely a metasediment. The mineral assemblage in the metasediment generally consists of fine-grained quartz, amphibole and some albite. Biotite is generally absent and only occurs close to the contact with the altered mafic flow, where it poikilitically encloses amphibole. It should be emphasized that although potassic alteration is most extensive in the mafic flows, it is somewhat less extensive in the clotted rhyolite and is absent in most of the metasediments. Because of the close textural association of monazite and xenotime with biotite (*see* Photo 384.8), we suggest that the metasomatic fluids responsible for the breakdown of potassium-feldspars in the rhyolite crystallized both the biotite and REE phosphates in the adjacent mafic flows. The paucity of biotite (or micas, in general) and the absence of phosphates in the metasediment suggests a strong stratigraphic control on the fluid path.

Monazite and rutile are most common in the CL unit, although some fine-grained monazite was found in biotite in the clotted rhyolite, close to the contact with the altered mafic flow. Monazite grains (up to 200 µm) commonly occur in biotite and/or in chlorite that crystallized at the expense of biotite. Rutile is most common in the chloritic alteration zone and occurs as coarse dark grains and as finer-grained clear aggregates (*see* Photo 384.9) that probably crystallized from the partial breakdown of biotite and/or ilmenite-magnetite. The alteration sequence at Winston Lake is as follows: 1) silicification and partial recrystallization of the rhyolite to quartz + albite + minor sericite; 2) the breakdown of potassium feldspar and the crystallization of biotite, monazite and xenotime from the potassium-rich fluid and 3) partial breakdown of biotite to chlorite and rutile.

The Kidd Creek Mine geology, rhyolite geology and mineralogy are described in detail by Walker and Mannard (1974) and Coad (1985) and the paragenetic sequence of alteration mineralogy at Kidd Creek is described in detail by Schandl (1989) and Schandl et al. (1990). The mineral assemblage in the rhyolite consists predominantly of quartz + albite + carbonate + sericite + chlorite. Silicification, the earliest alteration in the rhyolite, is overprinted by carbonate which in itself is postdated by sericite and chlorite. Rutile occurs in fine-grained aggregates or stringers in both the sericite and chlorite. Fine-grained monazite and xenotime (less than 30 µm) were identified in the chloritic alteration zone, through the observation of wide pleochroic halos developed in the chlorite (*see* Photo 384.2).

GEOCHRONOLOGY: METHODS AND RESULTS

Methods

Rock crushing and mineral separation for geochronology were carried out using standard procedures including the utilization of the Wilfley table, heavy liquids and the Frantz isodynamic magnetic separator. Zircon and rutile were dissolved in HF using teflon bombs (Krogh 1973). Monazite fractions were dissolved in Savillex capsules using 6N HCl. Extraction of U and Pb was carried out following the method of Krogh (1973) for zircon and monazite. For rutile, this procedure was modified, using HBr and HNO_3 to purify the U solution (Corfu 1988). The U-Pb solutions were analyzed using a VG354 mass spectrometer equipped with a Daly detector.

U-Pb isotopic data for zircon, monazite and rutile from Winston Lake, monazite and rutile from Kidd Creek and monazite from Geco are presented in Tables 384.1 and 384.2 and plotted on Figures 384.2a and 384.2b. Results of age regression analyses are given in Table 384.3. The zircon and monazite data are all concordant or nearly concordant; thus, data points were fitted to a line forced through the origin of concordia.

Table 384.1. Isotopic data for zircon, monazite and rutile fractions from Winston Lake, Geco and Kidd Creek mines.

Sample	Weight (mg)	U (ppm)	Pb_{COM} (pg)	Measured $^{207}Pb/^{204}Pb$	Th/U	Corrected $^{206}Pb/^{238}U$	$^{207}Pb/^{235}U$	% DISC	$^{207}Pb/^{206}Pb$ Age (Ma)
Winston Lake									
1. z, Ab	0.010	50	12	284	0.62	0.52348	13.537	0.3±1.2	2720.7±4.1
2. z, Ab	0.008	43	7	336	0.61	0.52308	13.558	0.6±1.2	2724.5±3.4
3. m, Ab, 3 grp	0.056	320	9	12396	10.9	0.51476	12.971	0.1±0.6	2678.0±1.6
4. m, 21 gr	0.015	191	2	9681	27.7	0.51261	12.912	0.4±1.0	2677.3±2.2
5. m, Ab, 1 gr	0.012	51	1	3104	4.0	0.51348	12.917	0.2±0.8	2675.2±3.1
6. r, green	0.0490	5	11	142.2	0.03	0.50908	12.632	0.0±2.4	2652.5±4.0
7. r, blue, 15 gr	0.063	17	25	261.3	0.02	0.51165	12.684	-0.6±2.4	2651.0±3.3
8. r, blue, flat	0.245	19	29	958	0.02	0.50477	12.484	0.6±1.2	2647.0±2.6
9. r, black	0.325	16	81	384	0.32	0.49152	12.167	3.3±0.8	2648.4±2.6
Geco Mine									
10. m, Ab, 7 gr	0.017	1790	25	7098	8.3	0.51122	12.759	0.0±0.8	2662.1±3.2
11. m, flat, 7 gr	0.025	1425	90	2331	8.70	0.51005	12.715	0.1±1.4	2660.1±1.6
Kidd Creek Mine									
12. m, Ab, 7 gr	0.001	290	9	195.6	12.2	0.50425	12.560	1.2±0.8	2659.0±3.2

z - zircon; m - monazite; r - rutile; Ab - abraded; Pb_{COM} - Common Pb, including blank;
Th/U calculated from $^{208}Pb/^{206}Pb$ ratio and $^{207}Pb/^{206}Pb$ ageassuming concordance;
%DISC. - per cent discordance relative to $^{207}Pb/^{205}Pb$ age.

Table 384.2. Isotopic data for rutile fractions from Kidd Creek Mine.

Fraction	Weight (mg)	U (ppm)	PbCOM (pg)	Th/U	$^{207}Pb/^{204}Pb$	$^{206}Pb/^{204}Pb$
1. r, black	0.089	0.70	57	5.3	31.49±.12	106.66±.43
2. r, orange	0.077	0.65	136	2.1	18.47±.08	34.75±.14

Table 384.3. Summary of age data from Winston Lake, Geco and Kidd Creek mines.

Sample	Age (Ma)	Lower Intercept (Ma)	Probability of Fit (%)	Number of Points
WINSTON LAKE ZIRCON	2723 ± 2	—	16	2
WINSTON LAKEMONAZITE	2677 ± 1	—	30	3
WINSTON LAKE RUTILE	2651+6/-2	204	53	3
GECO MONAZITE	2661 ± 1	—	30	2
KIDD CREEK MONAZITE	2659 ± 3	—	—	1
KIDD CREEK RUTILE	2663 ± 28	—	—	2

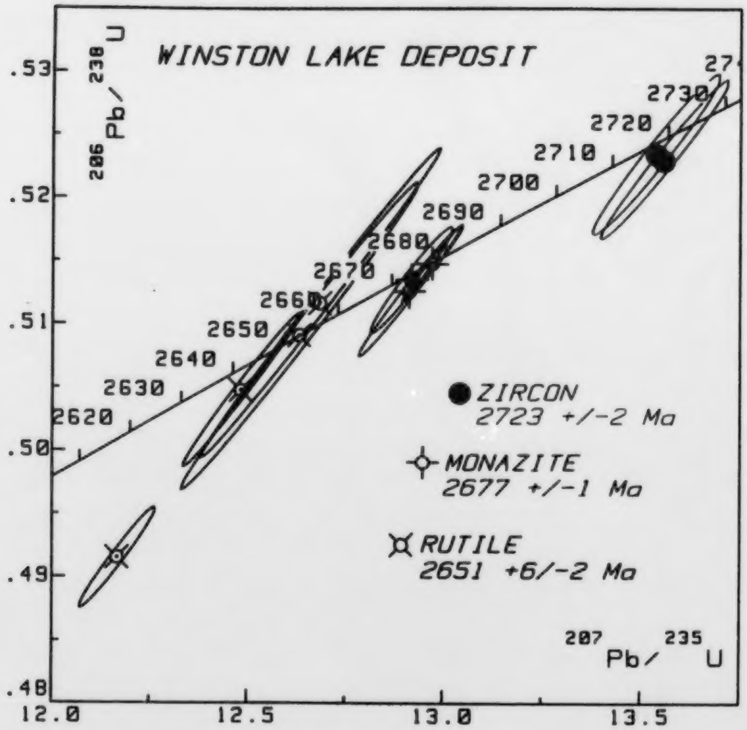

Figure 384.2a. ^{206}Pb/^{238}U vs. ^{207}Pb/^{235}U plot of zircon, monazite and rutile from the Winston Lake Mine.

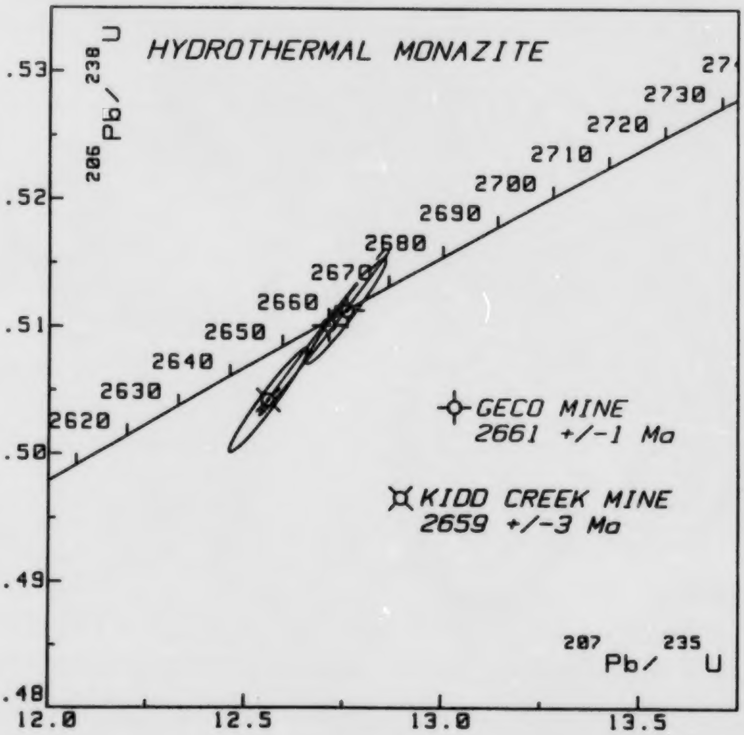

Figure 384.2b. ^{206}Pb/^{238}U vs. ^{207}Pb/^{235}U plot of monazite from Kidd Creek and Geco mines.

Table 384.4. Whole-rock analyses from the Winston Lake and Geco massive sulfide deposits.

Sample #	702-CL	702-CLR	702-131	687-106	687-CL	687CLR	660-CL	660-CLR	688-112	688-CL
SiO_2 %	29.8	78.9	64.8	63.1	26.4	76.9	30.3	81.8	66.6	26
TiO_2	1.4	0.31	0.65	0.78	1.47	0.37	1.31	0.3	0.49	1.41
Al_2O_3	18.8	9.21	14.6	13.8	20.3	10.4	19	8.81	13.6	20.2
Fe_2O_3*	14.2	1.68	5.24	4.97	16.1	1.41	16.1	1.19	3.57	18.2
MnO	0.07	0.02	0.06	0.1	0.06	0.02	0.06	0.02	0.06	0.04
MgO	23.3	3	3.5	6.43	22.3	3.16	21.5	1.66	5.29	21.8
CaO	0.23	1.05	4.5	1.09	0.25	3.18	0.51	0.73	4.15	0.11
Na_2O	0.34	3.79	5.99	7.3	0.06	4.2	0.29	4.23	5.26	0.02
K_2O	1.8	1.15	0.16	0.13	0.6	1.08	2.35	0.54	0.45	0.24
P_2O_5	0.31	0.05	0.24	0.11	0.22	0.07	0.23	0.04	0.06	0.2
LOI	8.16	0.77	0.47	2.23	10.1	0.54	7.85	0.47	1.08	10.2
TOTAL	98.6	100.1	100.3	100.1	98	99.4	99.6	100	100.6	98.6
Rb (ppm)	36	39	<10	20	39	43	55	20	21	16
Sr	<10	97	127	97	<10	92	<10	46	163	<10
Ba	266	193	118	126	106	208	273	192	134	143
Y	770	253	33	62	448	168	<10	253	18	314
Zr	116	707	114	119	141	75	118	677	68	117
Cr	5	8	166	203	467	5	343	5	146	467
La	768	105	4.8	2.1	684	768	11.6	32.4	2.5	714
Ce	1841	273	13.9	6.8	1781	1841	29.2	86.5	6	1747
Nd	886	145	10.2	4.9	888	886	12.9	48.6	5.5	856
Sm	14	29.4	3.1	1.6	163.5	14	3.5	14	1.8	147
Eu	4.3	2	1.3	6.83	6.1	4.3	0.25	1.57	1.25	6.1
Tb	26.1	4.3	0.54	0.32	14.8	26.1	0.62	3.89	0.23	12.4
Yb	31.6	20.5	1.9	19.3	23.2	36.1	1.1	19.3	1.4	16
Lu	3.29	3.01	0.28	0.23	2.59	3.29	0.2	2.81	0.22	2
Cs	2.4	0.3		0.3	2	2.4	1	0.2	0.5	1.3
U	-	2.1	0.3	0.3	-	-	0.3	1.5	0.2	-
Th	1.8	4.8	1.6	2	1.4	1.1	1	4.2	0.6	1.1
Sc	38.4	3.7	8.9	14.6	32.4	6.2	43.4	3.3	21.1	30.3
Hf	1.9	18.6	2.4	2.4	2.8	2	2	18.2	2.1	2.4
Au	19	5.7	4.9	20.9	38.6	8.6	6.7	11	4.5	10.1
Zn	905	26	79	678	2945	51	1027	32	282	3406
Co	30.2	9.8	34.3	15	16.8	7.1	39.6	6.5	9.2	19.3

Fe_2O_3* = FeO + Fe_2O_3.

Winston Lake: 702, 687, 660, 688, 665; Geco: G90-series.

Table 384.4. (continued)

Sample #	688-CLR	665-CL	665-CLR	G90-1	G90-2	G90-4	G90-7	G90-9	G90-10
SiO_2 %	75.4	36.7	78.2	67.2	97.8	83	73.6	56.1	51.9
TiO_2	0.49	0.96	0.3	0.31	0.02	0.09	0.05	0.13	2.71
Al_2O_3	10.4	13.8	7.71	16.8	0.33	9.31	15.8	7.55	13.1
Fe_2O_3*	0.92	16.9	3.07	2.26	0.34	2.44	0.33	17	18.3
MnO	0.02	0.12	0.04	0.04	0.03	0.02	0.02	0.05	0.21
MgO	5.62	21.5	5.41	1.22	<0.01	0.49	0.03	5	10.6
CaO	0.55	0.48	0.55	3.6	0.4	0.03	0.8	0.4	1.3
Na_2O	3.11	0.24	2.02	5.07	<0.01	0.19	4.6	0.73	0.38
K_2O	1.65	2.37	1.6	2.35	<0.01	2.53	4.22	2.25	<0.01
P_2O_5	0.07	0.18	0.05	0.09	0.01	0.02	0.02	0.03	0.74
LOI	1.16	5.62	0.77	1.39	0.39	1.47	0.85	3.7	0.84
TOTAL	99.6	98.9	99.9	100.5	99.3	99.8	100.4	93.1	99.9
Rb (ppm)	67	71	46	73	<10	47	195	117	14
Sr	62	<10	23	712	<10	16	86	22	27
Ba	228	250	245	947	143	250	175	905	82
Y	294	24	229	<10	<10	78	97	44	58
Zr	543	71	698	103	10	225	64	136	358
Cr	7	261	2	26	7	2	18	5	6
La	143	9.9	105	20.9	0.5	3.8	13.8	48.9	22
Ce	369	24.2	271	45.4	1	10.7	34.2	109.4	58.9
Nd	209	12.8	142	18.6	0.4	5.8	19	45.3	39.4
Sm	43.3	3.3	32.7	3.4	0.1	3.8	5.3	11.3	10.5
Eu	4.57	0.34	2.76	0.88	0.04	0.36	0.48	1.88	2.37
Tb	6.5	0.51	4.42	0.25	0.02	1.29	1.3	1.6	1.45
Yb	19.7	2.2	20.2	0.7	0.1	7	9.7	5.9	5.4
Lu	3.05	0.31	2.94	0.1	0.01	1.12	1.61	0.86	0.9
Cs	10.2	1.9	1.6	1.9	0.5	1.3	4.8	28.1	0.08
U	0.4	0.2	2	1.4	0.1	1.2	22.6	1.1	0.3
Th	4.9	1.2	4.3	4.3	0.1	3.2	29.3	5.2	1.2
Sc	10.2	36.4	6.4	4.1	0.1	0.9	4.8	3.4	30.7
Hf	14.5	1.8	17.1	2.8	0.1	7.7	4.6	4.9	6.6
Au	5.6	10	6.5	6	6.7	4.8	18	2128	349
Zn	35.4	1443	31.4	71	30	130	1.2	15.2	32.4
Co	5.3	30.4	15.2	7.5	0.9	2.2			

Fe_2O_3* = FeO + Fe_2O_3.
Winston Lake: 702, 687, 660, 688, 665; Geco: G90-series.

This is equivalent to averaging the $^{207}Pb/^{206}Pb$ ages. All errors are given at 95% confidence levels.

Results

Mineral separation is a major technical problem when dating hydrothermal rutile and monazite in greenschist facies deposits. The problem is related to the small grain size in the micaceous host minerals. For example, although rutile was observed in thin sections in samples from the Kidd Creek, Mattabi and Noranda deposits, no rutile was found in the heavy, non-magnetic fraction (where it is expected to be) in any of these samples. For the Kidd Creek sample, rutile and monazite were found embedded in sericite flakes in the light fraction which floated in methylene iodide. As rutile and monazite normally occur within micaceous minerals such as chlorite or sericite, which due to their large surface area are readily washed off the Wilfley table, it is likely that most of the rutile and monazite were lost during the Wilfley separation. Both rutile and monazite were recovered from the light methylene iodide fraction of the Kidd Creek sample by dissolving the sericite in HF at room temperature in an ultrasonic bath. More effective crushing and/or acid treatment methods are being developed to recover these fine-grained minerals from their micaceous hosts.

As both the Winston Lake and Geco deposits have been metamorphosed to middle amphibolite grade, there is a possibility that ages for some mineral fractions may represent cooling through a closure temperature for diffusion of Pb, rather than mineral formation. Zircon is well known to have an extremely high closure temperature, possibly in excess of 800°C. The age of the 2 zircon fractions, 2723 ± 2 Ma, therefore likely records eruption of the host rhyolite.

The closure temperature of monazite is estimated to be about 700°C (Parrish 1990) while that of rutile is estimated at about 400°C and has been shown to be grain size dependent (Mezger et al. 1989). Although monazite is unlikely to have been affected by peak metamorphism, any rutile which existed at this time would have been above its closure temperature. Age determinations were carried out on grains of different sizes and shapes to test for consistency. For the Winston Lake rhyolite sample, fine and coarse monazite grains from the rhyolite yield ages of no significance difference which also agrees with a large monazite grain from the chlorite alteration (analysis 5, Table 384.1). These three monazite fractions define an age of 2677 ± 1 Ma. Ages of two fractions of monazite from biotite alteration at the Geco Mine, one composed of equant grains and the other of flat grains, also agree within error at 2661 ± 1 Ma. Ages of coarse fractions of green and blue rutile from the Winston Lake rhyolite agree within error. A coarse fraction of black grains is slightly younger but somewhat discordant. A line regressed through these three fractions gives an age of 2651 +6/-2 Ma. A fraction of smaller, flat grains is slightly but distinctly younger than this age at 2647 ± 3 Ma and probably shows some diffusive loss of Pb. However, the difference in age is so small that the age of the coarse grains is likely close to their age of crystallization, which is therefore about 25 million years younger than that of the monazite.

The black and the orange rutile fractions from the Kidd Creek massive sulphide sample (*see* Table 384.2) both had much lower common U-Pb ratios than the samples from Winston Lake and Geco. Measured $^{207}Pb/^{204}Pb$ values are comparable to those of rutile from the adjacent Hemingway deposit (Schandl et al. 1990); hence the isotopic composition of the common Pb has a significant effect upon the age. Regressing the two data points on a Pb-Pb diagram gives an isochron age of 2663 ± 28 Ma. An initial common Pb value on this isochron would lie approximately midway between mantle and crustal values. On a concordia diagram, the data points are highly dependent on the value chosen for initial common Pb, but they are 5 to 30% above concordia, possibly due to U loss during the HF leaching process. Regressing the above two data points with the three points from the Hemingway deposit (Schandl et al. 1990) gives an age of 2654 ± 31 Ma but the data do not fit a line within 5% error.

Analysis of a very small fraction of monazite from the Kidd Creek sample produced a new concordant data point with a $^{207}Pb/^{206}Pb$ age of 2659 ± 3 Ma. The Pb is highly radiogenic so this analysis gives a much more accurate assessment of the age of hydrothermal activity.

GEOCHEMISTRY

Using X-ray fluorescence (XRF) at XRAL in Toronto, 20 representative whole rock samples were analyzed; major elements were determined on fused discs and trace elements on powder pellets. The same rocks were analyzed for REE by instrumental neutron activation analysis (INAA) at the SLOWPOKE reactor, University of Toronto. Analytical procedures and standards used followed the guidelines of Barnes and Gorton (1984).

Geco Mine

Major, trace and REE analyses for 5 representative rock types are shown in Table 4. G90-1 is the "grey gneiss", G90-4 is the "sericite schist", G90-9 is the "biotite schist" and G90-10 is the anthophyllite-cordierite-garnet rock at the base of the stratigraphic column. A fifth rock, G90-7, represents 1 of the many pegmatitic felsic dykes that cut through all rock units except the massive orebody. Some dykes are thought to have formed by metasomatic processes (Friesen et al. 1982).

All rocks have been subjected to amphibolite-grade metamorphism and to extensive metasomatic/hydrothermal alteration; thus the original chemistry has been significantly disturbed. Ti, the REE and highly charged cations are generally thought to be immobile components during metamorphism (Pearce 1975) and thus may be used as indicators of the rock type. At Geco, however, the interpretation based on trace and

REE geochemistry is not so straightforward, as remobilization of REE during post-ore hydrothermal alteration is evident from the unusually large amount of monazite and xenotime in biotite-rich alteration zones. The U-Pb age of monazite indicates that the REE were remobilized during regional metamorphism and our interpretation must take this into consideration.

The geochemistry of the anthophyllite-cordierite-garnet rock (G90-10) suggests that it was a separate (more mafic) unit from the overlaying sericite schist (*see* Table 384.4). The relatively high Fe_2O_3, P_2O_5, TiO_2, Sc, Zr and Y, low Cr, Zr/Y and La/Yb and the chondrite-normalized REE pattern (*see* Figure 384.3) of the rock is consistent with a highly fractionated tholeiitic basalt. The relatively high Mg content is attributed to alteration.

The geochemistry of the sericite schist (G90-4) is shown in Table 384.4. Low concentrations of Co, Cr, Sc and Eu, and relatively high concentrations of Zr, Y and HREE in this highly altered and silicified rock suggest a felsic precursor. The rock is depleted in LREE (*see* Figure 384.3) which is not surprising in view of the monazite concentration in the biotite-rich 4/2 copper zone which stratigraphically underlies the sericite schist analyzed in this study. It appears that REE were leached from the sericite schist and re-deposited as monazite and xenotime in the more mafic rock during potassium-metasomatism.

The major element geochemistry of G90-7 (pegmatitic felsic dyke) reflects its feldspar-rich mineralogy. The REE pattern is most similar to G90-4, but is markedly higher in incompatible elements such as Rb, Cs and Th. This would be consistent with G90-7 being derived by partial melting of G90-4. Lower concentrations of highly charged cations such as Zr, Hf, Ta and LREE could be attributed to residual accessory phases during melting.

The biotite schist (G90-9) is possibly a dacitic unit within the sericite schist. The partial replacement of quartz by chalcopyrite and pyrite resulted in the depletion of Si and an increase in Fe concentrations. The high LREE content, coupled with the abundance of monazite and xenotime in biotite suggests LREE mobilization during potassic alteration (*see* Table 384.4, Figure 384.3).

The quartz-feldspar-biotite gneiss, or "grey gneiss" (G90-1, Figure 384.3) is different from all the other rock types. The major and trace-element geochemistry and the steep REE pattern with rather low HREE concentrations and

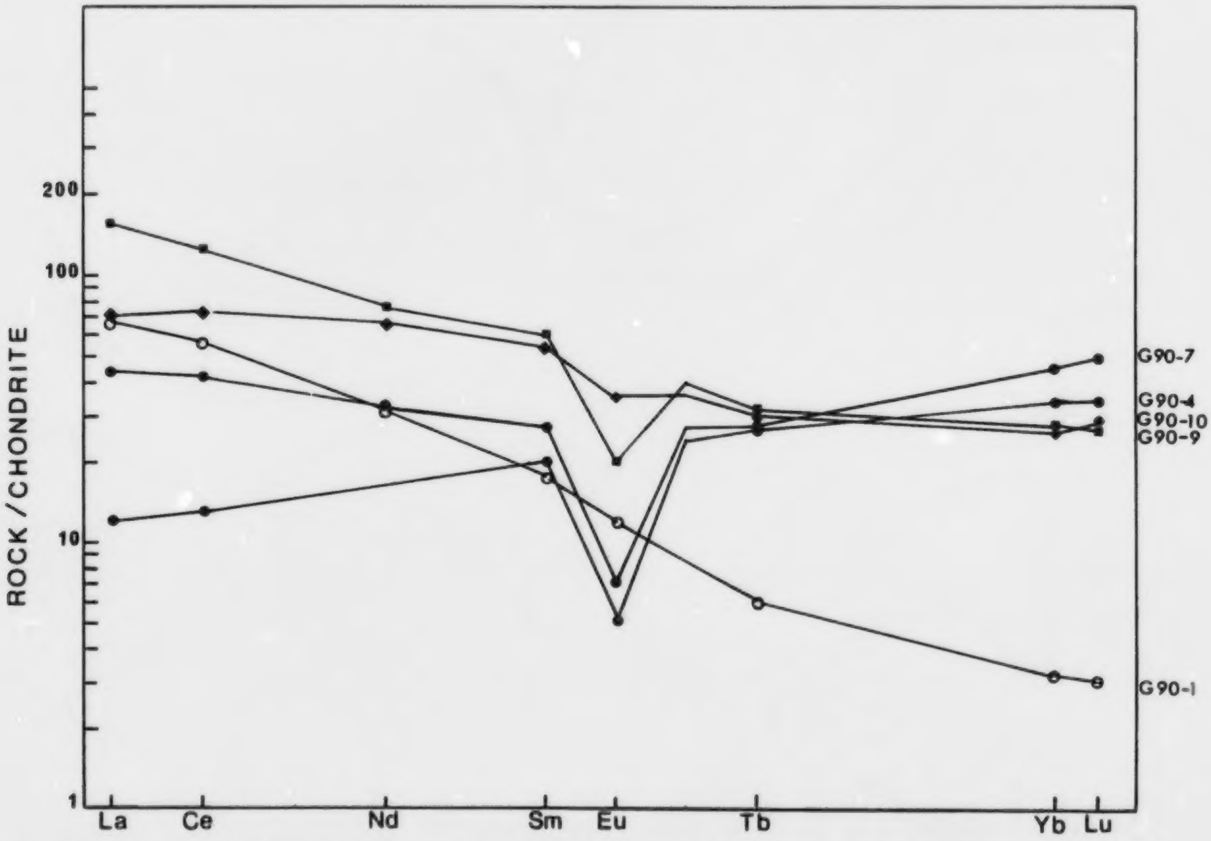

Figure 384.3. Chondrite normalised REE pattern of various rock types from Geco Mine. G90-10 (◊): "granite gneiss"; G90-4 (•): "sericite schist"; G90-9 (▪): "biotite schist"; G90-1 (o): "grey gneiss"and G90-7 (•): pegmatitic felsic dyke.

no Eu anomaly are all characteristics typical of primitive Archean grey gneisses. This rock shows no geochemical evidence of alteration.

Winston Lake Mine

The three rock types were analysed for major, trace and REE geochemistry from the Winston Lake massive sulfide deposit, including the "clotted rhyolite" (CLR), the "chlorite rock" (CL) and the metasediment that occurs between the two (*see* Table 384.4).

Although the rocks at Winston Lake are intensively altered, it is possible to distinguish between the three rock types from combined mineralogical and geochemical investigation. The clotted rhyolite (CLR) is characterized by high SiO_2, Na_2O and Zr. The chlorite rock (CL) is thought to be intensely altered basalt and is characterized by very low SiO_2 and high MgO, Al_2O_3 and basaltic concentrations of TiO_2, Cr and Sc. Pervasive hydrothermal alteration of the basalt to chlorite resulted in the transformation of most of the original whole rock chemistry to more or less chlorite composition. The metasediment is distinctive in having intermediate SiO_2 contents and high Na_2O.

The REE geochemistry of these rocks reveals a remarkable REE anomaly. The REE patterns for three of the chlorite rocks are steep and extremely high, exceeding 2000 times chondritic values of LREE (*see* Figure 384.4). No mafic igneous rocks are known with REE patterns like these and it is clear from the abundance of monazite and xenotime that REE have been introduced during alteration. It is significant that these three samples lie within the alteration zone defined by mine geologists.

There are two CL samples having much lower REE patterns (*see* Figure 384.5) that could well be representative of basalt and show little sign of REE enrichment. These samples lie outside the mineralized area. Unusually large negative Eu anomalies correlate with very low Ca and Sr concentrations, which are probably due to stripping of these elements during alteration.

The clotted rhyolites have REE patterns with the gentle slopes, high concentrations and steep negative Eu anomalies (*see* Figure 384.4) typical of rhyolites associated with mineralization (Lesher et al. 1986). Samples from the mineralized zone may have some LREE enrichment.

The metasediments have low flat REE patterns (*see* Figure 384.6) that could be consistent with basaltic material diluted by REE-poor detrital material. There is no sign of

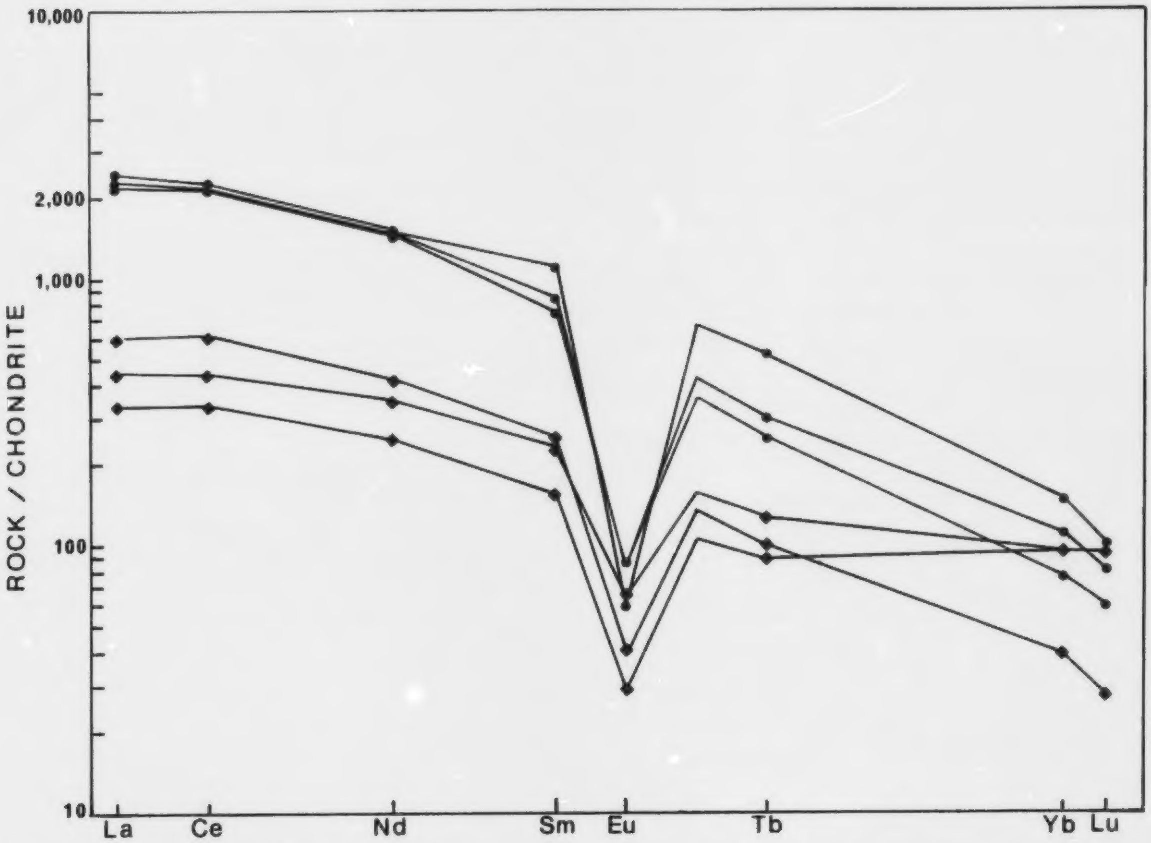

Figure 384.4. Chondrite normalised REE pattern of "clotted rhyolite" (CLR) and of 'chlorite rocks' (CL) from the alteration zone adjacent to the ore.

rhyolitic derived material or of REE enrichment. The absence of monazite is consistent with the lack of REE enrichment.

DISCUSSION

Our study is a necessary precursor to the reassessment of exploration targets for massive sulfide deposits in Archean terrains. The sericite-chlorite assemblage in greenschist-grade rocks, the coarse-grained muscovite-biotite (+ sillimanite + cordierite + anthophyllite + garnet) or biotite-chlorite assemblage in amphibolite-grade rocks clearly represents an overprint on massive sulfide mineralization at the three deposits studied.

The monazite shows a considerable range in U concentration and Th/U ratios. The monazite from the biotite/chlorite alteration zone at Winston Lake has relatively low U and low Th/U ratio, whereas the U concentration in monazite from the biotite zone at Geco Mine is much higher and closer to values of an igneous monazite. Rutile from the Winston Lake deposit has moderate U concentrations but very low Th/U. Hydrothermal monazite at Kidd Creek is similar to monazite at Geco and Winston Lake but the rutile is much lower in U and has crustal Th/U ratios.

Age results from hydrothermal monazite and rutile in the Winston Lake and Geco deposits indicate an association with regional metamorphism. The nearest area in which metamorphism has been dated is the Hemlo deposit in the Wawa Subprovince where metamorphic titanite from unmineralized rocks gives ages of 2678 to 2676 Ma (Corfu and Muir 1989). Monazite fractions clearly date mineral formation (a result of REE mobility) which accompanied the crystallization of biotite during prograde metamorphism. Results from rutile at Winston Lake probably date mineral formation by a retrograde metamorphic reaction, possibly accompanying breakdown of biotite to chlorite. Both these deposits are located near the southern boundary of the Quetico Subprovince. It is interesting to note that the time span of hydrothermal activity recorded by the minerals is similar to the time span of igneous activity associated with emplacement of S-type granites (2671 to 2665 Ma, Percival and Sullivan 1988) and granite pegmatites (2653 Ma, Percival and Sullivan 1988) in the western part of the Quetico Subprovince. Similar results have recently been found for Quetico granites associated with regional metamorphism in Minnesota (D.W. Davis, unpublished data). These granites typically contain high concentrations of monazite which may have been derived from remobilization of REE in the sediments (Sawka et al. 1986).

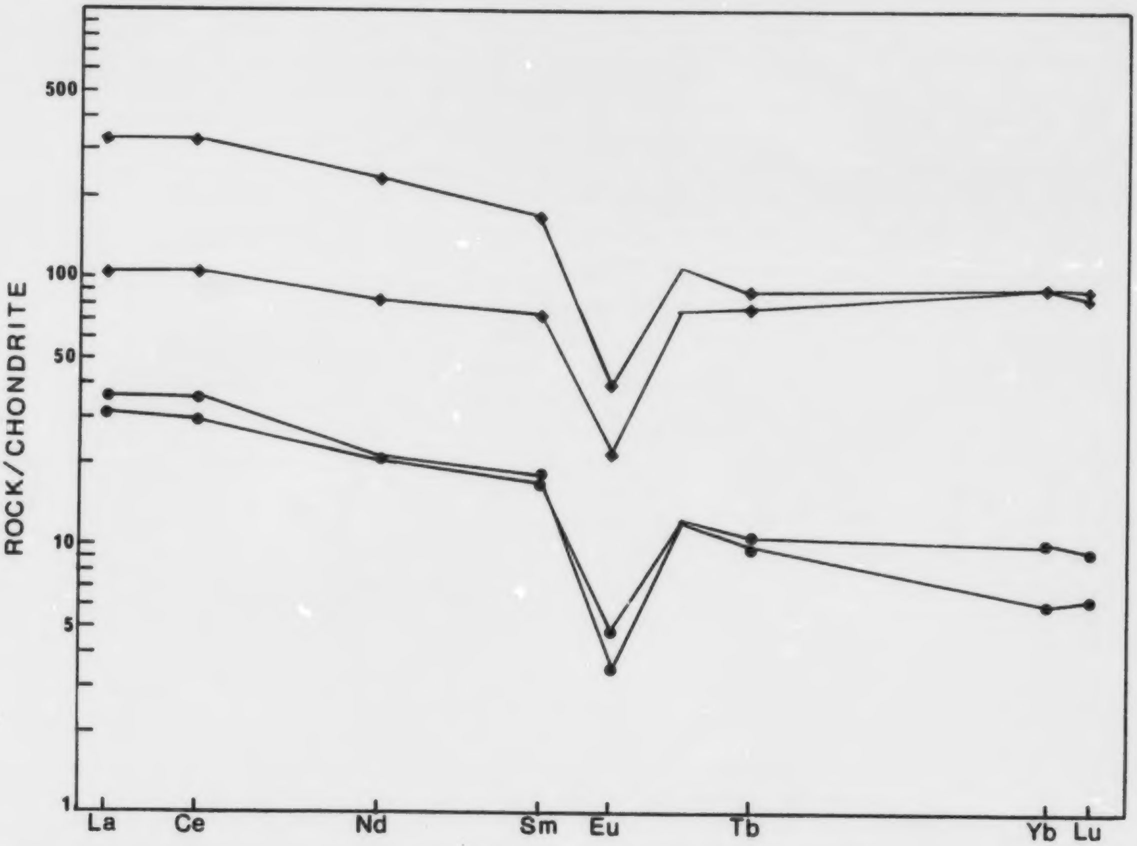

Figure 384.5. Chondrite normalised REE pattern of "clotted rhyolite" (◊) and of "chlorite rocks" (•) from outside the major alteration zone.

These age correspondences suggest that hydrothermal fluids which overprinted the ore deposits could have been derived from dewatering of metasediments which may have underthrust the Wawa Subprovince in the Winston Lake area. Since these sediments have been shown to contain a substantial amount of pre-2800 Ma detritus (Davis et al. 1990), it may be possible to test this model by measuring Nd isotopic ratios in both igneous and hydrothermal monazite. These determinations are currently being undertaken at the Geochronology Laboratory of the Royal Ontario Museum.

At Kidd Creek Mine, the age of hydrothermal monazite (2659 ± 3 Ma) and rutile (2663 ± 28 Ma) in samples collected from below the mineralized footwall rhyolite, appears somewhat younger than regional metamorphism (ca. 2680 Ma, Corfu and Muir 1989; Wong et al. 1991) and distinctly younger than volcanism (2717 ± 2 Ma, Barrie and Davis 1990; Nunes and Pyke 1981) which would have accompanied syngenetic mineralization. It is older than well-documented post-metamorphic hydrothermal activities in the Abitibi belt (Wong et al. 1991; Corfu and Muir 1989; Hanes et al. 1989; Jemielita et al. 1990) and may be older than the age of 2624 ± 62 Ma measured for the rutile in the Hemingway deposit, although this age cannot be resolved outside of error because of the large uncertainty associated with the common Pb component. It is noteworthy that the Kidd Creek rutile age is very close to a Sm-Nd isochron age of 2674 ± 40 Ma (Maas et al. 1986) measured on hydrothermally altered rocks associated with the ore body.

The monazite and rutile dates define either a post-metamorphic hydrothermal episode, or they represent the closing stages of regional metamorphism. Fuchsite collected from the altered ultramafic rocks in contact with the mineralized rhyolite in the east-trending shear zone at the Kidd Creek Mine and dated by $^{40}Ar/^{39}Ar$ at 2618 ± 8 Ma (Smith et al. 1991) suggests that post-metamorphic hydrothermal activity continued at Kidd Creek. We suggest that the Kidd Creek deposit might be located in an area of weakness in the crust that has been periodically reactivated by deep-seated tectonic and/or plutonic activity.

CONCLUSIONS

The significance of this study is that by using precise U-Pb geochronology of accessory phases from alteration zones of massive sulfide deposits it is possible to date the alteration presently associated with the deposits. Our results clearly show that the alteration assemblages in the rhyolite at Winston Lake, Geco and the Kidd Creek massive sulfide deposits are not primary and they did not form contemporaneously with mineralization. The sericite/biotite-chlorite assemblages at all three deposits formed at a later date and were contemporaneous with regional metamorphism, and with hydrothermal activities that represented the closing stage of, or postdated, regional metamorphism. Because of the presence of hydrothermal monazite in the alteration zones, the age obtained from these REE-rich accessory minerals also provides an age for the remobilization of REE around the three ore deposits studied.

To our knowlege, this is the first time that hydrothermal monazite was identified in the alteration halos of massive sulfide deposits, and these are the first age determinations on hydrothermal monazite associated with massive sulfides. Detailed petrographic work from other massive sulfide deposits, such as the Noranda-Millenbach and Mattabi mines suggests that hydrothermal monazite appears to be relatively common in alteration zones of Archean massive sulphide deposits. Our

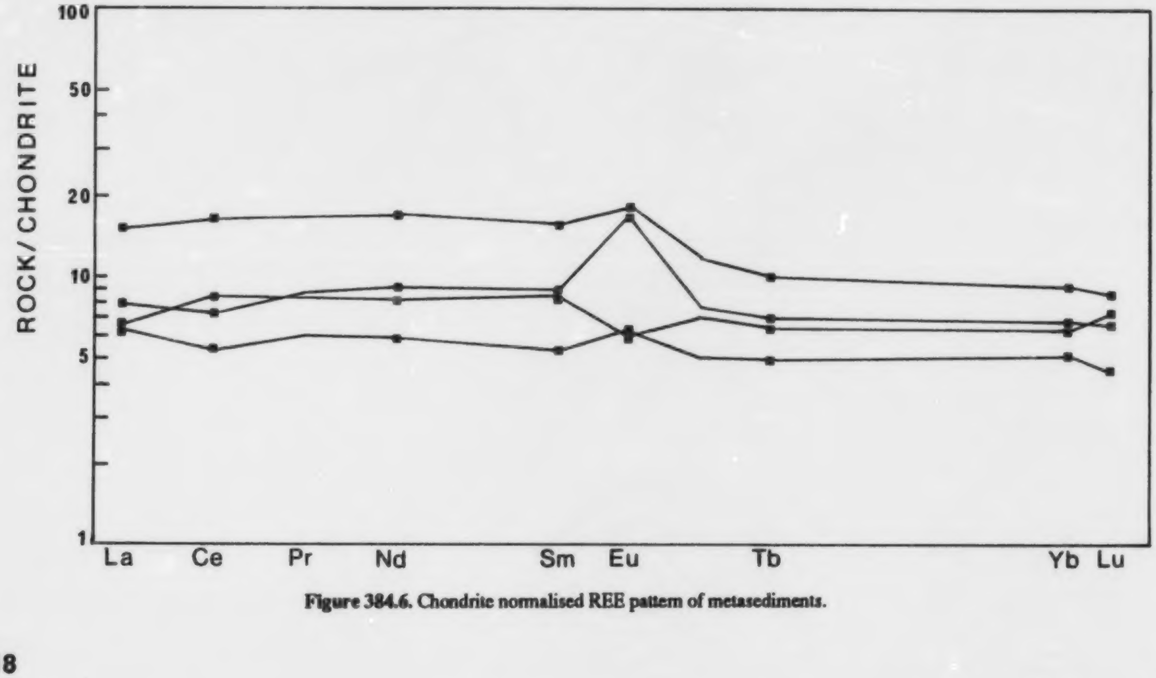

Figure 384.6. Chondrite normalised REE pattern of metasediments.

present work indicates that although the crystals are generally very small, monazite is potentially a very useful mineral for dating hydrothermal events in various environments.

We conclude that: 1) present alteration assemblages around the three Archean massive sulfide deposits postdated ore deposition; 2) extensive remobilization of REE was contemporaneous with this late alteration and not with the ore-forming processes as has been previously suggested by Campbell et al. (1984) and 3) the mobilization of the ore at Geco Mine and at Kidd Creek (Schandl et al. 1990) during late metasomatic/hydrothermal events implies that at least some of the stringer ore may have formed by the partial mobilization of the massive ore during post-depositional alteration.

ACKNOWLEDGMENTS

We would like to thank D. Brisbin, Senior Geologist, and V. Kelly, Chief Geologist, from Kidd Creek Mines Ltd. (Falconbridge) for supplying the samples for geochronology; R. Sim, Chief Geologist at Winston Lake, and F. Balint, Regional Exploration Manager of Noranda Mines Inc. (Minnova), for access to drill cores at Winston Lake; H. Lockwood, Chief Geologist at Geco Mine (Noranda Minerals Inc., Geco Division), for permitting sample collection from the mine and R. Reukel, Mine Geologist, for the tour of the mine. Their cooperation and generous help was essential for the success of this project. We also thank M. Back of the Department of Mineralogy, Royal Ontario Museum, for the identification (by X-ray diffraction) of numerous monazite and rutile grains used for geochronology. The support of an OGRF grant to M. P. Gorton is gratefully acknowledged.

REFERENCES

Barnes, S. J. and Gorton, M.P. 1984. Trace element analysis by neutron activation with a low flux reactor (SLOWPOKE II): Results for international reference rocks; Geostandards Newsletter, v.8, no.1, p.17–23.

Barrie, C.T. and Davis, D.W. 1990. Timing of magmatism and deformation in the Kamiskotia-Kidd Creek area, western Abitibi Subprovince, Canada. Precambrian Research, v.46, p.217–240.

Campbell, I.H., Lesher, C.M., Coad, P., Franklin, J.M., Gorton, M.P. and Thurston, P.C. 1984. Rare earth element mobility in alteration pipes below massive sulphide Cu-Zn sulphide deposits; Chemical Geology, v.45, p.181–202.

Coad, P.R. 1985. Rhyolite geology at Kidd Creek—a progress report; Canadian Institute of Mining and Metallurgy, v.78, no.874, p.70–83.

Corfu, F. 1988. Differential response of U-Pb systems in coexisting accessory minerals, Winnipeg River Subprovince, Canadian shield: implications for Archean crustal growth and stabilization; Contributions to Mineralogy and Petrology, v.98, p.312–325.

Corfu, F. and Muir, T.L. 1989. The Hemlo-Heron Bay greenstone belt and Hemlo Au-Mo deposit, Superior Province, Ontario, Canada. 2. Timing of metamorphism, alteration and Au mineralization from titanite, rutile and monazite U-Pb geochronology; Chemical Geology (Isotope Geoscience section), v.79, pp. 201–223.

Davis, D.W., Pezzutto, F. and Ojakangas, R.W. 1990. The age and provenance of metasedimentary rocks in the Quetico Subprovince, Ontario, from single zircon analyses: implications for Archean sedimentation and tectonics in the Superior Province; Earth and Planetary Science Letter, v.99, p.195–205.

Friesen, R.G., Pierce, G.A. and Weeks, R.M. 1982. Geology of the Geco base metal deposit; *in* Precambrian Sulphide deposits, H.S. Robinson Memorial Volume, Geological Association of Canada, Special Paper 25, p.343–362.

Hanes, J. A., Archibald, D.A., Hodgson, C.J. and Robert, F. 1989. Preliminary ^{40}Ar/^{39}Ar geochronology and timing of Archean gold mineralization at the Sigma Mine, Val d'Or, Quebec. Geological Survey of Canada Paper, v.89–1C, p.135–142.

Jemielita, R.A., Davis, D.W. and Krogh, T.E. 1990. U-Pb evidence for Abitibi gold mineralization postdating greenstone magmatism and metamorphism; Nature, v.346, p.831–833.

Krogh, T.E. 1973. A low contamination method for hydrothermal decomposition of zircon and extraction of U and Pb for isotopic age determination; Geochimica et Cosmochimica Acta, v.37, p.485–494.

Lesher, E. M., Goodwin, A. M., Campbell, I. H. and Gorton, M. P. 1986. Trace-element geochemistry of ore-associated barren, felsic metavolcanic rocks in the Superior Province, Canada; Canadian Journal of Earth Science, v.23, p.222–237.

Maas, R., McCulloch, M.T., Campbell, I.H. and Coad, P.R. 1986. Sm-Nd and Rb-Sr dating of an Archean massive sulfide deposit, Kidd Creek, Ontario; Geology, v.14, p.585–588.

Mezger, K., Hanson, G.N. and Bohlen, S.R. 1989. High precision U-Pb ages of metamorphic rutile: application to the cooling history of high grade terranes; Earth and Planetary Science Letter, v.96, p.106–118.

Morton, R. L. and Franklin, J. M. 1987. Two-fold classification of Archean volcanic-associated massive sulfide deposits; Economic Geology, v.82, p.1057–1063.

Morrison, I. R. and Sim, R. C. 1989. Winston Lake Project: Exploration to mining; unpublished company report, Minnova Inc., October 1989.

Nesbitt, B.E. and Kelly, W. 1980. Metamorphic zonation of sulphides, oxides, graphite in and around the orebodies at Ducktown, Tennessee; Economic Geology, v.75, p.1010–1021.

Nunes, P.D. and Pyke, D.R. 1981. Time-stratigraphic correlation of the Kidd Creek orebody with volcanic rocks south of Timmins, Ontario, as inferred from zircon U-Pb ages; Economic Geology, v.76, p.944–951.

Parrish, R.R. 1990. U-Pb dating of monazite and its application to geological problems; Canadian Journal Earth Science, v.27, p.1431–1450.

Pearce, J.A. 1975. Basalt geochemistry used to investigate past tectonic environments on Cyprus; Tectonophysics, v.25, p.41–61.

Percival, J.A., and Sullivan, R.W. 1988. Age constraints on the evolution of the Quetico belt, Superior Province, Ontario; *in* Radiogenic and Isotopic Studies: Report 2, Geological Survey of Canada, Paper 88–2, p.97–107.

Richards, J.P., Krogh, T.E. and Spooner, E.T.C. 1988. Fluid inclusion characteristics and U-Pb rutile age of late hydrothermal alteration and veining at the Musoshi stratiform copper deposit, central African copper belt, Zaire; Economic Geology, v.83, p.118–139.

Sawka, W.N., Banfield, J.F. and Chappell, B.W. 1986. A weathering-related origin of widespread monazite in S-type granites; Geochimica et Cosmochimica Acta., v.50, p.171–175.

Schandl, E.S. 1989. Talc-carbonate alteration of ultramafic rocks in the Kidd volcanic complex, the Slade-Forbes and the Munro asbestos deposits in the Abitibi Greenstone Belt, Timmins, Ontario; unpublished PhD thesis, University of Toronto, Toronto, Ontario.

Schandl, E.S., Davis, D.W. and Krogh, T.E. 1990. Are the alteration halos of massive sulfide deposits syngenetic? Evidence from U-Pb dating of hydrothermal rutile at the Kidd volcanic center, Abitibi Subprovince, Canada; Geology, v.18, p.505–508.

Smith, P.E., Schandl, E.S. and York, D. 1991. Timing of K-metasomatic alteration of the Kidd Creek massive sulphide deposit, Ontario, using $^{40}Ar/^{39}Ar$ laser dating of single crystals of fuchsite; *in* Program with Abstract, Geological Association of Canada—Mineralogical Association of Canada, v.16., p.116.

Walker, R.R. and Mannard, G.W. 1974. Geology of the Kidd Creek Mine—a progress report; Canadian Institute of Mining and Metallurgy Bulletin, v.67, p.41–57.

Wong, L., Davis, D.W., Krogh, T.E. and Robert, F. 1991. U-Pb zircon and rutile geochronology of Archean greenstone formation and gold mineralization in the Val d'Or region, Quebec; Earth and Planetary Science Letter (in press).

Grant 386 Modification of the Shallow Reflection Seismic Method for Urban Geophysical Studies in Southern Ontario

---

J.P. Greenhouse, D.C. Nobes, G.W. Schneider and M.A. Lockhard

Department of Earth Sciences, University of Waterloo

As southern Ontario becomes more urbanized, the need for good groundwater management becomes increasingly important. A major aid in this endeavour is a knowledge of the Quaternary subsurface geology. Shallow seismic reflection (SSR) surveys have been used to map the bedrock topography and delineate the overburden structure in northern Ontario, but this technique is not so well suited to conditions in southern Ontario. This project seeks to adapt SSR surveys so that they may be used more effectively in southern Ontario.

Different aspects of SSR surveys were isolated and examined to determine which parameters provided the optimum results for local conditions. The effects of different types of shotgun shells were assessed, as were the effects of gun design. Various shothole designs were examined to determine which provided the optimum shooting conditions. The results of these tests are presented, and a "standard" section is presented to contrast the effects of a survey shot with conventional parameters compared to a survey conducted with the newly proposed parameters.

INTRODUCTION

Southern Ontario is rapidly developing into a heavily urbanized center. As new and existing municipalities expand, the need for good groundwater management becomes increasingly important. Municipal engineers are continuously striving to search out and delineate new aquifers, as well as map out the extent of currently exploited aquifers. Hydrogeological consulting firms contracted for these tasks are finding that new geophysical techniques are required to map the Quaternary subsurface geology, particularly in semi-urbanized areas.

Shallow seismic reflection (SSR) surveys are a relatively new technique developed for overburden mapping. Of all the geophysical techniques, SSR is the only one with the inherent ability to image thick overburden deposits with a resolution that allows one to distinguish aquifer and aquitard sequences. Consultants are relying, to a considerable extent, on a version of the SSR technique known as Common Offset (CO). The CO technique has been largely developed by Dr. J. Hunter and his colleagues at the Geological Survey of Canada (Hunter et al. 1982), and is best suited for areas with fine-grained, water-saturated surface sediments which allow high frequency energy to be transmitted outwards and downwards from the shotgun shell source.

The Regional Municipality of York is covered with a thick veneer of dry, fairly coarse sediment such as the Halton Till or the sands and gravels of the Oak Ridges Moraine. Typical records obtained there with the CO technique (*see* Figure 386.1) are confused by low frequency, overlapping reflected events which, even if they are coherent, do not allow the resolution of the hydrogeological units that is required. This same problem has thwarted our efforts to image the water resources of the overburden in the Waterloo Region (Greenhouse et al. 1990). It is a fundamental limitation of the SSR technique that will have to be overcome if geophysics is to match the claims of its proponents.

This project seeks to adapt the SSR technique to typical southwestern Ontario conditions by examining:

(a) alternate energy sources
(b) different surveying techniques
(c) different processing techniques.

Since the earth acts as a low pass filter, a powerful high frequency energy source is essential to resolve thin seismic units at depth. Three components of the seismic energy source (the gun, the shotshell, and the shothole) were isolated, and examined individually to assess what effect each had on signal quality.

Most SSR surveys employ the CO technique developed by Hunter et al. (1982). However new seismic processing software packages allow SSR surveys to be conducted using the common midpoint (CMP) technique as well. We are currently examining these two techniques in an effort to determine which is best suited for conditions in southern Ontario.

Digital filtering of data can be carried out in both the time and frequency domain. Within the frequency domain there are also various filtering methods (such as semblance) available. Members of the Earth Sciences Department at the University of Waterloo have also been experimenting with singular value decomposition (SVD) filters for processing seismic records. This study will assess which filtering technique is most efficient.

Part (a) of the project is complete, and work continues on parts (b) and (c). This report summarizes our findings to date.

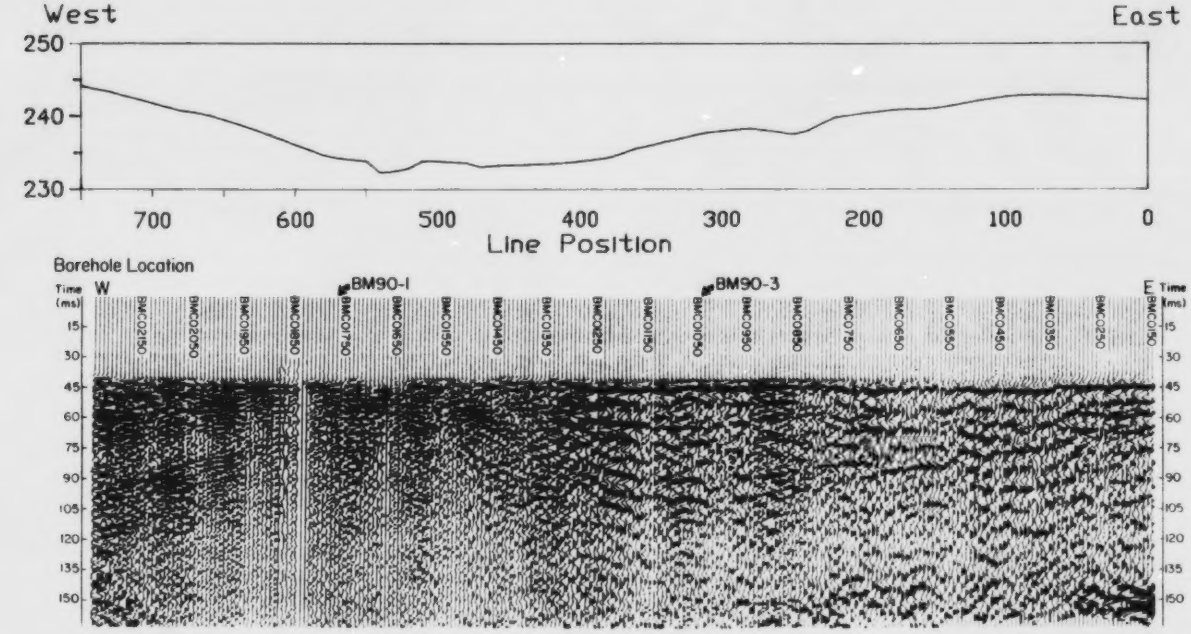

Figure 386.1. Seismic section collected at Bruce's Mill Conservation Area. Line topography is superposed.

ENERGY SOURCE TESTS

Tests of shotgun shells and gun design were conducted in specially fabricated shotholes and in the water of deep lakes or quarries. Water provides a uniform and repeatable medium to test a source. It does not, however, simulate well the shothole conditions encountered in the ground. For that we have attempted to design a "standard" shothole on the University of Waterloo Campus, one that can be used several times while providing the same shot-ground coupling.

Shot Shells

In order to assess what effect different shot charges have on signal quality, 12 gauge shotgun shells were packed with varying ratios of smokeless and black powder. Ratios of 7:3 and 3:7 of smokeless to black powder were used. Two types of smokeless powders were used (Hodgdon HS-7, a relatively slow-burning powder, and DuPont 700 X, a relatively fast-burning powder) with two types of black powder (XX, relatively slow-burning, and XXX, relatively fast-burning). This resulted in 8 different mixtures. Approximately 25 shells of each mixture were loaded.

Water was considered the optimum test medium for comparing these charges, since it is a homogeneous medium that will not alter its characteristics between shots. A deep water body was required so that bottom reflections would not coincide with (and thereby obscure) the direct arrival from the source. Kempenfeldt Bay (on Lake Simcoe) was chosen as a test site because it is deep (about 35 m) and is sheltered from winds. The testing took place during the summer of 1990.

Figure 386.2 depicts the experiment configuration. Two Zodiaks (inflatable boats) were tied together 5 m apart and then anchored in the centre of the bay. The shells were detonated in 60 cm of water beside one Zodiak, and the signal was recorded on hydrophones hanging below the second boat. The hydrophones were hung in a U-shaped array having its plane perpendicular to the direction of the shot. The shot depth coincided approximately with the centre of the "U" so that all hydrophones were roughly equidistant from the shot.

Frequency spectra were produced for each shot and examined to determine which mixtures produced the optimum signal. An example of these plots is shown in Figure 386.3. With a maximum peak around 1200 Hz, the frequency content of each shot does not differ significantly. However the power contained in each shot varies according to the powder mixture. Based on this test it was determined that a 7:3 mixture of smokeless to black powder was much more powerful than a 3:7 mixture. A second shell test was then conducted in 1991 to follow up the results of the first test.

The second test compared the power and frequency content of shells packed with smokeless and black powders mixed in a ratio of 8:2. Again, frequency content was found to be very similar between shots of different shells, so the optimum mixture was determined on the basis of power. Based on this test it was eventually determined that the 8:2 ratio of Hercules Bullseye pistol powder and XXX black powder provided the most powerful source. However these shells consistently ruptured on detonation, and extracting them from the chamber was extremely difficult. For practical purposes, then, the next most powerful mixture (with IMR HI-SKOR 700X in a ratio of 8:2) was chosen as the optimum mixture.

Gun Construction

A variation of the above test was repeated at Elora Quarry in the fall of 1990 to determine the effect of various gun constructions on signal quality. Four different guns were evaluated. Guns from Hyd Eng, the Ontario Geological Survey (2 designs), and the University of Waterloo were each fired 10 times in the water using the same type of shell. Gun dimensions are sketched in Figure 386.4. The experiment configuration was similar to that used during the shell tests, and depicted in Figure 386.2.

Frequency spectra were produced for each hydrophone for all 10 shots of each gun. Figure 386.5 depicts examples of these power spectra. Examination of these spectra show that they are extremely consistent for any one gun, but quite different between guns. This shows that the experiment is very repeatable, and that gun design does affect signal characteristics.

Two observations were made from this experiment. First, the University of Waterloo gun appears to produce a signal weak in energy in the 1000 Hz range. This may be related to the type of steel used to construct the gun, or it may be a function of chamber length. Second, the long Ontario Geological Survey gun appeared at the time to produce a much more powerful signal than the others. It was the only gun that recoiled when fired. Whereas the second arrival on the record was much stronger than for any of the other guns, the first (direct) arrival was much weaker. This suggests that the longer chamber focuses energy downwards so that most energy returns in reflection events rather than direct arrivals. Work on this data set also continues.

Standard Shotholes

In order to determine what effects shot depth, shot casings, and receiver depth have on signal quality for land records a "standard" shot hole is required. This hole will ideally not alter its characteristics with use, so that any differences observed in records recorded from signals created in this hole will be the result of the source itself.

A first attempt at standard shothole construction was made by grouting pipes of various materials and sizes into holes augured next to the Bauer Warehouse on the University of Waterloo campus. Five variations were prepared.

1. 5 cm steel pipe.
2. 10 cm steel pipe.
3. 5 cm steel pipe with 25 cm wide chamber for the basal 50 cm.
4. 5 cm PVC pipe.
5. 10 cm PVC pipe.

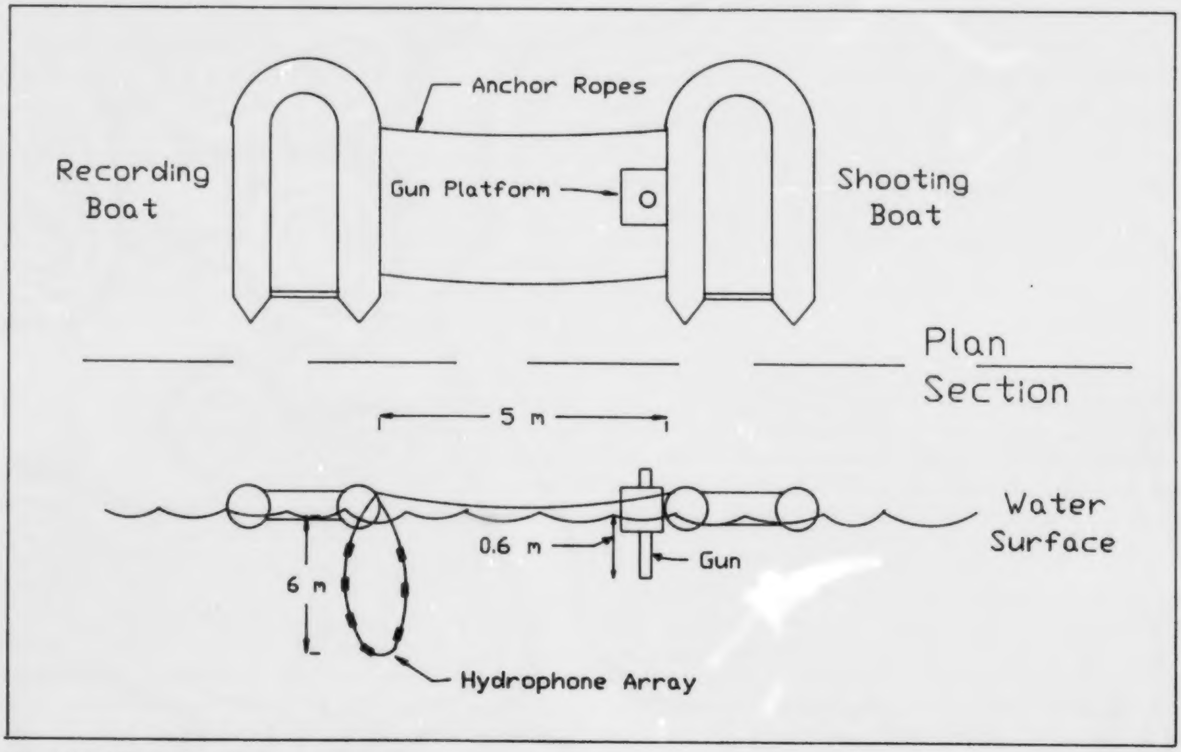

Figure 386.2. Source test experiment configuration.

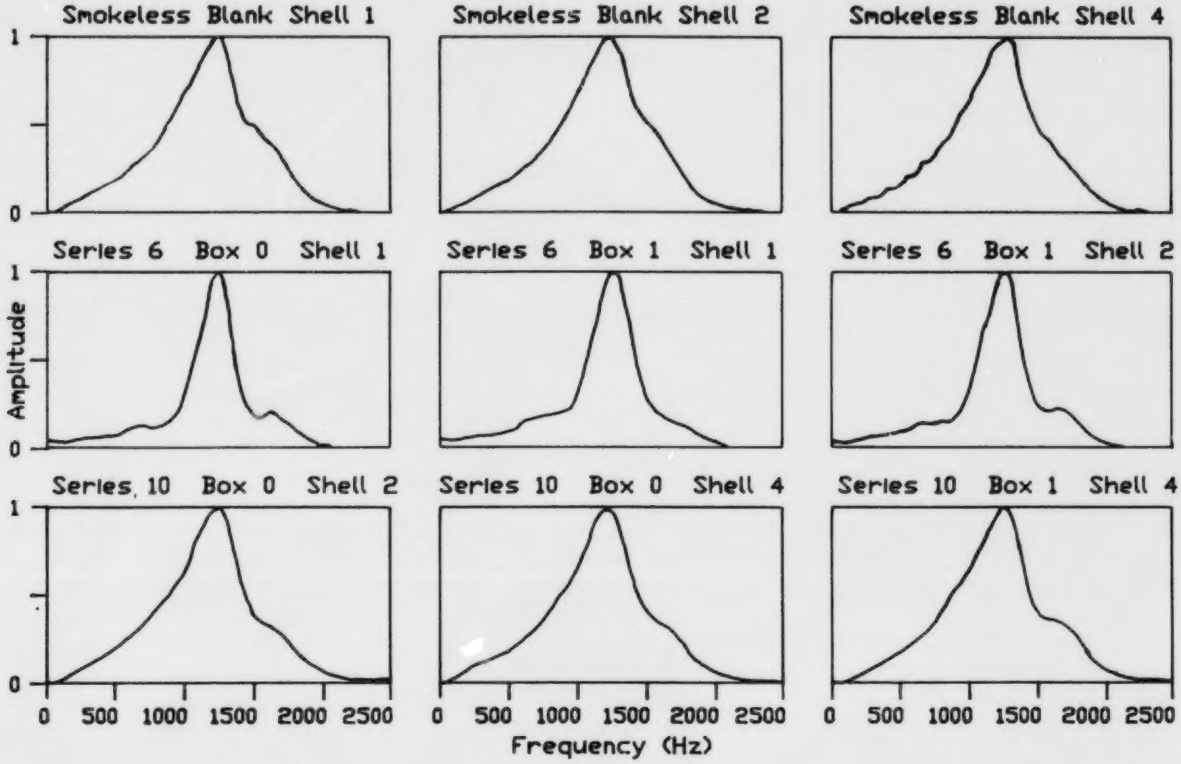

Figure 386.3. Examples of power spectra for first shell test. Note similarity between different shots of the same type of shell (horizontal row) and constant peak frequency (about 1200 Hz) for each shot.

All pipes were approximately 1.25 m long (except case number three which was 1.6 m long) and all were buried so that about 10 cm of the pipe protruded above ground. A schematic of the designs is presented in Figure 386.6. Oversize holes were augured for all pipes and gravel was packed around each pipe so that it fit snugly in its respective hole. The Ontario Geological Survey gun was then clamped so that it fired in the middle of these pipes at a depth of about 60 cm. For the steel chamber the shotgun was fired near the top of the chamber (at a depth of about 1 m). Prior to shooting, the shot hole was filled with water.

Ten shots were fired into each hole, and recorded on 12 geophones stretching away from the holes from 10 to 27.5 m distance. The geophones were not moved throughout the test, which took place on August 9. Physical changes to each shot hole were also noted after each shot. Generally the pipes sank down after 3 or 4 shots, as the percussion from each shot settled the gravel used to tamp the pipes in place.

Frequency spectra were produced for all 10 records of each hole to determine if the signal signature changed from shot to shot within one pipe. Unfortunately none of the pipes produced records with constant frequency characteristics. It was noteworthy, however, that the frequency characteristics of the records produced by shots fired in the PVC pipes were consistently much lower than those produced in the steel pipes. The frequency characteristics of the steel pipes is comparable to those of a normal shot hole (which was also recorded during the test).

This experiment was then repeated using the same materials (except the 10 cm PVC pipe) but cemented in place. Twelve geophones were arranged in an equidistant arc about the shots. Frequency spectra were once again generated for each shot, and variations noted from one shot to the next. Examples of the power spectra may be seen in Figure 386.7. While these plots were much more consistent than those from the previous experiment, there was still a noticeable difference in the signal between shots 1 and 10. The steel chamber appeared to have the best characteristics of this group. More of the shot energy was focused into the ground (the other casings all produced geysers of water when the shot was detonated, indicating that a portion of the shot energy was being transmitted upwards). The steel chamber also had the most repeatable signal characteristics, although these were not consistent enough for our purposes.

A further attempt at producing a standard shothole was completed in the spring of 1991. This time the shothole was a pit 2 m deep and 3 m across, lined with plastic and filled with water. A platform was placed over the pit so that the gun could be detonated in the centre of the pit at a depth of about 70 cm. The pit was large enough that the walls or floor were relatively

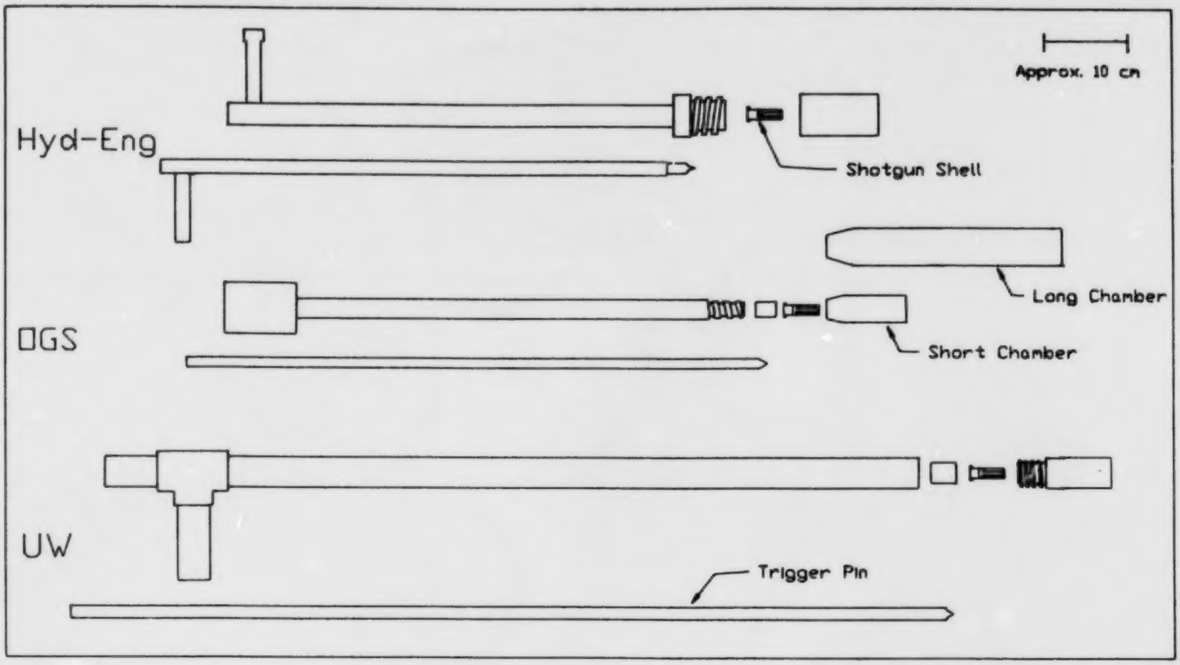
Approx. 10 cm
Hyd-Eng
Shotgun Shell
Long Chamber
OGS
Short Chamber
UW
Trigger Pin

Figure 386.4. Schematic diagram of the different gun designs evaluated.

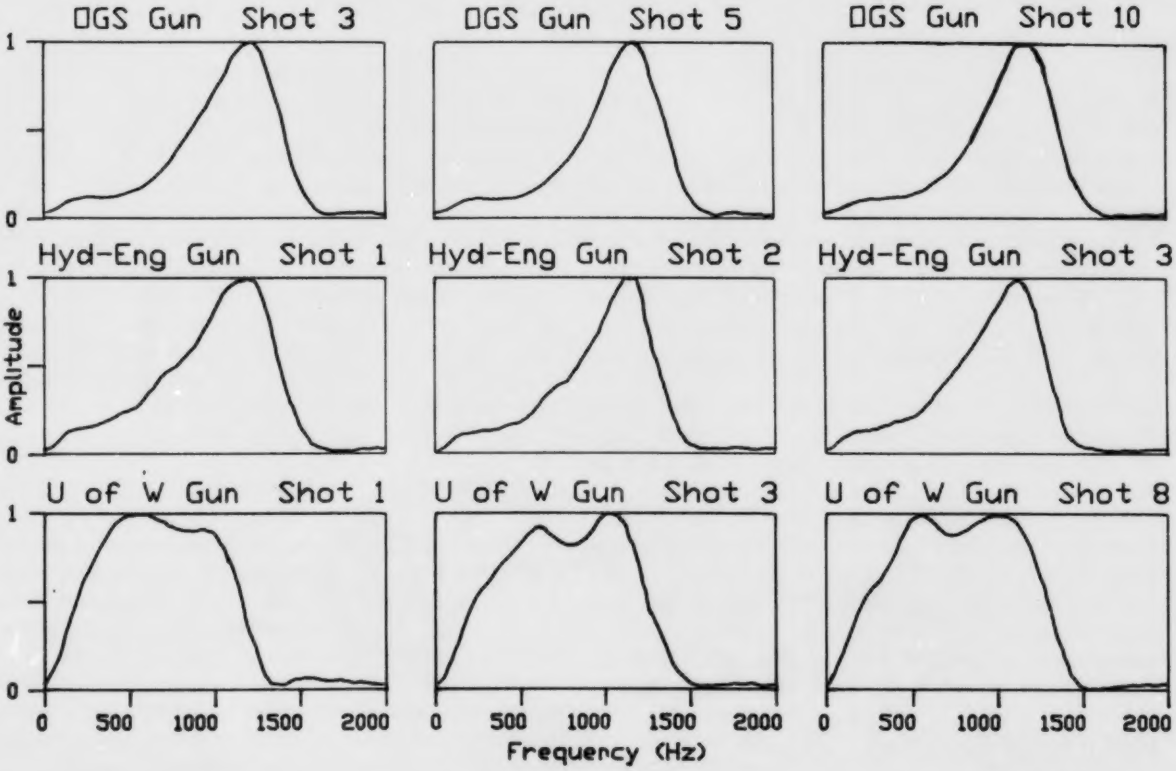

Figure 386.5. Examples of power spectra for each gun. Again note the similarity bewteen shots of the same gun (horizontal row). The University of Waterloo (U of W) gun appears to produce a signal weak in energy around 900 Hz.

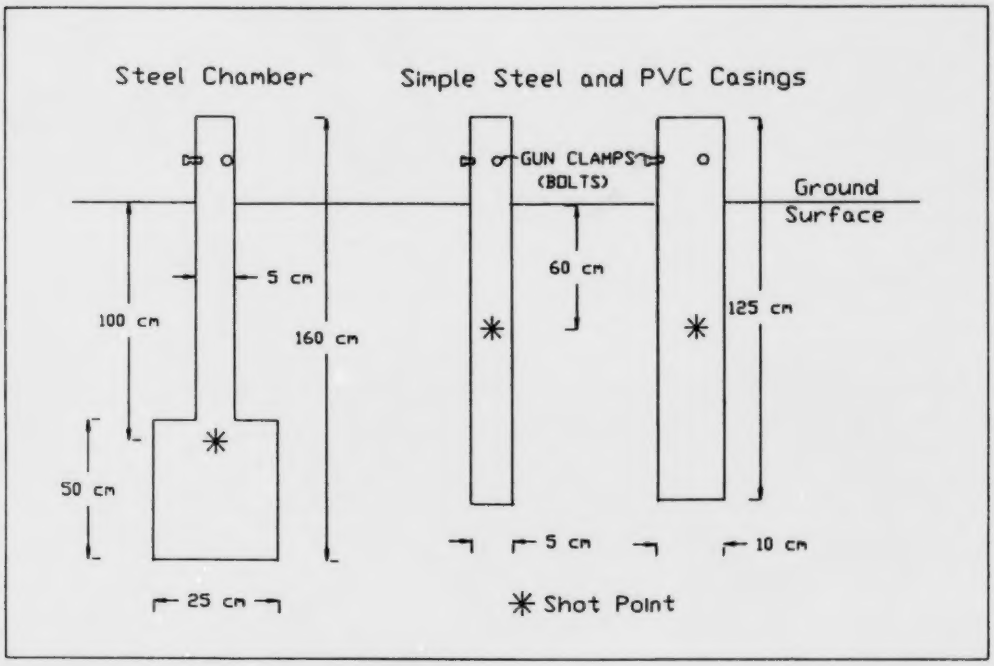

Figure 386.6. Schematic diagram of the original standard shothole designs.

undamaged by the shot, offering fairly uniform conditions for the duration of the test. An inelegant solution, it did provide consistent conditions for consecutive shots.

Although this configuration does not closely match the conventional practice of drilling a 5 to 10 cm wide hole about 1 m deep, it is a good approximation, since energy reaching the geophones must still travel through the near-surface, uncompacted overburden. Frequency spectra from consecutive shots in the pit are very similar, indicating that this shothole design does provide a consistent signal.

To assess the effects of shot depth on signal quality, several shots were fired in holes augured at the base of the pit before it was filled with water. These records were compared to records from conventional shotholes. The deeper shots resulted in records with a much higher frequency content than the shallow shots. While the conventional shotholes resulted in records with most energy in the 50 to 100 Hz range, the deeper shotholes resulted in records with much more energy around the 200 to 250 Hz range. As expected, this test indicates that detonating the shot at a deeper depth than the conventional 1 m enhances signal quality, since more high frequency energy is able to pass into the ground.

Additional Sources

Although not as widely used as the seismic "gun", other sources are used for SSR surveys. Of particular interest to us are the following: a small, portable sweep-frequency vibrator developed at the University of Utrecht (Nijhof 1990), a 50 calibre rifle used by the Kansas Geological Survey (Steeples and Miller 1990), and a pseudo random signal source based on existing technology in the acoustics laboratory of Dr. John Vanderkooy of the University of Waterloo.

Work to adapt Dr. Vanderkooy's technique is continuing, but is not funded by this project. The greatest difficulty may lie in generating a powerful enough signal that can be recorded by geophones some distance from the source. Seismic signals have been recorded on geophones 20 m from the source. We are inviting Dr. Nijhof to visit Ontario with his equipment and demonstrate it on the test section.

BRUCE'S MILL CONSERVATION AREA

The Geophysics/Geochemistry Section of the Ontario Geological Survey has established a test line in Bruce's Mill Conservation Area. This park is located south of Stouffville Side Road, about 8 km west of Stouffville. The survey line extends 1200 m from east to west, across Bruce's Creek (*see* Figure 386.8). Bruce's Creek was considered to be the surface expression of the Laurentian buried bedrock valley, originally described in Spencer (1894), and overburden thickness was expected to be as much as 250 metres.

In 1990 three rotasonic boreholes were drilled on this section. The central hole was located by the creek, while the two

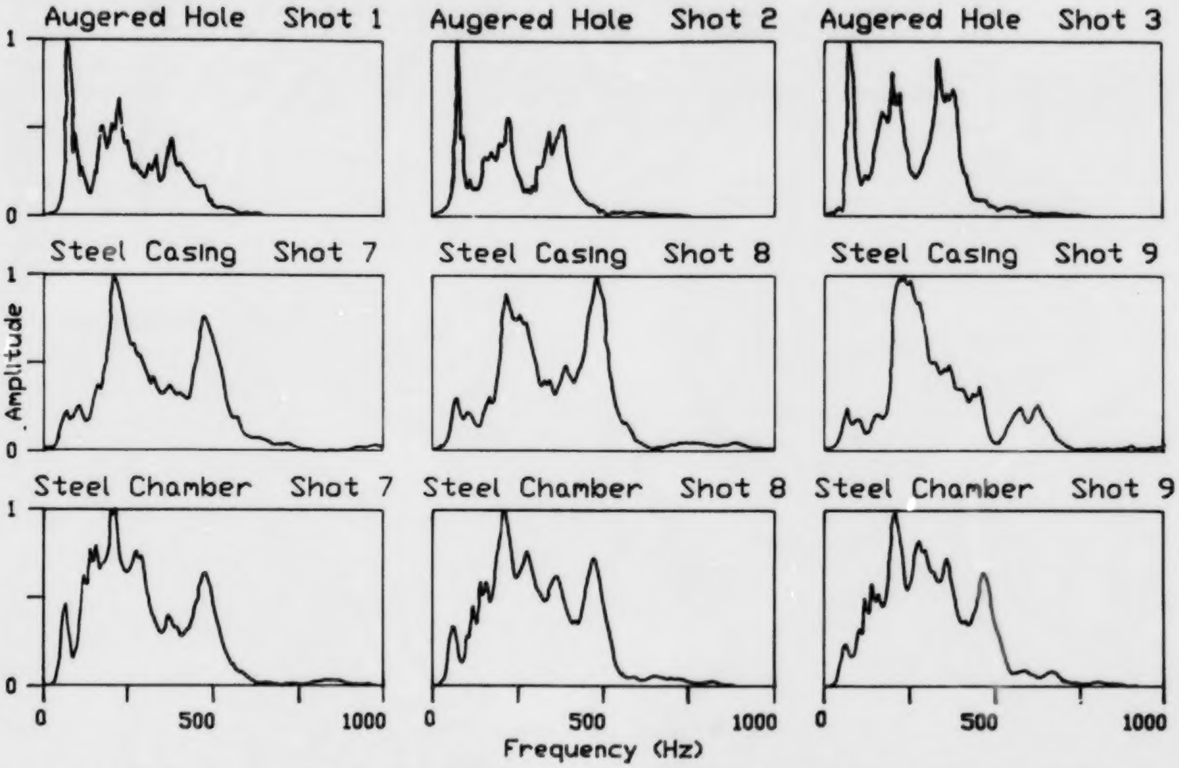

Figure 386.7. Examples of power spectra for cemented shotholes. Records are not very consistent between consecutive shots in the same hole.

others were placed about 250 m on either side of the creek. Drilling indicated that bedrock was not as deep as anticipated; all holes intercepted highly weathered Whitby shale at a depth of about 100 m. The overburden cored was typical of an ice margin environment with thin (1 to 3 m) units of silty till, sand, and sand and gravel alternating down the length of the boreholes.

The boreholes make clear that this site does not overlie the Laurentian bedrock valley, however, we continued with the seismic survey since the boreholes provide excellent stratigraphic control. The conditions encountered, thick sequences of coarse overburden over highly weathered bedrock, were considered representative of conditions throughout the Municipality and most of southern Ontario. This seismic section will now be used as a standard to compare to the new sections just created this summer using modified shooting, recording, and processing parameters.

1990 Survey Method

An east-west survey line was established that started approximately 500 m east of the creek and extended 600 m to the west of the creek (*see* Figure 386.8). A level survey was conducted along the line, which was found to have 10 metres of gentle relief along its length. The most prominent topographic expression is the valley incised by Bruce Creek. Figure 386.1 shows the topography along the survey line.

SSR data was collected on twenty-four 100 Hz marsh geophones spaced every 2.5 m and buried to a depth of about 10 to 20 cm. Each trace was composed of 1024 samples within a trace length of 150 milliseconds. A 300 to 1000 Hz bandpass analog filter was applied during the recording.

The signal was created by detonating a 12 gauge shotgun shell at a depth of about 1 m. Threefold stacking was employed at most shot points to ensure that sufficient energy was transmitted to the lower reflectors. While stacking improved the amplitude of the later reflections, it also degraded the high frequency content of all reflections, as the signals rarely stacked exactly in-phase.

A series of normal moveout (NMO) records was collected at the middle and either end of the survey line to determine the optimum shot/geophone spacing. Shots were fired into the 24 channel spread at intervals of 2.5 metres from distances of 47.5 to 17.5 m from the first geophone. The spread was then pulled forward 32.5 m, so that the next shotpoint was again 47.5 m distant from the first geophone.

This data set produced the 50 m CO section, a portion of which is shown in Figure 386.1. The same data set can be used to collect common midpoint (CMP) gathers (with 50, 55, 60, 65, 70 and 75 m offsets for each trace in the 6-fold gather) which will be processed this fall.

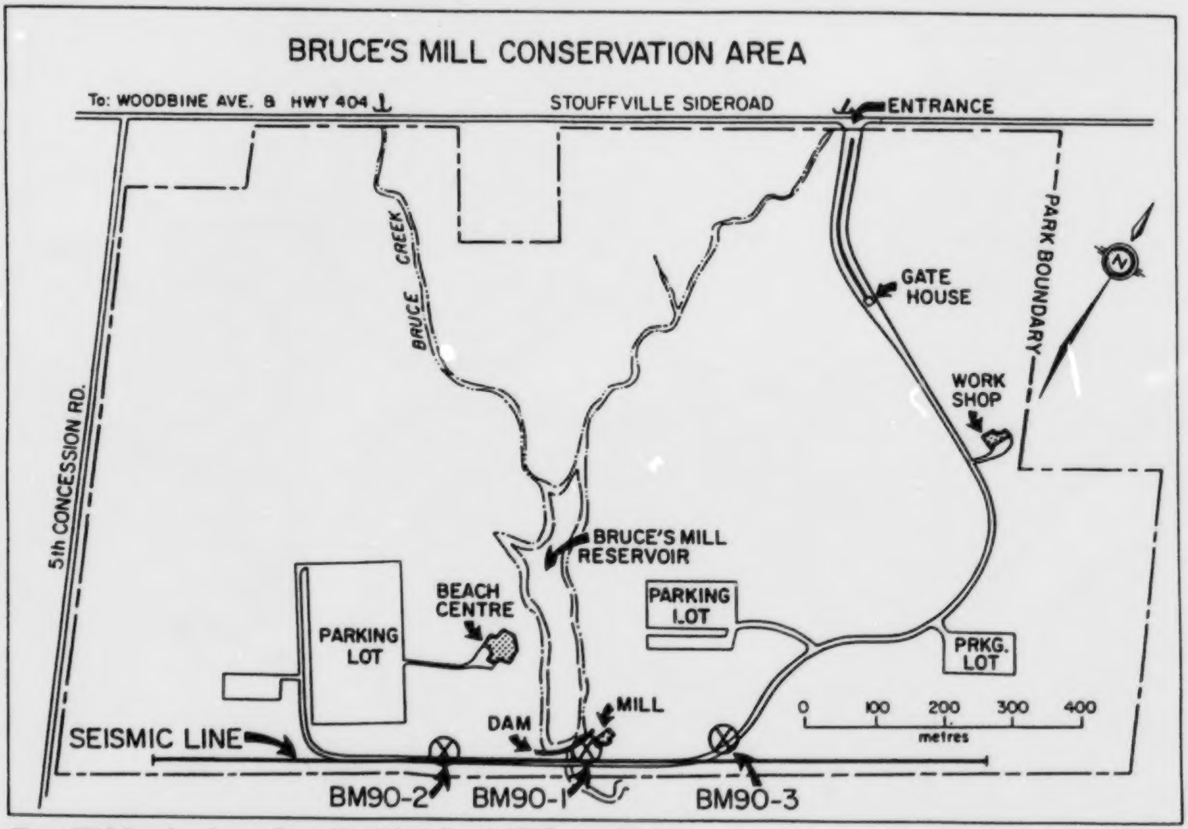
BRUCE'S MILL CONSERVATION AREA
To: WOODBINE AVE. & HWY 404
STOUFFVILLE SIDEROAD
ENTRANCE
PARK BOUNDARY
N
GATE HOUSE
WORK SHOP
BRUCE CREEK
5th CONCESSION RD.
BRUCE'S MILL RESERVOIR
PARKING LOT
BEACH CENTRE
PARKING LOT
PRKG. LOT
MILL
DAM
SEISMIC LINE
0
100
200
300
400
metres
BM90-2
BM90-1
BM90-3

Figure 386.8. Location of survey line and boreholes in Bruce's Mill Conservation Area.

Data quality deteriorates for spreads BMCO1550 to BMCO1950 (*see* Figure 386.1), which traverse Bruce Creek. This may occur because the surface material along this segment of the survey line is uncompacted fill. Both geophones and shot would be poorly coupled to the earth in such material, resulting in poor signal transmission and reception.

Processing

Each trace in Figure 386.1 was statically corrected by lining up the first arrivals, thought to be refractions from the water table. Preliminary velocity analysis indicates an average velocity of about 1800 m/s down to 100 milliseconds. At this velocity bedrock at 100 m depth should occur as a reflection at 110 milliseconds. The lack of a recognizable reflection at this time probably results from one of two factors. Either the seismic signal was not powerful enough to penetrate the dense basal till, or the acoustic impedance contrast between the till and weathered bedrock is small.

1991 Survey Method

This summer a portion of the test line between two of the boreholes (from BM90-1 to BM90-3, *see* Figure 386.8) was resurveyed. This survey was conducted with parameters that were determined in earlier phases of the project (and described in earlier sections of this paper). The OGS gun was used, since it has superiour energy in the 1000 to 1200 Hz band. Both shot and geophones were buried at 2 m depth, to reduce signal attenuation from low-pass earth filtering.

Only CO data was collected, with a 50 m offset. This dataset was just collected, and no comparison has yet been made with the section produced last year.

Borehole Logging

Vertical seismic profiling (VSP) was conducted in the two end boreholes (BM90-2 and BM90-3) in the summer of 1990. The data can be used to estimate average velocity as a function of depth, to locate reflecting horizons, and to construct a depth scale for the surface seismic sections.

Induction (conductivity) logs and complete geological cores were also obtained by the OGS in the three boreholes. These are also available for comparison with the seismic data.

SUMMARY

After isolating and examining each aspect of the seismic source, we determined that a number of modifications could be made to improve signal quality. The optimum shotshell is a "home-packed" shell with a mixture of pistol powder and black gunpowder in the ratio of 8:2 (pistol powder to black powder). Different guns produce different signals, when firing the same shells. The type of steel used may determine the frequency content of this signal. Deeper shotholes result in a much higher frequency signal being transmitted to the earth. Shallow shots have much of the high frequency content attenuated by the poorly compacted near-surface material which acts as a low-pass filter.

The improvement in data quality using these parameters, compared to the data quality of a record collected by conventional means (standard shotshells, shallow holes) is now being assessed.

ACKNOWLEDGEMENTS

We would like to thank the staff at Bruce's Mill Conservation Area for their helpful co-operation. Thanks are due to M. Barua and C. Clark for assistance during the 1990 field season, and J. Wong for the 1991 season. We are grateful to R. Barlow for the use of OGS equipment throughout the project.

REFERENCES

Greenhouse, J.P., Nobes, D.C., and G.W. Schneider 1990. Groundwater beneath the city: a geophysical study; *in* Proceedings, Fourth National Outdoor Action Conference, National WaterWell Association, p.1179-1191.

Hunter, J.A., Burns, R.A., Good, R.L., MacAuley, H.A. and Gagne, R.M. 1982. Optimum field techniques for bedrock reflection mapping with the multichannel engineering seismograph; Current Research, Part B, Geological Survey of Canada, Paper 82-1b, p.125-138.

Nijhof, V. 1990. Development of a small portable high frequency vibrator and its use in high resolution shallow seismic problems; *in* Abstracts, 52nd meeting of the European Association of Exploration Geophysicists, p.140-141.

Spencer, J.W., 1894. A review of the history of the Great Lakes; The American Geologist, v.24, p.289-301.

Steeples. D.W., and Miller, R.D., 1990. Seismic reflection methods applied to engineering, environmental, and groundwater problems; *in* Geotechnical and environmental geophysics, Society of Exploration Geophysicists, v.1, p.1-30.

Grant 389 Hydrogeological Implications of Buried Eskers in Essex County, Ontario: Results from Year 1

M.G. Sklash and O.A. Ibrahim

Department of Geology, University of Windsor, Windsor, Ontario N9B 3P4

There is a strong spatial similarity between the locations of buried eskers mapped by Morris (1989) and the anomalously young groundwater in the freshwater aquifer in Essex County, Ontario mapped by Crnokrak (1991). The freshwater aquifer in the study area is covered by more than 25 m of clayey silt to silty clay overburden that is generally considered to be a competent aquitard. We used a program of drilling, hydrometric monitoring, environmental isotope tracing and natural geochemical tracing to determine if one of the buried eskers could be related to rapid recharge of the freshwater aquifer. Our preliminary results are largely negative for this target: the target does not appear to be an esker and the freshwater aquifer contains water with very depleted $\delta^{18}O$ values which suggest recharge in the order of 10 000 years ago. A companion study on a second target esker gives much more encouraging results. The isotopic and geochemical data also suggest that the freshwater aquifer near Lake St. Clair is impacted by brine from the underlying bedrock.

INTRODUCTION

The main goal of this study is to determine whether eskers buried beneath clayey silt to silty clay glacial deposits are responsible for the anomalously young groundwater in the freshwater aquifer in central Essex County, Ontario. We use drilling, hydrometric, environmental isotope tracer and geochemical techniques to determine: (1) if one of the features mapped by Morris (1989) is a buried esker, (2) whether young groundwater occurs in the freshwater aquifer surrounding the target feature; and if the young groundwater is confirmed, (3) whether the young groundwater arrives vertically from above or laterally along the feature.

The Problem

The "freshwater aquifer" is a regional confined aquifer which underlies most of Essex, Kent and Lambton counties in Ontario and extends westward into Michigan. The aquifer consists of fractured bedrock subcrop and granular material of variable thickness (generally 1.5 to 6 m according to Gillespie and Dumouchelle 1989) draped upon the bedrock surface. The aquifer is known to thicken considerably in bedrock valleys, for example, in the Sarnia area (INTERA Technologies Ltd. 1987). According to Morris (Ontario Geological Survey, Sudbury, personal communication, 1991), the granular portion of the freshwater aquifer reported over much of the area is actually Catfish Creek Till. The clayey silt to silty clay deposits overlying the aquifer are commonly more than 30 m thick.

Although the freshwater aquifer supplies water for thousands of rural users, little is known about its regional flow characteristics. There have been some local investigations of the freshwater aquifer, especially in the Sarnia region (INTERA Technologies Ltd. 1987) and numerous local studies of the overlying clayey aquitard, mainly by researchers from the University of Waterloo. Results from these studies imply that the aquitard is commonly of sufficient thickness and of sufficiently low permeability (in the order of 2×10^{-10} m/s) to be widely suitable for waste disposal (Desaulniers et al. 1981). These detailed investigations support Allendorf's (1981) regional map of aquifer susceptibility to contamination that designates the areas in Essex County with thick deposits of clayey overburden as having a low probability of aquifer contamination.

The studies that suggest that the clayey overburden is an effective confining unit for the aquifer are based largely on two hydrogeological approaches: (1) standard hydrometric tests on the clayey overburden, such as Hvorslev tests for *in situ* permeability, and (2) analysis of vertical distributions of environmental isotope and natural chemical tracers in the groundwater within the clayey overburden. There are at least three problems with these approaches. First, Keller et al. (1986) recognized that extensive vertical fracturing can occur deep into unweathered till. These vertical fractures may not be obvious in vertical cores, especially since fracture frequency and fracture aperture decrease with depth. Keller et al. (1986) suggested that these fractures could profoundly affect permeability. Second, D'Astous et al. (1988) reported that augering tends to smear fractures in clayey soils, resulting in calculated permeabilities by single well test methods which are much lower than actual permeabilities. Smearing may also affect matrix permeability. Finally, since test drilling is expensive, *in situ* permeability testing and analysis of environmental isotope and natural chemical tracer distributions in the groundwater in the clayey overburden have been limited to small test sites. These sites may, or may not, be representative of the regional behaviour of the aquitard.

At the University of Windsor, we have conducted regional environmental isotope studies of the freshwater aquifer in Essex, Kent and Lambton counties in Ontario and in southeastern Michigan. The distributions of oxygen-18 (^{18}O) and tritium (^{3}H) in groundwater in the freshwater aquifer reflect the natural recharge, discharge and flow processes for the aquifer. The distinctive input functions of these tracer isotopes can be used to differentiate between groundwater recharged thousands of years ago during cooler climatic conditions, groundwater recharged during the last few thousand years under warmer climatic conditions, and groundwater recharged within the last few decades.

Briefly, ^{18}O is a stable isotope of oxygen that forms part of some natural water molecules. The concentration of ^{18}O in precipitation is largely controlled by temperature. Groundwater that was recharged from precipitation which fell during the cooler climatic conditions which dominated the area until about 10 000 years ago, has distinctly less ^{18}O than groundwater that was recharged during the warmer climatic conditions of the past several thousand years. Tritium is a radiogenic isotope of hydrogen (half-life of about 12.4 years) that forms part of some water molecules. Prior to the beginning of large scale atmospheric testing of thermonuclear devices in 1952, natural tritium concentrations in precipitation ranged from about 4 to 25 tritium units (TU), where 1 TU = 1 ^{3}H in 10^{18} ^{1}H atoms. Groundwater that was recharged by precipitation which fell before 1952 should now have less than 3 TU. Atmospheric testing of thermonuclear devices in the atmosphere resulted in increases in ^{3}H concentration of up to three orders of magnitude, reaching a peak of several thousand TU in 1963. Although ^{3}H concentrations in precipitation have decreased since 1963, the year in which an atmospheric test ban treaty was signed, groundwaters recharged since 1952 are characterized by tritium concentrations much greater than 3 TU. Desaulniers et al. (1981), Fritz and Fontes (1980) and others discuss the use of ^{18}O and ^{3}H for groundwater age determinations in more detail.

Figure 389.1, from Crnokrak (1991), shows the distribution of ^{18}O in the freshwater aquifer in Essex County. This map is based on groundwater samples collected from 35 domestic wells. According to Crnokrak (1991) and Desaulniers et al. (1981), the very depleted $\delta^{18}O$ values (-15 and -16 parts per thousand (‰)) in the northeastern and northwestern parts of the freshwater aquifer are characteristic of groundwater which

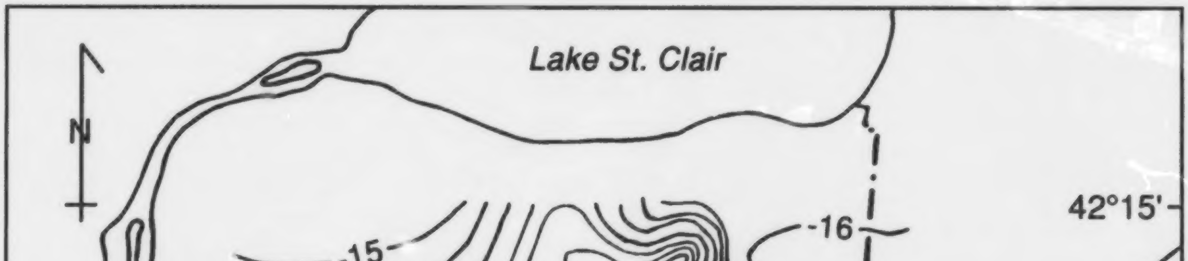

Figure 389.1. Distribution of ^{18}O in the freshwater aquifer in Essex County, Ontario (after Crnokrak 1991).

was recharged more than 10 000 years ago (the concentration notation for ^{18}O is explained in the "METHODS" section). The northward protrusion of groundwater with relatively enriched $\delta^{18}O$ values (-8 to -10 ‰) into the surrounding groundwater with more depleted $\delta^{18}O$ values, suggests that the central part of the freshwater aquifer contains younger groundwater.

Crnokrak's (1991) electrical conductivity (EC) and tritium data support this age distribution. She observed electrical conductivities in the freshwater aquifer that exceed 5000 µS/cm in the northeast and 3000 µS/cm in the northwest, but that are less than 500 µS/cm where the relatively enriched $\delta^{18}O$ values occur. More significantly, several of the wells in the zone of enriched $\delta^{18}O$ values have tritium concentrations characteristic of recharge within the last 40 years. Although Crnokrak's data must be viewed with some caution since her samples are from domestic wells, the repetition of the findings in numerous wells supports her results.

The location of this young groundwater is puzzling. Rapid vertical recharge through the thick aquitard has been considered to be unlikely in view of the measured low hydraulic conductivity and the presence of very old water deep in the aquitard (Desaulniers et al. 1981). Lateral flow from the closest obvious recharge area also seems improbable. Dillon (1987) estimated that the horizontal groundwater velocity in the freshwater aquifer is in the order of 2.5 m/a. This is consistent with a 3 m/a estimate for flow in the aquifer in Michigan (Long et al. 1988). Although Crnokrak's (1991) ^{18}O distribution in the freshwater aquifer is reasonable assuming this groundwater velocity, her tritium distribution cannot be explained in this manner. Groundwater containing anthropogenic tritium should only be found in the order of hundreds of metres from the recharge area. The nearest surface expression of the aquifer recharge area, however, is more than 10 km upgradient from some of the tritiated groundwater in the freshwater aquifer.

A clue to the origin of this young water may lie in a study by Morris (1989). Based on remote sensing, field mapping and drilling data, Morris (1989) suggested the possibility of a series of essentially north trending eskers buried beneath central Essex County. Morris (1989) first noted the buried eskers as lighter tones on remote sensing images that suggest enhanced drainage. These features coincide with the region of anomalously young groundwater in the freshwater aquifer.

We wanted to test two hypotheses which might explain the young groundwater. In the first hypothesis, groundwater velocities are very high along the reported eskers enabling rapid lateral groundwater movement from the closest obvious recharge area. In the second hypothesis, precipitation has recharged the freshwater aquifer rapidly by infiltrating through localized vertical fractures in the aquitard which are related to the settlement of the clayey deposits over the buried eskers.

Objectives

The main goal of this study is to determine whether eskers reported to be buried beneath clayey glacial deposits are responsible for the anomalously young groundwater noted in the central part of the freshwater aquifer in Essex County, Ontario. The primary objectives in the first year of the study were to: (1) confirm the existence of one of the buried eskers reported by Morris (1989), (2) confirm the existence of the anomalously young groundwater in the freshwater aquifer, and (3) examine the spatial relationship between the young groundwater and the target feature.

A companion study at the University of Windsor funded by the Ontario Ministry of the Environment, has the same goal and objectives and uses the same approach as this study. The Ontario Ministry of the Environment study targets a second reported esker. The findings from that study will be discussed only briefly here.

The Study Area

Figure 389.2 shows the location of our study area and drill sites in Essex County, Ontario. Our target is a north trending feature which runs parallel to, and just slightly east of,

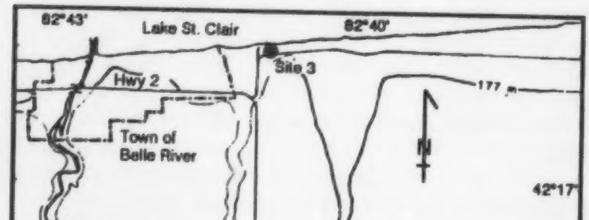

Figure 389.2. Location of study area and drill sites.

Rochester Concession Road No.2 from south of Highway 401 to Lake St. Clair. Both on the ground and on the 1:25 000 topographic map, the feature appears as an obvious linear ridge on the otherwise flat terrain. The target feature and the drill site locations were selected after consultation with Dr. T. Morris of the Ontario Geological Survey (personal communication, 1990). The three transects across the feature are in the eastern segment of the young groundwater noted by Crnokrak (1991).

Essex County is part of an extensive clay plain that has little relief (Chapman and Putnam 1984). The surficial deposits have been well documented by Vagners (1972), Vagners et al. (1973), Desaulniers et al. (1981) and Morris (1988, 1989). In the study area, surficial deposits are mostly clayey silt to silty clay till that range in thickness from about 25 to 40 m. The clayey deposits are considered to be an aquitard over the freshwater aquifer. Telford and Russell (1981) have mapped the bedrock geology of Essex County at 1:250 000. The Dundee Formation, a Middle Devonian limestone, subcrops beneath the study area.

Mellary and Nakashiro (1970) and Allendorf (1981) provide regional information on the water supply and contamination potential aspects, respectively, of the freshwater aquifer in Essex County. The aquifer consists of the fractured bedrock subcrop and granular material of variable but limited thickness draped upon the fractured bedrock surface. As mentioned previously, Morris (Ontario Geological Survey, Sudbury, personal communication, 1991) reports that the granular material is probably Catfish Creek Till. Based on potentiometric levels from water well records (Ontario Ministry of the Environment 1984), geochemical and isotopic data, the main recharge area for the freshwater aquifer in Essex County is the relatively high sandy area northwest of Leamington (Crnokrak 1991). From here, groundwater in the freshwater aquifer flows radially to the northern, eastern, and western parts of the county, and southward to nearby Lake Erie. According to Dillon (1987), the regional horizontal hydraulic gradient in the northern part of the freshwater aquifer is in the order of 0.001, reflecting the low relief; and the average groundwater velocity is in the order of 2.5 m/a.

METHODS

General Approach

Our problems are to determine: (1) if the target is an esker, (2) if there is anomalously young groundwater at the site, and (3) if there is anomalously young groundwater, did it arrive vertically from above or laterally along the feature. Our general approach to the recharge problem is to determine flow directions and relative groundwater ages along and perpendicular, to the target esker using environmental isotope, geochemical and hydrometric techniques. We installed a series of monitoring wells (Series A wells) in three transects oriented across the target (Sites 1, 2 and 3 on Figure 389.2). The monitoring network also includes selected domestic wells (Series B wells) located near the drill sites.

Specifically, the Series A boreholes should allow us to determine whether the target is an esker and if so, determine its dimensions. Analyses for ^{18}O and ^{3}H in the groundwater from the Series A wells should allow us to confirm or disprove the existence of the anomalously young groundwater reported by Crnokrak (1991). If the groundwater proves to be anomalously young and if the target acts as a localized, linear groundwater recharge area, hydraulic heads in the Series A wells should indicate flow directions away from the feature. Also, groundwater ages should increase away from the feature. These should be reflected in the tritium concentrations in the Series A and B wells, and ^{18}O concentrations and ^{14}C ages in the Series B wells. We also expect that the groundwater chemistry will become progressively more concentrated away from the feature. If instead, the target acts as a high permeability conduit for lateral recharge, we expect this to be apparent in the ^{18}O and groundwater age distributions (based on ^{3}H, ^{14}C, and hydrometric methods).

Drilling and Monitoring Well Installation

We used a hollow stem auger rig (CME Model 750) for all of the boreholes except two. We selected this type of rig mainly to minimize the introduction of drilling water into the aquifer. At OAI-4 and OAI-5a, we used rotary drilling with water. The drilling was completed between July 11 and August 28, 1990.

At each of the three sites, we first drilled a "deep" hole where we tried to drill through the feature to bedrock to determine the stratigraphy and the depth to the top of the aquifer. For this target, siting the first hole was easy since the feature forms an obvious surface ridge. The target in the companion study for the Ministry of the Environment and the other targets, have no obvious surface topography expression. After installing a monitoring well in the deep hole, we completed the site transect with a two or three level piezometer nest and one or two additional wells within a distance of about 100 m (Figures 389.3 to 389.5). At one deep hole at each site, we took Shelby tube samples every 3 m. For the other deep holes, we collected split spoon samples every 3 m. Samples were returned to the laboratory for subsequent physical tests.

The monitoring wells generally consist of 33 mm diameter schedule 40 PVC riser pipe with screw ends and O-rings and a 1.5 m long, No. 10 slotted schedule 40 PVC screen. The PVC materials had been pre-cleaned and plastic wrapped by the manufacturer. Only Well OAI-4 was different, it had a 57 mm diameter riser and its screen is 3 m long. Sand packs were emplaced to 0.3 m above the top of the screen. No sand packs were placed around OAI-3 and 6 due to collapse. Each well had a 1 m bentonite seal above the sand pack and a 0.6 m bentonite

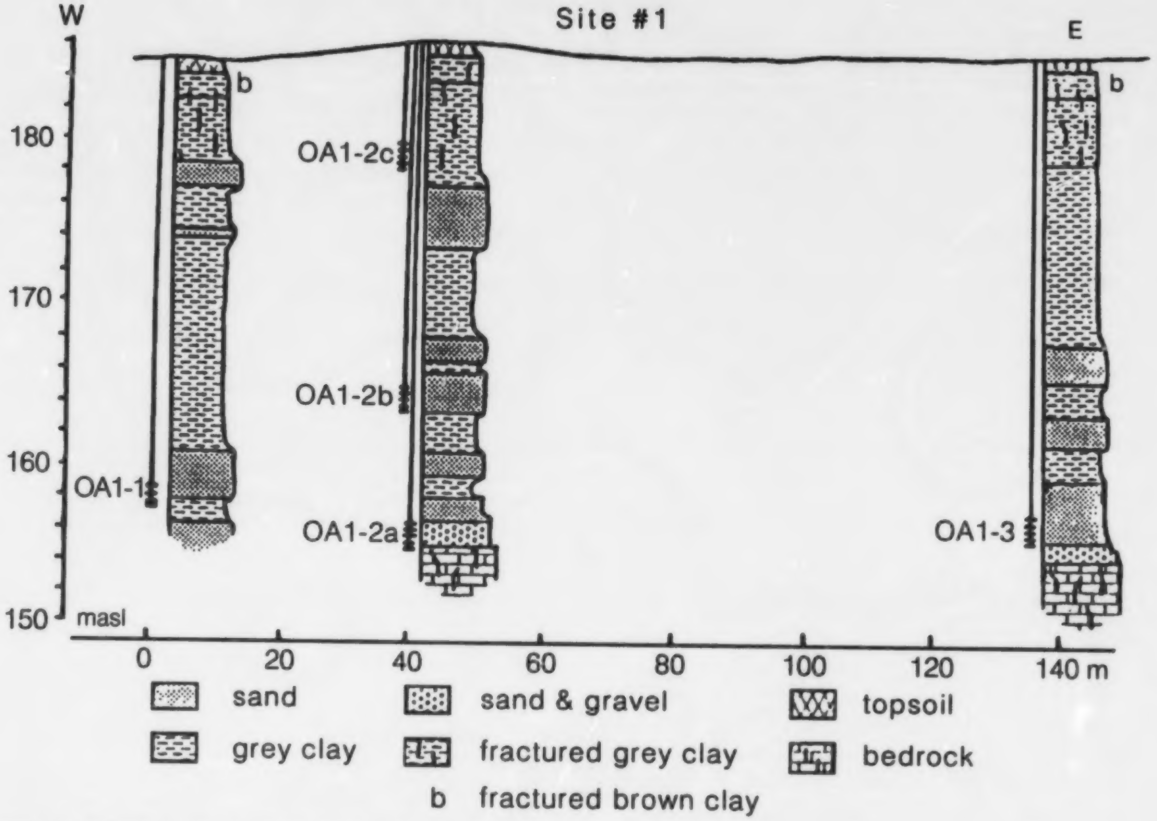

Figure 389.3. Geologic cross section at Site 1 and monitoring well depths.

seal near the surface. Locking metal surface casing protects each well.

Analytical Methods

Each well was purged two or three times after drilling and prior to the first sampling. Each purging removed more than ten times the volume of water standing in the well. Groundwater samples collected from wells for subsequent laboratory analysis were securely sealed in plastic bottles in the field. Porewater from Shelby tube samples was squeezed from Shelby tube cores using the apparatus designed by Orpwood (1984). To minimize evaporation, the cores had been tightly wrapped with plastic sheeting and electrical tape in the field and refrigerated until squeezing.

We prepared samples for ^{18}O analysis using standard methods. The prepared gas samples were analyzed at the University of Ottawa using a SIRA-12 mass spectrometer. The samples were analyzed for deuterium at the University of Waterloo using the zinc reduction method (Coleman et al. 1982) for sample preparation and a Micromass Model 602 mass spectrometer. The ^{18}O and deuterium (^2H) analyses are expressed in the standard delta (δ) notation in parts per thousand (‰) difference relative to the international standard Standard Mean Ocean Water (SMOW, Craig 1961), where:

$$\delta^{18}O \text{ or } \delta^{2}H = [(R_x - R_{SMOW})/(R_{SMOW})] \times 1000$$

and $R = {}^{18}O/{}^{16}O$ or $R = {}^{2}H/{}^{1}H$, and x = sample. The analytical precision for δ^2H and $\delta^{18}O$ measurements by mass spectrometry are better than ± 2 and ± 0.2 ‰, respectively.

Samples for ^3H analysis were submitted to the Isotope Laboratory at the Department of Earth Sciences, University of Waterloo but, owing to sample backlog at the laboratory, these results are not yet available. Sampling for ^{14}C analysis has been postponed in light of reported problems with methanogenesis and sulphate reduction in the freshwater aquifer in Essex County (Aravena, University of Waterloo, Department of Earth Science, personal communication, 1991).

We measured electrical conductivity in the field using a YSI Model 32 conductivity meter that automatically corrects readings to 25°C. Temperature and pH were also measured in the field using a Corning Model 103 pH meter. We determined alkalinity in the field by titration. Our samples were analyzed for major cations and sulphate at the University of Windsor using standard techniques. Chloride and nitrate analyses were done by ion analyzer at the University of Windsor.

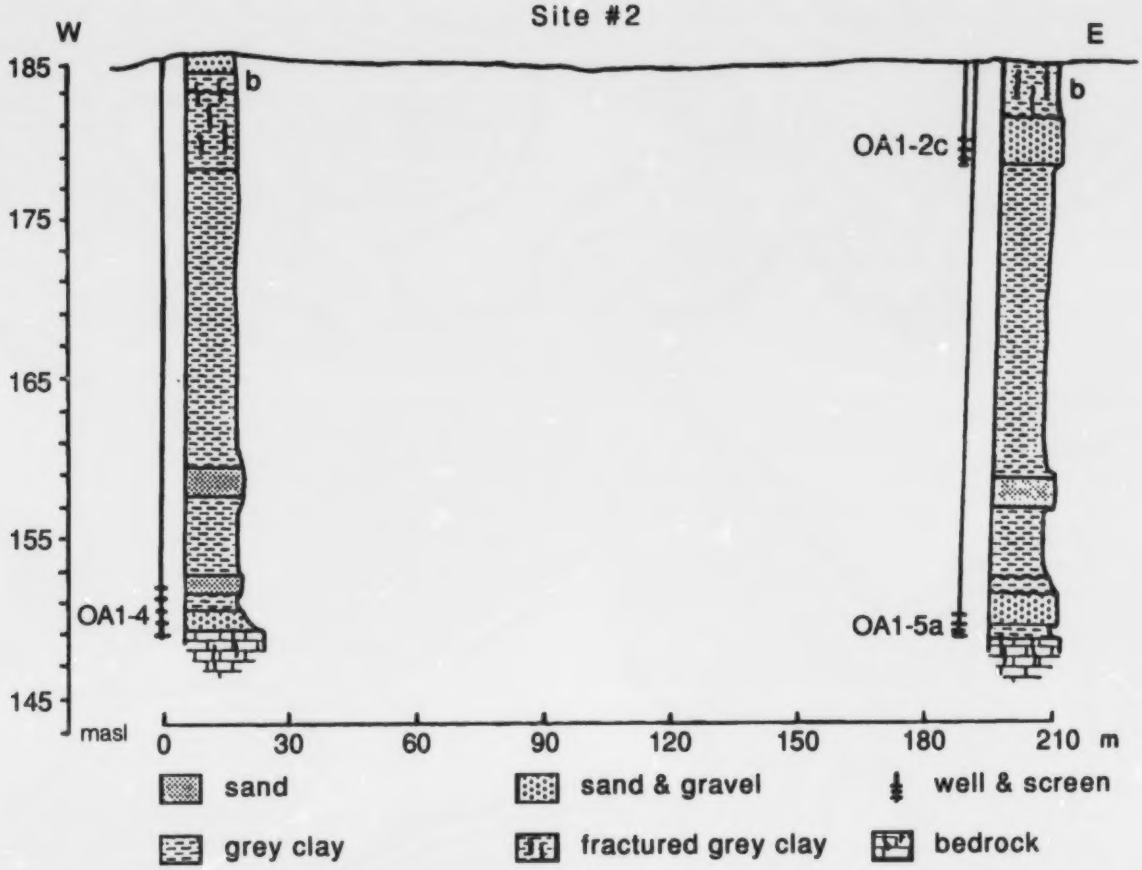
Site #2
W
E
185
175
165
155
145
masl
b
b
OA1-2c
OA1-4
OA1-5a
0
30
60
90
120
150
180
210 m
sand
sand & gravel
well & screen
grey clay
fractured grey clay
bedrock

Figure 389.4. Geologic cross section at Site 2 and monitoring well depths.

RESULTS AND DISCUSSION

Table 389.1 lists selected hydrometric, chemical and isotopic data from our study. We drilled a total of 12 boreholes in three transects (Figure 389.2). Figures 389.3 to 389.5 show both the geologic cross sections for the three sites and the screen depths for the Series A wells.

Although the relative elevations on each figure are correct the noted elevations are related to estimates from the topographic map.

Is the Feature a Buried Esker?

Based on our initial data, there is no clear indication that the feature is a buried esker. All of the drill sites are dominated by clayey silt to silty clay grey till interbedded with numerous sand units. Although sand layers constitute about 33% of the profile at OAI-2 and 20% at OAI-7, the thickest individual sand unit encountered in any borehole was less than 3 m. Bedrock was encountered at between 30 m (OAI-6) and 36 m (OAI-4 and 5) below ground surface. Although Wells OAI-2, 4, and 7 were drilled through the linear ridge, our preliminary

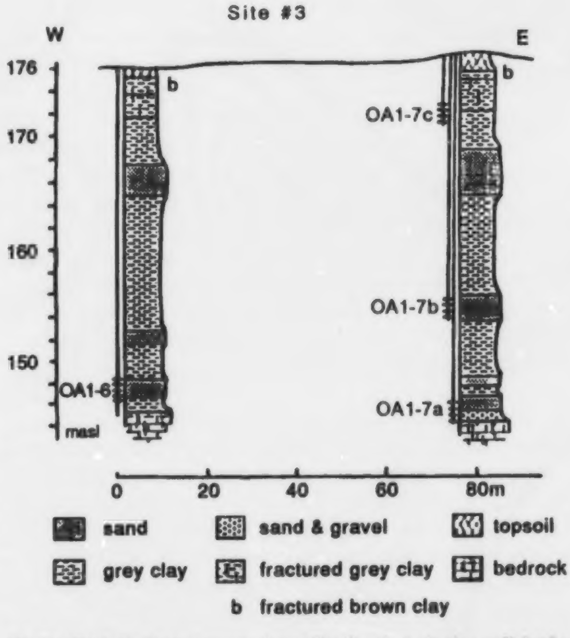
Site #3
W
E
176
170
160
150
masl
b
b
OA1-7c
OA1-7b
OA1-6
OA1-7a
0
20
40
60
80m
sand
sand & gravel
topsoil
grey clay
fractured grey clay
bedrock
b fractured brown clay

Figure 389.5. Geologic cross section at Site 3 and monitoring well depths.

conclusion is that there is no obvious esker beneath the ridge.

Do the Hydraulic Head Data Indicate Aquifer Recharge at the Feature?

Our hydraulic head data are expressed relative to local benchmarks, each arbitrarily assigned an elevation of 100 m. Our first hydraulic head data, collected on December 6, 1990, have not yet been corrected for possible density differences (*see* Table 389.1).

There is no clear indication that the hydraulic heads decrease away from the feature. The hydraulic head in the aquifer beneath the crest of the feature at Site 1 (OAI-2a) was 96.47 m. At OAI-1 and OAI-3, approximately 40 and 100 m away, the heads were marginally greater at 96.79 and 96.54 m, respectively. At Site 2, the hydraulic head in the aquifer beneath the crest of the feature (OAI-4) was 96.49 m. At OAI-5, approximately 200 m away, the head was the same. At Site 3, the hydraulic head in the aquifer beneath the crest of the feature (99.44 m at OAI-7a) was greater than the head at OAI-6 (99.15 m) which is approximately 80 m away.

The vertical hydraulic gradient at all of the sites was downward, which is consistent with recharge. The vertical hydraulic gradients on December 6, 1990 were: 0.07, 0.04, and 0.02 at Sites 1, 2, and 3, respectively.

Do the Isotopic Data Indicate Young Groundwater at the Feature?

The isotopic data do not indicate young groundwater in the freshwater aquifer at the feature. Figure 389.6 is a plot of the $\delta^{18}O$ and $\delta^{2}H$ values for the groundwater samples for which we have both types of data. For comparative purposes, we have included a sample of tap water from Lake St. Clair. Except for OAI-8, which is a 2 m deep well near the lake at Site 3, all of the samples fall near the $\delta^{18}O - \delta^{2}H$ line from Crnokrak (1991). The depleted $\delta^{18}O$ and $\delta^{2}H$ values in the freshwater aquifer samples (OAI-2a, OAI-7a) are typical of very old groundwaters which were recharged under cooler climatic conditions.

There is no indication of very recent recharge (similar to that at shallow wells OAI-8 and OAI-7c) nor is there indication of significant recharge of the freshwater aquifer from Lake St. Clair. The depleted $\delta^{18}O$ and $\delta^{2}H$ values in the groundwater from the sands within the till (OAI-2b and OAI-7b) are typical of the depleted waters in deeper till reported by Desaulniers et al. (1981). These depleted values suggest that the sand units are not connected to surface recharge.

Do the Isotopic and Geochemical Data Indicate Rapid Groundwater Movement Along the Feature?

Neither the isotopic nor geochemical data indicate that young groundwater rapidly moves northward along this feature. The regional trend in $\delta^{18}O$ contours in the freshwater aquifer shown in Figure 389.1 is from more recent, isotopically enriched waters in the south to older, isotopically depleted waters in the north. Along the feature, the $\delta^{18}O$ values at Sites 1 and 2 (-14.06 ‰ at OAI-2a and -15.26 ‰ at OAI-5a, Table 389.1) are consistent with the direction of this trend, however the $\delta^{18}O$ values are still characteristic of older, isotopically depleted waters. The opposite of this trend occurs between Sites 2 and 3 ($\delta^{18}O$ of -15.26 ‰ at OAI-5a and -13.31 ‰ at OAI-7a). We discuss a possible explanation for the data at Site 3 below.

In terms of chemistry, Crnokrak (1991) shows increasing electrical conductivities in the freshwater aquifer from south to north with electrical conductivities lower than 500 µS/cm in the young groundwater body. Figure 389.7 is a Schoeller diagram of the major ion chemistry along the feature. Although there is a strong indication of increasing concentrations from south (Sites 1 and 2) to north (Site 3), there is little change between Site 1 and Site 2.

Is there Brine in the Freshwater Aquifer?

Both the isotopic and chemical data suggest that the groundwater at Site 3 may be affected by brine from deeper formations. Long et al. (1988) found similar brine-affected groundwaters in the freshwater aquifer near Lake Huron. Dollar et al. (1987) report that Devonian strata (which subcrop beneath the study area) contain relatively dilute brines (total dissolved solids less than 30 g/L) whose stable isotopic compositions are indicative of recharge during a cooler climatic time, probably the last glaciation. Figure 389.8 shows that the groundwater at Site 3 is very different from the groundwater samples from the other sites in terms of $\delta^{18}O$ and chloride. OAI-6 from Site 3 is not plotted because we have no chloride analysis for it, however it is similar to the OAI-7a groundwater in terms of electrical conductivity (electrical conductivity at OAI-6 is 18,720 µS/cm compared to 20,400 µS/cm at OAI-7a).

Do the Isotopic and Geochemical Data Indicate Groundwater Movement Away from the Feature?

Figure 389.9 shows that at Sites 2 and 3, there is no significant difference between the $\delta^{18}O$ values in the freshwater aquifer at the feature and those further away as would be expected if recharge took place on the feature. The data at Site 1 suggest a progressively older water away from the feature however all of the $\delta^{18}O$ values are still characteristic of older, isotopically depleted waters (these wells are very close to the feature and similarity in $\delta^{18}O$ in the Series A wells at a given transect is expected). When we receive the $\delta^{18}O$ values from the Series B wells which are further from the feature and the tritium data from the Series A wells, we will be able to comment further on this.

Figure 389.10 is a Schoeller diagram of the major ion chemistry at Site 2. There is no clear indication of progres-

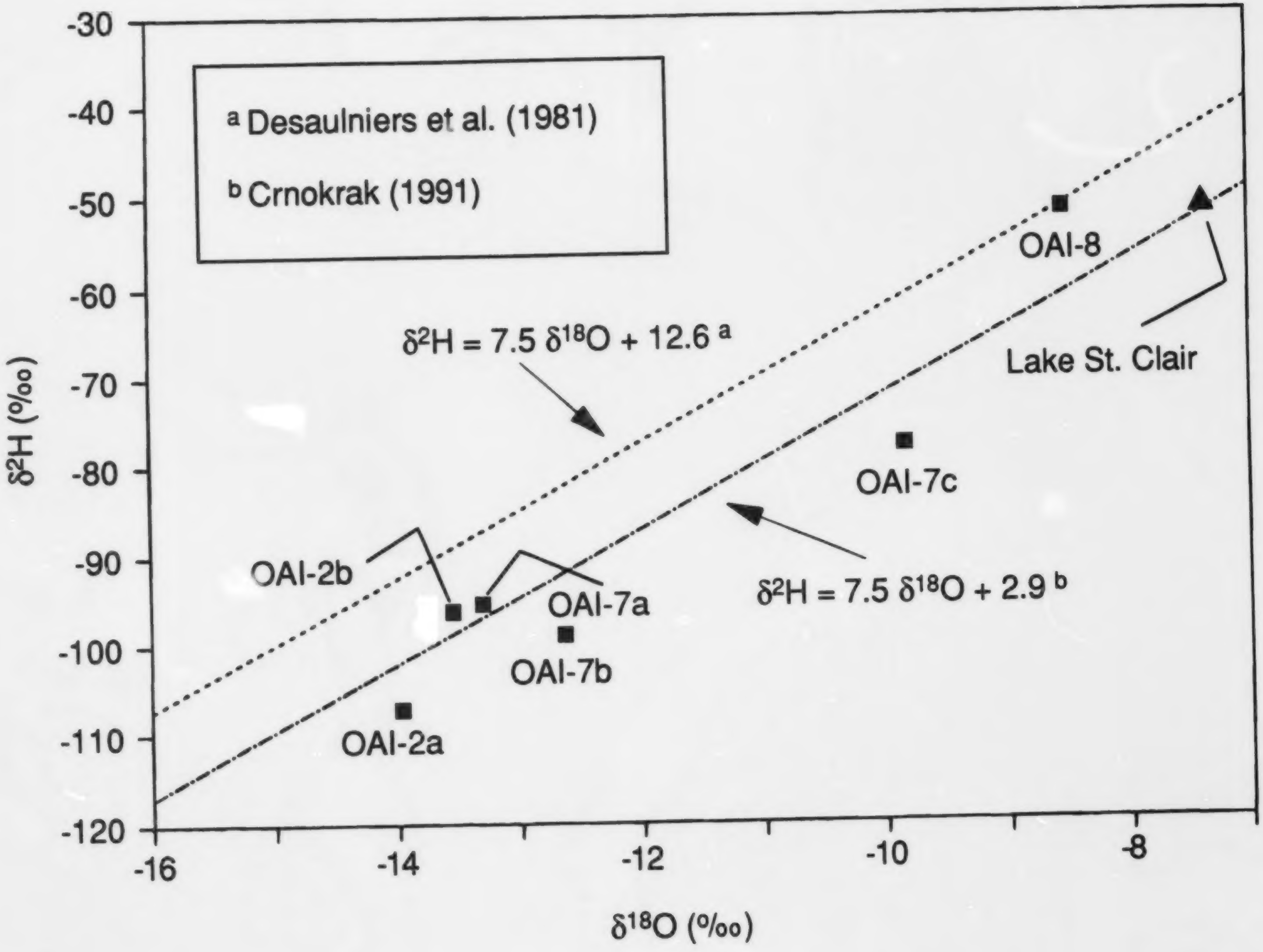

Figure 389.6. ^{18}O and ^{2}H concentrations in groundwater from monitoring wells. Also included are the meteoric water line for southwestern Ontario from Desaulniers et al. (1981), the $\delta^{18}O - \delta^{2}H$ relationship for the freshwater aquifer from Crnokrak (1991), and a Lake St. Clair water sample for comparative purposes.

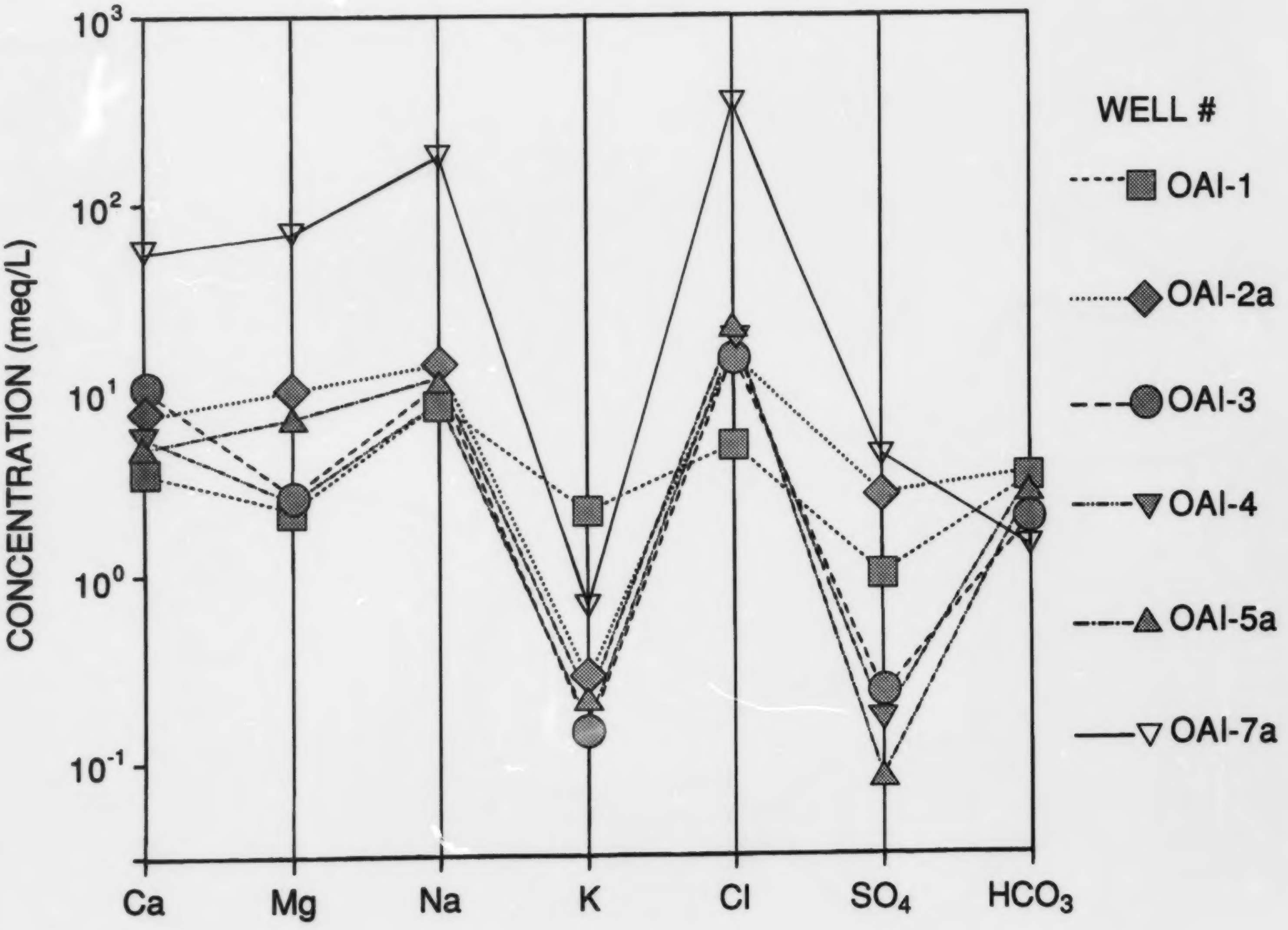

Figure 389.7. Schoeller diagram of groundwater chemistry trends along the feature.

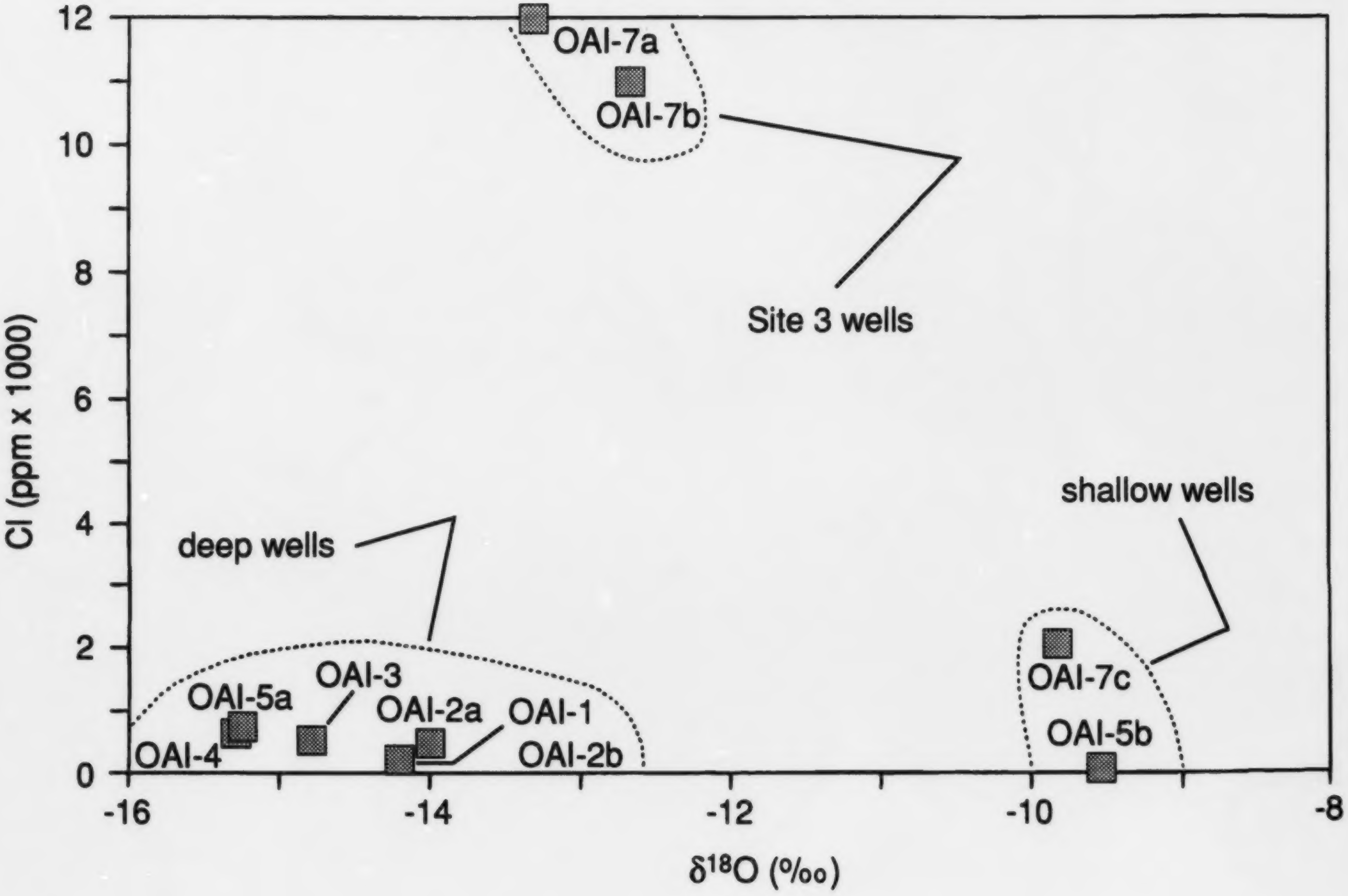

Figure 389.8. Chloride versus ^{18}O concentrations in groundwater from the monitoring wells.

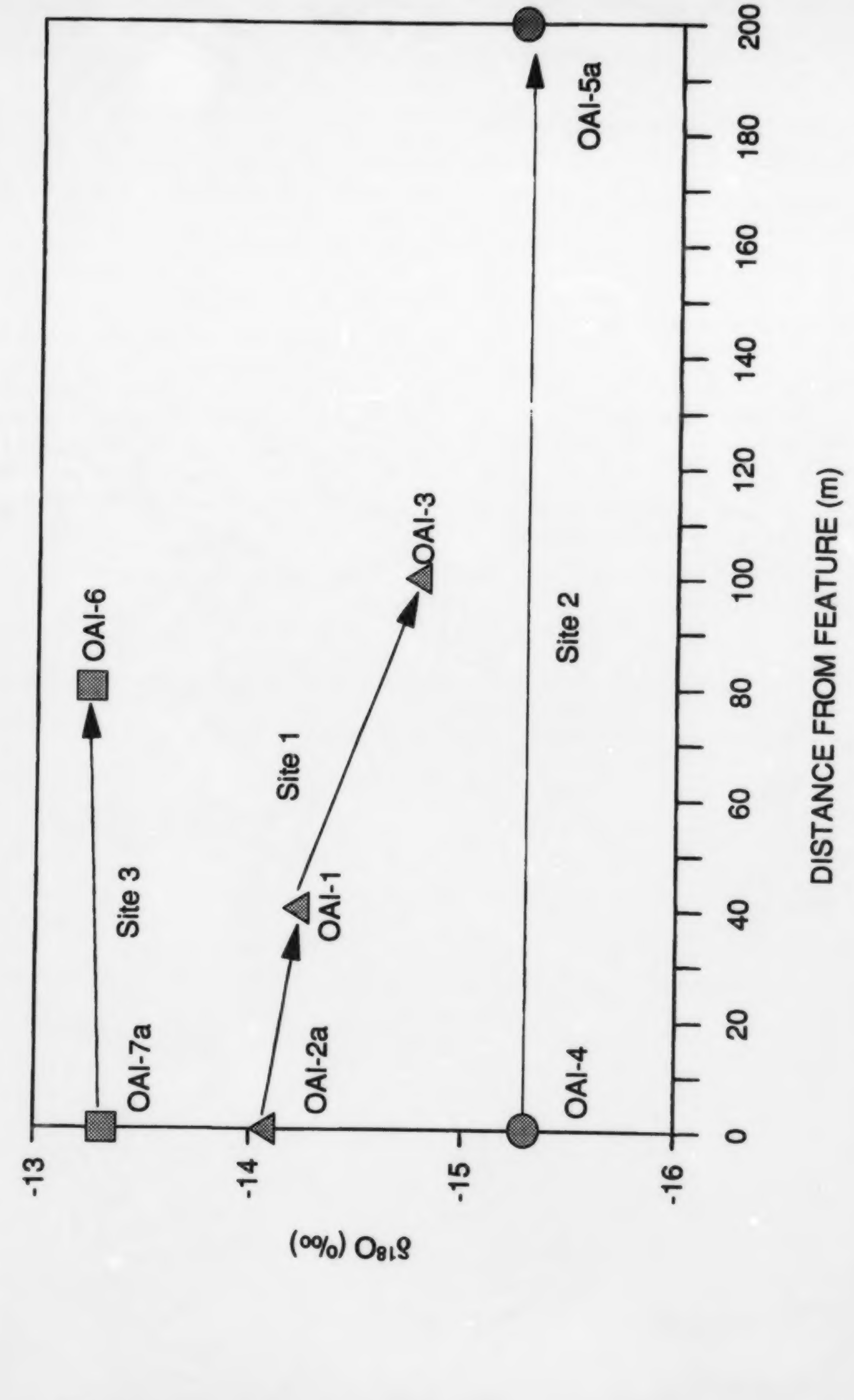

Figure 389.9. ^{18}O trends across the feature.

sively more concentrated waters away from the feature as would be expected if recharge took place on the feature. We obtained similar results at Site 1: the electrical conductivity in the aquifer at the feature (2600 µS/cm at OAI-2a) is greater than those away from the feature (1400 and 1750 µS/cm at OAI-1 and OAI-3, respectively).

Relative Ages of Groundwater in the Till and Aquifer

Figure 389.11 compares the $\delta^{18}O$ values of squeezed porewaters and groundwater samples from wells at each of the transects. In general, the groundwater follows the same trends as reported by Desaulniers et al. (1981): progressively more depleted in ^{18}O with depth, characteristic of older waters recharged under cooler climatic conditions. The close agreement between the squeezed and well samples indicates that the bentonite seals around the wells are effective.

At Site 1, the freshwater aquifer samples (OAI-1, 2a, and 3) have slightly more enriched to the same $\delta^{18}O$ values as the lowermost sample squeezed from the till. This suggests that the freshwater aquifer water is somewhat younger than or the same age as the groundwater at the bottom of the till. Since the freshwater aquifer samples at Site 2 (OAI-4 and 5a) are relatively depleted in ^{18}O compared to the lowermost squeeze samples from the till, and are collinear with the trend in the samples squeezed from the till, the groundwater in the freshwater aquifer is probably somewhat older than the till water. At Site 3, the squeeze sample trend in $\delta^{18}O$ changes from progressively more depleted with depth to progressively more enriched with depth. This trend is consistent with the relatively enriched freshwater aquifer $\delta^{18}O$ values at OAI-6 and 7. Since this site appears to be influenced by brine from deeper formations, the relative ages between the groundwater and the till cannot be determined with the available data.

Results from Target 2

A second target esker which crosses Highway 401 approximately 2.5 km west of Site 1 is being investigated by Ainslie (personal communication) in the companion study sponsored by the Ontario Ministry of the Environment. Ainslie's preliminary drilling results suggest that the second target is a buried esker. His initial hydraulic head, ^{18}O and tritium data indicate that young groundwater surrounds the target and that flow is away from the target.

Table 389.1 Selected hydrometric, geochemical and isotopic data from the monitoring wells.

Sample Number	Well Number	Depth (m)	Distance[1] (m)	Stage[2] (m)	Cl (ppm)	EC[3] (µS/cm)	$\delta^{18}O$ (o/oo)	δ^2H (o/oo)
1	OAI-1	28.0	40	96.79	177	1400	-14.21	
2	OAI-2a	32.0	0	96.47	550	2600	-14.06	-106.50
3	OAI-2b	23.0	0	97.39	39	1063	-13.57	-96.04
4	OAI-2c	7.6	0	98.16	38	1343		-63.79
5	OAI-3	31.0	100	96.54	545	1750	-14.79	
6	OAI-4	37.0	0	96.49	648	1775	-15.29	
7	OAI-5a	37.0	200	96.49	760	2600	-15.26	
8	OAI-5b	6.0	200	97.66	74	3320	-9.57	
9	OAI-6	31.0	80	99.15		18720	-13.24	
10	OAI-7a	32.0	0	99.44	12000	20400	-13.31	-95.51
11	OAI-7b	23.0	0	99.57	11000	24500	-12.66	-98.85
12	OAI-7c	7.6	0	99.94	2100	10300	-9.83	-77.88
13	OAI-D-8[4]	33.0	4200		4920		-7.39[5]	
14	OAI-D-9[4]	37.0			4980		-14.49	
15	OAI-8[6]	2.1					-8.53	-51.77
16	lakewater[7]					-7.37	-51.49	

NOTES

[1] Approximate distance from centre of feature.

[2] Stage is relative to 100 m benchmark for the site.

[3] EC is electrical conductivity.

[4] Domestic well samples.

[5] Probable analytical error.

[6] Shallow well in Site 3.

[7] Tap water sample, represents Lake St. Clair.

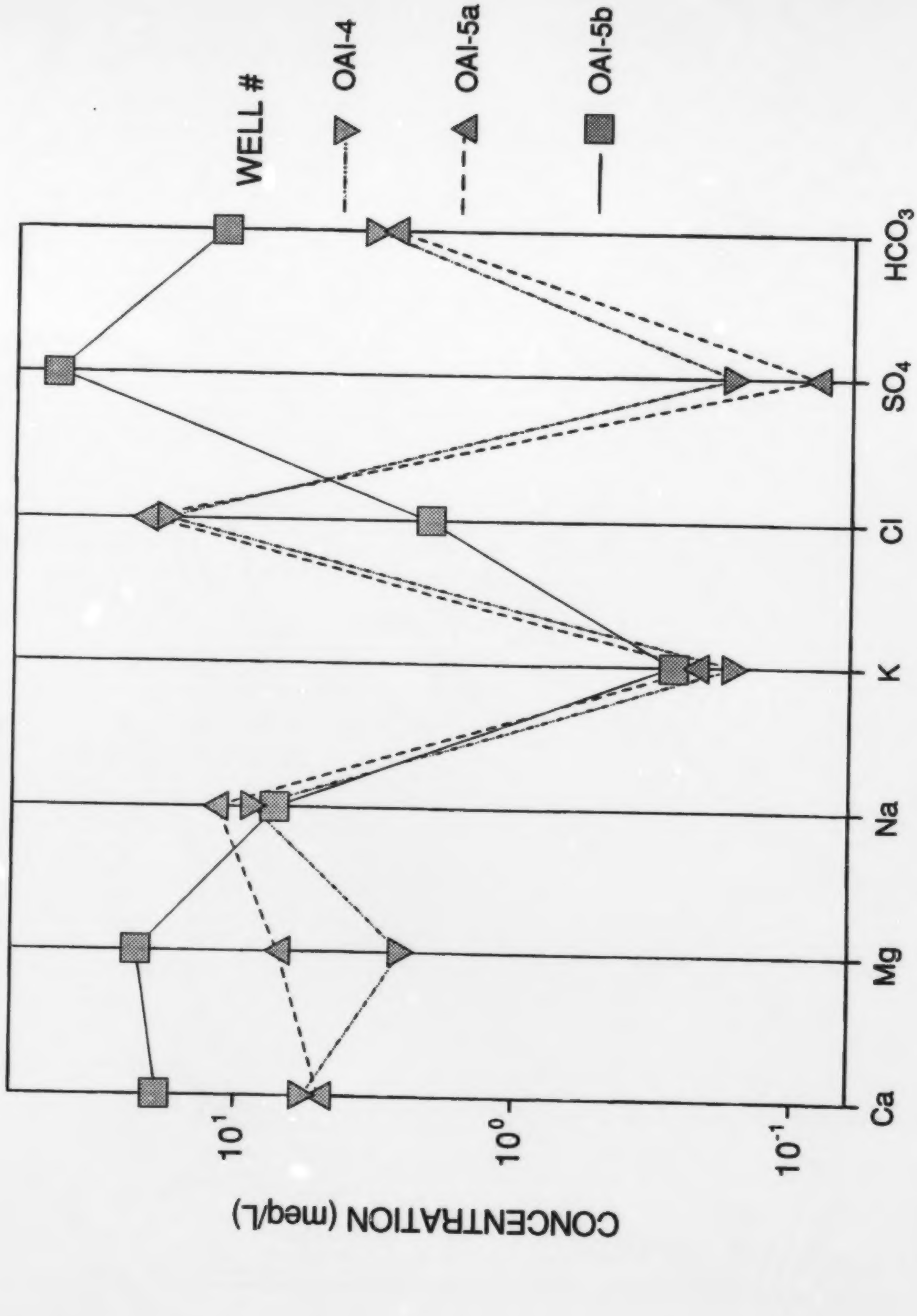

Figure 389.10. Schoeller diagram of groundwater chemistry trends across to the feature at Site 2.

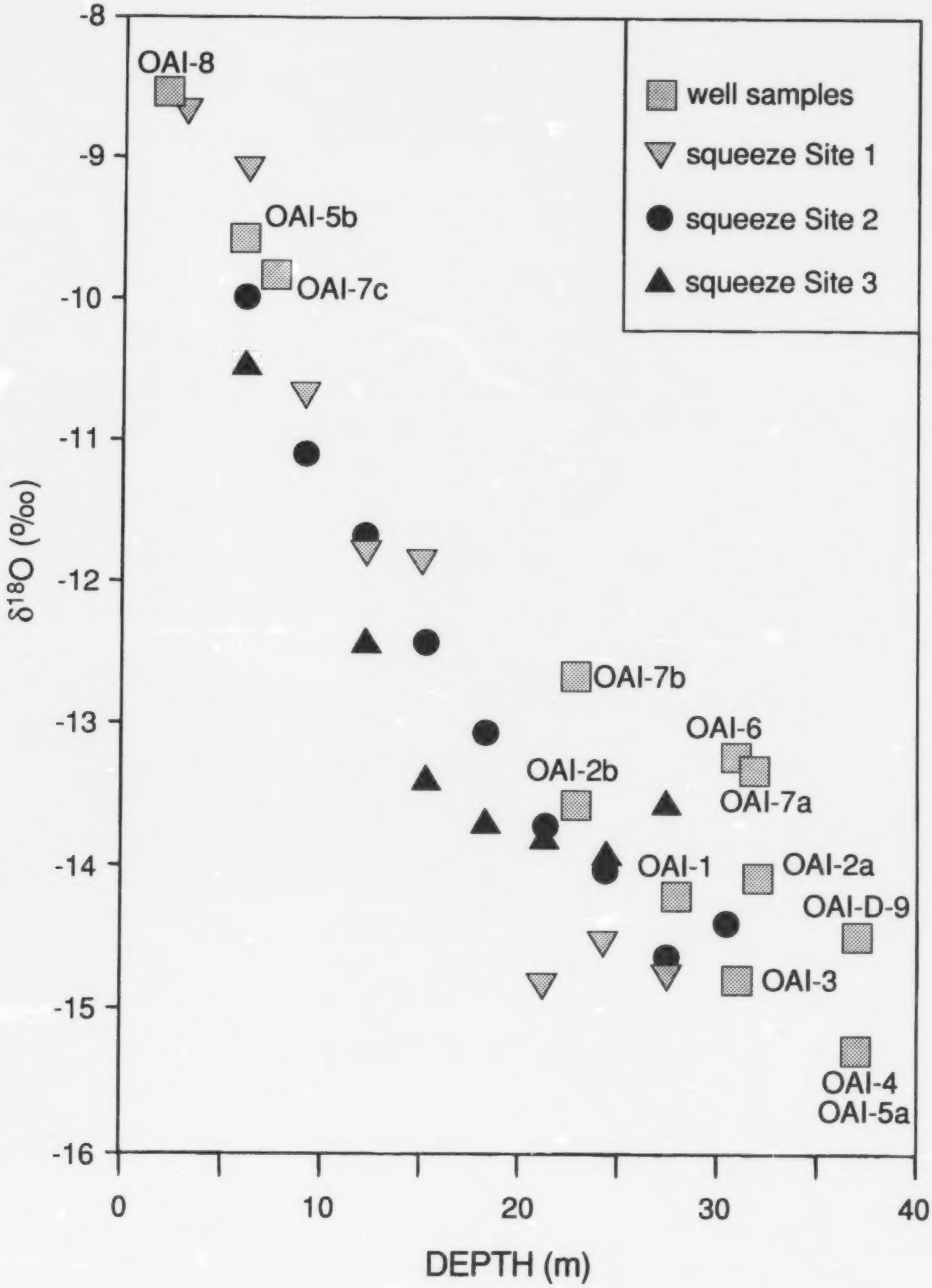

Figure 389.11. Comparison of vertical trends in ^{18}O concentration between groundwater samples from monitoring wells and samples squeezed from soil cores.

CONCLUSIONS

We used a program of drilling, hydrometric monitoring, environmental isotope tracing (^{18}O and deuterium) and natural geochemical tracing to determine: (1) if one of the features noted by Morris (1989) in central Essex County is a buried esker, (2) if the groundwater in the freshwater aquifer around the feature is anomalously young as noted by Crnokrak (1991), and (3) if the groundwater is young, did it arrive vertically from above or laterally along the feature.

Our preliminary results for this target are largely negative. There is no strong geological evidence that the target is a buried esker. Although the vertical hydraulic gradients at all three transects are downward suggesting recharge, horizontal hydraulic gradients perpendicular to the target are inconsistent. The ^{18}O, deuterium and major ion chemistry data indicate that the groundwater in the freshwater aquifer is old and that there is no apparent recharge from nearby Lake St. Clair. These data also suggest that there is no rapid movement of groundwater in the freshwater aquifer along the feature nor away from it. We have yet to reconcile our findings with those of Crnokrak (1991) and Morris (1989).

Although these results are largely negative, the results of a companion study on a nearby feature are largely positive. It appears that this second target is a buried esker and that there may be rapid vertical recharge of the freshwater aquifer along the feature.

The isotopic and geochemical data from this study suggest that the freshwater aquifer near Lake St. Clair is affected by brine from deeper bedrock aquifers.

ACKNOWLEDGEMENTS

We thank Tom Morris of the Ontario Geological Survey for his useful suggestions in planning this project. We are indebted to the Ontario Ministry of Transport, the Township of Rochester, and the residents of Charron Beach Road who permitted us to drill on their right-of-ways and property. Funding from the Ontario Ministry of the Environment, Environmental Youth Corps and Employment Canada SEED programs allowed us to hire additional field assistants for this project. Ontario Geoscience Research Grant 389 made this project possible.

REFERENCES

Allendorf, A. 1981. Susceptibility of Groundwater to Contamination, Windsor-Essex Sheet; Water Resources Branch, Ontario Ministry of the Environment, MOE Map S102.

Chapman, L.J., and Putnam, D.F. 1984. The Physiography of Southern Ontario, 3rd ed.; Ontario Geological Survey, Special Volume 2, 270 p.

Coleman, M.L., Shepherd, T.J., Durham, J.J., Douse, J.E. and Moore, G.J. 1982. Reduction of water with zinc for hydrogen isotope analysis; Analytical Chemistry, v.54, p.993–995.

Craig, H. 1961. Standard for reporting concentrations of deuterium and oxygen-18 in natural waters; Science, v.133, p.1833.

Crnokrak, B. 1991. An environmental isotope investigation of the freshwater aquifer in the St. Clair River – Lake St. Clair – Detroit River corridor; Unpublished M.A.Sc. thesis, University of Windsor, Windsor, Ontario.

D'Astous, A.Y., Ruland, W.W., Bruce, J.G.R., Cherry, J.A. and Gillham, R.W. 1988. Fracture effects in the shallow groundwater zone in weathered Sarnia-area clay; Canadian Geotechnical Journal, v.26, p.43–56.

Desaulniers, D.E., Cherry, J.A. and Fritz, P. 1981. Origin, age and movement of pore water in argillaceous Quaternary deposits at four sites in southwestern Ontario; Journal of Hydrology, v.50, p.231–257.

Dillon, M.M., Ltd. 1987. Essex County Landfill No. 3 Impact Analysis Report, v.11, 137 p.

Dollar, P., Frape, S.K., McNutt, R.H., Fritz, P. and Macqueen, R.W. 1987. Grant 249 Geochemical studies of formation waters from Paleozoicstrata, southwestern Ontario; *in* Geoscience Research Grant program, Summary of Research, 1986–1987; Ontario Geological Survey Miscellaneous Paper 136, p.57–65.

Fritz, P. and Fontes, J.Ch. (Eds). 1980. Environmental isotopes in groundwater hydrology; *in* Handbook of Environmental Isotope Geochemistry, Volume 1, The Terrestrial Environment; Elsevier Science Publishing Company, Amsterdam, 546 p.

Gillespie, J.L. and Dumouchelle, D.H. 1989. Ground water flow and quality near the upper Great Lakes connecting channels, Michigan; United States Geological Survey, Water-Resources Investigations report 88-4232, 82 p.

INTERA Technologies Ltd. 1987. Hydraulic properties of the fresh water aquifer, Sarnia, Ontario; Final report for Environment Canada, National Water Research Institute, 40 p.

Keller, C.K., van der Kamp, G. and Cherry, J.A. 1986. Fracture permeability and groundwater flow in clayey till near Saskatoon, Saskatchewan; Canadian Geotechnical Journal, v.23, p.229–240.

Long, D.T., Wilson, T.P., Takacs, M.J. and Rezabek, D.H. 1988. Stable-isotope geochemistry of saline near-surface ground water: East-central Michigan basin; Geological Society of America Bulletin, v.100, p.1568–1577.

Mellary, A.A. and Nakashiro, M. 1970. Groundwater Probability Map of Essex County; Ontario Water Resources Commission, Division of Water Resources, Map 3107-1.

Morris, T.F. 1988. Project Number 88-4. Quaternary geology of Essex County, southern Ontario; *in* Summary of Field Work and Other Activities in 1988; Ontario Geological Survey Miscellaneous Paper 141, p.399–401.

—— 1989. Project Number 88-4. Quaternary geology of Essex County, southern Ontario; *in* Summary of Field Work and Other Activities in 1989; Ontario Geological Survey Miscellaneous Paper 146, p.199–201.

Ontario Ministry of the Environment. 1984. Water Well Records for Ontario – Essex County 1946-1984; Bulletin 2–19, Groundwater Series, Toronto.

Orpwood, T.G. 1984. An evaluation of methods used to measure groundwater flow and transport characteristics in clayey deposits of two sites in Essex County, Ontario; Unpublished M.A.Sc. thesis, University of Windsor, Windsor, Ontario, 204p.

Telford, P.G. and Russell, D.J. 1981. Paleozoic Geology of the Windsor–Essex and Pelee Island Area, Southern Ontario; Ontario Geological Survey, Preliminary Map P.2396, scale 1:250 000.

Vagners, U.J. 1972. Quaternary Geology of the Windsor–Essex Area (Eastern Part), Southern Ontario; Ontario Department of Mines and Northern Affairs, Preliminary Map P.750, scale 1:50 000.

Vagners, U.J., Sado, E.V. and Yundt, S.E. 1973. Drift Thickness of the Windsor-Essex Area (Eastern Part), Southern Ontario; Ontario Division of Mines, Preliminary Map P.815, Drift Thickness Series, scale 1:50 000.

Grant 393 Metamorphic Petrology and Alteration Assemblages of the Hemlo Gold District

Yuanming Pan and Michael E. Fleet

Department of Geology, University of Western Ontario, London N6A 5B7

The C zone of the Williams mine and the North, South and Highway zones of the Golden Sceptre Resources property represent a diffuse westward extension of the main orebody of the Hemlo gold deposit. Similar to the main orebody, the North zone is situated approximately along the boundary between underlaying felsic rocks and overlying metasedimentary rocks. The principal ore-bearing rock of the North zone contains abundant phlogopite, carbonates and tremolite. In contrast, the C zone is entirely within the felsic rocks and is associated with intensively sheared lenses, in which mica schist with abundant relict quartz and oligoclase phenocrysts was apparently derived from the felsic host rocks.

A late calc-silicate alteration is characterized by mineral assemblages of epidote-group minerals, titanite, calcic amphibole, allanites, vesuvianite, pumpellyite, prehnite and armenite in the Golden Giant mine and of calcic amphibole, clinopyroxene, titanite and carbonates in the diffuse westward extension. Mineral equilibria suggest that this late calc-silicate alteration event occurred at about 300-400°C, < 2 kbar and in an aqueous fluid, and that XCO_2 increased from the Golden Giant mine to the diffuse westward extension. Values of $\log(f_{HF}/f_{H_2O})$ and $\log(f_{HCl}/f_{H_2O})$ calculated from compositions of phlogopite range from -5.1 to -6.0 and -4.2 to -4.8, respectively. Fluid-inclusion study on quartz and carbonate grains of the calc-silicate assemblages supports P-T-X estimates from mineral equilibria and suggests that the hydrothermal fluid responsible for this late calc-silicate alteration event probably resulted from mixing of a hot, saline solution with a cool, dilute solution. Native gold grains have been observed in direct association with calc-silicate assemblages in both the Golden Giant mine and the diffuse westward extension.

Two types of green mica schist occur in the Hemlo-Heron Bay greenstone belt. Chromium(Cr)-enriched green mica schist occurs in the Hemlo gold deposit and in the barite-rich occurrence to the west of the deposit. Geochemical characteristics, along with field relations and textural evidence, indicate that Cr-enriched green mica schist was most likely derived hydrothermally from mafic-ultramafic precursors. Vanadium(V)-enriched green mica schist appears to be restricted to the Hemlo deposit and contains a large number of unusual V-rich oxides and silicates. It is geochemically distinct form its Cr-enriched counterpart but is similar to quartz-oligoclase porphyritic host rocks.

The available data on structure, U-Pb geochronology, metamorphism, and hydrothermal alteration permit a reconstruction of the evolutionary history of the Hemlo-Heron Bay greenstone belt. Gold mineralization in the Hemlo gold deposit was broadly contemporaneous with a late calc-silicate alteration event, which was at least 30 Ma younger than the peak thermal metamorphism of the region.

INTRODUCTION

The Hemlo gold deposit contains approximately 80 Mt of ore at an average grade of 7.7 g/t Au (Harris 1989) and hosts the three biggest gold mines in current production in Canada: namely the Williams mine (Williams Operating Cooperation), the Golden Giant mine (Hemlo Gold Mines Incorporated), and the David Bell mine (Teck-Corona Operating Cooperation). The geology, mineral chemistry, geochemistry and metallogenic association of the main orebody have been described by Muir (1982), Cameron and Hattori (1985), Burk et al. (1986), Hugon (1986), Kuhns et al. (1986), Valliant and Bradbrook (1986), Walford et al. (1986), Muir and Elliott (1987), Corfu and Muir (1989a, 1989b), White and Barnett (1990), and Thode et al. (1991). However, the geological complexity of the Hemlo gold deposit as a whole, particularly in respect to its association with host rocks of high-intensity deformation, medium-grade metamorphism and pervasive alteration, has caused a lack of consensus among investigators regarding the style and timing of gold mineralization. As a result, almost all known ore-forming processes have been proposed for the gold mineralization in this deposit (Macdonald 1986).

The present study is a systematic investigation of the metamorphic petrology, mineral chemistry, geochemistry and rock-fluid interactions of the Hemlo gold district, with emphasis on the C zone of the Williams mine and the North zone of the Golden Sceptre Resources Limited property. This study follows on from our previous work on the nearby White River gold prospect of LAC Minerals Ltd., summarized in Fleet and Pan (1990).

GEOLOGICAL SETTING

The Hemlo gold deposit is situated within the late Archean (2800-2600 Ma; cf. Corfu and Muir 1989a, 1989b) Hemlo-Heron Bay greenstone belt, which is part of the larger east trending Schrieber-White River belt of the Wawa subprovince of the Superior Structural Province (Muir 1982). The geology of the Hemlo-Heron Bay greenstone belt, particularly the Hemlo mining district, has been studied extensively (Muir 1982, 1988; Macdonald 1986; Muir and Elliott 1987; Harris 1989; Corfu and Muir 1989a, 1989b; Fleet and Pan 1990; Thode et al. 1991).

The Hemlo-Heron Bay greenstone belt is comprised mainly of a sequence of highly deformed and metamorphosed volcanic and volcaniclastic sedimentary rocks, bordered by two granitoid complexes (the Pukaskwa Gneissic Complex to the south and the Gowan Lake Pluton to the north) and intruded by two granodiorites (the Heron Bay Pluton to the west and the Cedar Lake Pluton to the east) along its central axis. Muir (1982) has divided the supracrustal rocks into two groups near Heron Bay: the Playter Harbour Group (consisting of mainly tholeiitic basalt with subordinated intermediate to felsic tuffs and siltstone) to the south and the Heron Bay Group (consisting of mainly calc-alkalic pyroclastic rocks, tholeiitic basalt and calc-alkalic basalt) to the north.

Based on geochronological data, Corfu and Muir (1989a) suggested that the Hemlo-Heron Bay greenstone belt may represent two tectonically-contrasting terrains bordered by the Hemlo fault zone. Also, Corfu and Muir (1989a) recognized at least three generations of plutonism corresponding to major igneous bodies of the region: 2719 Ma to a marginal zone of the Pukaskwa Gneissic Complex, 2688-2684 Ma to the Heron Bay Pluton and the Cedar Lake Pluton, and 2678 Ma to the Gowan Lake Pluton.

All supracrustal rocks of the Hemlo-Heron Bay greenstone belt have been subjected to a complex history of deposition, magmatism, deformation, metamorphism and alteration. Muir and Elliott (1987) identified four generations of structures produced by at least two phases of deformation. Burk et al. (1986) and Fleet and Pan (1990) suggested that all supracrustal rocks have been subjected to at least two episodes of regional metamorphism. Fleet and Pan (1990) reported that an early regional metamorphism peaked at about 6 kbar and 500°C and was followed by a regional thermal metamorphism that climaxed at about 4 kbar and 580°C. Fleet and Pan (1990) also delineated a protracted phase of skarn development, which commenced during the waning of the regional thermal metamorphism along regional structural lineaments and terminated with a pervasive calc-silicate alteration at about 350°C and 1.5 kbar.

The Hemlo gold deposit is situated within the Heron Bay group of Muir (1982) and is contained within a major ductile, dextral shear zone (the Hemlo shear zone, Hugon 1986) at the lithological boundary between footwall felsic rocks and hanging-wall metasedimentary rocks (Burk et al. 1986; Kuhns et al. 1986; Valliant and Bradbrook 1986, Walford et al. 1986). The host rocks of the main orebody strike approximately 110° to 115° and dip 60° to 70° northeast. Metamorphic grade in the vicinity of the Hemlo gold deposit is middle-amphibolite facies, as indicated by the presence of garnet, sillimanite, kyanite, and staurolite in metapelitic rocks (Burk et al. 1986) and of tschermakitic/pargasitic hornblende, almandine garnet, and andesine in metabasites (Fleet and Pan 1990).

EXPERIMENTAL PROCEDURES

Over three hundred samples were collected from the Hemlo gold deposit and elsewhere in the Hemlo-Heron Bay greenstone belt during the first summer (1990) of the present study. Both surface samples and diamond-drill core materials were collected for the C zone of the Williams mine, and surface samples for the North and Highway zones of the Golden Sceptre Resources Limited property were also collected. Samples for the Golden Giant mine were obtained from an underground visit and diamond-drill core materials from the University of Western Ontario (Goad 1987). Elsewhere in the Hemlo-Heron Bay greenstone belt, surface samples were collected from a large number of localities and were complemented by diamond-drill core materials from the Core Library of the Ontario Ministry of Northern Development and Mines, Thunder Bay.

Mineral assemblages were examined by a combination of transmitted- and reflected-light microscopy, X-ray diffraction and electron-microprobe analysis. Chemical compositions of selected mineral grains were determined with a JEOL JXA-8600 Superprobe electron microprobe at the University of Western Ontario (operated at 15 kV, 10 nA, 20 second counts, 2-5 µm beam diameter, with minerals, pure metals and synthetic glasses as standards). X-ray-diffraction studies were performed on a Rigaku powder diffractometer (Cu $K\alpha$ radiation), a Gandolfi camera (Cr $K\alpha$ radiation), and a precession camera (Mo $K\alpha$ radiation). Whole-rock geochemical compositions were carried out at the X-Ray Assay Laboratories, Don Mills, Ontario. Major element oxide and S contents were determined by X-ray fluorescence spectrometry (XRF), Mo, Co, Ni, by inductively-coupled plasma spectrometry (ICP), V and Tl by directly-coupled plasma spectrometry (DCP), Au, Pt and Pd by a combination of fire-assay (FA) and DCP, La, Ce, Nd, Sm, Eu, Tb, Yb, Lu, As, Sb, Cs, Rb, Sr, Sc, Hf, Zr, Ta, Nb, Th, U by instrumental neutron activation analysis (INAA). Fluid-inclusion study was carried out on a LINKAM TH600 programmable heating-cooling stage operated according to the guidelines of Macdonald and Spooner (1981).

THE DIFFUSE WESTWARD EXTENSION OF THE HEMLO GOLD DEPOSIT

The diffuse westward extension of the main orebody includes the C zone of the Williams mine and the North, South and Highway zones of the Golden Sceptre Resources

Limited property (*see* Figure 393.1). The C zone and the North zone are currently being mined as open-pit operations.

The C Zone of the Williams Mine

The C zone of the Williams mine is located at the west end of the Williams property, and is strata-bound within the felsic rocks (*see* Figure 393.1; Valliant and Bradbrook 1986; Walford et al. 1986). It consists of a number lenticular, siliceous gold-bearing units with a total strike length of up to 300 m and thickness attaining 25 m. The C zone has a total reserve of 3.9 Mt grading 3.98 g/t Au (Valliant and Bradbrook 1986).

The felsic rocks enclosing the C zone are similar to their counterparts which underlain the main orebody and are mainly composed of quartz and oligoclase phenocrysts, with fine-grained quartz, microcline and albite, muscovite and pyrite as groundmass. The ore-bearing bodies of the C zone are commonly seen to be intensively sheared lenses on surface outcrops (*see* Photo 393.1) or thin layers, in which muscovite schist, microcline gneiss and green mica schist are the most common lihtologies. Generally, these ore-bearing rocks retain a porphyritic texture which is represented by abundant large grains of quartz and oligoclase (*see* Photo 393.3; Walford et al. 1986, Muir 1988, Harris 1989), and are apparently derived from their host rocks, as indicated by textural evidence and trace-element geochemistry (discussed below). All ore-bearing rocks of the C zone commonly contain abundant calc-silicate aggregates (*see* Photo 393.4) or veins. Representative compositions of minerals from the C zone are given in Table 393.1.

The large quartz and oligoclase grains in the ore-bearing rocks of the Hemlo gold deposit have been referred to as "clasts" or "eyes" by local geologists. In the C zone, these

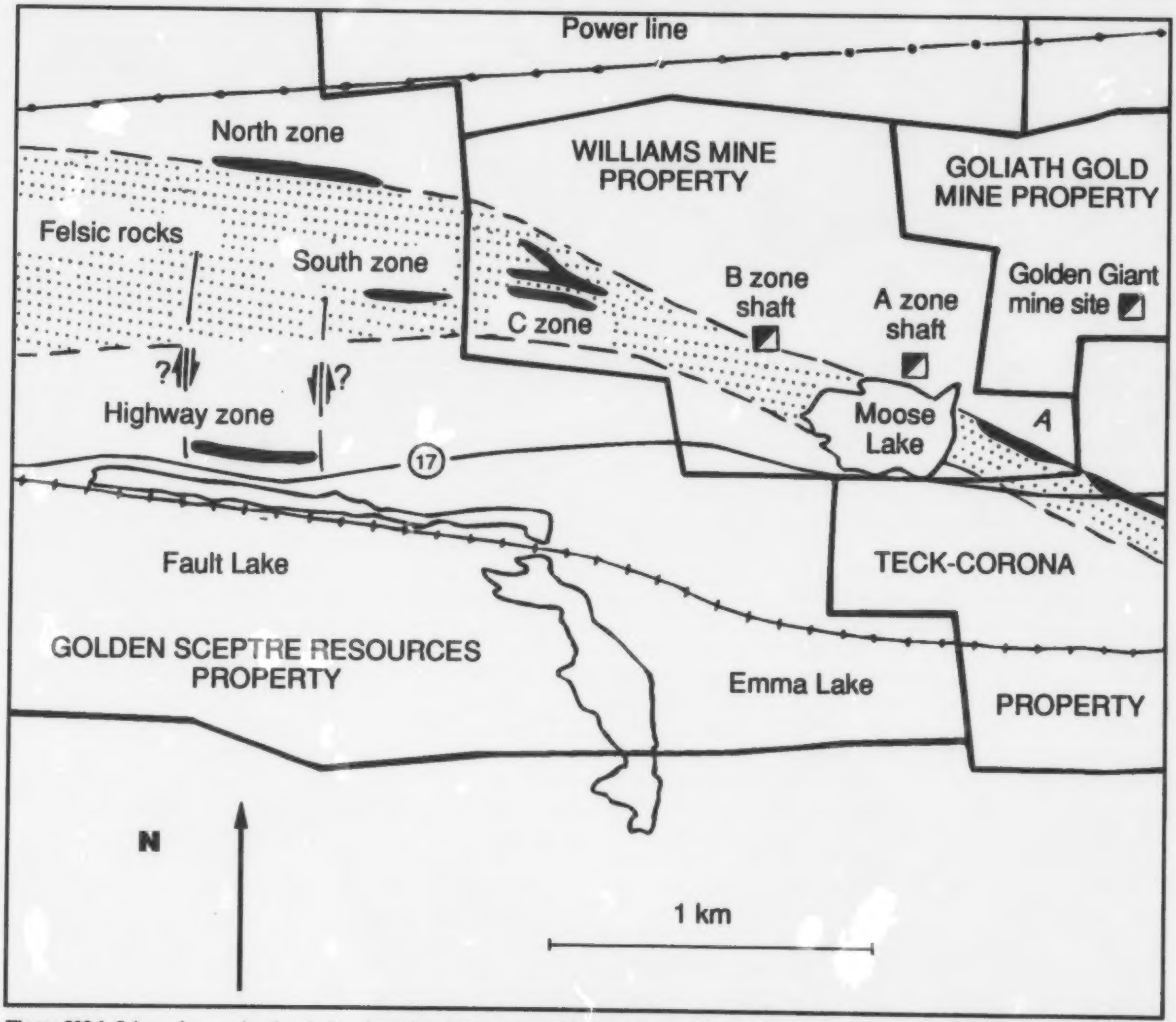
Power line
North zone
WILLIAMS MINE PROPERTY
GOLIATH GOLD MINE PROPERTY
Felsic rocks
South zone
C zone
B zone shaft
A zone shaft
Golden Giant mine site
?
?
Highway zone
Moose Lake
A
17
Fault Lake
TECK-CORONA
GOLDEN SCEPTRE RESOURCES PROPERTY
Emma Lake
PROPERTY
N
1 km

Figure 393.1. Schematic map showing the locations of surface ore zones (black) of the Hemlo gold deposit: felsic host rocks are stippled, hanging-wall metasedimentary rocks to the north are in white, lithologies to the south of the felsic rocks are not differentiated (modified from Muir 1989). The possible relationship between Highway zone and South zone is suggested by faulted section along Trans-Canada Highway 17.

Table 393.1. Representative mineral compositons of the C zone.

Mineral	**plagioclase**		**calcic amphibole**		**clinopyroxene**		**titanite**	**chlorite**	**talc**	**phlogopite**
Sample			**W8840 /147c**	**W8840 /147m**	**W8840 /147c**	**W8840 /147m**	**W8840 /147**	**W8840 /98**	**W8840 /98**	**W8840 /98**
SiO_2 (wt. %)	64.37	64.68	58.73	53.32	55.12	52.50	31.32	31.95	40.56	61.45
TiO_2			0.00	0.00	0.00	0.11	32.81	0.00	1.38	0.00
Al_2O_3	22.61	22.66	0.90	2.41	0.38	1.90	4.95	16.31	16.37	0.36
V_2O_3			0.00	0.00	0.00	0.11	0.00	0.00	0.00	0.00
FeO*			1.71	15.68	3.21	10.60	0.33	7.65	4.60	3.12
MnO			0.07	0.25	0.75	0.52	0.02	0.17	0.03	0.00
MgO			23.28	13.57	16.31	10.58	0.10	30.27	21.16	30.12
CaO	3.38	3.40	13.96	11.84	25.99	23.81	29.23	0.00	0.02	0.00
BaO	0.04	0.00	0.00	0.00	0.00	0.03	0.31	0.00	0.11	0.00
Na_2O	9.42	9.52	0.10	0.43	0.15	0.39	0.00	0.00	0.13	0.00
K_2O	0.00	0.00	0.01	0.11	0.02	0.00	0.03	0.00	10.06	0.00
F			0.00	0.00	0.00	0.00	0.90	0.00	0.54	0.00
Cl			0.00	0.00	0.00	0.00	0.03	0.00	0.02	0.00
F, Cl=0			0.00	0.00	0.00	0.00	0.39	0.00	0.23	0.00
Total	**99.82**	**100.3**	**98.76**	**97.61**	**102.0**	**100.5**	**99.64**	**86.35**	**94.72**	**95.05**
on the basis of	**8 (O)**		**23 (O)**		**6 (O)**		**4 (Si)**	**14 (O)**	**11 (O)**	**23 (O)**
Si	2.837	2.838	7.932	7.780	1.986	1.973	4.000	3.098	5.787	3.952
^{IV}Al	0.163	0.162	0.068	0.220	0.014	0.027		0.902	2.213	0.027
^{VI}Al	1.011	1.010	0.076	0.195	0.002	0.057	0.657	0.962	0.540	0.000
Ti			0.000	0.000	0.000	0.003	3.150	0.000	0.148	0.000
V			0.000	0.000	0.000	0.003	0.000	0.000	0.000	0.000
Fe			0.193	1.913	0.097	0.333	0.036	0.620	0.548	0.167
Mn			0.008	0.031	0.023	0.017	0.002	0.014	0.003	0.000
Mg			4.686	2.952	0.876	0.593	0.020	4.373	4.503	2.889
Ca	0.160	0.160	2.020	1.851	1.003	0.959	4.000	0.000	0.003	0.000
Ba	0.008	0.000	0.000	0.000	0.000	0.000	0.016	0.000	0.005	0.000
Na	0.805	0.810	0.026	0.122	0.010	0.028	0.000	0.000	0.036	0.000
K	0.000	0.000	0.002	0.020	0.001	0.000	0.004	0.000	1.835	0.000
F			0.000	0.000	0.000	0.000	0.363	0.000	0.244	0.000
An (%)	16.4	16.5								
Fe/(Fe + Mg)			0.04	0.39	0.10	0.36		0.12	0.11	0.05

c denotes analysis on grain core.
m denotes margin.
wt. % is weight percent.
* is total iron content.

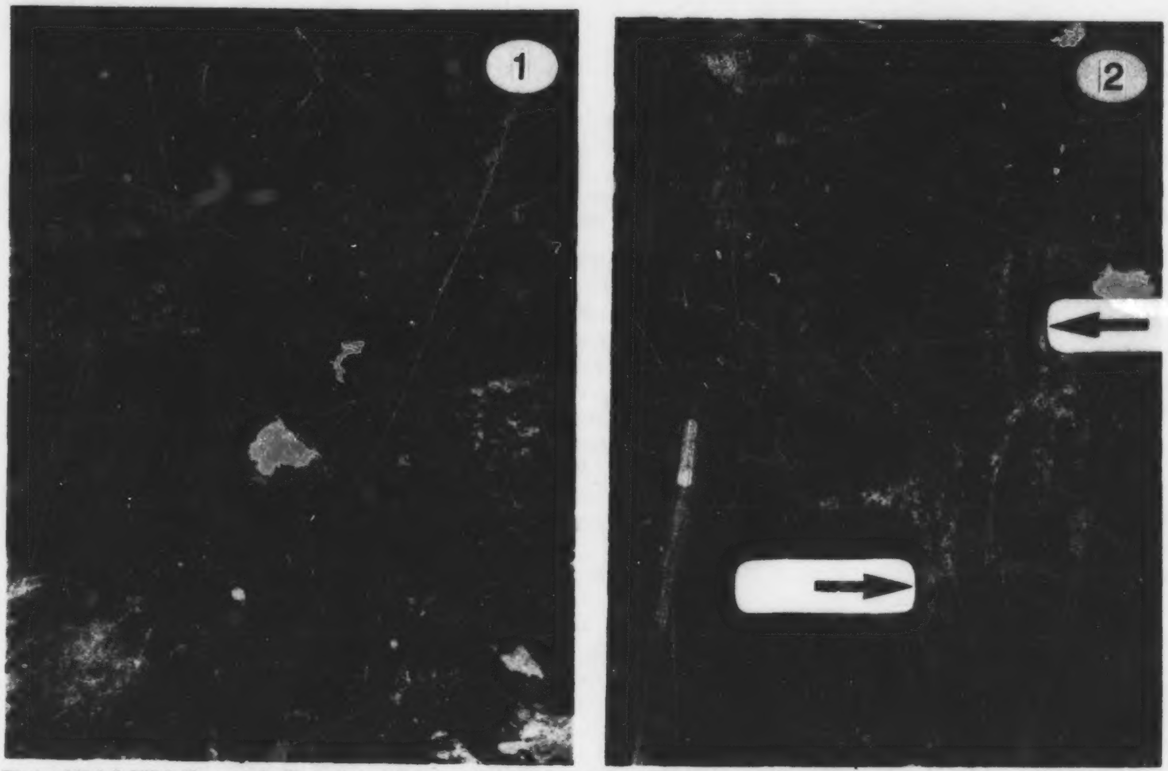

Photos 393.1 & 393.2. Photographs illustrating rocks, minerals and their textures in the Hemlo gold deposit: 393.1) intensively sheared lens (outlined) within less deformed felsic rocks from the C zone, 393.2) phlogopite- (black), carbonate- (white) and tremolite-rich rocks of the North zone.

quartz and oligoclase grains in the ore lenses are flattened and oriented parallel to the schistosity (*see* Photo 393.3). In quartz grains, deformation is also reflected by severe undulated extinction. Oligoclase grains (An16, Table 393.1) are commonly altered partly to sericite and, locally, display undulated extinction. Both albite and Carlsbad twins are common in oligoclase grains and exhibit curved twin boundaries. Locally, myrmekitic texture has also been observed in oligoclase grains from the C zone. Although myrmekitic texture is commonly considered to have resulted from post-magmatic or post-consolidation reactions, it is generally confined to igneous rocks. Myrmekitic texture also occurs in metamorphic rocks (Ashworth 1986). In the Hemlo area, myrmekitic texture has not been observed in rocks of metamorphic origin (cf. Fleet and Pan 1990).

The felsic rocks of the C zone, as in many other parts of the Hemlo gold deposit, are commonly intruded by quartz-oligoclase porphyritic dikes. These dikes cross-cut each other, indicating multiple generations, but are remarkably similar in composition and texture. Various degrees of both deformation and alteration are observed in most quartz-oligoclase porphyritic dikes, but there are some that show only microscopic alteration with little or no evidence of deformation. The C zone and its host felsic rocks are also intruded by north trending and steeply dipping Proterozoic diabase dikes and lamprophyre dikes. On the surface, the economic mineralization of the C zone is concentrated between three diabase dikes (Walford et al. 1986).

Representative whole-rock compositions of various rock types from the C zone are reported in Table 393.2. Similar to the main orebody (cf. Cameron and Hattori 1985; Harris 1989; Thode et al. 1991), anomalously high concentrations of V, Mo, Ba are associated with some ore-bearing rocks of the C zone. However, the As, Sb and Tl contents are considerably lower than these in the main orebody. Ore-bearing rocks of the C zone are remarkably similar in their low 3d-transition metals to their host felsic rocks (*see* Table 393.2), with exceptions of V and Cr in green mica schist (Pan and Fleet 1991c, and described below). The ore-bearing rocks and their host rocks of the C zone are also characterized by low total rare-earth-element abundances, compared to most supracrustal rocks of the Hemlo-Heron Bay greenstone belt (*see* Table 393.2; cf. Fleet and Pan 1990; Pan et al. 1991a).

Visible gold grains, along with gold tellurides, are locally abundant in small quartz veins on surface outcrops of the C zone. In the present study, maximum gold values from the C zone tend to correlate with samples containing abundant calc-silicate aggregates, as indicated by high Ca concentration (*see* Table 393.2). Carbonate-rich rocks without calc-silicates are not significantly enriched in Au (*see* Table 393.2).

The North Zone of the Golden Sceptre Resources Limited Property

The Golden Sceptre Resources Ltd. property of the Hemlo Gold Mines Incorporated is located to the west of the Williams

Table 393.2. Representative whole-rock compositions of the C zone.

Sample	**[illegible]0 [illegible]3**	**18840 /80**	**18840 /96**	**18840 /98**	**18840 /112**	**18840 /123**	**18840 /143**	**18840 /144**	**18840 /147**
SiO_2 (wt. %)	59.3	70.6	67.5	35.0	77.3	46.0	53.4	15.9	68.2
TiO_2	0.58	0.46	0.50	0.16	0.11	0.27	0.44	0.03	0.33
Al_2O_3	17.4	14.4	18.3	2.70	2.82	11.6	15.1	1.18	12.8
Fe_2O_3*	5.72	1.44	2.28	3.44	6.46	3.00	5.55	2.59	2.13
MnO	0.11			0.12		0.10		0.07	0.07
MgO	2.45	1.79	1.31	5.69	2.26	5.53	4.74	7.95	2.79
CaO	5.12	2.28	0.25	13.5	2.75	11.0	5.54	42.1	4.59
Na_2O	4.39	3.73	0.24	0.37	0.44	1.35	3.21	0.05	6.70
K_2O	1.74	2.69	5.85	1.38	0.91	6.10	4.93	0.08	0.67
P_2O_5	0.25	0.12	0.10	0.02	0.02	0.08	0.07	0.04	0.07
L.O.I.	2.54	1.16	2.62	5.62	3.70	9.62	5.08	28.4	1.77
Total	**100.0**	**100.2**	**99.1**	**84.0**	**99.0**	**96.8**	**98.2**	**98.4**	**100.2**
Au (ppb)	46	42	80	>10000	>10000	1800	690	520	210
S (ppm)	1100	1260	642	39000	8950	8240	12800	5600	2450
As	3	4	2	36	25	12	16	43	2
[illegible]	0.7	1.8	1.0	3.0	1.1	6.1	0.8	0.3	1.4
[illegible]	14	29	16	89	500	132	25	4	30
Tl	<2	<2	<2	<2	<2	<2	<2	<2	<2
Cs	2	4	5	2	<1	1	1	<1	<1
Ba	1150	1040	1200	142000	19500	18700	1000	<10	333
Rb	58	69	116	16	19	64	34	16	20
Sr	1690	106	11	1330	566	475	173	101	188
Cr	270	240	220	130	450	150	180	36	270
V	93	105	92	141	244	121	86	66	48
Sc	10.2	8.4	8.6	2.5	2.1	3.3	6.8	1.4	5.3
Ni	5	34	22	4	12	6	32	<1	8
Co	14	16	21	2	4	7	20	<1	7
Th	5	1	1	<1	<1	1	1	1	1
U	1.0	<0.5	<0.5	<2.0	<1.0	<0.5	<0.5	<0.5	<0.5
Zr	186	109	88	<10	15	80	75	<10	63
Hf	5	3	2		1	2	2	<1	2
Nb	20	17	<10	10	<10	<10	<10	<10	<10
La	57.0	15.7	3.0	2.4	5.1	14.1	10.5	2.6	8.6
Ce	113	31	7	4	8	26	20	5	17
Nd	45	14	<5		<5	10	7	<5	7
Sm	7.9	2.2	0.7	0.3	0.5	1.6	1.4	0.4	1.1
Eu	2.2	0.9	0.4	0.4	0.5	0.7	0.6	0.2	0.5
Yb	3.0	0.7	0.5	<1.0	<1.0	0.3	0.4	<0.2	0.3
Lu	0.44	0.10	0.07	<0.10	<0.10	0.05	0.06	<0.05	0.05

wt. % is weight percent.
Fe_2O_3*, total iron content.
L.O.I., loss on ignition.
ppb, parts per billion.
ppm, parts per million.

property and contains three zones of anomalously-high and yet erratic Au-enrichment, referred to as the North, South and Highway zones (*see* Figure 393.1). The North zone contains approximately 100,000 tonnes of ore averaging 3.42 g/t Au (Goad 1987). The North zone, similar to the main orebody to the east, is essentially situated along the contact between hanging-wall metasedimentary rocks and footwall felsic rocks. The hanging-wall metasedimentary rocks and the footwall felsic rocks of the North zone are generally similar in texture, mineralogy and composition to those in the C zone and the main orebody.

Phlogopite-carbonate schist (*see* Photo 393.2) is the principal ore-bearing rock of the North zone and contains phlogopite (up to 60 %), carbonates (both calcite and dolomite, 70 %), quartz (20 %), oligoclase (30 %), microcline (25 %), and muscovite (10 %). Locally, quartz and oligoclase are also present as relict phenocrysts in the phlogopite-carbonate schist from the North zone, similar to those in the C zone (described above). Phlogopite and carbonates appear to be alteration products (*see* Photo 393.2). Phlogopite in ore-bearing rocks of the North zone appears to have crystallized from two different parageneses. The two generations of phlogopite, one defining schistocity and the other in cross-cutting veins, are generally similar in composition, except for a slightly higher halogen content in the latter. Massive tremolite aggregates are locally abundant and commonly occur along foliation planes. Molybdenite is also locally present and generally occurs on the surface of foliation planes. Carbonates, phlogopite, talc, clinopyroxene, chlorite, titanite, microcline and tourmaline are also common constituent of these tremolite aggregates (*see* Calc-silicate Alteration). In contrast to the main orebody and the C zone, potassic alteration is generally less developed in the North zone, and microcline is only locally abundant and muscovite is generally rare. Representative compositions of minerals from the North zone are listed in Table 393.3.

Representative whole-rock compositions of the North zone are reported in Table 393.4. Barium, and to some extends, S, As, Mo are enriched in the North zone, but V and Cr are generally low, consistent with the absence of green

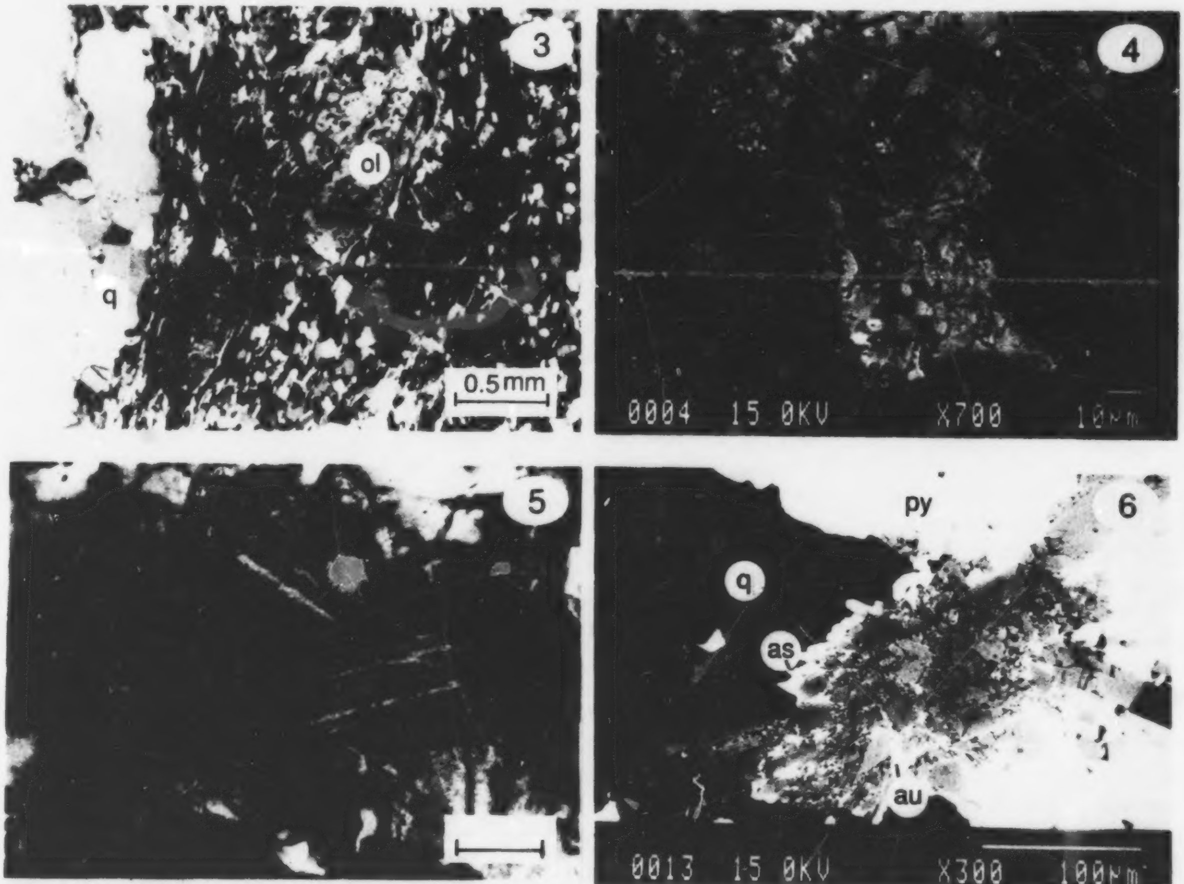

Photos 393.3, 393.4, 393.5 & 393.6. Photomicrographs illustrating rocks, minerals and their textures in the Hemlo gold deposit: 393.3) relict quartz (q) and oligoclase (ol) phenocrysts in V-enriched green mica schist of the C zone, 393.4) calcic amphibole (zoned) and calcite aggregate from the C zone, 393.5) prismatic vanadoan pumpellyite-(mg) with well-developed twin in cross-cutting vein from the Golden Giant mine, 393.6) antimonian vesuvianite aggregate associated with native arsenic (as), native gold (au) and pyrite (py) from the Golden Giant mine.

Table 393.3. Representative mineral compositions of the North zone.

Mineral	**phlogopite**		**calcic amphibole**			**talc**	**titanite**
Sample	**Gsp10**	**Gsp23**	**Gsp10**	**Gsp23 core**	**Gsp23 rim**	**Gsp23**	**Gsp10**
SiO_2 (wt. %)	40.66	40.40	57.12	57.97	58.26	62.95	31.07
TiO_2	0.27	2.00	0.10	0.04	0.01	0.00	32.95
Al_2O_3	15.04	15.30	1.56	0.66	0.81	0.23	4.69
V_2O_3	0.00	0.00	0.00	0.05	0.00	0.00	0.00
FeO*	8.45	7.36	4.71	3.99	4.07	2.11	0.91
MnO	0.01	0.05	0.12	0.10	0.10	0.00	0.05
MgO	21.68	20.91	21.05	22.04	22.05	30.45	0.02
CaO	0.00	0.00	12.83	13.74	13.26	0.00	29.30
BaO	0.00	0.04	0.00	0.01	0.00	0.00	0.35
Na_2O	0.01	0.03	0.46	0.15	0.25	0.00	0.00
K_2O	9.57	10.15	0.13	0.08	0.08	0.00	0.01
F	0.15	0.00	0.00	0.00	0.00	0.00	0.69
Cl	0.00	0.00	0.00	0.00	0.00	0.00	0.01
F,Cl=0	0.06	0.00	0.00	0.00	0.00	0.00	0.29
Total	**95.78**	**96.24**	**98.08**	**98.84**	**98.89**	**95.74**	**99.76**
on the basis of	**22 (O)**		**23 (O)**			**11 (O)**	**4 (Si)**
Si	5.816	5.744	7.874	7.916	7.937	3.991	4.000
^{IV}Al	2.184	2.256	0.126	0.084	0.073	0.009	
^{VI}Al	0.351	0.308	0.128	0.022	0.058	0.009	0.711
Ti	0.030	0.213	0.010	0.004	0.001	0.000	3.189
V	0.000	0.000	0.000	0.006	0.000	0.000	0.000
Fe	1.011	0.876	0.543	0.455	0.464	0.112	0.098
Mn	0.001	0.006	0.014	0.012	0.011	0.000	0.006
Mg	4.623	4.431	4.326	4.487	4.477	2.880	0.004
Ca	0.000	0.000	1.895	2.010	1.935	0.000	4.040
Ba	0.000	0.002	0.000	0.000	0.000	0.000	0.017
Na	0.003	0.009	0.123	0.041	0.065	0.000	0.001
K	1.745	1.841	0.024	0.014	0.015	0.000	0.001
F	0.067	0.000	0.000	0.000	0.000	0.000	0.281
Cl	0.000	0.000	0.000	0.000	0.000	0.000	0.002
Fe/(Fe + Mg)	0.18	0.17	0.11	0.09	0.09	0.04	

wt. % is weight percent.
* is total iron content.

mica schist. In the North zone, visible gold grains are locally present on surface outcrops and have also been found in direct association with tremolite aggregates, but samples analyzed by the present study have gold values lower than 2000 ppb (*see* Table 393.4).

CALC-SILICATE ALTERATION

Mineral Assemblages

Alteration in the Hemlo gold deposit is predominated by potassic varieties, as indicated by abundant microcline and muscovite (cf. Kuhns 1986; Walford et al. 1986; Muir 1988; Harris 1989; and this study). Other alteration styles, such as silicification, carbonization and tourmalinization, are also present in the Hemlo gold deposit, but are generally of limited intensity and only of local significance. A pervasive, late calc-silicate alteration was recognized and suggested to have occurred in spatial and probably temporal association with gold mineralization in a shear zone at the nearby White River gold prospect of LAC Minerals Ltd (Fleet and Pan 1990). A late calc-silicate alteration has also been observed in the hanging-wall metasedimentary rocks of the Williams mine (Walford et al. 1986). The present study demonstrates this calc-silicate alteration also occurred in the Hemlo gold deposit and elsewhere in the Hemlo-Heron Bay greenstone belt.

Harris (1989) reported that calc-silicate minerals, along with carbonates, are generally rare in the main orebody, except for some parts of the David Bell mine. The present study has identified a large number of calc-silicate minerals, including epidote-group minerals, tremolite, titanite, pumpellyite-group minerals, antimonian vesuvianite, garnet, prehnite, and armenite in the Golden Giant mine. Some of these calc-silicate minerals, including pumpellyite-group minerals, antimonian vesuvianite and garnet, appear to be restricted to Vanadium(V)-enriched green mica schist and are characterized by unusually high V concentrations (described below; *see* also Pan and Fleet 1991b, 1991c). With rare exceptions, these calc-silicate minerals occur as mono- or bi-mineralic assemblages, in cross-cutting veins or along foliation planes (*see* Photo 393.5). Multiple-mineral veins are also locally present but are commonly zoned. Native gold grains, along with native arsenic, have been observed locally in direct association with calc-silicate assemblages in the Golden Giant mine; i.e., antimonian vesuvianite aggregates (*see* Photo 393.6).

In the diffuse west extension, calcic amphibole (the tremolite-actinolite series) is the most abundant calc-silicate mineral and occurs, along with calcite, dolomite and locally clinopyroxene (the diopside-hedenbergite series), as massive aggregates in cross-cutting veins or along foliation planes (*see* Photo 393.3). Calcic amphibole and clinopyroxene are predominantly Mg-rich, whereas Fe-rich varieties occur only as thin layers rimming their respective Mg-rich grains (Photo 393.3). Other minerals in these calc-silicate assemblages are phlogopite, talc, titanite, quartz, microcline, albite, barite, apatite, monazite, and sulfides (mainly pyrite and pyrrhotite). As mentioned above, maximum gold values in the C zone tend to correlate with samples containing abundant calc-silicate aggregates. Native gold grains within the calc-silicate aggregates have been observed in both C zone and North zone.

Calc-silicate assemblages, as cross-cutting veins and infilling along foliation planes or small-fold noses, have also been observed at many other localities throughout the Hemlo-Heron Bay greenstone belt, particularly in amphibolites. These calc-silicate assemblages are commonly predominated by epidote, with variable amounts of titanite, prehnite, garnet, actinolite, clinopyroxene, microcline, albite, quartz, calcite and pyrite. At the contact with the Heron Bay Pluton, near Moose Lake on Trans-Canada Highway 17, an assemblage of clinopyroxene, garnet, prehnite, epidote, actinolite, chlorite, titanite, microcline, quartz and pyrite is present as cross-cutting veins within garnet amphibolite. Although chemical analyses of all mineral phases have not yet been completed, preliminary results on element partitioning between mineral pairs (e.g. Fe/Al in the prehnite-garnet pair and the prehnite-epidote pair, Mg/Fe in the clinopyroxene-actinolite pair and the actinolite-chlorite pair) support textural evidence and suggest that this mineral assemblage may have crystallized in equilibrium.

P-T-X-T Constraints

(1) Mineral Equilibria

The stabilities of some of the calc-silicate minerals, such as prehnite, epidote, vesuvianite, pumpellyite, and garnet are reasonably well-known from hydrothermal experiments (Ito and Arem 1970; Taylor and Liou 1978, Schiffman and Liou 1981, Hochella et al. 1982) and from observations on the presently active geothermal fields (Bird et al. 1984). The mineral assemblages described above, similar to those at the White River gold prospect, probably indicate that the calc-silicate alteration in the Hemlo gold deposit likely formed at about 300-400°C, < 2 kbar and in an aqueous fluid (cf. Fleet and Pan 1990). The unusual compositions, such as an extremely high concentration in V, of some calc-silicates in the Gold Giant mine (Pan and Fleet 1991a, 1991b, and 1991c) must be largely attributable to their host-rock geochemistry (discussed below), and may also have some significant influences on their stabilities (cf. Ito and Arem 1970).

The obvious change in mineral assemblage from the main orebody (Golden Giant mine) to the diffuse westward extension (e.g. prehnite-, epidote-, vesuvianite-bearing to tremolite-, phlogopite-dominant) may indicate an increase in X_{CO_2} in the hydrothermal fluid from east to west (cf. Thompson 1971; Taylor and Liou 1978; Hochella et al. 1982). This is also indicated by a marked increase in carbonates of the calc-silicate aggregates from the main orebody to the diffuse

Table 393.4. Representative whole-rock compositions of the North zone.

Sample	**Gsp1**	**Gsp3**	**Gsp5**	**Gsp11**	**Gsp12**	**Gsp16**	**Gsp17**	**Gsp19**	**Gsp23**
SiO_2 (wt. %)	46.7	61.8	59.0	70.0	60.6	59.9	54.7	59.0	69.6
TiO_2	0.30	0.37	0.35	0.31	0.27	0.40	0.37	0.37	0.38
Al_2O_3	9.72	14.3	16.2	13.1	12.6	15.3	16.2	13.9	13.9
Fe_2O_3*	3.66	1.79	1.87	1.27	3.13	3.07	2.01	2.31	0.47
MnO	0.16								
MgO	9.68	3.28	3.36	2.21	4.92	2.97	4.31	4.22	1.34
CaO	15.6	5.51	5.78	3.41	7.40	4.87	7.16	5.16	1.89
Na_2O	3.04	7.27	8.20	6.77	6.92	6.98	6.29	2.75	5.41
K_2O	1.75	1.41	1.32	1.08	0.57	2.63	3.45	6.63	3.19
P_2O_5	0.07	0.08	0.08	0.05	0.06	0.04	0.10	0.08	0.07
L.O.I.	7.24	3.08	2.93	1.85	1.93	2.54	3.93	3.16	1.08
Total	**98.3**	**99.0**	**99.3**	**100.2**	**98.5**	**98.8**	**98.7**	**98.3**	**98.8**
Au (ppb)	480	1600	1800	230	570	570	620	310	100
S (ppm)	1920	1200	1550	1400	4220	4220	3100	711	1250
As	2	3	4	3	4	7	4	4	2
Sb	0.5	0.5	0.5	1.1	1.9	0.7	0.3	0.7	0.8
Mo	344	23	24	14	64	7	10	17	21
Tl	<2	<2	<2	<2	<2	<2	<2	<2	<2
Cs	2	1	1	1	1	2	1	1	<1
Ba	2760	512	1270	624	270	417	1610	5720	12500
Rb	28	33	28	21	23	41	49	58	28
Sr	229	119	179	135	267	150	222	205	403
Cr	73	130	130	190	72	87	86	100	170
V	98	36	73	68	68	89	29	85	18
Sc	9.5	4.0	4.5	3.0	9.6	8.6	5.7	9.0	0.9
Ni	4	4	4	3	10	3	2	4	<1
Co	9	7	8	4	10	8	8	8	14
Th	<1	<1	1	1	1	1	1	1	1
U	<0.5	<0.5	<0.5	<0.5	<0.5	<0.5	<0.5	<0.5	<0.5
Zr	53	68	73	70	63	85	85	81	71
Hf	1	2	1	2	1	1	2	2	2
Nb	<10	11	14	<10	<10	14	<10	<10	17
La	8.1	7.3	7.9	11.0	9.8	7.2	9.6	6.5	7.2
Ce	13	13	13	19	14	14	18	15	14
Nd	6	6	6	7	6	6	7	6	6
Sm	1.2	1.1	0.9	1.2	1.2	1.2	1.3	1.0	0.9
Eu	0.5	0.6	0.6	0.3	0.4	0.5	0.7	0.2	0.5
Yb	0.04	0.4	0.4	0.2	0.4	0.4	0.4	0.4	0.3
Lu	0.05	0.05	<0.05	<0.05	0.07	0.06	0.06	0.06	0.05

wt. % is weight percent.
Fe_2O_3*, total iron content.
L.O.I., loss on ignition.
ppb, parts per billion.
ppm, parts per million.

westward extension and is further directly supported by an increase in the estimated CO_2/H_2O ratio in fluid inclusions in quartz grains (described below).

(2) HF and HCl Fugacities

High halogen concentration is one of the characteristic features of calc-silicates and their associated minerals in the Hemlo gold deposit, indicating that a highly saline fluid was responsible for the calc-silicate alteration event (Pan et al. 1991b). Munoz (1984), based on experimental studies on the temperature and compositional (Fe-Mg-Al) dependence of F = OH and Cl = OH exchange reactions in biotite and phlogopite, has formulated the following expressions to calculate HF and HCl activity in the coexisting hydrothermal solutions.

$$\log(f_{H_2O}/f_{HF}) = 2100/T + 1.52X_{Mg} + 0.42X_{Ann} + 0.20X_{Sid} - \log(X_F/X_{OH})$$

$$\log(f_{H_2O}/f_{HCl}) = 5151/T - 5.01 - 1.93X_{Mg} - \log(X_{Cl}/X_{OH}).$$

Values of $\log(f_{HF}/f_{H_2O})$ and $\log(f_{HCl}/f_{H_2O})$, calculated at a temperature of 350°C and a pressure of 1 kbar (discussed above), show no systematic change from the main orebody and the diffuse westward extension and range from -5.1 to -6.0 and -4.2 to -4.8, respectively. It is noteworthy that a substantial amount of Cl is present only in antimonian vesuvianite in the Hemlo gold deposit. Such a high Cl concentration is most likely attributable to some unknown mineral-structural factor(s), because Cl is remarkably constant at about 1 Cl atom per formula unit (50 cations; cf. Pan and Fleet 1991c) and is known to strongly partition to an aqueous solution.

(3) Fluid Inclusion Study

Quartz and carbonates (calcite and dolomite) in calc-silicate assemblages of the Hemlo gold deposit contain at least four types of primary fluid inclusions (cf. Roedder 1984) according to the number of phases present at room temperature: (Type I) liquid phase, (II) liquid + gas, (III) liquid + gas + one daughter mineral, (IV) liquid + vapour + more than one daughter mineral. Type II inclusions are by far the most abundant primary inclusions in both quartz and carbonates. Halite, as identified optically, is the most common daughter mineral, and the presence of both halite and sylvite in Type IV inclusions in a titanite grain has been confirmed by energy-dispersive analysis. Other unidentified daughter minerals, including some opaque phases, are also present as both Type III and IV inclusions but are generally rare. There is an increase in estimated CO_2/H_2O ratio in inclusions from the main orebody to the diffuse westward extension. Such a trend appears to extend further to the west in the Hemlo-Heron Bay greenstone belt, as CO_2-rich inclusions (double-ringed) have been observed in vein quartz grains from the barite-rich occurrence. The presence of these CO_2 rich inclusions is probably attributable to the abundance of graphitic materials to the west (Pan and Fleet 1991a).

Homogenization temperatures (all to liquid) of primary inclusions in both quartz and carbonate grains show a wide and yet similar range of variation from about 200 to 400°C (*see* Figure 393.2a). It is also noted that there is no significant difference in homogenization temperatures between the main orebody and the diffuse westward extension. Salinity of primary inclusions in both quartz and carbonates, as determined by final melting temperatures of ice (cf. Potter et al. 1978), also has a wide and similar range of variation but appears to be more abundant in two populations at about 10 and 20 equivalent wt. % NaCl, respectively (*see* Figure 393.2b). However, primary inclusions with intermediate values of salinity are present in both quartz and carbonates (*see* Figure 393.2b). Inclusions of higher salinity are commonly higher in homogenization temperature as well (*see* Figure 393.3). Such a linear correlation is commonly attributed to mixing of a hot, saline fluid with a cold, dilute fluid (Craw and Koons 1989).

(4) Timing

It is almost certain that the low- to very-low-grade calc-silicate alteration in the Hemlo gold deposit postdated the regional thermal metamorphism, as the calc-silicate assemblages

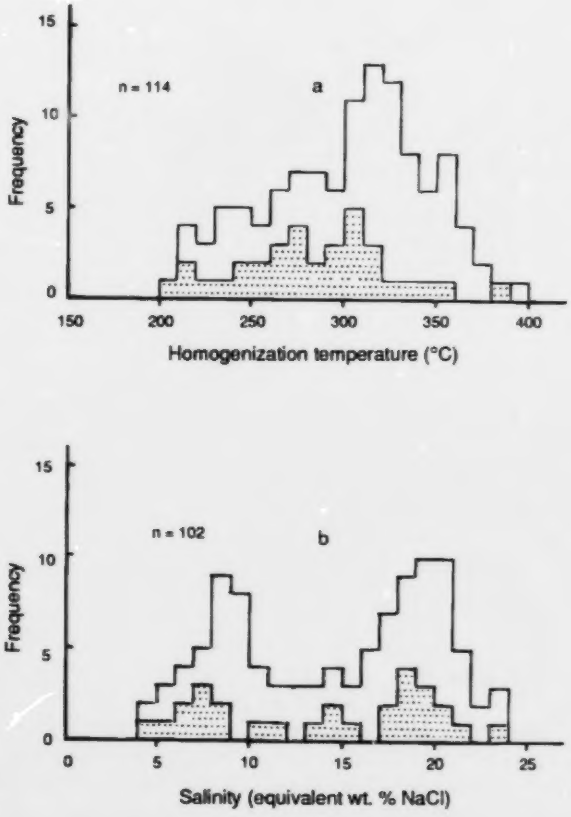

Figure 393.2. Histograms illustrating homogenization temperature (a) and salinity (b) of fluid inclusions in quartz (white boxes) and carbonates (dotted boxes) associated with calc-silicates from the Hemlo gold deposit.

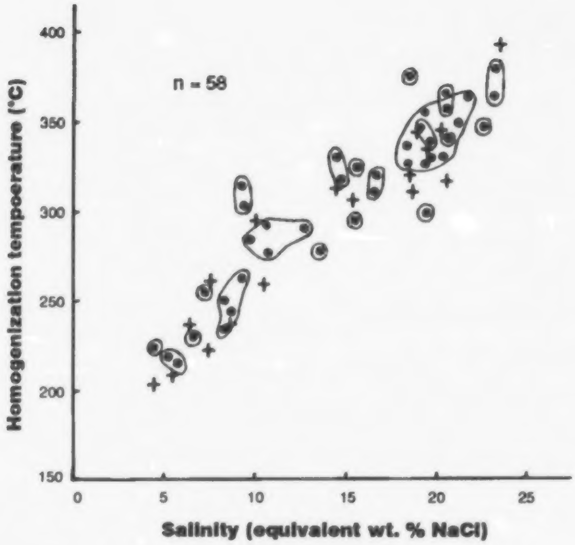

Figure 393.3. Homogenization temperature as a function of salinity for fluid inclusions in quartz (solid circles) and carbonates (crosses) associated with calc-silicates from the Hemlo gold deposit. Inclusions from individual quartz grains are outlined.

occur commonly in cross-cutting veins or as infillings along the foliation planes. Recently, Corfu and Muir (1989a, 1989b) reported the U-Pb age data from zircon, titanite, rutile, and monazite of the Hemlo gold deposit and its vicinity. Monazite is a common constituent of the late calc-silicate alteration. Therefore, the age data of monazite from 2644-2637 Ma may represent the timing of the late calc-silicate alteration in the Hemlo gold deposit. Corfu and Muir (1989b) obtained different U-Pb age data on different varieties of rutile. It is noteworthy that some of the U-Pb age data from rutile are similar to those from monazite. Titanite, replacing rutile and barian tomichite in V-enriched green mica schist (cf. Harris 1989, and described below) and along with other calc-silicates in veins, is most likely part of the late calc-silicate alteration in the Hemlo gold deposit. On the other hand, titanite grains from the ore zones yielded uniformed ages at 2672-2670 Ma (Corfu and Muir 1989b), which are considerably older than these from rutile and monazite. However, recent observations (Pan and Fleet 1991b) suggest that lanthanides and actinides may be mobile in titanite under hydrothermal conditions and therefore an application of such titanite for U-Pb age dating may be erroneous.

GREEN MICA SCHISTS

Green mica schists have been reported to occur at several localities in the Hemlo-Heron Bay greenstone belt (Patterson et al. 1983; Cameron and Hattori 1985; Harris 1989). The following summarizes some important findings on mineralogy, geochemistry and possible genesis of green mica schists from the Hemlo gold deposit and the barite-rich occurrence west of the Hemlo deposit. More detailed documentation and discussion of these green mica schists and their associated lithologies can be found in Pan and Fleet (1991a, 1991b, 1991c).

The Hemlo Gold Deposit

There are two types of green mica schists (Vanadium(V)- and Chromium(Cr)-enriched) in the Hemlo gold deposit, corresponding to the presence of V- and Cr-rich muscovite, respectively (Pan and Fleet 1991a, 1991c). Cr-enriched green mica schist is mainly composed of Cr-bearing muscovite (less than 1 wt. % Cr_2O_3), quartz, alkali feldspar, plagioclase and variable amounts of sulfides. V-enriched green mica schist, on the other hand, contains a large number of exotic V-rich oxides (rutile, barian tomichite, hematite, karelianite, chromite, hemloite and cafarsite; cf. Harris 1989) and some of the most V-rich silicate minerals (Pan and Fleet 1991c). Quartz and oligoclase "eyes" are not uncommon in V-enriched green mica schist (*see* Photo 393.3), but are typically absent in its Cr-enriched counterpart.

Harris (1989) reported that green mica in the Hemlo gold deposit is a 2M vanadian muscovite with less than 8.5 weight percent V_2O_3 and a 2M muscovite structure. This is the case for many analyses obtained in this study (*see* Figure 393.4). However, higher V contents for green mica analyses have been obtained from both the Golden Giant mine and the C zone of the Williams mine (Table 393.5). It is noteworthy that a few analyses from the C zone of the Williams mine contain up to 17.6 wt. % V_2O_3 (i.e. analysis 1 in Table 393.5) and should be classified as roscoleite. An X-ray-diffraction study indicates that the Hemlo roscoelite, similar to its less V-enriched counterpart (Harris 1989), also possesses a 2M muscovite structure. In the C zone, phlogopite is a minor constituent in roscoelite-bearing samples and contains as much as 10.1 wt. % V_2O_3, which results in a high proportion

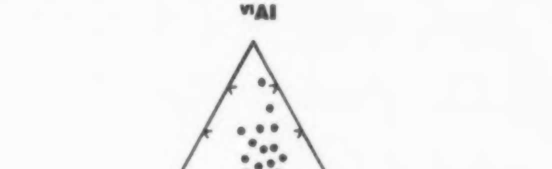

Figure 393.4. V-(Fe* + Mg)-^{VI}Al triangle illustrating compositional ranges of V-rich green mica (circles) and vanadian phlogopite (crosses) from the Hemlo gold deposit.

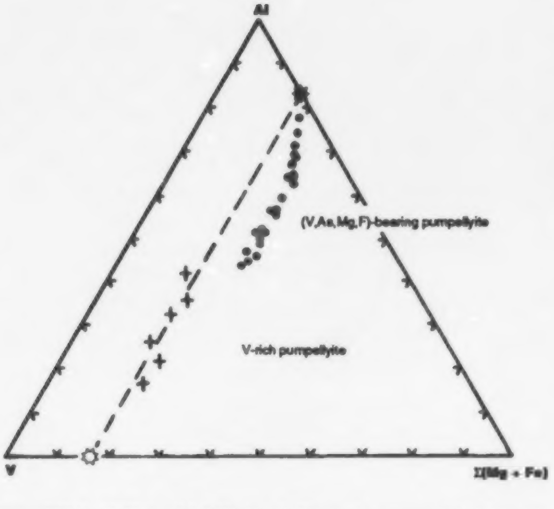

Figure 393.5. Al-(Fe* + Mg)-V triangle illustrating compositional ranges of pumpellyite-group minerals from the Hemlo gold deposit. Solid star, ideal pumpellyite-(Mg); open star, $Ca_8(Mg_2V_2)V_8Si_{12}O_{56-N}(OH)_n$.

of octahedral vacancies and, consequently, a significant deviation from the trioctahedral formula (Table 393.5).

High V concentrations in titanite, epidote-clinozoisite series and garnet have been previously reported by Harris (1989) and have also been obtained by the present study (*see* Table 393.6; Pan and Fleet 1991c). Pan and Fleet (1991b) also reported allanite-(La) and allanite-(Ce) contain up to 8.1 and 7.8 wt. % V_2O_3, respectively (*see* Table 393.6).

There are two texturally and compositionaly distinct pumpellyite group minerals in the V-enriched green mica schist (*see* Figure 393.5): prismatic grains in cross-cutting veins and along foliation planes (*see* Photo 393.5) and fine-grained aggregates in close association with vanadian titanite. The latter contains up to 25.7 wt. % V_2O_3 and results in a possible new end-member in the pumpellyite group with V as the most dominant cation in both X and Y sites (cf. Passaglia and Gottardi 1973). The prismatic grains are also characterized by a considerable amount of V (1.7 to 13.6 wt. % V_2O_3) and, additionally, high concentration in As, Mg and F (Table 393.6; Pan and Fleet 1991c). Vesuvianite in the V-enriched green mica schist of the Golden Giant mine is an unusual antimonian variety (11.2 to 21.2 wt. % Sb_2O_3, cf. Bradshaw 1972) and, additionally, is characterized by a considerable amount of V and Cl (up to 4.3 wt. % V_2O_3 and 1 wt. % Cl; *see* Table 393.6).

V-rich muscovite, defining the schistosity, is most likely broadly contemporaneous with the peak thermal metamorphism of the region. Based on a transmitted electron microscopy (TEM) study on microstructures in microcline from the Williams mine, White and Barnett (1990) concluded that potassic metasomatism (responsible for the formation of potassium feldspar and muscovite) most likely occurred during cooling after the peak of the regional thermal metamorphism. Also, Malsiwec et al. (1986) obtained a uniform $^{40}Ar/^{39}Ar$ age at 2671 Ma for green mica of the Hemlo gold deposit. Calc-silicates and phlogopite, on the other hand, in cross-cutting veins or along foliation planes, are part of the late calc-silicate alteration (Fleet and Pan 1990; Pan and Fleet 1991c; Pan et al. 1991b). Two-episodes of crystallization are also supported by contrasting patterns of chemical zonation in these vanadian silicates: green V-rich muscovite locally shows a decrease in V from core to margin, whereas the calc-silicates commonly exhibit an increase in V from core to margin (Pan and Fleet 1991c).

The Barite-Rich Occurrence

At the barite-rich occurrence, 21 km west of the Hemlo gold deposit, green mica schist, graphitic schist, sericitic schist, and a barite-rich unit occur as a conformable zone up to 50 m thick that can be traced by geology and geophysics for 6 km (Patterson et al. 1983). The green mica schist from this area contains feldspars, green mica, quartz, rutile, chromite, titanite, tourmaline, garnet, phlogopite, chlorite, and variable amounts of carbonates (calcite and ankerite) and sulfides (pyrite, pyrrhotite, sphalerite, chalcopyrite and pentlandite). Fluorite is rare and is invariably restricted to cross-cutting veins. Feldspars and green mica are the most abundant constituents, feldspars becoming more abundant toward the barite-rich unit (Pan and Fleet 1991a).

Green mica shows a wide range of composition and is characterized by high concentrations of both Ba and Cr (up to 10.3 and 6.4 wt. % BaO and Cr_2O_3, respectively; *see* Table 393.7). The compositional variation in green mica exists not only in different grains analyzed but also is also expressed in pronounced chemical zonation within individual grains. Such chemical zonation in green mica involves both Ba and Cr, which commonly exhibit an antipathetic relationship: the core zone contains higher Cr and lower Ba than the margin. Minor constituents in green mica from this area include Ti, Mg, Fe and Na (up to 5.8 wt. % TiO_2, 2.4 wt. % MgO, 1.3 wt. % FeO*, and 0.9 wt. % Na_2O; *see* Table 393.7). X-ray-diffraction study indicates that the green mica possesses a 2M1 muscovite structure and, therefore, is a barian-chromian muscovite.

There are two kinds of feldspars in green mica schists from the study area: alkali feldspar-hyalophane-celsian series and plagioclase series. Plagioclase, invariably a minor constituent, is present in both cross-cutting veins and the rock matrix, but with distinct composition: albite (An < 1 %) in the former and oligoclase or andesine (An_{22} to An_{36}) with a minor amount of Sr (up to 0.4 wt. % SrO) in the latter. Members of the alkali feldspar-hyalophane-celsian series, on the other hand, are the most abundant minerals in green mica schists, but celsian-dominant members are restricted to the barite-rich unit. The analytical data of the alkali feldspar-hyalophane-celsian series from this area are summarized in Figure 393.6 and fall into four groups: (1) Cn_{0-15}, (2) Cn_{25-30}, (3) Cn_{40-47}, and Cn_{65-96}, and show three compositional discontinuities (cf. Gay and Roy 1968).

Table 393.5. Representative compositions of V-rich micas from the Hemlo gold deposit (weight per cent).

	V-rich muscovite							**vanadian phlogopite**		
Analysis	**1**	**2**	**3**	**4**	**5**	**6c**	**7m**	**8**	**9**	**10**
SiO_2	41.79	41.31	47.60	45.12	44.82	42.63	45.44	39.04	39.13	38.91
TiO_2	0.21	0.56	0.31	0.67	0.65	0.45	0.74	1.07	1.02	1.00
Al_2O_3	18.98	20.25	19.45	18.31	18.42	20.87	25.55	15.56	15.76	15.50
V_2O_3	17.55	16.43	14.94	16.65	16.57	13.72	6.76	10.10	9.63	9.44
Cr_2O_3	0.29	0.30	0.19	0.30	0.34	0.24	0.15	0.21	0.13	0.15
FeO*	1.15	1.16	0.96	1.22	1.05	3.76	2.64	4.01	4.46	4.02
MgO	2.18	2.67	3.26	3.12	3.14	2.34	2.42	15.67	15.32	15.46
MnO	0.08	0.01	0.06	0.0	0.0	0.02	0.03	0.06	0.06	0.02
BaO	3.29	4.35	0.31	1.85	1.96	0.95	0.90	0.98	1.00	1.02
CaO	0.0	0.0	0.0	0.0	0.0	0.01	0.0	0.0	0.0	0.0
Na_2O	0.16	0.12	0.16	0.13	0.15	0.06	0.05	0.08	0.09	0.08
K_2O	9.76	8.16	9.63	9.38	8.98	10.16	9.30	9.63	9.81	9.37
F	0.0	0.0	0.0	0.0	0.0	0.0	0.0	0.37	0.32	0.28
O=F	0.0	0.0	0.0	0.0	0.0	0.0	0.0	0.16	0.14	0.14
Total	**95.44**	**95.31**	**96.86**	**96.76**	**96.08**	**95.20**	**94.06**	**96.63**	**96.58**	**95.16**
chemical formulae calculated on the basis of 22 oxygens										
Si	6.079	6.005	6.530	6.343	6.332	6.135	6.349	5.615	5.637	5.663
^{IV}Al	1.921	1.995	1.470	1.657	1.668	1.865	1.651	2.385	2.363	2.337
^{VI}Al	1.333	1.474	1.670	1.377	1.399	1.675	2.555	0.263	0.313	0.322
Ti	0.022	0.061	0.032	0.071	0.069	0.048	0.078	0.115	0.110	0.110
V	2.034	1.915	1.643	1.877	1.877	1.583	0.757	1.165	1.112	1.102
Cr	0.033	0.034	0.021	0.034	0.038	0.026	0.017	0.024	0.014	0.018
Fe	0.122	0.141	0.110	0.143	0.124	0.407	0.277	0.482	0.537	0.490
Mg	0.472	0.579	0.666	0.653	0.661	0.506	0.504	3.358	3.289	3.354
Mn	0.009	0.002	0.007	0.0	0.0	0.003	0.003	0.008	0.007	0.003
OCT	4.037	4.206	4.419	4.155	4.168	4.245	4.191	5.415	5.382	5.399
Ba	0.187	0.248	0.017	0.102	0.108	0.054	0.055	0.055	0.056	0.059
Ca	0.0	0.0	0.0	0.0	0.0	0.002	0.0	0.0	0.0	0.0
Na	0.045	0.033	0.042	0.035	0.041	0.017	0.013	0.023	0.027	0.023
K	1.814	1.514	1.685	1.681	1.618	1.870	1.661	1.767	1.803	1.740
X	2.046	1.795	1.744	1.818	1.767	1.943	1.729	1.845	1.886	1.822
F	0.0	0.0	0.0	0.0	0.0	0.0	0.0	0.168	0.144	0.131

FeO* is total iron content as FeO.
c denotes core.
m, margin.
Cl is not detectable.

Table 393.6. Representative compositions of other V-rich silicates from the Hemlo deposit (weight per cent).

	epidote-group minerals			pumpellyite		garnet		vesuvianite		titanite
	clz	epd	aln			core	margin			
SiO_2	37.41	36.50	32.14	32.45	33.23	35.45	36.51	31.90	33.61	29.68
TiO_2	0.0	0.06	0.21	0.0	1.13	0.0	0.27	0.03	0.36	18.63
Al_2O_3	26.24	22.95	15.61	13.52	4.55	12.79	3.37	9.11	13.60	1.45
V_2O_3	5.91	8.06	8.46	13.62	25.67	9.15	18.48	0.79	4.34	18.52#
Cr_2O_3	0.22	0.27	0.40	nd	0.56	0.21	0.41	nd	nd	0.31
As_2O_3	0.0	0.0	nd	4.77	nd	nd	nd	0.02	0.22	nd
Sb_2O_3	nd	nd	nd	0.	nd	nd	nd	21.21	11.29	nd
FeO*	2.51	5.57	8.34	1.73	3.34	4.24	4.98	6.36	0.83	0.31
MgO	0.07	0.11	0.40	5.13	2.10	0.05	0.0	0.07	2.83	nd
MnO	0.06	0.14	1.26	0.16	0.50	0.26	0.41	2.93	0.20	0.31
ΣRE_2O_3	nd	nd	19.64	nd	nd	nd	nd	nd	nd	nd
BaO	0.02	0.08	nd	nd	0.09	0.0	nd	nd	nd	nd
CaO	22.65	22.84	11.76	21.97	20.56	36.77	34.11	25.95	30.28	28.78
Na_2O	0.05	0.10	0.17	0.01	0.14	0.0	0.01	0.04	0.15	0.00
K_2O	nd	nd	nd	nd	0.09	nd	0.14	nd	nd	0.00
F	nd	nd	0.0	0.73	0.0	1.33	0.0	0.00	0.46	0.33
Cl	nd	nd	0.0	0.0	0.0	0.0	0.02	1.04	0.95	0.00
O=F,Cl	0.0	0.0	0.0	0.31	0.0	0.56	0.0	0.24	0.41	0.14
Total	95.66	96.49	98.39	93.79	91.96	99.56	98.71	99.20	98.40	97.98
Si	3.008	2.979	2.987	11.035	11.942	2.684	3.008	17.786	17.508	4.000
As	0.0	0.0	—	0.847	—	—	—	0.005	0.059	0.000
Ti	0.0	0.004	0.015	0.0	0.305	0.0	0.017	0.012	0.143	1.888
Al	2.486	2.133	1.709	5.414	1.928	1.145	0.328	6.059	8.974	0.231
V	0.381	0.521	0.630	3.710	7.397	0.557	1.221	0.355	1.812	1.667
Cr	0.004	0.016	0.029	—	0.159	0.013	0.027	—	—	0.033
Fe	0.154	0.338	0.583	0.493	1.003	0.270	0.343	2.966	0.363	0.035
Mg	0.014	0.013	0.055	2.599	1.123	0.002	0.0	2.438	2.196	—
Mn	0.008	0.010	0.099	0.046	0.151	0.016	0.029	0.033	0.086	0.008
ΣRE	—	—	0.670	—	—	—	—	—	—	—
Ba	0.001	0.016	—	—	0.012	0.0	—	—	—	—
Ca	1.994	2.979	1.173	7.998	7.917	2.992	3.012	15.502	16.902	4.156
Sb	—	—	—	0.008	—	—	—	4.876	2.425	—
Na	0.008	0.012	0.027	—	0.100	0.0	0.002	0.039	0.156	0.000
K	—	—	—	0.788	0.043	—	0.015	—	—	0.000
F	—	—	0.0	0.0	0.0	0.320	0.0	0.000	0.756	0.140
Cl	—	—	0.0		0.0	0.0	0.003	0.979	0.841	0.000
				49.0						
Oxygens	12.5	12.5	12.5		49.0					
Cations						8.0	8.0	50.0	50.0	4(Si)

clz, clinozoisite.
epd, epidote.
aln, allanite-(Ce).
*, total iron as FeO.
#, V_2O_5.
nd, not determined.

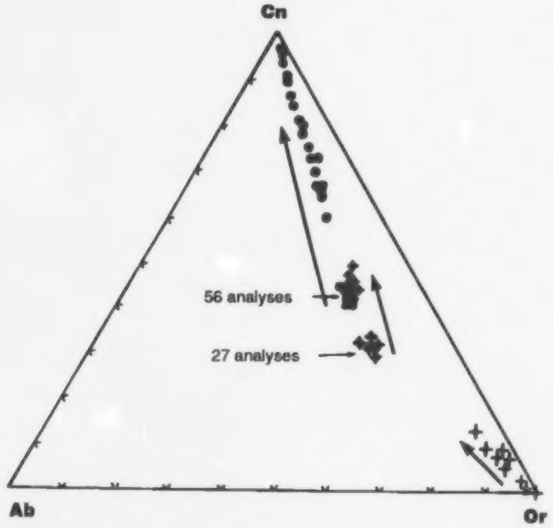

Figure 393.6. Celsian(Cn)-orthoclase(Or)-albite(Ab) triangle illustrating the compositional range of the alkali feldspar-hyalophane-celsian series from the barite-rich occurrence west of the Hemlo gold deposit.

Rutile and chromite occur as porphyroblasts in green mica schists and are commonly partly or completely replaced by green mica aggregates. Chromite is characterized by very high concentrations of Mn and Zn (up to 13 wt. % MnO and 8.9 wt. % ZnO and, therefore, is a zincian-manganoan variety (*see* Table 393.7; Pan and Fleet 1991a). Tourmaline occurs only as a minor constituent in close association with pyrite and green mica and is essentially dravite with a considerable amount of Cr (up to 9.8 wt. % Cr_2O_3).

The textural and chemical evidence described above indicates that Cr-enriched green mica schist probably formed in three stages. Chromite and rutile appear to have crystallized earliest, as they occur as relict porphyroblasts and are replaced by green mica aggregates. The concordance between the schistosity of green mica schist and the penetrative foliation in all supracrustal rocks of the region indicates that the main mineral assemblage, including barian feldspar, barian-chromian muscovite, quartz, plagioclase, garnet, tourmaline, titanite, ankerite, pyrite and sphalerite, formed broadly contemporaneous with the regional thermal metamorphism. The third generation assemblage, in cross-cutting veins and along foliation planes, probably corresponds to the late calc-silicate alteration observed elsewhere in the Hemlo-Heron Bay greenstone belt. The presence of phlogopite instead of calc-silicates is readily attributable to elevated X_{CO_2}, which is confirmed by fluid-inclusion observation and may be related to local abundance of graphitic material.

Geochemistry and Genesis

Whole-rock analyses for Vanadium- and Chromium-enriched green mica schists and their associated rocks of the Hemlo-Heron Bay greenstone belt are reported in Tables 393.8 and 393.9. The Cr-enriched green mica schists from the Hemlo gold deposit and the barite-rich occurrence are remarkably similar in most geochemical compositions to each other, but are distinct from their V-enriched counterpart of the Hemlo gold deposit (*see* Figure 393.7). V-enriched green mica schist in the Hemlo gold deposit (Table 393.8) is characterized by anomalously high concentrations of Au, V, Cr, Ba, As, Mo, Tl, as are other ore-bearing rocks of this deposit (Cameron and Hattori 1985; Harris 1989; Thode et al. 1991). Cr-enriched green mica schists from both localities are characterized by high concentrations of Ba, As and 3d-transition metals (Cr, V, Ni, Co, Ti, Mn, Sc), but not Au, Mo and Tl (Tables 393.8 and 393.9). Cr-enriched green mica schists are also characterized by low total REE abundances and flat chondrite normalized REE patterns, similar to those in mafic-ultramafic rocks (Pan and Fleet 1991a, 1991c). V-enriched green mica schist is generally low in total REE abundances, but high light REE abundances have been obtained by the present study and are attributable to preferential remobilization of LREE over HREE during the late calc-silicate alteration.

As noted by Pan and Fleet (1991b), elements commonly considered to be "immobile", such as REE, appear to have been locally remobilized during late hydrothermal alteration in the Hemlo gold deposit. Therefore, application of trace-element geochemistry alone to deduce possible protoliths for host rocks in the Hemlo deposit may be misleading. In the barite-rich occurrences west of the Hemlo deposit, Cr-enriched green mica schist contains well-preserved relict mafic-ultramafic fragments (tremolite-talc-phlogopite schist) and is structurally overlain by metamorphosed mafic-ultramafic

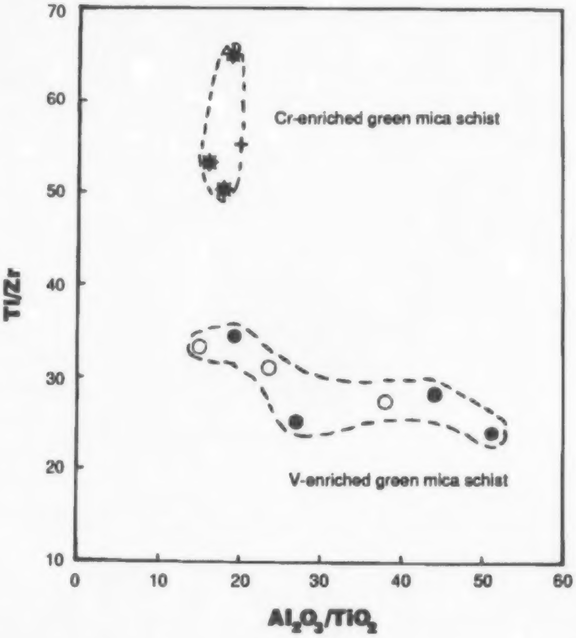

Figure 393.7. Ti/Zr versus Al_2O_3/TiO_2 plot comparing V-enriched green mica schist and Cr-enriched green mica schist of the Hemlo gold deposit.

Table 393.7. Representative mineral compositons of the Cr-enriched green mica schist from the barite-rich occurrence.

Mineral	**green mica**			**phlogopite**	**feldspar**				**tourmaline**	**chromite**
Analysis	**PR-4m**	**NE-4**	**PR-5**	**PR-3**	**PRBUr**	**PR-2c**	**PR-2m**	**PR-1c**	**NE-2c**	**NE-3**
SiO_2 (wt. %)	42.03	43.48	43.75	39.97	33.40	53.78	48.32	64.31	35.39	
TiO_2	0.86	0.73	5.84	0.97					0.11	0.03
Al_2O_3	32.61	29.51	29.45	14.80	27.38	21.36	22.26	18.51	27.20	14.91
Cr_2O_3	0.63	6.39	3.36	1.84					9.82	50.41
FeO*	1.19	0.00	0.23	7.00					0.51	14.05
MnO	0.00	0.00	2.24	0.56					0.00	10.71
MgO	2.06	1.88	0.00	19.06					9.10	1.45
ZnO									1.24	8.67
CaO	0.00	0.00	0.00	0.03	0.00	0.00	0.06	0.00	0.00	
BaO	10.31	4.16	3.07	2.56	39.10	15.08	22.41	1.34	2.08	
Na_2O	0.30	0.72	0.68	0.11	0.10	1.75	1.31	0.19	0.00	
K_2O	6.80	8.53	8.80	8.31	0.32	8.16	6.01	16.15	0.00	
F	0.00	0.00	0.00	2.10						
F=0	0.00	0.00	0.00	0.88						
Total	**96.79**	**95.40**	**97.43**	**96.44**	**100.3**	**100.7**	**100.4**	**100.5**	**85.63**	**100.2**
on the basis of	**22 (O)**	**8 (O)**	**29 (O)**	**4 (O)**						
Si	5.991	6.039	5.892	5.701	2.041	2.716	2.579	2.985	5.858	
^{IV}Al	2.009	1.961	2.108	2.299	0.959	0.284	0.421	0.015		
^{VI}Al	3.291	2.869	2.566	0.188	1.014	0.987	0.979	0.998		0.608
Ti	0.090	0.076	0.591	0.104						0.001
Cr	0.066	0.702	0.358	0.207						1.379
Fe	0.125	0.000	0.026	0.835						0.406
Mn	0.000	0.000	0.000	4.050						0.313
Mg	0.432	0.389	0.450	0.068						0.074
Zn										0.221
Ca	0.000	0.000	0.000	0.005	0.000	0.000	0.004	0.000		
Ba	0.573	0.226	0.162	0.144	0.937	0.299	0.470	0.024		
Na	0.081	0.194	0.178	0.030	0.012	0.166	0.135	0.017		
K	1.221	1.511	1.512	1.512	0.025	0.527	0.410	0.956		
F	0.000	0.000	0.000	0.947						

c denotes analysis on grain core.
m, margin.
wt. % is weight percent.
FeO* is total iron content.

Table 393.8. Whole-rock compositions of green mica schists and associated rocks from the Hemlo gold deposit.

Lithology	**green mica schist**							**GS**	**MB**	**QOP**
Sample	**1**	**2**	**3**	**4**	**5**	**6**	**7**	**8**	**9**	**10**
SiO_2 (wt. %)	83.5	81.8	73.5	60.8	60.6	65.5	67.1	64.24	52.8	67.6
TiO_2	0.07	0.13	0.26	0.33	1.05	0.79	0.72	0.45	0.61	0.26
Al_2O_3	3.11	6.68	7.12	6.12	17.1	14.1	13.6	13.74	12.3	11.8
Fe_2O_3*	4.89	4.62	5.95	1.78	7.25	3.64	3.02	5.01	9.19	3.24
MgO	0.29	0.47	0.28	0.13	0.59	0.69	0.61	1.07	9.77	1.86
CaO	<0.01	<0.01	0.03	0.21	0.34	0.34	0.19	2.87	9.12	3.91
Na_2O	0.11	0.20	0.28	0.50	0.95	1.87	0.47	3.87	2.92	4.52
K_2O	1.64	2.56	0.38	4.39	6.56	5.48	5.17	2.46	1.39	3.31
P_2O_5	0.02	0.02	0.08	0.09	0.10	0.15	0.15	0.09	0.23	0.08
L.O.I.	3.31	2.93	3.93	0.85	5.23	2.62	3.77	5.74	1.08	1.93
Total	**99.0**	**99.7**	**95.6**	**91.7**	**100.3**	**98.9**	**100.1**	**99.55**	**99.8**	**98.6**
Au (ppb)	10000	2900	10000	10000	2900	1300	370	60	370	510
S (ppm)	23300	15600	34400	33200	23800	12400	4700	15800	<50	8140
As	14	23	61	94	160	170	150	1408	<2	14
Sb	19.0	5.4	280	540	30	130	<0.2	1.3	nd	2.0
Hg (ppb)	nd	nd	nd	nd	nd	nd	430	nd	nd	nd
Mo (ppm)	7000	3090	24000	916	37	60	<5	21	<5	17
Tl	<2	<2	72	53	14	22	nd	nd	nd	<2
Cs	<1	1	2	2	5	2	4	2	8	1
Ba	17900	2200	3950	147000	4580	32500	5500	810	441	862
Rb	37	53	31	24	118	72	87	86	49	36
Sr	189	16	32	621	22.0	651	144	302	417	57
Cr	550	490	630	710	780	470	1640	235	620	350
V	5710	2550	2170	255	216	162	160	72	220	131
Sc	6.1	2.9	4.6	2.0	22.0	14.9	22.0	9.5	42.6	5.1
Ni	4	13	8	8	151	72	300	41	120	2
Co	2	3	8	9	43	26	76	21	48	4
Mn	65	47	56	64	67	33	160	180		<2
Th	<1	<1	1	<1	1	2	1.1	2.7	1.8	<1
U	<0.5	<0.5	<0.5	<2	0.6	0.6	<0.5	0.9	<0.6	<2
Zr	15	33	62	58	118	95	66	122	67	87
Hf	<1	<1	<1	<1	3	3	3	3	<1	2
Nb	26	24	73	23	11	17	<10	15	<10	<10
Al_2O_3/TiO_2	44	51	27	19	16	18	19	31	20	45
Ti/Zr	28	24	25	34	53	50	65	22	55	18

GS is an average of 12 graphitic schists.
MB, metabasite.
QOP, quartz-oligoclase porphyry.
wt. %. weight per cent.
ppb, parts per billion.
ppm, parts per million.
L.O.I., loss on ignition.
nd, not determined.

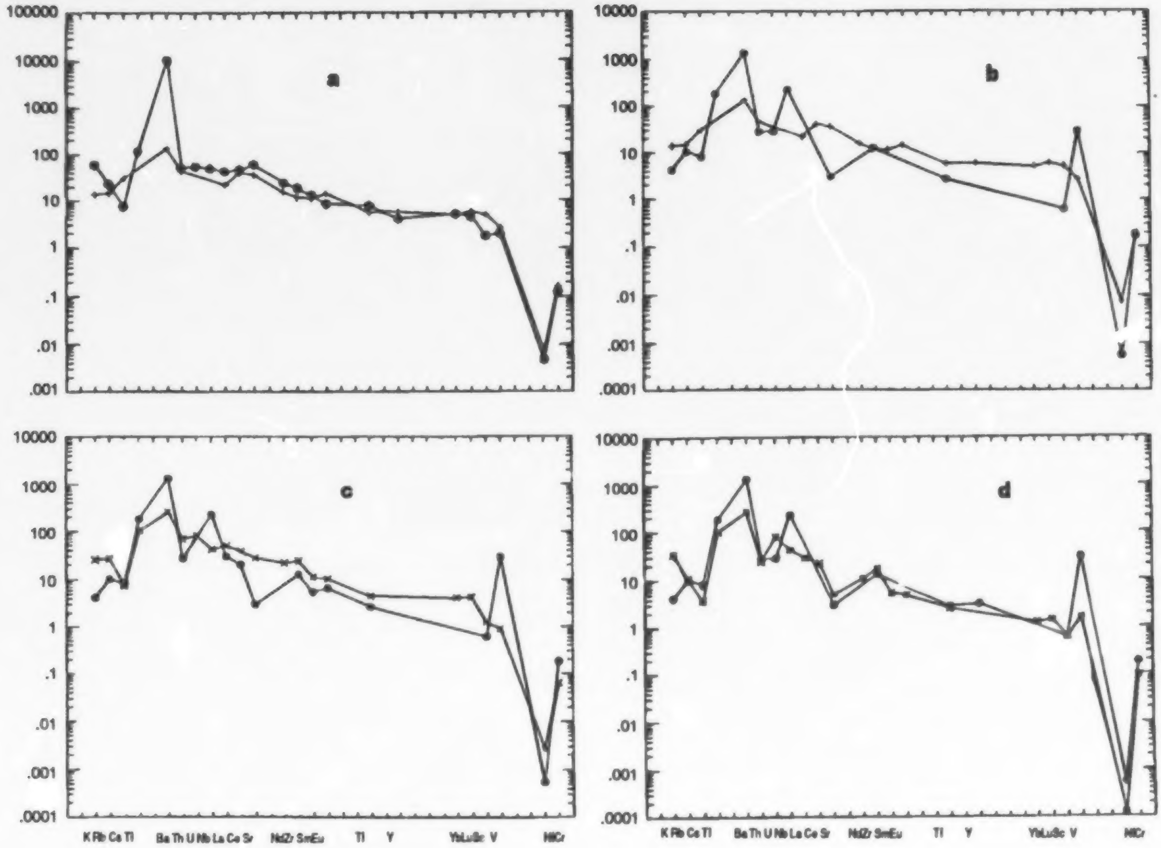

Figure 393.8. Trace-element geochemistry in: a) Cr-enriched green mica schist (stars) and metabasites (crosses); b), c) and d) V-enriched green mica schist (circles) and metabasites (+), graphitic schist (x) and quartz-oligoclase porphyry (*), respectively. Note the difference in scales between (a) and the rest.

rocks (Pan and Fleet 1991a). Similarly, mafic-ultramafic fragments are common in the hanging-wall metasedimentary rocks at the Hemlo deposit and are probably represented by biotite-rich lenses in the ore zones (Kuhns et al. 1986). It has been demonstrated above that Cr-enriched green mica schist from both localities are remarkably similar in geochemistry to metamorphosed mafic-ultramafic rocks (Figure 393.8a). Pan and Fleet (1989) showed that Cr-rich skarn at the White River gold prospect was metasomatically derived from mafic-ultramafic host rocks within a regional-scale fracture zone during a phase dilation. The barite-rich occurrence and the Hemlo gold deposit are situated within the Heron Bay-Black River fault zone and the Hemlo shear zone, respectively (Brown et al. 1985; Hugon 1986). Therefore, it is conceivable that the high levels of Cr in these areas resulted from a selective enrichment of this element during extensive hydrothermal alteration of mafic-ultramafic rocks within regional structural lineaments.

V-enriched green mica schist of the Hemlo deposit, on the other hand, differs considerably from metamorphosed mafic-ultramafic rocks (*see* Figure 393.8b) and metasedimentary rocks (*see* Figure 393.8c), but does resemble quartz-oligoclase porphyry (*see* Figure 393.8d), except for those elements believed to have been introduced by metasomatism (e.g. K, Tl, Ba and V). This favorable comparison is consistent with the presence of relict quartz and oligoclase phenocrysts within the V-enriched green mica schist from the C zone of the Williams mine. It is possible that these quartz and oligoclase phenocrysts were volcanic in origin, as previously suggested by Kuhns et al. (1986) and Muir (1988). However, the abundances of light REE in the V-enriched green mica schist are lower than those in felsic metavolcanic rocks. The felsic metavolcanic rocks in the Hemlo-Heron Bay greenstone belt are characterized by anomalously high LREE abundances (Pan et al. 1991a). It is most likely therefore that the V-enriched green mica schist from the Hemlo deposit was derived from the felsic (quartz-oligoclase porphyritic) host rocks.

If the quartz-oligoclase porphyritic rocks were indeed the protolith of the V-enriched green mica schist at the Hemlo deposit, V and Cr must have been introduced from

Table 393.9. Whole-rock compositions of green mica schist and associated rocks from the barite-rich occurrence.

Sample	PR-1	PR-2	PR-3	PR-4	PRBU	PR-20	PR-21	PR-22	PR-23	MTVL
SiO_2	41.79	49.30	53.70	54.90	39.10	69.60	48.50	65.90	67.10	45.40
TiO_2	0.61	0.71	0.84	0.85	0.48	0.56	0.63	0.58	0.61	0.97
Al_2O_3	11.10	12.20	15.40	17.00	9.68	8.62	11.40	9.78	10.10	11.70
Fe_2O_3*	10.90	18.10	11.20	8.15	4.68	9.67	10.20	10.10	9.22	18.80
MgO	3.77	1.11	1.13	1.47	0.76	1.09	3.71	1.27	1.42	7.49
MnO	0.15	0.07	0.07	0.09	0.04	0.08	0.15	0.07	0.14	0.67
CaO	6.38	1.29	1.22	1.78	1.99	nd	6.09	0.05	0.01	10.10
BaO	0.91	2.05	3.88	3.94	26.69	1.78	1.13	1.88	2.19	nd
Na_2O	1.14	3.87	3.90	4.68	1.92	0.20	1.15	0.25	0.25	1.13
K_2O	3.30	1.43	2.43	2.53	0.97	2.59	3.51	2.85	3.05	0.49
P_2O_5	0.05	0.04	0.03	0.04	0.11	0.04	0.06	0.05	0.05	0.09
L.O.I.	13.50	9.93	6.08	4.70	3.62	4.54	13.40	6.00	4.54	1.39
Total	**100.5**	**100.4**	**100.3**	**100.6**	**90.20**	**100.0**	**100.7**	**100.1**	**100.3**	**98.40**
S	1.95	4.47	2.70	1.80	4.47	0.68	1.68	2.27	0.37	nd
As	2400	1900	2200	2700	59	1400	2200	3300	1900	14
Sb	160	1.6	2.0	1.2	3.5	49	94	21	14	0.8
Mo	nd	nd	nd	nd	18	140	nd	30	18	nd
Hg	27	18	14	nd	9	72	57	45	23	nd
Sc	52.5	45.6	64.6	45.6	11.6	24.0	48.6	31.3	40.6	62.7
V	200	220	330	280	76	190	230	190	28	270
Cr	4930	1920	2600	2740	290	8620	4720	9170	10900	410
Co	210	100	1400	160	23	26	170	210	13	67
Ni	1200	520	680	860	49	130	1100	1400	66	140
Hf	nd	2	nd	nd	17	nd	nd	nd	nd	3
Nb	10	16	nd	nd	69	nd	11	nd	nd	24
Th	4.5	0.7	nd	nd	2.3	nd	5.9	nd	nd	3
U	1.4	nd	nd	1.9	2.5	nd	2.9	nd	0.8	1.6
Zr	67	44	57	65	21	39	71	43	41	83
W	85	21	38	35	19	87	78	63	45	nd
Rb	89	50	71	83	19	45	92	52	54	16
Sr	95	381	501	667	1570	29	107	19	29	87
Al/Ti	18	17	19	20	20	15	18	17	17	12
Ti/Zr	55	96	88	77	137	86	53	81	89	70
Cr/Ni	4.1	3.7	3.8	3.2	5.9	66	4.3	6.6	165	2.9
Th/U	3.2				0.9		2.0			0.4

MTVL is a sample of mafic metavolcanic rocks (garnet amphibolites).
All oxides and S are in weight per cent.
All trace elements, except Hg in parts per billion, are in parts per million.
Fe_2O_3* is total iron content.
L.O.I. is loss of ignition.
nd is not detectable.

Table 393.10. Summary of metamorphic and hydrothermal history of the Hemlo-Heron Bay greenstone belt.

	Structure	Age (Ma)
Calc-silicate alteration (350°C, < 2 kbar)	F_4	2632-2645*
Potassic alteration (500°C, 3 kbar)	F_3	2671**
Regional thermal metamorphism (580°C, 3-4 kbar)	F_3	2678* (?)
Regional Barrovian metamorphism (500°C, 6-6.5 kbar)	F_1 (?)	

F_1 to F_4 are structural elements of Muir and Elliott (1987).
*, U-Pb ages of Corfu and Muir (1989b).
**, $^{40}Ar/^{39}Ar$ age of Malsiwec et al. (1986).

external sources. Mafic-ultramafic rocks are common in the Hemlo deposit and its vicinity. Elevated V and Cr abundances have been obtained from less altered mafic-ultramafic lenses in the hanging-wall metasedimentary rocks (*see* Tables 393.8 and 393.9). The details of how V and Cr were introduced into the quartz-oligoclase porphyry have been obscured by polymetamorphism and multiple generations of alteration of the Hemlo-Heron Bay greenstone belt. However, it is possible that V and Cr were introduced into the quartz-oligoclase porphyry after pre-concentration in altered mafic-ultramafic rocks (as a result of mass loss; cf. Pan and Fleet 1991a) and fixed in green mica and oxides during the waning stage of the regional thermal metamorphism. Pan and Fleet (1989) identified a similar two stage concentration and remobilization of Cr in the Cr-rich skarn of the White River gold prospect.

V-enriched green mica schist of the Hemlo deposit may also represent a volcanoclastic unit, in which V and Cr have been pre-concentrated by sedimentary processes. High concentrations of V and Cr are not uncommon in sedimentary rocks with the "red bed" U-V-Cu deposits perhaps being best known examples (Foster 1959). Metasedimentary rocks of the Hemlo-Heron Bay greenstone belt are somewhat elevated in V and other transition metals and this has been attributed to contributions from mafic-ultramafic components, but their U and Cu abundances are not notable enriched (Pan et al. 1991a.)

DISCUSSION AND CONCLUSIONS

Table 393.10 is a summary of our reconstruction of the metamorphic and hydrothermal history of the Hemlo-Heron Bay greenstone belt, along with structural data of Muir and Elliott (1987) and geochronolgical data of Corfu and Muir (1989b) and Malsiwec et al. (1986). An early regional Barrovian-type metamorphism was first recognized by Burk et al. (1986) in metapelites from the David Bell mine and has also been delineated in rocks from the White River property (Fleet and Pan 1990). Unfortunately, the relationship of this metamorphic event with early generations of structures (e.g. F1 and F2 of Muir and Elliott 1987) is uncertain owing to the lack of early fabrics in the critical samples examined (kyanite-bearing samples, Fleet and Pan 1990). The regional Barrovian-type metamorphism was followed by a regional thermal metamorphism, which was broadly contemporaneous with the main ductile shear deformation (F3). During the waning stage of the regional thermal metamorphism, a pervasive potassic alteration occurred along regional structural lineaments and is indicated by abundant micas and microcline in the Hemlo gold deposit (White and Barnett 1990), the White River gold prospect (Fleet and Pan 1990), and the barite-rich occurrence (Pan and Fleet 1991a). This alteration event, apparently, was strongly controlled by the compositions of the associated host rocks. This is demonstrated by the significant Ba component in the barite-rich occurrence (Pan and Fleet 1991a) and some parts of the Hemlo gold deposit (Harris 1989), and is further manifested by the formation of Cr- and Fe-rich skarns in association with mafic-ultramafic rocks at the White River gold prospect (Pan and Fleet 1989, Fleet and Pan 1990). Still later, the late calc-silicate alteration, first recognized on the White River gold prospect, has been observed in the Hemlo gold deposit and elsewhere in the Hemlo-Heron Bay greenstone belt by this study. This late calc-silicate alteration can be related to late brittle structures (F4, Muir and Elliott 1987) and occurred at about 2632-2645 Ma (cf. Corfu and Muir 1989b).

There is no evidence of regional metamorphism in the diffuse westward extension of the main orebody, because metamorphic minerals (such as sillimanite, garnet, staurolite, etc.), which are indicators of the amphibolite-facies metamorphism in the country metasedimentary rocks of the main orebody, are typically absent. Moreover, the well-preserved quartz-oligoclase phenocrysts in the V-enriched green mica schist and other ore-bearing rocks of the C zone argue against the possibility that all metamorphic minerals in ore zones have been obliterated by late hydrothermal fluid. These observation are consistent with post-metamorphic models (Walford et al. 1986; White and Barnett 1990), but not pre- or syn-metamorphic models (Cameron and Hattori 1985; Burk et al. 1986; Kuhns et al. 1986; Valliant and Bradbrook 1986). As mentioned above, native gold grains occur commonly in direct association with calc-silicate assemblages (*see* Photo 393.6). Our petrographic observation and preliminary geochemical data also have shown that ore-bearing rocks from the C zone almost invariably contain abundant calc-silicates. These findings are similar to those at the White River gold occurrence. We therefore suggest that gold mineralization in the Hemlo gold deposit also was broadly contemporaneous with this late calc-silicate alteration event.

ACKNOWLEDGEMENTS

We thank G. Skrecky and J. Gray of the Williams Operating Cooperation, D. McIlveen and P. Johnson of the Hemlo Gold Mines Incorporated, W. Stone of McMaster University, and M. Smyk and B. Schnieders of the Ontario Ministry of Northern Development and Mines, Thunder Bay for logistical assistance in the field, and R.L. Barnett, Y. Cheng, J.A. Forth and D.M. Kingston for technical assistance.

REFERENCES

Ashworth, J.R. 1986. Myrmekite replacing albite in prograde metamorphism; American Mineralogist, v.71, p.895–899.

Bird, D.K., Schiffman, P., Elders, W.A., Williams, A.E. and McDoewell, S.D. 1984. Calc-silicate mineralization in active geothermal fields; Economic Geology, v.79, p.671–695.

Bradshaw, N.D. 1972. An antimonian vesuvianite from the Bau mining district, Sarawak, Malaysia; Mineralogical Magazine, v.38, p,894–896.

Brown, P., Carson, D., Cooper, P., Farr, E., Gibson, J., Harvey, J., Hog, W., MacIsaac, N., Mackie, B., Nash, W. and Pierce, G. 1985. Golden Giant joint venture properties—Hemlo; *in* Gold and Copper—Zinc Metallogeny Within Metamorphosed Greenstone Terrain, Hemlo-Manitouwadge-Winston Lake, Ontario, Canada, Geological Association of Canada—Canadian Institute of Mining and Metallurgy, Toronto, 1985, p.58–65.

Burk, R., Hodgson, C.J., and Quartermain, R.A. 1986. The geological setting of the Teck-Corona Au-Mo-Ba deposit, Hemlo, Ontario, Canada; *in* Proceedings of Gold'86, an International Symposium on the Geology of Gold, p.311–326.

Cameron, E.M., and Hattori, K. 1985. The Hemlo gold deposit, Ontario: a geochemical and isotopic study; Geochimica et Cosmochimica Acta, v.49, p.2041–2050.

Corfu, F., and Muir, T.L. 1989a. The Hemlo-Heron Bay greenstone belt and Hemlo Au-Mo deposit, Superior Province, Ontario, Canada. 1. Sequence of igneous activity determined by zircon U-Pb geochronology; Chemical Geology, v.79, p.183–200.

——1989b. The Hemlo-Heron Bay greenstone belt and Hemlo Au-Mo deposit, Superior Province, Ontario, Canada. 2. Timing of metamorphism, alteration and Au mineralization from titanite, rutile and monazite geochronology; Chemical Geology, v.79, p.201–223.

Craw, D., and Koons, P.O. 1989. Tectonically induced hydrothermal activity and gold mineralization adjacent to major fault zones; *in* The Geology of Gold Deposits: The Perspective in 1988, Economic Geology, Monograph 6, p.471–478.

Fleet, M.E. and Pan, Y. 1990. Metamorphic petrology and gold mineralization of the White River gold prospect, Hemlo area; Ontario Geological Survey, Open-File Report.

Foster, M.D. 1959. Geochemistry and mineralogy of the Colorado Plateau uranium ores; Part 10. Chemical study of the mineralized clays; United States Geological Survey, Professional Paper 320, p.121–132.

Gay, P. and Roy, N.N. 1968. The mineralogy of the potassium-barium feldspar series. III. Subsolidus relationships; Mineralogical Magazine, v.36, p.914–932.

Goad, R.E. 1987. The geology, primary and secondary chemical dispersion of the Hemlo Au deposit metal occurrences, northwestern Ontario; unpublished M.Sc. thesis, The University of Western Ontario, London, Ontario, 578p.

Harris, D.C. 1989. The mineralogy and geochemistry of the Hemlo gold deposit, Ontario; Geological Survey of Canada, Economic Geology Report 38, 88p.

Hochella, M.F., Jr., Liou, J.G., Keskinen, M.J., and Kim, H.S. 1982. Synthesis and stability relations of magnesium idocrase; Economic Geology, v.77, p.798–808.

Hugon, H. 1986 The Hemlo gold deposit, Ontario, Canada: a central portion of a large scale, wide zone of heterogeneous ductile shear; in Proceedings of Gold'86, an International Symposium on the Geology of Gold, p.379–387.

Ito, J. and Arem, J.E. 1970. Idocrase: synthesis, phase relations and crystal chemistry; Amercian Mineralgist, v.55, p.880–912.

Kuhns, R.J. 1986. Alteration styles and trace elements dispersion associated with the Golden Giant deposit, Hemlo, Ontario, Canada; *in* Proceedings of Gold'86, an International Symposium on the Geology of Gold, p.340–354.

Kuhns, R.J., Kennedy, P., Cooper, P., Brown, P., Mackie, B., Kusins, R., and Friesen, R. 1986. Geology and mineralization associated with the Golden Giant deposit, Hemlo, Ontario, Canada; *in* Proceedings of Gold'86, an International Symposium on the Geology of Gold, p.327–339.

MacDonald, A.J. ed., 1986. Proceedings of Gold'86, an International Symposium on the Geology of Gold , 517p.

MacDonald, A.J., and Spooner, E.T.C. 1981. Calibration of a LINKAM TH600 programmable heating-cooling stage for microthermometric examination of fluid inclusions; Economic Geology, v.76, p.1248–1258.

Malsiwec, A., McMaster, D. and York, D. 1986. The dating of Ontario's gold deposits; Ontario Geological Survey, Miscellaneous Paper 130, p.107–114.

Muir, T.L. 1982. Geology of the Hemlo area, district of Thunder Bay; Ontario Geological Survey, Report 218, 65p.

——1988. Hemlo tectono-stratigraphic study; in Summary of Field Work and Other Activities, Ontario Geological Survey, Miscellaneous Paper 141, p.226–239.

Muir, T.L., and Elliott, C.G. 1987. Hemlo tectono-stratigraphic study; *in* Summary of Field Work and Other Activities, Ontario Geological Survey, Miscellaneous Paper 137, p.117–129.

Munoz, J.L. 1984. F-OH and Cl-OH exchange in micas with application to hydrothermal deposits; *in* Micas, Review in Mineralogy, v.13, p.469–491.

Pan, Y., and Fleet, M.E. 1989. Cr-rich calc-silicates from the Hemlo area, Ontario; The Canadian Mineralogist, v.27, p.565–577.

—— 1991a. Barian feldspar and barian-chromian muscovite from the Hemlo area, Ontario; The Canadian Mineralogist, v.29 (in press).

——1991b. Vanadian allanite-(La) and vanadian allanite-(Ce) from the Hemlo gold deposit, Ontario, Canada; Mineralogical Magazine (in press).

——1991c. Vanadium silicate minerals in the Hemlo gold deposit: mineral chemistry and geochemistry; *in* Program with Abstracts, Geological Association of Canada-Mineralogical Association of Canada, v.16, p.A94.

Pan, Y., Fleet, M.E., and Stone, W.E. 1991a. Geochemistry of metasedimentary rocks in the late Archean Hemlo-Heron Bay greenstone belt, Superior Province: implications for provenances and tectonic setting; Precambrian Research (in press).

—— 1991b. Calc-silicate alteration in the Hemlo gold deposit, Ontario: mineral assemblages, P-T-X constraints and association with gold mineralization; *in* Program with Abstracts, Geological Association of Canada-Mineralogical Association of Canada, v.16, p.A94.

Passaglia, E. and Gottardi, G. 1973. Crystal chemistry and nomenclature of pumpellyites and julgoldites; The Canadian Mineralogist, v.12, p.219–223.

Patterson, G.C., Mason, J.K. and Schnieders, B.R. 1983. Thunder Bay resident geologist area, north central region; *in* Report of Activities 1983, Ontario Geological Survey, Miscellaneous Paper 117, p.77–106.

Potter, R.W., Clynne, M.A., and Brown, D.L. 1978. Freezing point depression of sodium chloride solutions; Economic Geology, v.73, p.284–285.

Roedder, E. 1984. Fluid Inclusions; Review in Mineralogy, v.12, 644p.

Schiffman, P., and Liou, J.G. 1981. Synthesis and stability relations of Mg-Al pumpellyite, $Ca_4Al_5MgSi_6O_{21}(OH)_7$; Journal of Petrology, v.21, p.441–474.

Taylor, B.E. and Liou, J.G. 1978. The low-temperature stability of andradite in C-O-H fluids; American Mineralogist, v.68, p.444–448.

Thode, H.G., Ding, T. and Crocket, J.H. 991. Sulphur isotope and element geochemistry studies of the Hemlo gold deposit, Ontario: sources of sulphur and implications for the mineralization process; Canadian Journal of Earth Sciences, v.28, p.13–25.

Thompson, A.B. 1971. PCO_2 in low-grade metamorphism: zeolite, carbonate, clay mineral, prehnite relations in the system of $CaO\text{-}Al_2O_3\text{-}SiO_2\text{-}CO_2\text{-}H_2O$; Contributions to Minerαlogy and Petrology, v.33, p.145–161.

Valliant, R.I., and Bradbrook, C.J. 1986. Relationship between stratigraphy, faults and gold deposits, Page-Williams mine, Hemlo, Ontario, Canada; *in* Proceedings of Gold'86, an International Symposium on the Geology of Gold, p.355–361.

Walford, P., Stephens, J., Skrecky, G., and Barnett, R. 1986. The Geology of the "A" zone, Page-Williams mine, Hemlo, Ontario, Canada; *in* Proceedings of Gold'86, an International Symposium on the Geology of Gold, p.362–378.

White, J.C., and Barnett, R.L. 1990. Microstructural signatures and glide-twins in microcline, Hemlo, Ontario; The Canadian Mineralogist, v.28, p.757–769.

Conversion Factors for Measurements in Ontario Geological Survey Publications

Conversion from SI to Imperial			Conversion from Imperial to SI		
SI unit	*Multiplied by*	*Gives*	*Imperial unit*	*Multiplied by*	*Gives*
			LENGTH		
1 mm	0.039 37	inches	1 inch	**25.4**	mm
1 cm	0.393 70	inches	1 inch	**2.54**	cm
1 m	3.280 84	feet	1 foot	**0.304 8**	m
1 m	0.049 709 7	chains	1 chain	20.116 8	m
1 km	0.621 371	miles (statute)	1 mile (statute)	**1.609 344**	km
			AREA		
1 cm²	0.155 0	square inches	1 square inch	**6.451 6**	cm²
1 m²	10.763 9	square feet	1 square foot	**0.092 903 04**	m²
1 km²	0.386 10	square miles	1 square mile	2.589 988	km²
1 ha	2.471 054	acres	1 acre	0.404 685 6	ha
			VOLUME		
1 cm³	0.061 02	cubic inches	1 cubic inch	**16.387 064**	cm³
1 m³	35.314 7	cubic feet	1 cubic foot	0.028 316 85	m³
1 m³	1.308 0	cubic yards	1 cubic yard	0.764 555	m³
			CAPACITY		
1 L	1.759 755	pints	1 pint	0.568 261	L
1 L	0.879 877	quarts	1 quart	1.136 522	L
1 L	0.219 969	gallons	1 gallon	**4.546 090**	L
			MASS		
1 g	0.035 273 96	ounces (avdp)	1 ounce (avdp)	28.349 523	g
1 g	0.032 150 75	ounces (troy)	1 ounce (troy)	**31.103 476 8**	g
1 kg	2.204 62	pounds (avdp)	1 pound (avdp)	**0.453 592 37**	kg
1 kg	0.001 102 3	tons (short)	1 ton (short)	**907.184 74**	kg
1 t	1.102 311	tons (short)	1 ton (short)	**0.907 184 74**	t
1 kg	0.000 984 21	tons (long)	1 ton (long)	**1 016.046 908 8**	kg
1 t	0.984 206 5	tons (long)	1 ton (long)	**1.016 046 908 8**	t
			CONCENTRATION		
1 g/t	0.029 166 6	ounce (troy)/ ton (short)	1 ounce (troy)/ ton (short)	34.285 714 2	g/t
1 g/t	0.583 333 33	pennyweights/ ton (short)	1 pennyweight/ ton (short)	1.714 285 7	g/t

OTHER USEFUL CONVERSION FACTORS

1 ounce (troy per ton) (short)	20.0	pennyweights per ton (short)
1 pennyweight per ton (short)	0.05	ounces (troy) per ton (short)

Note: Conversion factors that are in bold type are exact. The conversion factors have been taken from or have been derived from factors given in the Metric Practice Guide for the Canadian Mining and Metallurgical Industries, published by the Mining Association of Canada in co-operation with the Coal Association of Canada.